Effects of Foundation Characteristics and Building Separation Gap on Seismic Performance of Mid-rise Structures Incorporating Soil-Foundation-Structure-Interaction

By

Quoc Van Nguyen

A thesis submitted in fulfilment

of the requirement for the degree of

Doctor of Philosophy

School of Civil and Environmental Engineering

Faculty of Engineering and Information Technology

University of Technology Sydney (UTS)

July 2017

CERTIFICATE OF ORIGINAL AUTHORSHIP

I hereby certify that the work embodied in this Thesis is the result of original research and has not previously been submitted for a degree nor has it been submitted as part of requirements for a degree except as fully acknowledged within the text.

I also certify that the thesis has been written by me. Any help that I have received in my research work and the preparation of the thesis itself has been acknowledged. In addition, I certify that all information sources and literature used are indicated in the thesis.

Signature of Candidate

Production Note:
Signature removed prior to publication.

(Quoc Van Nguyen)

Sydney, July 2017

ACKNOWLEDGMENT

This PhD project could not have been possible without the assistance, understanding, and guidance rendered by numerous people throughout the project.

The author would very much like to express his appreciation and gratitude to his principal supervisor, Associate Professor Behzad Fatahi, for his limitless support, tireless contributions, and guidance throughout this work. The author would also like to very much thank his co-supervisors, Dr. Harry Far, and Associate Professor Hadi Khabbaz for their presence and willingness to help throughout the years.

Furthermore, the author would like to thank staff of the Faculty of Engineering and IT team, especially Dr. Matthew Gaston, Mr. Phi Nguyen, Mr. Christopher Dundov and Mr. Jason Chen for their extensive assistance in conducting the advanced computations on Faculty clusters.

Warm thanks to my friends and colleagues for sharing their time and friendship with the author and rendered precious help. Special thanks to Dr. Aslan Sadeghi Hokmabadi and Mr. Ruoshi Xu for their collaboration and kind assistance during the project. The author also feels a deep sense of gratitude to all the academic and non-academic staff in the Faculty of Engineering and Information Technology for the help rendered.

Words are not enough to thank my family for the support they have given me during this long and sometimes difficult journey. The author would very much like to express his love and gratitude to his mother, wife and two kids for their love and support, and for instilling in me the value of learning and providing me outstanding opportunities to do so throughout my life. Without their endless help, I would not be able to achieve and enjoy these successes.

LIST OF PEER-REVIEWED PUBLICATIONS BASED ON THIS RESEARCH

PEER-REVIEWED JOURNAL PAPERS

1. Nguyen, Quoc Van, Fatahi, Behzad and Hokmabadi, S Aslan. 2016. 'The effects of foundation size on the seismic performance of buildings considering the soil-foundation-structure interaction', *Structural Engineering and Mechanics*, Vol. 58, No. 6 (2016), page 1045-1075.

   DOI: http://dx.doi.org/10.12989/sem.2016.58.6.1045.

2. Nguyen, Quoc Van, Fatahi, Behzad and Hokmabadi, S Aslan. 2017. 'Influence of Size and Load-Bearing Mechanism of Piles on Seismic Performance of Buildings Considering Soil–Pile–Structure Interaction', *International Journal of Geomechanics*, Vol. 17, No. 7 (2017), page 04017007-1-22.

   DOI: 10.1061/(ASCE)GM.1943-5622.0000869.

3. Fatahi, Behzad, Nguyen, Quoc Van, and Xu, Ruoshi. 2017. 'The response of mid-rise buildings sitting on pile foundations to seismic pounding'. *International Journal of Geomechanics. (Accepted)*

PEER-REVIEWES CONFERENCE PAPERS

4. Nguyen, Quoc Van, Fatahi, Behzad and Khabbaz, Hadi. 'Three dimensional numerical simulation to predict performance of laterally loaded piles on clay-sand layered slope'. *International Conference GeoMontreal 2013*, Sep-Oct 2013, Montreal, Canada.

5. Nguyen, Quoc Van, Fatahi, Behzad and Hokmabadi, S Aslan, 'Influence of Shallow Foundation Characteristics on Seismic Response of Mid-rise Buildings Subjected to Strong Earthquakes', *International Conference GeoChina 2016*, July 25-27, 2016, Shandong, China, Page 117-124.

ABSTRACT

Seismic waves travel many kilometres and pass through soil layers close to the ground surface before hitting the structures. The seismic induced dynamic behaviour of structures built on soft soil is highly dependent on the soil properties and the foundation type due to their interactions during an earthquake event. The design of building structures needs to consider seismic soil-foundation-structure interaction, where the building responses vary significantly depending upon the fixity of the base condition due to the interaction between the ground and the foundation as well as the building structures. This interaction is called "Seismic Soil-foundation-structure-interaction" (SSFSI). For a typical soil and foundation, SSFSI analysis shows lower natural frequency of the structural system and higher effective damping ratio compared to the traditional analysis with fixed base condition. This can considerably alter the response of the building frames under the seismic excitations by influencing the structural demand of the building as well as amplifying the lateral deflections and inter storey drifts of the superstructure. This phenomenon is highly influenced by the foundation type (i.e. shallow and deep foundation) and may change the performance level of buildings in the performance based design approach. Therefore the interaction should be considered in design of buildings subject to seismic activities so as to provide a safe and cost effective structural system.

In this study, a rigorous numerical modelling approach was developed and used to build numerical tests for different foundation types and sizes as well as the pounding effects between buildings. The results consisted of lateral deformation, inter-storey drifts, levelling shear forces of the structures, foundation rocking, impact force and pile responses. These perimeters cover a wide range of earthquake inputs and foundation characteristics.

The first step was that the soil-pile-interaction numerical behaviour was investigated in a case study of lateral loaded pile considering the shear plastic deformation of the layered sloping ground including sand and clay layers. Appropriate subroutines were adopted to simulate the soil-pile-interaction which included the incorporation of gapping and sliding (in normal and tangential directions) at the interface. A wide range of parameters for this numerical modelling was validated through comparison with an array of a full-scale lateral loaded pile experiments.

Secondly, dynamic characteristics of soil-foundation-structure system were investigated for seismic response of a mid-rise moment resisting building on shallow foundation under four well-known earthquakes. By adopting a direct calculation method, the numerical model can perform a fully nonlinear time history dynamic analysis for three-dimensional numerical model with different foundation sizes where the infinite boundary, sliding and separation in soil-foundation was taken into account. In addition, the influence of foundation sizes on natural frequency and structure response spectrum was also studied. The results confirmed that when the size of shallow foundation is reduced, the natural period would lengthen, the base shear would reduce significantly while the lateral deformation, inter-storey drift and foundation rocking would increase.

Thirdly, the comprehensive pile foundation investigation concludes that the type and size of a pile foundation that supports mid-rise buildings in high-risk seismic zones can alter the dynamic characteristics of the soil-pile-foundation system during an earthquake due to soil-structure-interaction. It is not true to believe that longer piles can provide safer condition under earthquake loading. In fact, by increasing the length of floating piles the structure undergoes more maximum lateral deflection, more inter-story drift and more total maximum levelling shear force but less foundation rocking. This can be explained due to the fact that longer pile foundation has higher contact surface with surrounding soil which enable them to absorb extra seismic energy. This finding can be the recommendation for design engineers that the pile should not lengthen too much to reduce the seismic effects.

Finally, the separation gap between moment resisting and two shear wall braced buildings on pile foundation under seismic loading was studied. The result from this numerical modelling showed that pounding impact influences the distribution of shear force which disturbs the natural vibration and in extreme case, causes collapse. The outcome of this study provides essential insight to geotechnical and structural engineers when designing neighbouring structures in earthquake prone areas.

TABLE OF CONTENTS

LIST OF FIGURES

LIST OF TABLES

LIST OF ABBREVIATIONS

Full text	Abbreviation
American Society of Civil Engineers design code	ASCE
Boundary element method	BEM
Building Seismic Safety Council	BSSC
Complete quadratic combination	CQC
Earthquake design category	EDC
Earthquake Wave Equation Analysis for Piles	EQWEAP
Federal Emergency Management Agency	FEMA
Global Positioning System	GPS
International Building Code	IBC
Linear dynamic procedure	LDP
Linear static procedure	LSP
National Earthquake Hazards Reduction Program	NEHRP
National Computational Infrastructure	NCI
Nolinear dynamic procedure	NDP
Nonlinear static procedure	NSP
Seismic Soil-foundation-structure-interaction	SSFSI
Seismic soil–pile–structure interaction	SSPSI
Single degree of freedom	SDOF
Soil-foundation-structure interaction	SFSI
Soil-pile-structure interaction	SPSI
Soil–structure-interaction	SSI
Structure-soil-structure-interaction	SSSI
Thin layer method	TLM

LIST OF NOTATIONS

$a(t)$	raw data record
$a_c(t)$	corrected acceleration record
$a_0(t)$	acceleration correction
$2a$	width of the foundation
A	Area, foundation width, cohesion
A_{loop}	area of the hysteresis
$[A]$	Damping matrix
B	width of the pile
B_b	width of building
B_f	width of foundation
B_s	width of soil model
c	damping coefficient, soil cohesion
c_h	damping coefficient in horizontal direction
c_θ	damping coefficient in rotation direction
$\widetilde{c}$	equivalent damping coefficient
C_1, C_2, C_3, C_k	modification factor for pseudo lateral load, constant
c'	cohesion, effective cohesion
c_p, c_s	velocities of the normal wave and shear wave
CL	clayey soil
$[C]$	damping matrix
D	diameter of pile
$Drift$	maximum inter-storey drifts of the building
d_p, d_s	distributed damping in the normal and shear directions
d_c	decay coefficient
d_{i+1}, d_i	Deflection at level $(i+1)$ and (i)
$d_i(t)$	deflection history at level (i)
E	Young's modulus, modulus of elasticity of concrete
E_a, E_b, E_c, E_d, E_e	Soil classification according to AS1170.4 (2007)
E_s	soil subgrade reaction
E_p	Young's modulus of pile

E_{x}	soil reaction
F	force
F_{x}	vertical distribution of seismic force at each level
f	natural frequency
f_1, f_2	first and second mode frequencies in Rayleigh damping
f_c'	compressive strength of concrete
f_{n}	natural frequency of mode *n*
f_{y}, f_{sy}	yield strength
G	shear modulus, permanent action
G_0	average shear modulus
G_{max}	maximum shear modulus
G_{sec}	secant shear modulus
G_{tan}	tangent shear modulus
H	height of the structure, shear force, soil thickness, soil height
H_s	height of soil model
h	clearance or gap, height of level
h_s	floor slab thickness
h_f	foundation thickness
I	moment of inertia
I_p	moment of inertia of pile
I_x, I_y	moment of inertia about *x* axis and y axis
IE	bending stiffness of the beam
k	stiffness
k_h	stiffness in horizontal direction
k_i	soil resistance in segment (i)
k_y	lateral stiffness
k_θ	stiffness in rotation direction, rocking stiffness
$\widetilde{k}$	equivalent stiffness
$\overline{k}$	stiffness of the structure fixed at the base
$[K]$	stiffness matrix
L	length

L_b	length of building
L_f	length of foundation
L_{FE}	length of finite element section
L_{INF}	length of infinite element section
m	mass
M	bending moment
$[M]$	mass matrix
M_w	moment magnitude of earthquake in Richter scale
P	lateral load
p	load, contact pressure
p_i	load in segment (i)
P_0	amplitude of harmonic force
P_{x}	axle force from structure applied to pile head
PI	plasticity index
PGA	peak ground acceleration
q_{s}	lateral distributed load from soil to the pile
q_{y}	lateral distributed load along the beam
Q	Impose Action, shear force along the pile
R_{int}	reduction factor
r_{in}	inner radius of the pile
r_{out}	outer radius of the pile
$SDOF$	single degree of freedom
S	slope (or rotational deflection) of the pile, distance
S_a	response spectrum acceleration, spectral acceleration
S_{DS}	design earthquake motion
s_{i}	minimum distance between adjacent structure at level (i)
S_u	undrained shear strength
$(S_u)_{soil}$	undrained shear strength of soil
$[(S_u)_{int}]$	reduce shear strength at the interface
SD	separation gap
Δ	lateral deflections in $P-\Delta$ effect
Δ_{i1}, Δ_{i2}	lateral deflections of neighbouring structures

T	fundamental period
$\widetilde{T}$	effective fundamental period
T_0	characteristic period of the response spectrum
T_1 and T_2	limits of a time interval
t	time
u_0	structural distortion
u_t^0	total initial lateral displacement
u_t	total lateral displacement
$\widetilde{u_g}$	equivalent input motion
u_i, u_j	material particle displacement
$u_i(t)$	horizontal displacement history at level (i)
$u_0(t)$	horizontal displacement history at level (0)
$\ddot{u}_i$	material particle acceleration
V	pseudo lateral load, shear force
V_S	shear wave velocity
V_{S0}	average shear wave velocity
$v_c(t)$	corrected velocity record
W	total dead load and anticipated live load
$\overline{W}$	total dead load and anticipated live load of structure fix at base
W_D	dissipated energy
W_S	the maximum strain energy
x_i	position of pile at segment (i)
Y	deflection, pile deflection
y_i	deflection in segment (i)
z_i	depth of soil at segment (i)
α, β	mass damping coefficient and stiffness damping coefficient
γ	shear strain, unit weight
$\dot{\gamma}_1$ and $\dot{\gamma}_2$	two local slip velocity components
γ_c	cyclic shear strain, shear strain
γ_{max}	maximum shear strain
$\dot{\gamma}_{eq}$	equivalent slip rate
ε	strain of concrete material

ε_{yield}	strain at yield point
Z	damping ratio
Θ	angle
μ	coefficient of friction
μ_r, μ_p	residual coefficient of friction, peak coefficient of friction
ν	Poisson's ratio
ξ_0	hysteretic damping
Ξ	damping ratio
$\widetilde{\xi}$	equivalent damping ratio
ρ	density, mass density
σ, σ'	normal stress, effective normal stress
σ_y, σ_{yield}	yield stress of concrete material
τ	shear strength
τ_1 and τ_2	two orthogonal components of shear stress
τ_{cr}, τ_{crit}	critical shear stress
τ_{eq}	equivalent shear stress
τ_c	shear stress
φ, φ'	internal frictional angle, effective internal frictional angle
ψ	dilation angle
ω, ω_0	natural frequency
ω_i, ω_j	natural angular frequency for mode (i) and (j)
$\widetilde{\omega}$	equivalent natural frequency
$\phi, \emptyset$ and $\emptyset'$	friction angle and effective friction angle

Chapter 1 INTRODUCTION

1.1 General

The seismic soil–foundation–structure interaction (SSFSI) in each case of construction plays an important role to the response of that structure. With the differences in foundation types and sizes, the interaction surfaces and their mechanical properties will provide different responses to the structure. These responses depend on the types of loads, especially in the case of the earthquake waves transferring from far distance. The foundation is a part of a structure system in which the gravity load and live load from the structure are applied to. However, the seismic load comes from some depths of the earth and transfers the load to the structure via foundation. This demands the survival of structure even if they occur a few times in hundred years, suddenly without prediction.

This study aims to numerically analyse the building response under different earthquakes. The main components of seismic building response includes displacement, deflection, and drift of each floor, levelling shear forces, foundation rocking and also the recorded acceleration at any point in models. This can produce the response spectrums and dominant frequency. All of these parameters need to satisfy certain requirements from design codes.

In order to determine the seismic response of structures, the assumption that the structure is fixed at its base has been made frequently in practice. In general, this assumption can be acceptable if the ground under the structure is stiff enough (similar to structure founded on solid rock). However, when the soil under the structure is soft, two modifications factors need to be considered to determine the seismic response. First of all, the imposed motion to the structure is different from free field motion due to the presence of the structure and foundation. Secondly, additional dynamic deformations are induced within the structure due to the soft soil underneath. According to Kramer (1996), soil–structure-interaction (SSI) is the process in which response of the soil influences the motion of the structure and also response of the structure influences the motion of the soil.

The importance of seismic soil–foundation–structure interaction (SSFSI) in earthquake prone areas employing different types of foundations continues to increase. Unfortunately, research into SSFSI has not kept up with overall demand and it is very

limited in comparison to other geotechnical and structural engineering research topics. In particular, the numerical study of SSFSI has attracted limited attention due to the number of assumptions while the full-scaled experiment has been unfeasible.

Current understanding about the seismic soil–foundation–structure interaction (SSFSI) is insufficient and requires more comprehensive studies. Various parameters represent the complicated nature of dynamic soil properties, soil–foundation–structure system, and earthquake properties need to be verified.

1.2 Highlighted features of this study

Initially, this research is to provide a rigorous study into the performance of soil-pile interaction under the lateral loads producing a clear multiple layered soil and single pile response using the well-known Mohr–Coulomb failure criterion (based on two soil properties, namely friction angle, $\emptyset$, and cohesion, c). The verified results of this study provides a subroutine capturing soil-structure-interation that can be assigned to interface elements in numerical modelling. In this study, this interface model is developed as a FORTRAN subroutine embedded into ABAQUS, which is a multiphysic Finite Element Analysis commercial package. Three-dimensional numerical models are also developed using the above mentioned equation to investigate the effects of soil-structure-interaction in dynamic behaviour of structures on soft soils.

By adopting a direct calculation method, the numerical model can perform a fully nonlinear time history dynamic analysis to realistically simulate the dynamic behaviour of soil, foundation, and structure under seismic excitations. This three-dimensional numerical model accounts for the nonlinear behaviour of the soil medium and structural elements. Infinite boundary conditions are assigned to the numerical model to simulate quiet boundaries, and appropriate contact elements capable of modelling sliding and separation between the foundation and soil elements are also considered.

In shallow foundation models, due to natural period changing when foundation size varies, there is a significant change in building response when comparing with fixed base condition. It is concluded that the size of foundation influences the dynamic characteristics and the seismic response of the building due to interaction between the soil, foundation, and structure, and therefore design engineers should carefully consider these parameters in order to ensure a safe and cost effective seismic design.

In the second seismic model, soil-pile interaction modelling is applied to determine the response of building considering seismic soil–foundation–structure interaction (SSFSI) influenced by size and load-bearing mechanism of foundation. The study provides an excellent insight into the behaviour of structures under a broad range of input parameters. Moreover, due to the complexity of numerical modelling and large required memory, there are very few numerical studies on this topic. This study provides a simple and reliable approach that can speed up the numerical studies, which is one of the most significant contribution to the study of seismic soil–foundation–structure interaction.

In addition, pounding between adjacent buildings is adding another layer of complexity into the study due to the interaction between floors of buildings that needs to be considered in order to obtain the impact forces. With the help of the Cluster supercomputers from University of Technology Sydney and National Computational Infrastructure (NCI) Australia, different numerical results have been obtained including lateral building deflections, inter-storey drifts, structural shear forces, foundation rocking, lateral pile deflections, impact force histories and locations, and the distributions of bending moments and shear forces of the piles. The findings of this study will give engineers a better understanding of the possible effects of seismic pounding on the seismic performance of buildings, and the response of end-bearing piles in soft soils. It is confirmed that the separation gap influences the pounding dynamic characteristics and the seismic response of the building, and therefore design engineers and urban planner should carefully consider these parameters in order to ensure a safe seismic design from the pounding effects.

In this study, it takes averagely a week to solve a single model on Cluster supercomputers with average output file size of 80 GB. It clearly shows a significant required computer power that is currently unfeasible to solve using a personal computer.

1.3 Objectives and Scope of Study

The research presented in this thesis focus on four main problems of seismic soil–foundation–structure interaction (SSFSI) which can be summarised as below:

(1) The nonlinear three-dimensional soil-pile interaction under lateral loading;
(2) The effect of foundation size on performance of buildings considering SSFSI;

(3) The influence of size and load-bearing mechanism of pile on performance of buildings considering SSFSI;
(4) Response of mid-rise buildings sitting on pile foundations considering SSFSI and pounding between buildings.

The main objective of this study is to find the response of regular mid-rise moment resisting building under earthquake loading sent from a distance underneath the soil medium, in order to ensure that the design is safe and reliable. To do that, the research work consisted of 3 steps:

Step 1. Studying, in depth, the nonlinear three-dimensional soil-pile interaction numerical modelling under lateral loading. The soil-pile response in term of $p-y$, rotational displacement, bending moment, and gap opening behind the pile is investigated. Mohr-coulomb failure criteria is adopted to implement the soil plasticity.

Step 2. Developing the nonlinear three-dimensional model to simulate seismic soil–foundation–structure interaction. Four well-known earthquakes are selected to apply to the foundation.

Step 3. The superstructure is modelled with several element types to meet all requirements from Australian design codes. The building response is reported for various foundation conditions.

Step 4. Conducting a large number of full-scale numerical modelling with different types and sizes of foundation and pounding impact between buildings with different separation gaps.

1.4 Organisation of the Thesis

The structure of this thesis reflects the three main topics about seismic soil-foundation-structure interaction (SSFSI). It is organised as follows:

Chapter 2 presents a basic summarised historical review of soil foundation interaction under static lateral load and seismic soil–foundation–structure interaction (SSFSI). Chapter 2 also provides the background to the subsequent chapters by presenting a summary of research into previous work with their limitations and future work recommendations.

Chapter 3 describes the details of numerical modelling used throughout the research capturing soil-foundation interaction in a case study of lateral loaded pile on clay-sand layered slope. The predictions are compared with experiment results.

Chapter 4 presents the effect of foundation size on performance of buildings considering SSFSI. In this chapter, the foundation size is changed then the building performance is recorded and discussed.

Chapter 5 presents the effect of pile size and load-bearing mechanism on performance of buildings considering SSFSI. The moment-resisting mid-rise building under different pile sizes and load-bearing mechanisms is analysed.

Chapter 6 focuses on pounding between mid-rise buildings on pile foundation under seismic loadings. Two shear-wall braced buildings and a moment-resisting building staying next to each other with different separation gaps causing pounding effect are analysed.

Chapter 7 concludes the thesis for current study and provides some recommendations for further work.

Chapter 2 LITERATURE REVIEW

2.1 General

One of the most common challenges that civil engineers face is the problem of structure-soil-structure-interaction (SSSI) and soil-foundation-structure interaction (SFSI) when the buildings are located in potential earthquake areas. They have become increasingly essential for most seismic analysis and structural design. The structural designer usually assumes the structure in a fixed-base condition. If the ground is stiff enough, the earthquake input is applied directly to the foundations in the form of acceleration. The fixed-base condition is used widely today as it is simple and the structure response is reasonable to design the structure details. By that way, the influence of the structure-soil-structure-interaction is ignored.

Historically, this problem has attracted a number of scholars who did study the soil-structure-interaction when the building was to be built in poor unfavourable geotechnical conditions like frequent seismic activity or soft soil. However, the current design codes like ASCE, NEHRP, Australia and New Zealand standard have several limitations which are usually neglected. Some of these components are influenced by soft soil and the effect of kinematic interaction.

The deformations, floor drift and column shear forces of a structure under earthquake condition are affected by the characteristics of interactions between three main components namely the structure, the foundation, and the soil media surrounding the foundation. The complexity of soil-structure-interaction (SSI) or structure-soil-structure-interaction (SSSI) and especially seismic soil–foundation–structure interaction (SSFSI) problems and the limited standards and unavailability of validated analysis techniques routinely forces design engineers to apply simple techniques and ignore the presence of the building foundation in structural design. As the range of application continues to increase for current design codes, greater demand is placed on SSFSI.

Unfortunately, meeting simultaneously of two disciplines of structural and geotechnical engineering is the major challenge of seismic soil–foundation–structure interaction problems. In addition, the current understanding regarding the influence of SSFSI is somewhat unsatisfactory due to the complex nature of interactions between each component in the soil-structure system. Moreover, conducting full-scale experiment for

the mid-rise buildings under an earthquake is impossible. As a result, most currently proposed theories have to use a number of significant underlying assumptions based on observations of earthquake performance. The advantage of using numerical modelling to study SSFSI is that the mechanism can be obtained without any assumptions being made in advance.

In this chapter, the principles related to seismic soil–foundation–structure interaction (SSFSI) in addition to review of design codes will be summarised.

2.2 Seismic soil-foundation-structure interaction concept

The earlier approach for structure design under seismic loading comes from ground response analysis. In the ideal situation, the earthquake-induced acceleration applied to the superstructure is determined from propagation of the stress wave through the earth material to beneath the structure. However, there are a number of uncertainties about this faced in practice which force earthquake engineers to use empirical methods and seismic hazard analysis. The concept of SSFSI comes from geotechnical earthquake engineering which deals with design and construction of buildings in order to resist the strike of earthquakes. This type of engineering requires a certain level of understanding about geology, seismology, earthquake engineering, geotechnical and structural engineering as well as the consideration of social, economic and political factors.

Kumar (2008) mentioned that geological data and principles are important for planning, design, construction and maintenance of civil engineering works. The primary responsibility of a geologist is to determine the location of a fault, investigate the fault in terms of either active or passive, as well as evaluate historical records of earthquakes and their impact on a site. The main earthquake parameters from these studies are peak ground acceleration and magnitude of earthquake.

In seismology study, it is important to understand the dynamic properties of soil in that site. This includes an investigation for the possibility of liquefaction of the soil because liquefaction causes complete loss of soil shear strength, bearing capacity failure, excessive settlement, soil sliding or slope movement. These liquefaction factors result in unfavourable soil conditions in term of geotechnical engineering. It is not accurate and safe for engineers to assume soil properties remain unchanged while earthquake waves pass through soil. There has been a number of scholars who have investigated

experimentally the dynamic properties of the soil during earthquake excitation. These properties include shear modulus, modulus reduction and damping variation with cyclic strain.

According to Kramer (1996), ground motions that are not influenced by the presence of structures are referred to as *free-field motions*. However, when a structure founded on solid rock is subjected to an earthquake, the extremely high stiffness of the rock constrains the rock motion to be very close to the free - field motion. Structures founded on rock are considered to be fixed-base structures. On the other hand, the same structure would respond differently if supported on a soft soil deposit. First, the inability of the foundation to conform to the deformations of the free-field motion would cause the motion of the base of the structure to deviate from the free-field motion. Second, the dynamic response of the structure itself would induce deformation of the supporting soil. This process, in which the response of the soil influences the motion of the structure and the response of the structure influences the motion of the soil, is referred to as *soil-structure interaction.*

Soil-structure interaction has little effect on the dynamic response of many structures and foundation systems. In other cases, however, its effects can be significant. Whether neglecting of its effects is conservative or aggressive depends on the details of the problem at hand and must be evaluated on a case-by-case basis.

The analysis of soil-structure-interaction and the concept of SSFSI can be quite complicated in terms of both understanding and applying. Wolf (1985) suggested a simplified model with a single degree of freedom (SDOF) system. This model can be used for both a one storey building or equivalent multi-storey building on the soil foundation with respect to its dominant motion mode. The structure has mass (m), stiffness (k) and damping coefficient (c), and its natural frequency (ω_0) is as follows:

$$\omega_0 = \sqrt{\frac{k}{m}} \tag{2.1}$$

and hysteretic damping (ξ_0) is:

$$\xi_0 = \frac{c\omega_0}{2k} \tag{2.2}$$

However, when the supporting soil is compliant, the foundation can translate and rotate. The stiffness and damping characteristics of such a system can be represented by the translational and rotational springs and dashpots as shown in Figure 2.1, where:

- k_h and c_h are stiffness and damping in the horizontal direction;
- k_θ and c_θ are stiffness and damping in the rotational direction, respectively;
- h is the height of the structure; $2a$ is the width of the foundation;
- u_0 is the amplitude of the base relative to the free-field motion (u_g);
- u is the structural distortion; and u_t is the total lateral displacement of the system.

This system can be replaced by an equivalent model shown in Figure 2.2

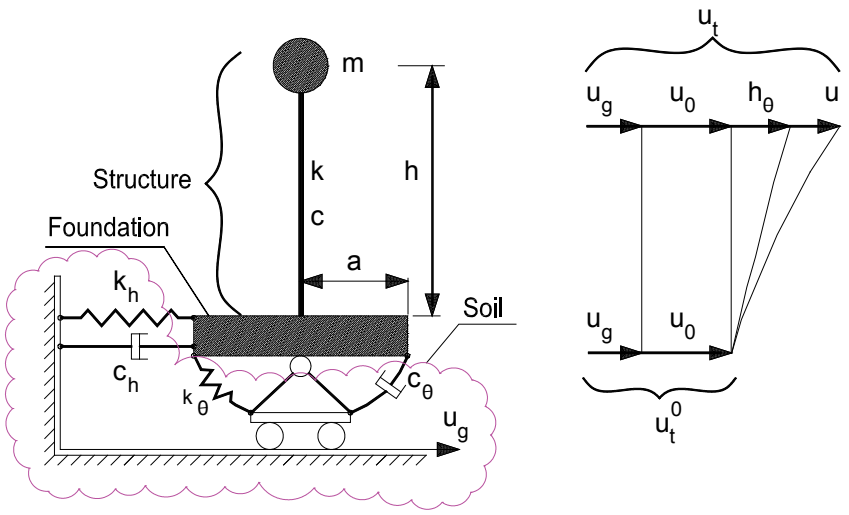

Figure 2.1 Soil-structure interaction model including SDOF structure and idealised discrete system to represent the supporting soil (after Wolf 1985)

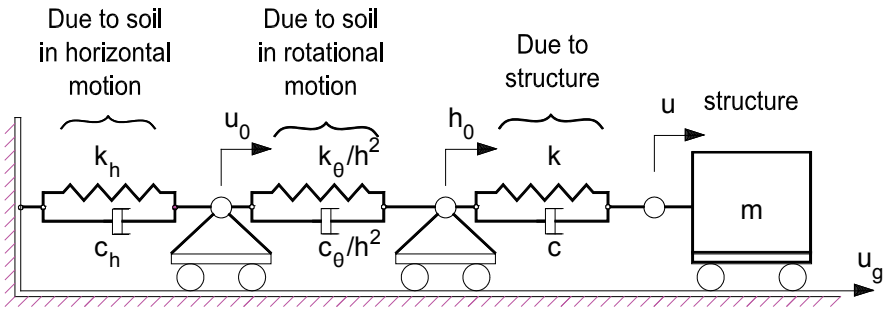

Figure 2.2 Equivalent soil-structure interaction model (after Wolf 1985)

As explained by Wolf (1985), the motion equation of system in Figure 2.2 can be expressed in matrix form as follows:

$$\begin{bmatrix} k_h + \frac{k_\theta}{h^2} & -\frac{k_\theta}{h^2} & 0 \\ -\frac{k_\theta}{h^2} & k + \frac{k_\theta}{h^2} & -k \\ 0 & -k & k \end{bmatrix} \begin{Bmatrix} u_0 \\ u_0 + h\theta \\ u_0 + h\theta + u \end{Bmatrix} + \begin{bmatrix} c_h + \frac{c_\theta}{h^2} & -\frac{c_\theta}{h^2} & 0 \\ -\frac{c_\theta}{h^2} & c + \frac{c_\theta}{h^2} & -c \\ 0 & -c & c \end{bmatrix} \begin{Bmatrix} \dot{u}_0 \\ \dot{u}_0 + h\dot{\theta} \\ \dot{u}_0 + h\dot{\theta} + \dot{u} \end{Bmatrix} + \begin{bmatrix} 0 & 0 & 0 \\ 0 & 0 & 0 \\ 0 & 0 & m \end{bmatrix} \begin{Bmatrix} \ddot{u}_0 \\ \ddot{u}_0 + h\ddot{\theta} \\ \ddot{u}_0 + h\ddot{\theta} + \ddot{u} \end{Bmatrix} = \begin{Bmatrix} 0 \\ 0 \\ -m \end{Bmatrix} \ddot{u}_g \tag{2.3}$$

where

$$\xi = \frac{c}{2k\omega};\ \xi_h = \frac{c_h}{2k_h\omega_h};\xi_\theta = \frac{c_\theta}{2k_\theta\omega_\theta}\ ;\omega_s = \sqrt{\frac{k}{m}};\ \omega_h = \sqrt{\frac{k_h}{m}};\ \omega_\theta = \sqrt{\frac{k_\theta}{mh^2}} \tag{2.4}$$

After solving these equations

$$u_0 = \frac{\omega_s^2}{\omega_h^2}\frac{1+2i\xi}{1+2i\xi_h}u;\ h\theta = \frac{\omega_s^2}{\omega_\theta^2}\frac{1+2i\xi}{1+2i\xi_\theta}u \tag{2.5}$$

And *u* is expressed as:

$$\left(1 + 2\xi - \frac{\omega^2}{\omega_s^2} - \frac{\omega_s^2}{\omega_h^2}\frac{1+2i\xi}{1+2i\xi_h}\frac{\omega_s^2}{\omega_\theta^2}\frac{1+2i\xi}{1+2i\xi_\theta}\right)u = \frac{\omega^2}{\omega_s^2}u_g \tag{2.6}$$

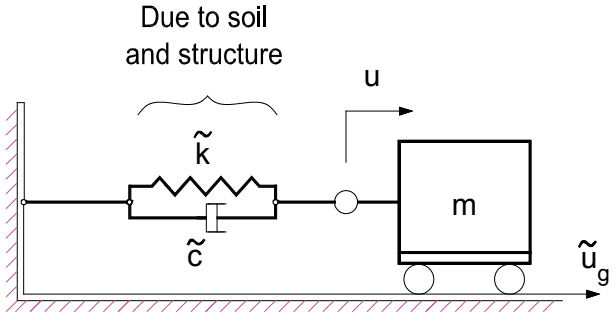

Figure 2.3 Equivalent one degree of freedom (after Wolf 1985)

Figure 2.3 displays the equivalent system of a full one degree of freedom soil-structure interaction system in which the equivalent natural frequency ($\widetilde{\omega}$), equivalent damping ratio ($\tilde{\xi}$), and equivalent input motion ($\tilde{u}_g$), are calculated as below:

$$\frac{1}{\widetilde{\omega}^2} = \frac{1}{\omega_s^2} + \frac{1}{\omega_h^2} + \frac{1}{\omega_\theta^2} \tag{2.7}$$

$$\tilde{\xi} = \frac{\widetilde{\omega}^2}{\omega_s^2}\xi_s + \frac{\widetilde{\omega}^2}{\omega_h^2}\xi_h + \frac{\widetilde{\omega}^2}{\omega_\theta^2}\xi_\theta \tag{2.8}$$

$$\tilde{u}_g = \frac{\widetilde{\omega}^2}{\omega_s^2}u_g \tag{2.9}$$

Equations (2.7) and (2.8) indicate that when the seismic soil-structure interaction is taken into account the natural frequency of the equivalent system ($\widetilde{\omega}$) is always lower while the damping ratio ($\tilde{\xi}$) is always greater than those of the fixed-base structure. In other words, the important properties of full soil-structure system compared to fixed-base structure are affected significantly by seismic soil-structure interaction which is to reduce the natural frequency and increase the damping ratio.

According to Veletsos and Meek (1974), compared to a fixed-base system, the soil-foundation-structure interaction (SFSI) has two basic effects on the structural response: *(i)* the soil-structure system has an increased number of degrees of freedom and thus modified dynamic characteristics, and *(ii)* a significant part of the vibration energy of the soil-structure system may be dissipated by radiating waves emanating from the vibrating foundation-structure system back into the soil, or by hysteric material damping in the soil. Either way this means that a soil-structure system has a longer natural period of vibration than its fixed-base counterpart.

The seismic soil-foundation-structure interaction (SSFSI) was developed to explain the consequent effect of considering the soil-structure interaction on the total response of the structure. The simplified SDOF model is subjected to an arbitrary input motion. In general, two key mechanisms are involved during a seismic soil-foundation-structure interaction: *kinematic interaction* and *inertial interaction*. On the one hand, kinematic interaction occurs because stiff foundation elements in the soil cause the foundation motion to deviate from the free field ground motion. Kinematic interaction

could also be due to ground motion incoherence, foundation embedment effects, and wave scattering or inclination (Stewart *et al.* 1999b). On the other hand, inertial interaction results from the inertia developed in the structure as its own vibration produces base shear, moment, and torsional excitation. These loads in turn cause displacements and the foundation to rotate relative to the free field condition (Kramer and Stewart 2004). Fundamentally, the size of a foundation can influence the kinematic and inertial interactions mainly by altering the mass and stiffness of the soil-foundation system, which in turn influences the seismic response of the superstructure.

2.3 Soil-foundation-structure interaction analysis: procedures for design

2.3.1 General design procedure considering seismic loading

According to Kumar (2008), geotechnical earthquake engineering deals with the design and construction of projects. The objective of this field of study is to understand the effect of earthquakes. Geotechnical earthquake engineering requires an understanding of geology, seismology and earthquake engineering. Furthermore, practice of geotechnical earthquake engineering also requires consideration of social, economic and political factors. The primary responsibility of a geologist is to determine the location of a fault, investigate the fault in terms of either active or passive, as well as evaluate historical records of earthquakes and their impact on the site. The studies help to define design earthquake parameters. The important design earthquake parameters are peak ground acceleration and magnitude of anticipated earthquake. The very first step in geotechnical earthquake engineering is to determine the dynamic loading from the anticipated earthquake. The anticipated earthquake is also called the design earthquake.

According to Kumar (2008), a geotechnical earthquake engineer should perform the following duties:

- Investigates the possibility of liquefaction at the site (liquefaction causes complete loss of soil shear strength, causing bearing capacity failure, excessive settlement or slope movement).
- Calculates settlement of structure caused by anticipated earthquake.

- Checks the bearing capacity and allowable soil bearing pressures, to make sure that the foundation does not suffer a bearing capacity failure during the design earthquake.
- Investigates for slope stability due to additional forces imposed due to design earthquake. Within this, lateral deformation of slope also needs to be studied due to anticipated earthquake.
- Studies the effect of earthquake on the stability of retaining walls.
- Analyses other possible earthquake effects, such as surface faulting and resonance of the structure.
- Develops site improvement techniques to mitigate the effect of anticipated earthquake. These include ground stabilisation and ground water control.
- Determines the type of foundation, (shallow or deep), best suited for resisting the effect of design earthquake.
- Assists the structural engineer by investigating the effect of ground movement due to seismic forces on the structure.

Building designers need to fully understand the earthquake load in order to deal with them cautiously in the design phase. It is important to remember that "Earthquakes don't kill people, buildings do" (Hough and Jones 2002). Thus we cannot control the earthquake but we can design the building to survive from earthquake strike.

The following factors affect and are affected by the design of the building (Kramer 1996):

- *Torsion*: Torsion is one of the main reactions of the building and occurs when earthquake sends the load to the building in the form of movement, velocity or acceleration. Buildings have their own centre of mass. If their mass is uniformly distributed then the geometric centre of the floor and the centre of mass may coincide. Due to the movement of the foundation caused by earthquake, uneven mass distribution will position the centre of mass outside of the geometric centre causing "torsion" generating stress concentrations. A certain amount of torsion is unavoidable in every building design. Symmetrical arrangement of masses, however, will result in balanced stiffness against either direction and keep torsion within a manageable range.
- *Damping*: The building vibration will gradually come to an end resulting from damping. Buildings, in general, are poor resonators to dynamic shock and

dissipate vibration by absorbing it. Earthquake structural designers need to consider damping as an important factor during which natural vibration is absorbed.

- *Ductility*: While ductility is the physical characteristic of a material to bend, flex, or move, it fails after considerable deformation has occurred. Non-ductile materials (such as poorly reinforced concrete) fail abruptly by crumbling.
- *Strength*: Strength is the property of a material to resist and bear applied forces within a safe limit. It should be fully understood to apply to any components within the structure based on the mechanism of the components.
- *Stiffness*: Stiffness of a material is the degree of resistance to deflection or drift. Serviceability of each component is influenced directly by stiffness of material. A poor design for a structure can satisfy the strength requirement (safety condition) but not the serviceability.
- *Building Configuration*: Building size, shape, structural and nonstructural elements are defined as building configuration. It determines the way seismic forces are distributed within the structure, their relative magnitude, and problematic design concerns. During seismic design procedures, building configuration should change to meet design conditions.

The below sections are presenting the current design codes for seismic soil-foundation-structure interaction under earthquake loading.

2.3.2 National Earthquake Hazards Reduction Program (NEHRP)

One of the most widely used design codes is the National Earthquake Hazards Reduction Program (NEHRP) from America. The NEHRP's Recommended Provisions for Seismic Regulations for New Buildings and Other Structures have contained procedures for soil-structure interaction analysis. These were originally developed between 1975 and 1977 by the Applied Technology Council Committee on Soil-Structure Interaction (ATC3 Committee 2C). These procedures affect the analysis of seismic demand in structures by modifying the base shear for a fixed-base structure to that for a flexible-base structure with a longer fundamental mode period and a different (usually larger) system damping ratio (BSSC 1997).

The 1997 edition of NEHRP titled “Recommended Provisions for Seismic Regulations for New Buildings and Other Structures”, from Buildings Seismic Safety Council (BSSC 1997) provides detailed procedure including the impedance functions for incorporating the influence of the soil-structure interaction in the determination of design earthquake forces and lateral deflections of structures. Incorporating these effects has a direct result on reducing the base shear applied to the structure, and consequently the lateral forces and overturning moments, while those effects can either increase or reduce the lateral deflections.

The foundation stiffness factors can be derived from a simple model of a rigid mat bonded to an elastic half space following the method initially developed by Gazetas *et al.* (1991). The model can take into account foundation shape, embedment, and the condition of the soft soil over the stiff layer. In addition, simplified expressions for the ‘pile axial and rocking stiffness values’ as well as the influence of the ‘pile cap on the pile group seismic response’ are provided by NEHRP (BSSC 1997). However, the suggested method in NEHRP suffers from the shortcomings corresponding to the application of the substructure method, such as assuming linear behaviour for the soil during the excitation and using general approximation to estimate the material and geometric damping properties for the soil.

General analysis and design requirements of NEHRP for all buildings contain direct effects, $P-\Delta$ effects, torsion, overturning, continuity, diaphragms, walls nonstructural components, structures sharing common elements, building separation and vertical earthquake effects. All of these requirements are important and cover most aspects of structure response and seismic soil-foundation-structure interaction (SSFSI) which is considered clearly. In the 1997 NEHRP Guidelines for the Seismic Rehabilitation of Buildings, the analysis procedures include linear static procedure (LSP), linear dynamic procedure (LDP), nonlinear static procedure (NSP) and nolinear dynamic procedure (NDP).

According to BSSC (1997), under the Linear Static Procedure (LSP), the distribution over the height of the building, and the corresponding internal forces together with system displacements are determined using a linearly-elastic, static analysis. In other words, the building is modelled with linearly-elastic stiffness and equivalent viscous damping that approximate values expected for loading, close to the yield point. Further

in each floor the design earthquake demands for the LSP are represented by static lateral forces whose sum is equal to the pseudo lateral load defined by Equation (2.10).

$$V = C_1 C_2 C_3 S_a W \tag{2.10}$$

where:

V = Pseudo lateral load.

C_1 = Modification factor to related expected maximum inelastic displacements to displacements calculated for linear elastic response. C_1 = 1.5 for T < 0.10 second, C_1 = 1.0 for $T <$ T_0 second.

T = fundamental period of the building in the direction under consideration. If soil-structure interaction is considered, the effective fundamental period $\tilde{T}$ shall be substituted for T.

T_0 = Characteristic period of the response spectrum, defined as the period associated with the transition from the constant acceleration segment of the spectrum to the constant velocity segment of the spectrum.

C_2 = Modification factor to represent the effect of stiffness degradation and strength deterioration on maximum displacement response.

C_3 = Modification factor to represent increased displacements due to dynamic $P - \Delta$ effects.

S_a Response spectrum acceleration, at the fundamental period and damping ratio of the building in the direction under consideration.

W Total dead load and anticipated live load.

The vertical distribution of seismic force at each level F_x is the product of vertical distribution factor and pseudo lateral load. The horizontal distribution of seismic forces shall be distributed according to the distribution of mass at that floor level. The floor diaphragm needs to be designed to resist the effect of inertia forces developed at each level and the structural deformation is based on pseudo lateral load **(**2.10**)**

Under the Linear Dynamic Procedure (LDP) the linearly-elastic, dynamic analysis are used and the acceptance criteria of LDP are similar to those for the LSP (BSSC 1997). The LDP includes two analysis methods, namely, the Response Spectrum and Time-History Analysis Methods. The Response Spectrum Method uses peak modal responses calculated from dynamic analysis of a mathematical model. Only those modes contributing significantly to the response need to be considered. Modal responses are combined using rational methods to estimate total building response quantities.

Nonlinear Static Procedure (NSP) and Nonlinear Dynamic Procedure (NDP) are similar to those in linear types (LSP and LDP); however, a model directly incorporating inelastic material is used to determine the displacement, drift and internal forces to compare with allowable values. NDP is carries out using time-history analysis, so the design displacement is not established using target displacement. The design displacement is determined directly from dynamic analysis using ground motion histories.

Applied Technology Council code, ATC-40 (1996), suggests a similar procedure to account for the effects of the soil-structure interaction. Moreover, simplified recommendations to model the deep foundations are provided. NEHRP from the 2003 edition onward, including 2009 version (BSSC 2009) eliminates the detailed procedure to derive foundation stiffness factors and covers almost the same materials as in ASCE 7-10.

2.3.3 Australian and New Zealand codes

Whilst Australia and New Zealand have developed the code for earthquake design and the seismic soil-foundation-structure interaction (SSFSI) is mentioned, the code does not suggest how to design in consideration of these effects. The NZS1170.5 (2004) has some limitations of earthquake design code in term of SSFSI.

The New Zealand code requires consideration of foundation deformations when calculating building deflections. It even specifies that foundation flexibility should be included in the modelling of the structure. However no guidance or references are provided in commentary in terms of how to include foundation flexibility in the analysis model. Due to the complicated modelling, the flexibility of foundation has frequently been ignored in the industry practice.

AS1170.4 (2007) is the Australian code used to design for earthquake actions. The earthquake actions are determined by considering the site hazard, sub-soil conditions, type and configuration of the structure. The Standard also provides the means for reducing earthquake loads on a structure by achieving set levels of ductility. Materials design Standards then provide detailing to enable the selected structural ductility to be achieved.

The AS1170.4 (2007) separates the soil under the structure into 5 categories (Class A_e, B_e, C_e, D_e or E_e) covering from hard rock to very soft soil. The type of soil is determined by geotechnical engineers but is only needed if the structure is tall. In the analysis step, AS1170.4 (2007) requires at least a static analysis to be done and then lists the earthquake design category (EDC I, EDC I and EDC III) for each type of soil and height of structures.

- EDC I - Earthquake design category I in which the equivalent earthquake load is simply taken as 10% of the seismic mass to be applied at each floor level.
- EDC II - Earthquake design category II requires a static analysis (dynamic analysis can be used if desired) and also sets out the method including the spectral shape factor, the structural ductility and performance factors, the natural period of vibration of the structure. A simple method for distributing the earthquake actions to the levels of the structure is also provided.
- EDC III - Earthquake design category III requires a full dynamic analysis in design. This one is required for the highest hazard levels and tallest structures.

However, the Australian code AS1170.4 (2007) does not address the soil-structure interaction effects for seismic design of structures explicitly. Consequently, structural designers are not able to include those important effects in the analysis and design procedure using AS1170.4 (2007). Because of this problem, the seismic design is not adequately safe due to amplification of lateral deflections and corresponding inter-storey drifts which can possibly change the performance levels of the buildings.

2.3.4 American Society of Civil Engineers design code (ASCE 7-10)

Section C9.0 - Earthquake loads of ASCE 7 is primarily based on the 2000 edition of NEHRP which is prepared by the Building Seismic Safety Council (BSSC) under

sponsorship of the Federal Emergency Management Agency (FEMA). This section denotes that if the option to incorporate the effects of the soil-structure interaction is exercised, the following method is permitted to be used in the determination of the design earthquake forces and the corresponding displacements of the structure in the case that the model used for structural response analysis does not directly incorporate the effects of the foundation flexibility.

The ASCE code accounts for decreasing the base shear and increasing the modified deflection due to the soil-structure interaction corresponding to the fundamental (first) mode of vibration. From this value, the modified storey drifts can be evaluated. In addition, ASCE code employs a spring-dashpot model with SDOF structure similar to what has been illustrated in Figure 2.1 to calculate the modified period and damping ratio of the structure due to the soil-structure interaction.

$$\tilde{T} = T\sqrt{1 + \frac{\bar{k}}{k_y}\left(1 + \frac{k_y \bar{h}^2}{k_\theta}\right)} \tag{2.11}$$

$$\bar{k} = 4\pi^2\left(\frac{\bar{W}}{gT^2}\right) \tag{2.12}$$

where, $\bar{k}$ is the stiffness of the structure fixed at the base, k_y and k_θ are lateral and rocking stiffness of the foundation, respectively, and g is the gravity acceleration.

Unfortunately, ASCE code does not give any equation to calculate this foundation stiffness. It only suggests that the stiffness of spring representing the foundation dynamic behaviour can be calculated by principles of foundation mechanics and soil properties. To do that, ASCE categorises various cases into six site classes in conjunction with the design earthquake motion (S_{DS}) to determine the shear wave velocity ratio V_S/V_{SO} and shear modulus ratio G/G_0 as in Table 2.1.

ASCE code also separates the effect of soil-structure interaction to the modified deflection into total deflection and rocking component. Guin and Banerjee (1998) noted that with the use of the ASCE code, the seismic soil-structure interaction may increase the overall displacement of the superstructure in comparison to the fixed-base condition due to the rotation of foundation.

ASCE7-10 employs a simplified method to account for the soil-structure interaction. This method represents the subsoil by a series of springs and dashpots

(impedance functions), and the superstructure as a SDOF oscillator. Thus, it does not address the coupled behaviour of the soil-structure system.

Table 2.1 Value of V_S/V_{SO} and G/G_O considering strain compatibility (ASCE7-10, 2010)

Site Class	Value of V_s/V_{so}				Value of G/G_0			
	$S_{DS}/2.5$				$S_{DS}/2.5$			
	≤ 0.1	0.4	≥0.8		≤ 0.1	0.4	≥0.8	
A	1.00	1.00	1.00		1.00	1.00	1.00	
B	1.00	0.97	0.95		1.00	0.95	0.90	
C	0.97	0.87	0.77		0.95	0.75	0.60	
D	0.95	0.71	0.32		0.90	0.50	0.10	
E	0.77	0.22	a		0.60	0.05	a	
F	a	a	a		a	a	a	

Note: *Use straight-line interpolation for intermediate values of* $S_{DS}/2.5$*, where:*

a *should be evaluated from site specific analysis;*

V_{so} *is the average shear wave velocity for soil deposit beneath the foundation at small strain levels (10-3% or less);*

G_0 $(= \gamma V_{so}^2/g)$ *is the average shear modulus for the soil deposit beneath the foundation at small strain levels, and* γ *is the average unit weight of the soil deposit. The design earthquake motion is provided in the code, and the site is classified based on the upper 30m of the site profile with respect to the soil properties such as the shear wave velocity.*

Additionally, linear equivalent behaviour for the subsoil is assumed. In addition, this method does not capture directly any non-linearity of the soil as it assumes linear behaviour for the soil during the solution process. Strain-dependent modulus and damping functions (Figure 2.4) are only taken into account in an average sense (Table 2.1), in order to approximate some effects of soil non-linearity.

The above mentioned process is for shallow foundations and ASCE 7-10 does not offer any procedure for pile foundations. The process explained in ASCE 7-10 can also be found in Veletsos (1993) and Stewart *et al.* (1998). International Building Code (IBC, 2012) refers to the similar procedure to account for the effects of the soil-structure interaction in structural designs.

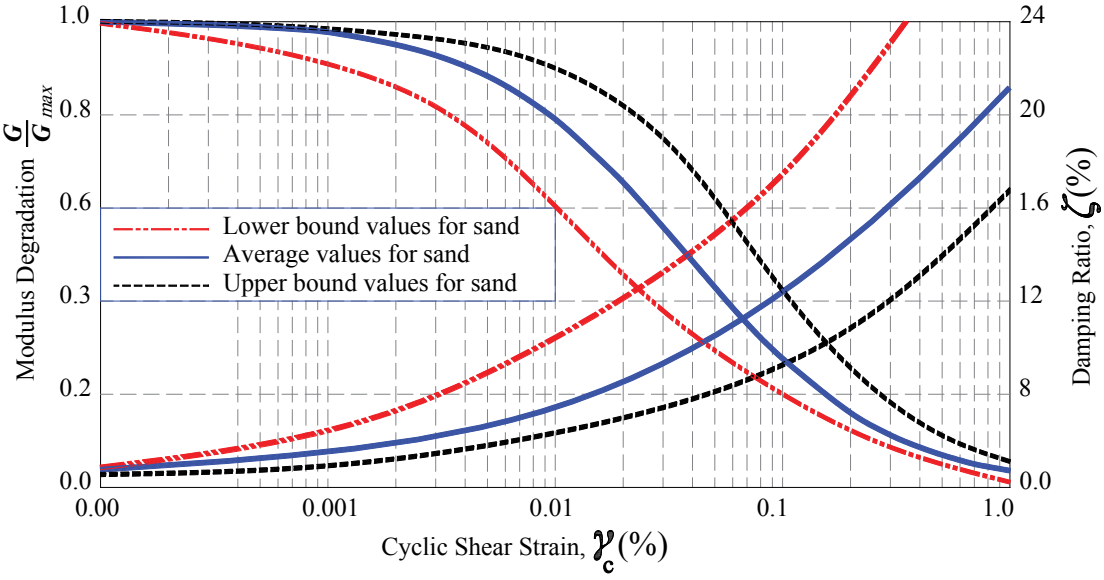

Figure 2.4 Damping ratio and Modulus Degradation depending on cyclic shear strain for cohesionless soil (after Seed *et al.* 1986)

There have been several researchers mentioning the limitation of the current design codes and effects of this limitation. They compared the building response under fixed base condition and the condition that seismic soil-foundation-structure interaction is taken into account (Tabatabaiefar *et al.* 2014b; Hokmabadi and Fatahi 2015; Mekki *et al.* 2016; Kumar *et al.* 2016). There have been a number of suggestions and recommendations from these studies which have stated that seismic soil-foundation-structure interaction (SSFSI) brings significant differences from the current design codes.

2.4 Well-known earthquakes used for benchmark analysis

Earthquakes do not kill people but inadequately designed buildings do (Hough and Jones 2002). No one knows when the earthquake will happen and we cannot predict how it will affect the buildings. It is reasonable if there is collective information about earthquakes, such as position, time, and frequency of occurrence. In this section, four well-known earthquakes namely 1940 El Centro, 1968 Hachinohe, 1994 Northridge and 1995 Kobe, usually used as benchmark earthquakes will be described.

2.4.1 The 1940 El Centro earthquake

The El Centro earthquake occurred on 18th of May, 1940 in the Imperial Valley in Southern California near the international border of the United States and Mexico. This was the first major earthquake to be recorded by professional equipment to obtain an

accelerogram. Kramer (1996) reported that large earthquakes produce ground motions with different characteristics at different points on the ground surface. The spatial variation of ground motion, whether on worldwide, regional, or local scales, is important in both seismology and earthquake engineering. In fact, the instruments for the El Centro area were still limited before1940 El Centro earthquake. It was attached to the El Centro Terminal Substation Building's concrete floor, and not in a free-field location. The record may have underrepresented the high frequency motions of the ground because of soil-structure interaction of the massive foundation with the surrounding soft soil. This earthquake happened significantly in about a minute then reduced to small accelerations.

However, several researchers (e.g., Clough and Chopra 1966; Seed *et al.* 1969; Hartzell and Heaton 1983) reported that the majority of energy released during the 1940 El Centro earthquake occurred within the first 15 seconds. The recording showed that the earthquake consisted of 13 sub-events within 5 minutes. Nine people were killed during the earthquake due to building collapse and 80% of buildings at Imperial were damaged to some degree (Figure 2.5). Unfortunately, in the business district of Brawley, all structures were damaged and about 50% had to be condemned. The shock caused 40 miles of surface faulting on the Imperial Fault, part of the San Andreas system in southern California. It was the first strong test of public schools designed to be earthquake-resistive after the 1933 Long Beach quake. Fifteen such public schools in the area had no apparent damage. The earthquake also caused substantial damage to irrigation systems over a very wide area of the valley with a number of breached locations of the canals within Imperial Irrigation District. Total damage was estimated at about $6 million. The magnitude was approximately 6.9 - 7.1 (Clough and Chopra 1966).

Figure 2.5 (a) shows the position of the 1940 El Centro earthquake, and its recorded acceleration from a concrete floor of El Centro Terminal Substation Building is plotted in Figure 2.5 (b) while the damaged pictures are shown in Figure 2.5 (c) and Figure 2.5 (d).

The 1940 El Centro earthquake provided a strong-motion seismograph which is considered to be the first example of major earthquake recording made very close to the fault rupture. It has become a well-known earthquake for researchers and studied as a far-field strong earthquake.

(a) 1940 El Centro earthquake map (from Google map 2016)

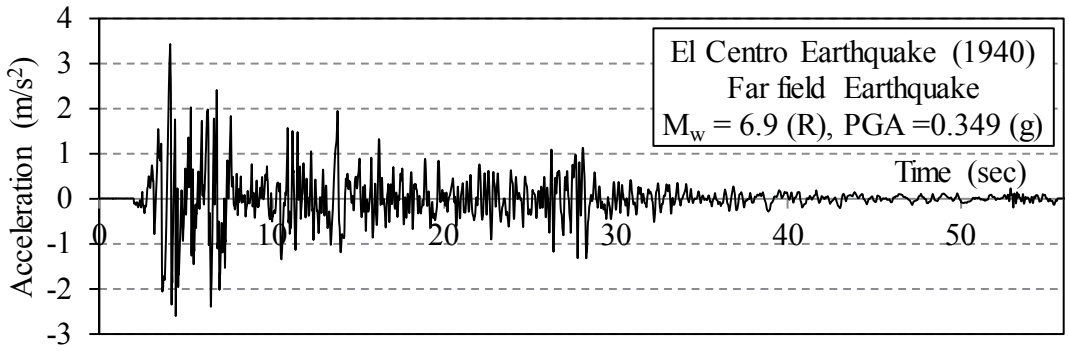

(b) Acceleration recored of earthquake

(c) Imperial's 100,000 gallon water tank that collapsed in the earthquake (Photo: U.S. Coast and Geodetic Survey, Hemple 1941)

(d) Collapsed buildings in Imperial, California, in which four people died. (Photo: U.S. Coast and Geodetic Survey, Hemple 1941)

Figure 2.5 1940 El Centro earthquake details

2.4.2 The 1968 Hachinohe earthquake

Yuen *et al.* (1969) reported that the 1968 Hachinohe earthquake (or the 1968 Tokachi earthquake) occurred at 0:48:55 UTC on 16th of May, 1968 in the area offshore Aomori and Hokkaido, Japan. The epicentre of the earthquake is at 40.80°N 143.40°E, 26 km depth and about 100 km to the east of Hachinohe. It has magnitude of 8.25 at the epicentre but the seismic load was sent to the land and created a maximum of 6 meters high Tsunami but 2.8 meters high at Hachinohe. There were about 47-52 people killed and 281-330 injured. Hachinohe was one of the worst affected with damages to the buildings, water pipes and gas pipes. There were 4 nearest ports to the epicentre to record the earthquake and calculate response spectra; they are Muroan Port, Aomori Port, Hachinohe Port and Miyako Port.

The collected data included the digitized records on the main shock from the earthquake strike and had the largest recorded aftershock. The earthquake triggered 15 strong-motion accelerograms in the network of ports and Harbour Research Institute. The maximum horizontal acceleration of 29 gals was recorded at Hachinohe Port. There were a large number of aftershocks and about 120 accelerograms were obtained in the network. All the accelerograms were collected at the Earthquake Resistant Structure Laboratory in Port and Harbour Research Institute for processing. Information included determination of maximum acceleration and digitisation, and preliminary analyses such as calculation of the response spectra and Fourier spectra (Kanamori 1971). The study of this earthquake also included the main shock and two aftershocks (largest and second largest aftershock) which occurred at different times on the same day (May 16, 1968), different locations and in depth of 7.1, 33 and 37 km, respectively (Suzuki 1971; Kanamori 1971).

Although the 1968 Hachinohe earthquake occurred in the sea, the complex seismic wave hit the land and created Tsunami. Based on the data collected from accelerograms, it has attracted a number of researchers to study the characteristics and influence to the SSFSI (e.g., Kanamori 1971; Fatahi and Tabatabaiefar 2013; Tabatabaiefar *et al.* 2013; Hokmabadi 2014).

(a) 1968 Hachinohe earthquake map (after Yuen *et al.* 1969)

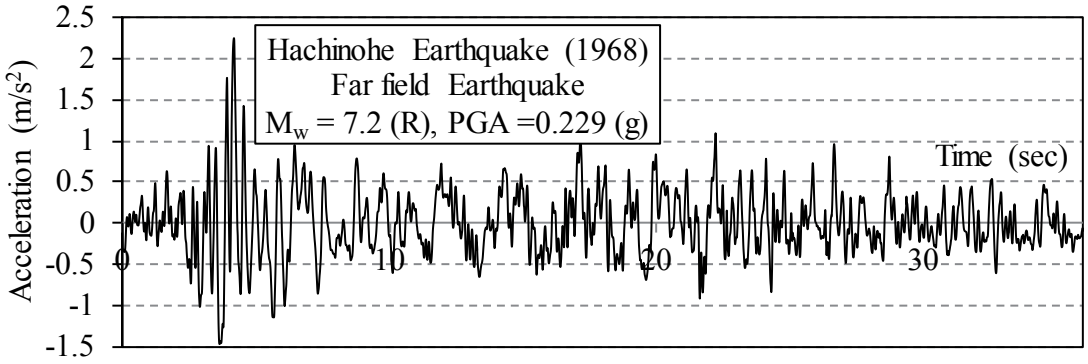

(b) Acceleration recorded of earthquake (from Hachinohe port record)

Figure 2.6 1968 Hachinohe earthquake details

2.4.3 The 1994 Northridge earthquake

Northridge is a city of 50,000 people in 1994 located near Los Angeles, Southern California, USA. Yegian *et al.* (1995) traveled to Los Angeles to survey just after the Northridge earthquake occurred on January 17, 1994 at 4:30:55 AM PST. According to the report of Yegian *et al.* (1995) and Wald *et al.* (1996), the earthquake had its epicentre in Reseda, a neighbourhood in the San Fernando Valley in Los Angeles, California, USA.

The duration of the earthquake was 10-30 second across locations. This was a 6.7 magnitude blind thrust earthquake as it occurred along a thrust fault that did not show signs on the surface of the Earth. The instrument recording showed that the earthquake had ground acceleration of 1.8 g (16.7 m/s^2). This was the highest ever in an urban area in North America and its strong ground motion effect is still evident in areas around 360 km from the epicentre. In addition, the 1994 Northridge earthquake had the fastest peak ground velocity ever, 6.59 km/h, near Rinaldi Receiving Station.

Reports of others (e.g., Wald *et al.* 1996 and Donnellan 1994) also summarised that 57 people were killed and more than 8,700 injured. Between $13 and $40 billion of property was damaged, making it one of the costliest natural disasters in America. The earthquake caused damages up to 125 km away with worst effect in the West San Fernando Valley, and the cities of Santa Monica, Simi Valley and Santa Clarita. One of the well-known affected apartment complexes was the Northridge Meadows in which sixteen people were killed due to collapsed buildings. The earthquake gained worldwide attention due to damages to the vast freeway network. The network consisted of the Santa Monica Freeway, Interstate 10, known as the busiest freeway in America. This congested nearby surface roads for three months while the freeway was being repaired. The quake produced unusually strong ground acceleration in the range of 1.0 g and the damage from the quake revealed that some structural specifications needed to be revised. Most casualties and damage occurred in multi-storey wood-framed buildings. Broken gas lines, collapse of wooden buildings and fallen electricity line were the main factor which created fires. Water pipes were broken and thousands of people lost their public water service. The earthquake also damaged unreinforced masonry buildings and houses on steep slopes suffered from damage.

Thio and Kanamori (1996) studied the source complexity of the 1994 Northridge earthquake and it relation to aftershock mechanisms by inverting the P and SH waveforms recorded by the IRIS and IDA/IRIS network. Their results showed that the main-shock rupture is consistent with the results from other investigations, which favour slip occurring at larger depth. These works are important for earthquake input of any numerical modelling or small scale experiment when SSFSI are investigated.

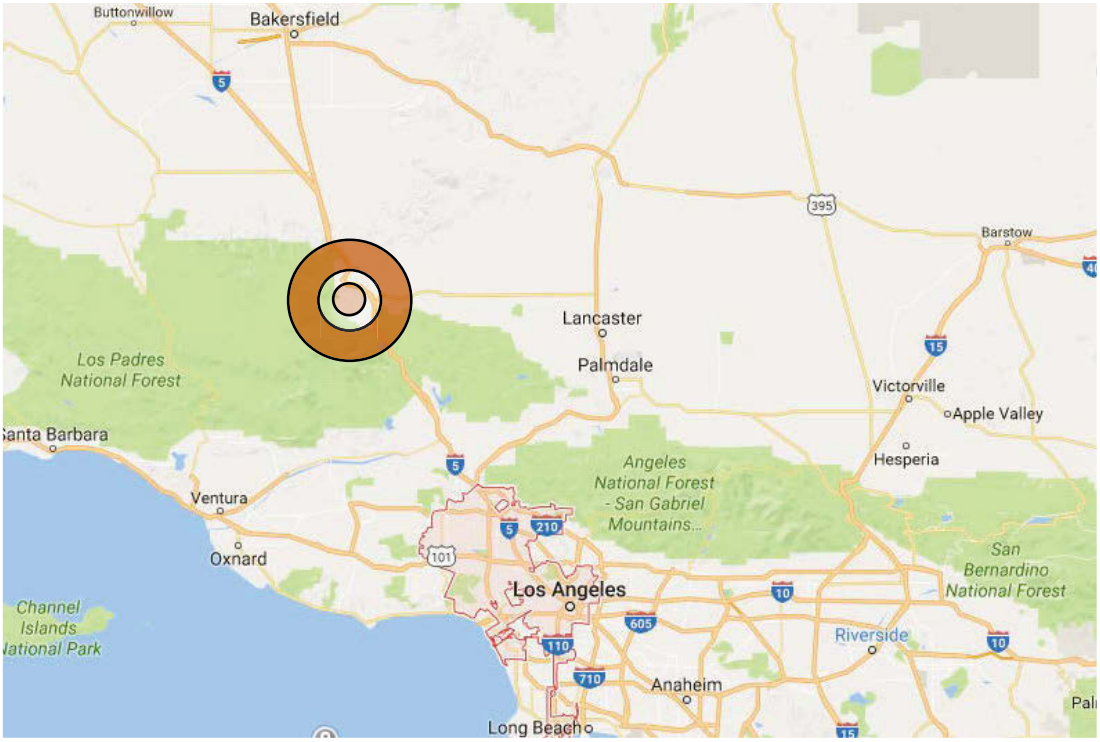

(a) 1994 Northridge earthquake map (from Google map 2016)

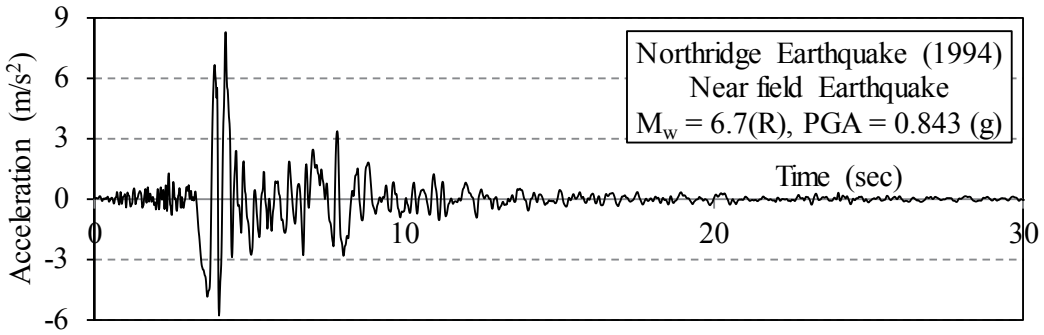

(b) Acceleration recorded of earthquake (from FEMA library, Hall *et al.* 1994)

(c) Kaiser Permanente building collapsed due to earthquake (from FEMA photo library, Hall *et al.* 1994)

(d) Golden State Freeway at Gavin Canyon collapsed as a result of earthquake (from FEMA photo library, Hall *et al.* 1994)

Figure 2.7 1994 Northridge earthquake details

There were a number of changes made to the building codes after this earthquake. Amongst these were the advances in technology associated with testing system, design and modelling, structural connections, structural forms and seismic force resisting systems.

2.4.4 The 1995 Kobe earthquake

Several researchers (e.g., King *et al.* 1995; Koketsu *et al.* 1998; Yoshimi and Higashihara 1999; Horwich 2000) reported for a very sad event at 20:46:53 UTS time on January 17, 1995 called The 1995 Kobe earthquake (or the Great Hanshin earthquake). The epicentre of this earthquake was at 34.59°N 135.07°E in the southern part of Hyōgo Prefecture, Japan, known as Hanshin, and at 17 km beneath the surface and about 20 km away from Kobe city centre. The peak acceleration is 0.8 g and the magnitude is of 6.8. There were 6434 people killed and total damage was about US$200 billion. The type of earthquake was strike-slip and it was the second worst earthquake in 20th century Japan after the Great Kantō earthquake of 1923.

Report of Horwich (2000) has some minor differences. The brunt of the quake was felt in a swath roughly 20 kilometres long and 2 kilometres wide within a metropolitan area of 4 million people. The intensity of the quake as measured on the Richter scale, 7.2, does not capture its full force, since it was accompanied by an extraordinary horizontal movement of 1.5–2 meters, a vertical thrust of 1.2 meters, and a twisting motion as well. The port facilities, constituting the world's sixth largest container port and the source of 39% of Kobe's gross industrial output, were a shambles. In the city, 100,000 buildings were destroyed, close to an equal number half destroyed, and 183,000 partially destroyed. The entire underground water system was ruptured, as was much of the sewage system, the gas system, the power system, the rail system, and the main coastal highway, one elevated section of which rolled over on its side. Hundreds of fires broke out, mainly in the older industrial and residential sections of the city, and burned uncontrollably because backup water supplies were either inadequate or non-functioning. Over 300,000 people became homeless on that cold January day. Sixty-five hundred eventually died as a result of the quake—600 or 700 in the fires, the rest in collapsing structures.

Wald (1996) summarised that Jma, Fukiai and Takatori earthquake recording stations provided different earthquake recordings. There were three twelve-storey

buildings, near Takatori earthquake recording station, supported by pile foundation and these suffered shear and compressive failure (probably due to rocking) near the pile head. Some scholars found that there was not any evidence of soil liquefaction and the main factor that caused the damage to the structure was the inertial forces. According to Wald (1996), data recorded from strong-motion, teleseismic and geodetic data were recorded from several stations and by a number of owners. For strong-motion recorded data, there were nineteen stations and three owners while there were fourteen teleseismic stations. Geodetic data consisted of Global Positioning System (GPS) and levelling-line resurvey data made by Hashimoto *et al.* (1996). The GPS data is a combined set of data from both continuous recording and campaign-type surveys. As with the strong-motion data, the station coverage on Awaji Island is not particularly dense, but another station indicates about 1 m of right-lateral displacement to the southeast, which places an important constraint on the amount of shallow slip along the northeast portion of the Nojima fault.

As a result, the data which should be used for seismic research comes from different recording stations with different data. They should be selected for each study depending on each aspect and purpose of that study.

(a) 1995 Kobe earthquake (after King *et al.* 1995)

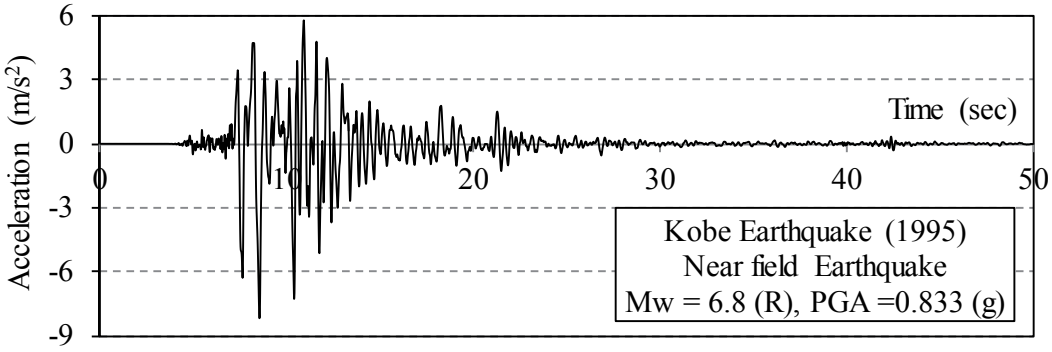

(b) Acceleration recorded of earthquake (from JMA library, Koketsu *et al.* 1998)

c) Damage at Minatogawa, Kobe (from JMA library, Koketsu *et al.* 1998)

(d) Damage in Sannomiya (from JMA library, Koketsu *et al.* 1998)

(e) 1 km of Hanshin expressway collapsed (from JMA library, Koketsu *et al.* 1998)

Figure 2.8 1995 Kobe earthquake details

In addition, researching about soil-structure interaction of the 1995 Kobe earthquake, Hayashi and Takahashi (2004) mentioned that there was a clear uplift of the base mat and the separation between the foundation and soil due to the rocking of the superstructure.

2.5 Soil-pile interaction under lateral loading

There is a number of potential sources of lateral load to the structure such as vehicle acceleration and braking, wind, wave or debris loading, ice forces, lateral earth pressures, vessel impact, seismic loading or slope movement. The response of a laterally loaded pile foundation is significantly important in structure design for such loads. Basically, the load-deflection $(p - y)$ related to this problem has been studied extensively by a number of researchers with theoretical, experimental and numerical modelling methods (Poulos 1971; Lin *et al.* 2014; Byrne *et al.* 2015; Sorensen *et al.* 2015; Li and Yang 2017). This $(p - y)$ concept is proposed by the Winkler Spring Method in which there is a number of soil springs along the pile which are modelled as the soil resistance. The soil is linear, therefore, spring stiffness is constant depending on soil characteristic, obtained from experimental investigation or from analytical calculations.

Referring to (Reese *et al.* 2006), when a vertical pile under a lateral load applied to the head, the surrounding soil will deform into three parts. The front part, where the soil is compressed, experiences a passive lateral soil resistance while the behind part, where the soil is tensile or the gap is opened, is active lateral soil resistance. In addition, the two side parts make up the area where the soil and pile surface slip relatively called friction parts. The pile-soil system usually creates the maximum lateral displacement at the top of the pile and minimum or even negative displacement (opposite direction) at the bottom of the pile (referring to Figure 2.9 (a) and (b)).

Due to the different displacements at each point along the pile from the top to the bottom, the $p - y$ method assumes that there is a finite number of pile segments in which each segment of the pile holds the same soil resistance k_i [unit: F/L^2] and the same horizontal displacement y_i [unit: L]. As a result, the soil resistance to each segment is p_i [unit: F/L] or soil reaction per unit length of pile can be found from Equation (2.16):

$$p_i = k_i y_i \tag{2.13}$$

In addition, the soil resistance k is converted from the horizontal modulus of subgrade reaction k_h as in Equation (2.14).

$$k_i = k_h B \tag{2.14}$$

where *B* is the width of the pile.

As shown in Figure 2.9 (e) and (f), the upper part of the pile generates higher soil resistance as it contains higher lateral deflection.

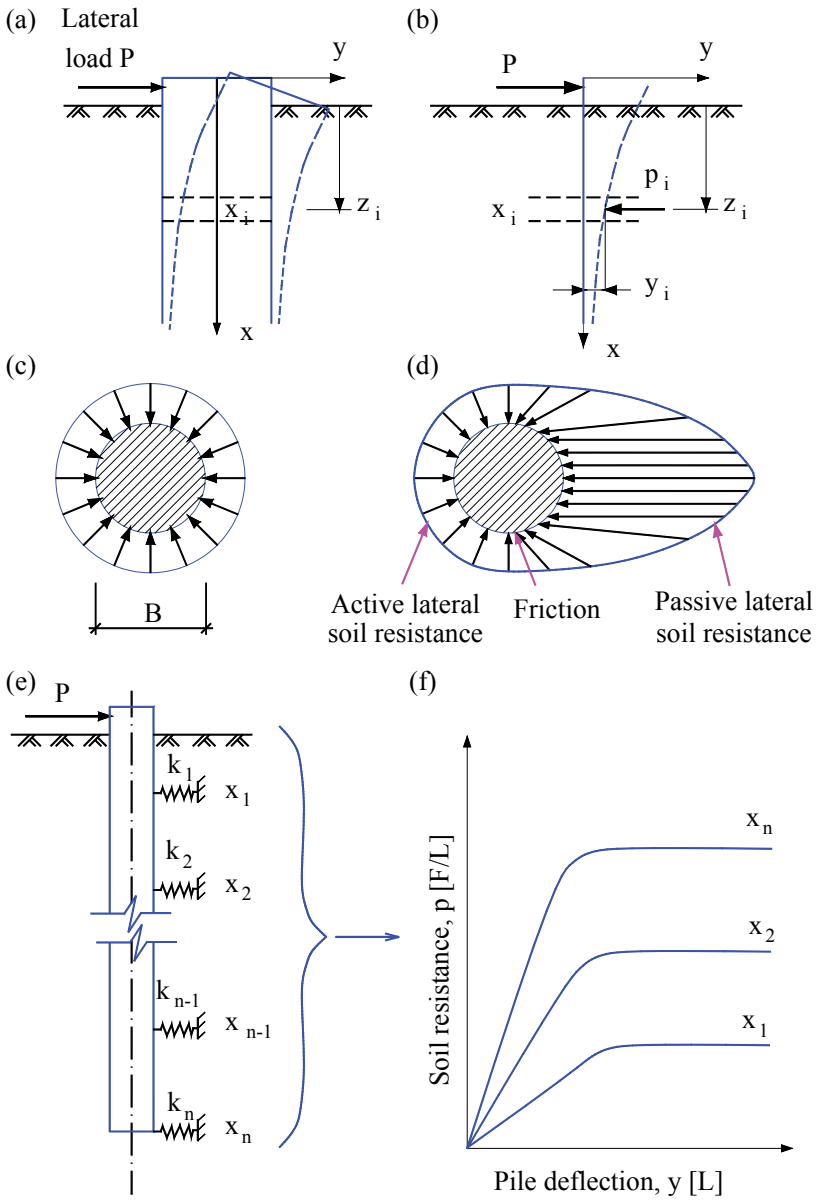

Figure 2.9 Soil – pile system under lateral loading (after Reese *et al.* 2006)

For the development of a general equation for a laterally loaded pile, the theory of the elastic beam is adopted widely to calculate rotational displacement, bending

moment and shear force along the pile. The application of this method is very challenging when the soil is nonlinear, the soil is layered or the pile is placed near a slope. For these cases, the $p - y$ method is applied by dividing the pile into more segments in which the soil and pile can hold equal soil resistance. For this case study there has been a number of solutions to address the nonlinear problems including experiments in laboratory, full-scaled experiment, theoretical methods and numerical modelling (Nimityongskul 2010).

Laboratory based research into the laterally loaded soil-pile system in purely cohesive soil is limited in comparison to studies on a pile in purely frictional soil. The key reason for this limitation is the inherent difficulty and additional time required for testing when preparing large clay samples. Samples of soil need to be hydraulically consolidated or manually compacted in testing chambers of various sizes of pile which can be tedious and time consuming. This type of clay sample preparation is far more difficult than that required to prepare sand samples for testing, where simple vibration techniques are used to achieve a particular density. Pile, lateral loading and related equipment for testing purposes also require several gauges installed along the pile surface and in centre-line and in soil medium which make the testing preparation is more difficult (e.g., Robertson *et al.* 1989; Nimityongskul 2010).

In an attempt to reduce model preparation times, many civil engineering researchers choose to adopt small scale laterally loaded pile model testing. Model pile can be as small as 50mm in width/diameter, but most of them adopt piles between 20 mm and 100 mm in diameter. The size of the testing soil tank generally ranges from 500 mm in each size up to 5000 mm. Recently, Sorensen *et al.* (2015) conducted the small-scale test of laterally loaded rigid piles with applied overburden pressure to investigate the quasi-static behaviour of laterally loaded, non-slender piles installed in cohesionless soil. There were twenty-three static tests with aluminium piles with diameter of 60 to 100 mm in a new and innovative test because the tests were conducted in a pressure tank to ensure the overburden pressure is applied to the soil.

The soil-structure interaction of single short, stiff laterally loaded pile was investigated by Lin *et al.* (2014) with a full instrumented experiment. A hollow steel pipe pile with a length of 1.524 m, a thickness of 6.4 mm and a diameter of 102 mm was installed in well-graded sand and subjected to increasing lateral load. In this test, flexible shape acceleration arrays, thin tactile pressure sheets, and in-soil null pressure sensors

were installed along the pile and in the surrounding soil. The sensors attached to the pile were used to develop the compressive soil-pile interaction pressures and the lateral displacement along the pile length. The tactile pressure sheet sensors provided the soil-pile interaction compressive pressures on the circumference of the pile at a specific depth and along the length of the pile.

The measured soil-pile interaction compressive pressures combined with the measured lateral displacement along the pile length were used to develop the soil-pile interaction force-displacement relationships ($p-y$ curves) using direct measurements. In addition, in order to deal with increasing of the lateral pile displacement, the in-soil null pressure sensor measurements were used to develop the distribution of horizontal stress changes around the pile. The result from this small scaled experiment was compared and obtained good agreement with current results of the laterally loaded pile. However the results of this test for bending moment and shear force along the length of the pile were different from back-calculation procedure using strain measurements with curve fitting. This can be explained by the $p-y$ method and its curve fitting back-calculation for a complex soil profile may introduce a significant error.

Note that the beam theory applied for a vertical pile in soil can be summarised as in Figure 2.10 and Equation (2.15)

$$S=\frac{dy}{dx};\ M=E_pI_p\frac{d^2y}{dx^2};\ V=E_pI_p\frac{d^3y}{dx^3};\ p=E_pI_p\frac{d^4y}{dx^4} \tag{2.15}$$

where E_pI_p is flexural stiffness of pile;

y is lateral deflection of pile;

x is depth below the pile head;

p is soil reaction per unit length of pile;

S is rotational deflection of pile;

M, V are bending moment and shear force along the pile, respectively.

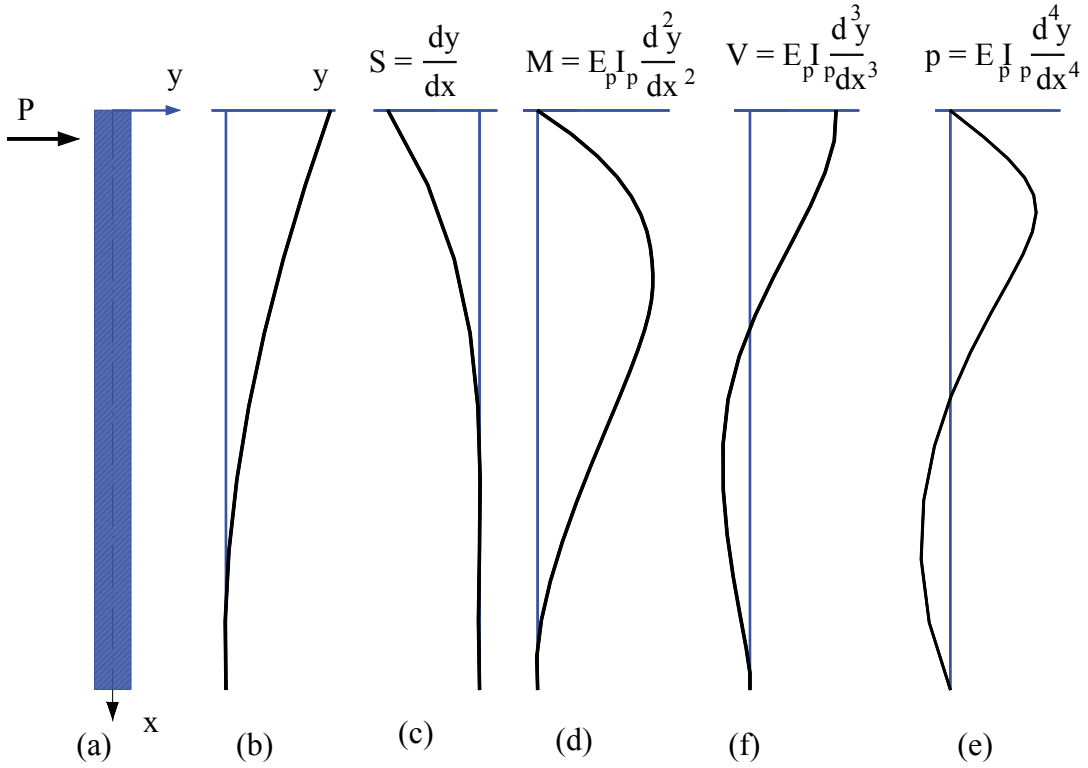

Figure 2.10 Beam theory applied for a vertical pile in soil

Numerical modelling of a laterally loaded pile has been studied widely recently with verification exercise (e.g., Kok and Huat 2008; Nimityongskul 2010; Nguyen*, et al.* 2013).

Kok and Huat (2008) used finite element analysis PLAXIS 2D Version 8 to simulate the soil-pile model and its interaction placed near an excavation. The soil model was plain strain in two dimensional modelling (fifteen-nodes triangle element provides a fourth order interpolation for displacement and the numerical interation involves twelve Gauss points) while the pile was adopted with beam element. Mohr-Coulumb soil model was adopted for soil model and the results were compared to previous work (e.g., Carrubba *et al.* 1989; Guo 2002).

Full-scaled experiments and numerical model verification work (Nimityongskul 2010) was comprehensive for a single pile on layered soil slope. The position of the pile was changed relatively to the slope crest. The distances from the slope crest to the pile centre were -4D, 0D, 2D, 4D and 8D, where D is the outside diameter of the pile. All tests were conducted using displacement control and the same load protocol. The test results

of first baseline pile were different from the second baseline pile due to testing at different time of the year. This indicates that changes in soil condition due to seasonal weather affected the lateral response of piles. The other lateral loading tests were conducted under similar soil conditions.

Nimityongskul (2010) stated that the observations during the lateral loading tests include gaps forming behind the piles and heaving of the ground in front of the baseline piles. This observation is consistent with other lateral loading tests in cohesive soils. For the lateral loading tests for the piles near the slope, in addition to the observed gap behind the test piles, cracking of the ground around the pile and on the slope were also observed. During the test, the first major crack observed during the testing occurred on the slope face directly in front of the test pile. Following this were cracks that formed along a line with an angle of approximately 45 degrees from the pile axis perpendicular to the loading direction. The observed crack patterns on the ground are not symmetric indicating that actual soil failure mechanisms may be different from theories.

In addition, Nimityongskul (2010) processed the full-scale $p - y$ curves with back-calculation for each test result by using 2D Finite Difference program for solving the governing beam equation *(LPILE)*.

Li and Yang (2017) investigated the $p - y$ approach for a laterally loaded pile in frozen soils, including seasonally frozen soils and perennially frozen ground, or permafrost, which exist extensively in Alaska and other cold regions. Lateral load for this study was earthquake in the form of a cyclic, quasi-static lateral load which was applied near the top of the pile (about 900 mm above the ground surface) at a loading cyclic rate of around 0.04 cm/s. The soil in this model was layered into 3 layers which the pile was installed through. During the earthquake loading to the pile head, all force, horizontal displacement on the head of the pile were recorded. Back-calculation of $p - y$ curves from experiment data also was processed to determine rotational displacement, bending moment and shear force along the top half of the pile. Results from modelling the test pile using the proposed p-y curve agree well with the test results. The proposed $p - y$ curve was further validated by independent field test data. It is concluded that the proposed $p - y$ curve is capable of modelling both seasonally frozen and perennially frozen silts in frozen soil-pile interaction analyses during short-term lateral loading. Recommendations

from Li and Yang (2017) are provided on how to select soil parameters for constructing frozen-silt $p - y$ curves.

2.6 Seismic soil-foundation-structure interaction for shallow foundation

Shallow foundation is one of the most common foundation solutions for buildings. It is a spread footing foundation which has a wider bottom portion than the load-carrying walls. The wider part will spread the dead load and live loads from the structure to the soil for better stability. However, the earthquake loading applied to the structure is more complicated when considering soil-foundation-structure interaction (Hokmabadi 2014). There has been a number of scholars who devoted their effort on the topic by experiment, analysis and numerical modelling (e.g., Mason *et al.* 2013; Fatahi *et al.* 2014; Hokmabadi 2014; Tabatabaiefar and Fatahi 2014). Unfortunately, full-scale testing of Soil-foundation-structure interaction of shallow foundation of mid-rise building under earthquake loading is costly and in most cases unfeasible. For this reason, testing is generally limited to small scale models because these can provide a cost effective and convenient alternative. However, one concern associated with the scaled experiment is the presence of scale effects. On the other hand, numerical modelling allow users to build the actual full-scale, do as many tests as they want providing that these numerical models need to verify and improve until they work well. The following sections provide a general summary of past experimental research into soil-foundation-structure interaction of shallow foundation.

In general, seismic shallow foundation design does not consider the ground response; civil engineers usually use either a pseudo-static approach or a dynamic response approach (e.g., AS1170.4 2007; ASCE 7-10 2010; GB50011 2010). Firstly, in the pseudo-static analysis, the effects of the dynamic earthquake-induced loads on the foundation are represented using static forces and moments. Typically, the pseudo-static forces and moments are calculated by applying a horizontal force equal to the weight of the structure times a seismic coefficient through the centre of gravity of the structure. The seismic coefficient is generally a fraction of the peak ground acceleration for the design earthquake and may also be dependent upon the response characteristics of the structure, the behaviour of the foundation soils, and the ability of the structure to accommodate permanent seismic displacement. Secondly, in a dynamic response analysis, the dynamic stiffness and damping of the foundation are incorporated into a numerical model of the

structure to evaluate the overall seismic response of the system and the interaction between the soil, foundation and structure.

The buildings with shallow foundations are the common foundation solutions which can reduce costs for construction if the safety and serviceability requirements are satisfied. The model of shallow foundation needs to check the bearing capacity and maximum settlement under static, live and dynamic loading. These are followed by routine engineering design procedures mentioned by Poulos and Davis (1980), Bowles (2001) and Nguyen *et al.* (2013).

Liu and Dobry (1997) investigated experimentally, the seismic response of shallow foundation on liquefiable sand with eight centrifuge models. The soil was put in the box of 458 mm x 300 mm with the depth is 157 mm; however only some depth from the top was compacted. The acceleration of 16g was applied to the bottom of the box as earthquake excitation. The first series of tests focused on the effect of the depth of soil compacted under the foundation on the footing acceleration and settlement. The results found that, when the compaction depth increased and approached the total thickness of the soil deposit, the footing acceleration during shaking increased but its settlement decreased. In another words, in stronger soil, earthquake causes larger acceleration to the structure but smaller settlement of the whole building.

Hayashi and Takahashi (2004) also studied how the soil-foundation-structure interaction affected the earthquake response of building by testing a building with shallow foundation under 1995 Hyogoken-Nanbu Earthquake (usually known as 1995 Kobe earthquake). They found that the damage reduction effects, by soil-foundation-structure interaction, greatly depend on motion characteristics, number of stories and horizontal capacity of earthquake resistance of buildings. As a result, base mat uplift should be considered in soil-foundation-structure interaction studies.

Torabi and Rayhani (2014) conducted a three dimensional Finite Element Analysis utilising linear elastic single degree of freedom (SDOF) structure and a nonlinear elasto-plastic constitutive model for soil behaviour, in order to capture the nonlinear foundation–soil coupled response under seismic loadings. There are two concepts of “fixed-base” and “flexible-base” building which are taken into account in any soil-foundation-structure interaction evaluation process. The fixed-base refers to a building placed on very strong soil or rock to be considered as a rigid base. On the other

hand, flexible-base refers to a building founded on a soil deposit which enables the foundation of the building to vibrate under seismic loading. Their study concluded that a rigid slender structure is highly susceptible to the soil-foundation-structure interaction effect, including alteration of natural frequency, foundation rocking and excessive base shear demand. However, there are some assumptions to this modelling; for example, the structure is elastic and the soil is elasto-plastic and the model is using Rayleigh damping. They used 2 frequencies f_1 = 0.5 Hz and f_2 = 5 Hz and damping ratio ζ = 12% to calculate the mass and stiffness damping coefficients. It is claimed that these parameters contain experimental response spectra and encompass natural frequencies of site and structure and the predominant frequency of input motion.

Stewart *et al.* (1999) used analytical methods to investigate the seismic soil-foundation-structure interaction (SSFSI) effect on the structural response. The analysis procedures were similar to provisions in some building codes but incorporated more rationally, the influence of site conditions and the foundation embedment, flexibility, and shape on foundation impedance. The implementation of analysis procedures and system identification techniques was illustrated using a building shaken during the 1994 Northridge earthquake. The result of these analysis procedures predicted that the observed soil-foundation-structure interaction effects on the building response accurately.

Hokmabadi *et al.* (2014b) made a comparison in different foundation conditions amongst fixed-base, shallow foundation, float pile foundation and FLAC numerical modelling. It was found that the FLAC model could employ a full nonlinear hysteretic damping algorithm representing the variations of damping ratio and shear modulus versus cyclic shear strain. Numerical results were verified by experiment results including foundation rocking, base shear, floor deformation and inter-storey drifts. The results showed that there was a good agreement confirming the reliability of the numerical modelling. The main conclusion is that shallow foundation causes higher deformation and drift but lower base shear and rocking of the foundation. These conclusions clearly showed that soil-foundation-structure interaction significantly affects the current assumption of the structure under seismic loading.

Several researchers such as Sbartai (2016), Sameti and Ghannad (2016) and Chen (2016) studied the seismic soil-foundation-structure interaction (SSFSI) phenomena and its influence on seismic response of the building by using Winkler (substructure) methods

and the numerical methods. (Tabatabaiefar *et al.* (2014a), Hokmabadi *et al.* (2014b), and Hokmabadi and Fatahi (2015) adopted advanced numerical models which have a number of advantages over the Winkler methods, especially their ability to conduct time history analyses while considering effects such as the nonlinear stress–strain behaviour of the soil and the superstructure, material and radiation damping, advance boundary conditions, and interface elements.

Sameti and Ghannad (2016) investigated the equivalent linear model for existing soil-structure system and concluded that the concept of equivalent linearization could be extended for the soil-structure systems, in which the strength ratio (defined as the ratio of the yielding strength to the elastic strength demand) was known rather than the ductility ratio. The nonlinear soil-structure system was replaced by a linear single-degree-of-freedom (SDOF) system, which can capture the response of the actual system with sufficient accuracy. The dynamic characteristics of the equivalent linear SDOF system were determined through a statistical approach. The superstructure was modelled by an inelastic SDOF system with bilinear behaviour, and the homogeneous half space beneath the structure by a discrete model, following the Cone Model. To cover a wide range of soil-structure systems, Sameti and Ghannad (2016) conducted a comprehensive parametric study, using a set of non-dimensional parameters for the soil-structure system. The accuracy of the equivalent linear parameters was then assessed and laid in an acceptable range. The results confirm that the proposed equivalent linear model can capture the simultaneous effects of soil-structure interaction (SSI) and non-linearity in the super-structure concerning the maximum inelastic response of the soil-structure system.

Similarly, Chen (2016) studied the dynamic interaction for two adjacent rigid foundations embedded in a viscoelastic soil layer with dynamic loading in the form of vibrations originating from one of the rigid foundations placed in the soil layer, which are subjected to harmonic loads of translation, rocking, and torsion. These dynamic responses of the rigid surface foundations were solved from the wave equations by taking into account their interaction. The solution was formulated using the frequency domain boundary element method (BEM), in conjunction with Kausel–Peek Green's function for a layered stratum and the thin layer method (TLM) to account for the interaction between the two foundations. This approach allows us to establish a mathematical model for

determining the compliance functions of the two adjacent foundations with regard to their spacing, substratum depth, masses, shapes, embedding, load intensity, and frequencies of excitation. The soil heterogeneity was taken into account for the cases of one or two layers of soils over a rigid bedrock and semi-infinite soil. The analysis of the present study indicates that the effect of several parameters on the dynamic interaction response of two adjacent foundations is nonnegligible. In particular, the dominant influence of some parameters, such as the heterogeneity of the soil, shape of the foundations, and the load intensity, compared to the other ones was clearly revealed.

Lu *et al.* (2016) used a simplified nonlinear sway-rocking model as a preliminary design tool for their seismic soil structure interaction analysis. The nonlinear load-displacement response of shallow foundation was captured during strong earthquake loading by this model where foundation bearing capacity is fully mobilised. Soil non-homogeneity was modelled with variation of soil stiffness and strength with depth to create the saturated clay half-space for heavily-load structures resting on it. In this study, functions of the factor of safety against vertical bearing capacity failure (FSv) and the moment-to-shear ratio (M/H) were used to express the load-displacement relations of the shallow foundation when the swaying and rocking motions were taken into account. A rigorous finite-difference numerical modelling was used to calibrate and validate the above nonlinear sway-rocking method and the conclusion was made that the concept of this model gives engineers more degrees of freedom in defining their own model components, providing a good balance between simplicity, flexibility and accuracy despite some limitations of the current implementation.

For the system of soil-structure-interaction under the seismic loading forces sent from the epicentre to the structure, the small strain soil medium properties are different from the static large strain properties. There has been a number of studies dealing with the relationship between shear modulus ratio G/G_{max} and damping ratio ξ with cyclic shear strain γ; among them are Hardin and Drnevich (1972), Vucetic and Dobry (1991) and Sun *et al.* (1988) for cohesive soil and Hardin and Drnevich (1972), Seed and Idriss (1969) and Seed *et al.* (1986) for cohesionless soil.

Star *et al.* (2015) designed and constructed a simple test structure, which was a shallow foundation of a one floor building on layered soil, which experienced combined base shear and moment demands. There was reinforced concrete as the shallow

foundation and a top reinforced concrete slab which was braced with steel columns and braces holding 2:1 aspect ratio in plan view to facilitate a variable amount of over-turning for shaking in two orthogonal directions. That structure was tested in two field sites with representative shear-wave velocity values of around 95 m/s and 190 m/s while the vibration force from a controllable shaker system was applied on the top slab of the structure and the foundation mat. There were several accelerometers, pressure cells and displacement transducers attached to the system to record history response. A test program was designed to provide high quality data for validation of SSI models under realistic boundary conditions, a wide range of load amplitudes, and a wide frequency range. While forced vibration tests were performed on a portable steel column structure, this test structure was reconfigurable to provide alternate structural stiffnesses and tests were performed with shaking applied in both the short and long directions of the oblong structure.

Rocking of a soil-structure system subjected to near-fault pulses was investigated recently by Masaeli *et al.* (2015) considering foundation uplifting and soil plasticity. In that research, the medium-to-high-rise buildings with different aspect ratios based on shallow raft foundation at stiff-to-rock sites was studied. Seismic loading in a form of input ground motion as mathematical directivity and fling pulses were used while the superstructure was assumed to have three different boundary conditions, including (a) fixed-base, (b) linear soil-structure interaction (SSI), and (c) nonlinear SSI. The period T_p of the prevailing pulse was a key parameter governing effects of nonlinear SSI. The normalised acceleration response spectra reveal that despite beneficial effects of foundation uplifting and soil yielding in most cases, there are some minor regions in which the response accelerations are amplified. In addition, more slender buildings significantly benefited from uplifting and soil yielding when subjected to short- and medium-period directivity pulses compared to squat structures. However, response amplifications with respect to fixed-base structures were considerable in the case of slender structures subjected to medium- or long-period directivity pulses. This shown that neglecting the SSI effects on seismic performance of rocking structures with shallow foundations, as mostly assumed in common practice, may give rise to inaccurate estimations of force demands against near-fault pulse-like ground motions. Furthermore,

the envelope of residual foundation tilting θ_r is limited to 0.015 rad, in case of directivity pulses.

Some studies (e.g., Gajan and Kutter 2008; Anastasopoulos *et al.* 2010) based on analytical and experimental research found that the material and geometric nonlinearities in soil may be beneficial to the seismic response of a structure.

Several studies adopted elasto-plastic behaviour of soil during unload-reload cycles as well as tension-less interface between the top surface of underlying soil and the bottom surface of the foundation allowing the simulation of the uplift and the rocking mode of vibration. The recent works by Mergos and Kawashima (2005); Arredondo and Reinoso (2008) and Gazetas *et al.* (2013) focused on the energy dissipation due to foundation uplifting and soil yielding known as "rocking isolation" and found that the soil-foundation system can absorb a significant amount of seismic input energy and as a result the structure would be protected. This should be true for total shear force in each level as well as the shear force of each column or wall which may be the most important factor causing superstructure collapse.

Gazetas *et al.* (2013) investigated the response of surface foundation of a superstructure on inelastic homogeneous soil to large overturning moments. The footing covered a wide range of shapes and aspect ratios and the soil was characterised by an elastic (small-strain) shear modulus G_0 and undrained shear strength S_u, and a G/G_0 versus γ curve appropriate for medium-plasticity clays. Three stages of foundation performance, ranging from the initial elastic fully-bonded response, to the nearly-elastic but nonlinear response with the foundation partially detaching and uplifting from the soil, and finally to the ultimate stage where full mobilisation of soil bearing failure mechanisms were developed. Simple to use formulas or charts were developed for all stages of response in terms of dimensionless parameters, prominent among which is the static factor of safety against bearing capacity failure under purely vertical loading. As reported by Gazetas *et al.* (2013) research on seismic soil-structure interaction over the last decades has mostly relied on the following assumptions: (1) the soil was assumed as linear or most equivalent-linear elastic material; (2) the soil-structure interaction was assumed as fully bounded contact. However, over the last 20 years, the recorded motion of 1994 Northridge earthquake and 1995 Kobe earthquake revealed that seismic loading transmitted onto shallow foundation induced significant nonlinear inelastic action in soil

and interaction between soil and structure. Recently, soil model and soil-structure interaction has been assumed to be inelastic and their behaviour would be changed during the earthquake excitation (see Bao *et al.* 2012; Sameti and Ghannad 20143 and Kumar *et al.* 2016).

2.7 Seismic soil-foundation-structure interaction for pile foundation

Soil-foundation-structure interaction for pile foundation under seismic loading has attracted a number of authors who have conducted laboratory tests, numerical modelling or theoretical research into soil model, soil-pile-structure behaviour or structure response. Hokmabadi *et al.* (2014b) mentioned that the seismic soil-pile-structure interaction (SSPSI) can benefit the structural system under seismic loading because it can lengthen the fundamental period and raise the damping if compared with fixed-based condition. They also concluded that fixed-base assumption in design could be misleading and neglecting the influence of SSPSI could lead to unsafe design, particularly for structures founded on soft soils.

The well-known Winkler method for beam-on-elastic foundation has been used widely for seismic soil-foundation-structure interaction (SSFSI). This beam is assumed to be Euler-Bernoulli beam where there is some assumption of the beam needing to be adopted like small deflection of the beam, and that only the beam is subjected to lateral load (the load which its direction is right angle to the axis of the beam). The governing equation is:

$$EI\left(\frac{d^4y}{dx^4}\right) + E_x(y) = q_y \tag{2.16}$$

where EI is bending stiffness of the beam, E_x is the soil reaction (i.e., the spring's stiffness), q_y is lateral distributed load along the beam.

Hetényi (1971) proposed the governing equation as shown in Equation (2.17) for beam-on-elastic-foundation but the axial load was taken into account which was the case for pile foundation.

$$EI\left(\frac{d^4y}{dx^4}\right) + P_x\left(\frac{d^2y}{dx^2}\right) + E_s(y) = q_s \tag{2.17}$$

where, EI is bending stiffness of the beam, E_s is the soil subgrade reaction (i.e., the spring's stiffness), P_x is axial force from structure applied to pile head, and q_s is lateral distributed load from soil to the pile. For the cases including earthquake, $q_s = 0$ as there is no load applied to the pile rather than soil reaction. However in the case of earthquake loading, the value of q_s is varied during the earthquake excitation.

The solution to solve Equation (2.17) when $q_s = 0$ was proposed by several researchers using numerical method but with some assumptions such as pile rigidity. The linear or nonlinear soil-pile interface springs can be employed. The $p - y$ curve solution can be used to model nonlinear stiffness of soil-pile and they come from the semi-empirical relationships.

The modified Winkler method should be applied for the complex models when soil-pile gap, cyclic degradation or rate dependency exists (see Allotey and El Naggar 2008; Gazetas and Apostolou 2004). Using the analytical model to investigate the soil-pile-structure-interaction, Malhotra (2010) discussed the available models and required modifications to $p - y$ relationship considering the model on the soft soil under seismic loading.

Boulanger *et al.* (1999) studied experimentally and analytically the seismic soil–pile–structure interaction (SSPSI). The analysis used the dynamic beam on nonlinear Winkler foundation ($p - y$ analysis) while the experiment used series of dynamic centrifuge model tests. In fact dynamic $p - y$ analysis has a long history of development and application for seismic loading and it can be performed with computer. Comparing several results of dynamic $p - y$ method, Wang *et al.* (1998) confirmed that calculations were sensitive with the detail of nonlinear springs and dashpots but these different codes gave similar results if the detail of model were similar to each other. In order to validate the *p-y* analysis, experimental tests of Boulanger *et al.* (1999) were performed using the earthquake simulator on the 9-m-radius centrifuge at the University of California at Davis. There were two layers of soil in the model which is soft clay on dense sand and nine different earthquake motions for single and group of piles under the structure.

Similar to the structure on shallow foundation, the structure response for building on pile foundation also includes floor displacement and deflection, inter-storey drift, levelling shear force, and foundation rocking. In addition, the pile and pile group response

under seismic load including bending moment, shear force and deflection should be taken into account (Hokmabadi *et al.* 2014; Kumar *et al.* 2016).

Mylonakis *et al.* (1997) used substructuring method to analyse the seismic response of bridge piers founded on vertical piles and pile group in multiple-layered soil. The method reproduced semi-analytically both the kinematic and inertial soil-structure-interaction, in a simple realistic way. Vertical S-wave propagation and the pile-to-pile interplay were treated with sufficient rigor, within the realm of equivalent-linear soil behaviour, while a variety of support conditions of the bridge deck on the pier could be studied with the method. The ground motion was specified at outcropping elastic rock in both frequency and time domains manners. A parametric study explored the role of soil-structure interaction by elucidating the key phenomena and parameters associated with the interplay between seismic excitation, soil profile, pile-foundation, and superstructure. This solution found that there were some errors when radiation damping due to pile oscillation and rotation of pile head were ignored.

Gazetas *et al.* (1991) studied the dynamic interaction for floating pile group and developed a comprehensive set of dimensionless graphs for dynamic interaction factor versus frequency for vertical, horizontal and rocking harmonics excitation at the head of each pile. Several other scholars have also showed that the dynamic response of pile groups differ substantially from their static response when consider the soil-structure-interaction (Boulanger *et al.* 1999; Chu 2006; AS2159 2009; Chau *et al.* 2009).

The work on kinematic seismic response of single piles and pile groups were conducted by Fan *et al.* (1991). Research by finite element method on nonlinear response of single piles under lateral inertial and seismic load was conducted by Badoni and Makris (1996). In this study, hysteretic and radiation damping were modelled realistically within the practical rang of amplitudes and frequencies and the results were calibrated and validated against five well instrumented full-scale experiments and typical values for the range of the model-parameters were provided. The developed method and the calibrated model were used to predict the inertial and seismic response of one of the piles for Ohba bridge near Tokyo, Japan. The dynamic head-force-displacement loops under harmonic force with amplitude P_0 = 400 kN of single pile embedded into the Ohba-Ohashi soil deposit, was determined.

Han (2002) found that the seismic behaviour of tall buildings could be affected by non-linear soil-pile interaction during strong earthquakes. This investigation was done by numerical modelling and validated by full-scale experiment of a single pile and group of piles. The adopted foundation included three conditions namely rigid base, linear soil-pile system and nonlinear soil-pile system. The results were then compared to each other. The soil model was simulated by a boundary zone model with non-reflective interface. For the stiffness and damping of pile foundation in non-linearity problem, the approximate analysis was considered as an efficient technique to obtain solution. In order to solve analytical equation, a computer program was developed by the author based on Novak's method and non-reflective boundary. Both theoretical and experimental solutions showed that the dynamic response of pile was very sensitive to the properties of the soil in the vicinity of pile shaft.

Comparing models developed for fixed base, shallow and pile foundations, some studies showed that maximum lateral deflections at each level of the same superstructure reduce from shallow foundation, to pile foundation and then to fixed base condition (e.g. Hokmabadi *et al.* 2014b; Kumar *et al.* 2016; Chang *et al.* 2016).

Chang *et al.* (2016) analysed the case where the superstructure was subjected to earthquake in bevel angle by decomposing the excitation in both longitudinal and transverse directions. To do that they used transformation from pile-soil-pile element to equivalent pier underneath the raft for the sake of the simplified modelling for seismic response of rectangular foundation on pile subjected to horizontal earthquakes. The method was found compatible to three dimensional finite element method which could be further developed for more complex problems for soil-pile-soil interaction.

Chang *et al.* (2014) presented a numerical one-dimensional wave equation analysis technique for a model of structure on piles and pile groups subjected to seismic horizontal ground motions in liquefiable zones. The soil-pile system under earthquake, was separated into free field ground response analysis and pile response analysis. The so-called Earthquake Wave Equation Analysis for Piles (EQWEAP) procedure was introduced for piles subjected to horizontal earthquake excitations. The nonlinearities of the concrete piles were modelled using the approximate tri-linear moment–curvature relationships. Although the analysis was in one dimension, it was found to be effective and able to provide a rapid estimation in foundation design when seismic pile behaviour

is of interest. The advantages of Chang *et al.* (2014) model were the time efficiency of the seismic analysis and design of pile foundations and the relative simplicity of the analysis.

Recently, seismic soil-pile-interaction behaviour have been studied deeply with several methods (e.g., Emani *et al.* 2016; Chen *et al.* 2016; Durante *et al.* 2016; Hamayoon *et al.* 2017). Emani *et al.* (2016) studied inelastic response spectrum for seismic soil-pile structure interaction when their structures resting on deep foundations (pile foundation) were subjected to entirely different kind of vibrations than those resting on shallow foundations. Their work generated response spectrum for single-pile within pile group supported structures using inelastic dynamic soil-pile interaction analysis. The soil non-linearity of the numerical modelling included both separation at soil-pile interface and the plasticity of the near-field soil. In order to model the boundary in seimic modelling, the radiation boundary condition was incorporated in the form of a series of far-field dampers which assume that this boundary can absorb the out-going waves. The synthetic time histories compatible with design (input) response spectra at the base of pile were used to investigate the effects of kinematics and inertial interaction between soil-pile system to generate the inelastic response spectra for the structure.

Durante *et al.* (2016) conducted an experiment using shaking table for soil-pile-interaction scaled model which comprised of an oscillator connected to a single or group of piles embedded in a bi-layer deposit. The input earthquake was applied to the bottom of a shaking table which were controlled with five pairs of hydraulic pumps while the soil was compacted into a laminar container and some piles were installed inside the soil. The outcomes of this experiment were acceleration, displacement and strain in soil and in piles from a number of accelerometers, displacement transformers and strain gauges. The test result revealed that due to the soil-structure interaction effect, pile response differed significantly from fixed base condition.

For all numerical or experimental models to investigate the seismic soil-foundation-structure interaction (SSFSI), the effect of the boundaries is very important factor. In general, the boundaries in earthquake direction should absorb all earthquake wave without any reflection effect. In order to do that, the soil container in experiment model should satisfy the same dynamic shear stiffness with the soil (Hokmabadi 2014) while in the numerical modelling the boundaries should be quiet boundary (e.g.,

Maheshwari *et al.* 2004) or free field boundaries (Mylonakis *et al.* 1997; Tabatabaiefar 2012; Hokmabadi 2014; Hamayoon *et al.* 2017).

2.8 Seismic soil-foundation-structure interaction considering pounding between adjacent buildings

The separation gap between building is a critical parameter for urban development. Some city councils require a minimum separation gap among new buildings. One of the reason for this gap is seismic pounding because when the separation gap between buildings and structures is not wide enough, particularly during major earthquake events; this can cause them to collide, causing local damage, or in extreme cases, to collapse. There have been a larger number of studies that investigated the impact that the separation gap has on the seismic response of mid-rise buildings supported on piles while seismic soil-pile-structure interaction (SSPSI) is considered (e.g., Rosenblueth 1986; Park and Hashash 2004; Chouw and Hao 2012).

Recently, the Christchurch earthquake on 22 February 2011 had a strong aftershock (moment magnitude of 6.3) following a strong main earthquake on 4 September 2010 (moment magnitude of 7.1). Chouw and Hao (2012) investigated this event and found that pounding might have induced damage. Unfortunately, many adjacent buildings had inadequate separation gap or in many cases had even no gap, as a result, the heavy damage of several buildings and bridges on Avon River were observed (see Figure 2.11).

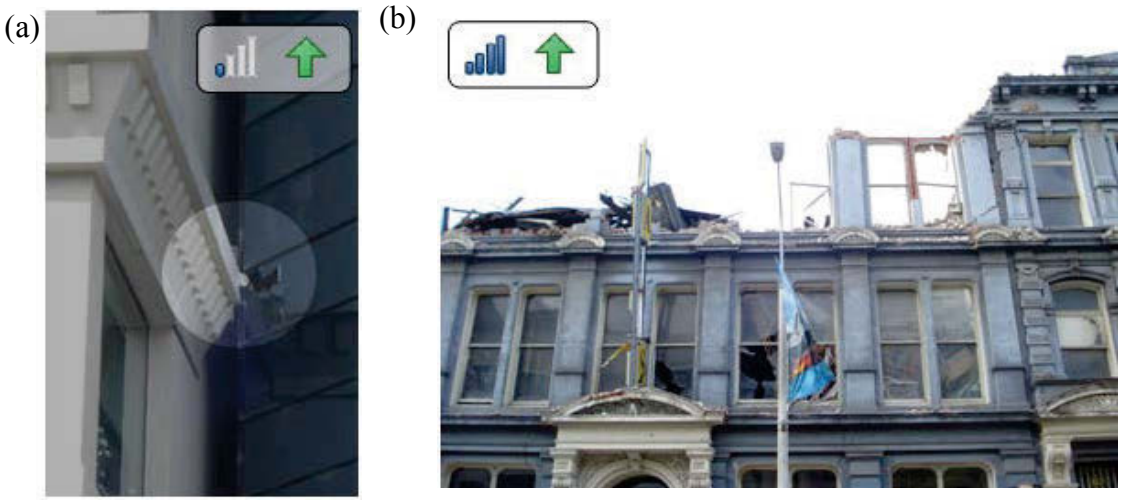

Figure 2.11 Pounding caused buildings damaged in the 2011 Christchurch earthquake (a) floor damaged the column, (b) loss of top floor (Cole *et al.* 2012)

In addition, the 1985 Mexico earthquake striked the Mexico city and the damage due to pounding between buildings caused about 40% of the total damage to buildings which partially or entirely collapsed, while 15% of the buildings collapsed primarily due to collisions during this seismic event (Rosenblueth and Meli 1986).

Hong *et al.* (2003) investigated the critical building separation distance in reducing pounding risk under earthquake excitation by numerical method for both single and multiple degree of freedom systems. The results revealed that that evaluation of the critical separation distance is a one-sided barrier crossing problem while the problem of structural design under seismic excitations is a two-sided crossing problem. Since the crossing rate for the latter is always larger than that for the former, the critical separation distance calculated based on two-sided crossing is always conservative. The ratio of the critical separation distance obtained from one-sided crossing to that from two-sided crossing ranges from about 0.83 to 0.95. Since the peak responses based on the two-sided crossing rather than one-sided responses are often considered and available for structural design purpose, the former were employed in the complete quadratic combination (CQC) rule to estimate the critical separation distance. Numerical results indicate that if the seismic excitation is modelled as the white noise, the ratio of the critical separation distance obtained from random vibration analysis to the one obtained by directly using the CQC rule varies from about 0.8 to about 1.1 for most cases considered. Furthermore, Carbonari *et al.* (2011) studied the effect of soil-pile-structure interaction (SPSI) on a coupled wall-frame building through a finite element analysis and concluded that the effects of SPSI should be considered in structural design because it would amplify the global seismic response of buildings, particularly the lateral displacement and inter-storey drifts. On this basis, the effects of SSI should be considered when studying the seismic pounding because it is caused by the relative lateral movement of two adjacent structures.

Shakya and Wijeyewickrema (2009), Chouw and Hao (2012), Mahmoud *et al.* (2013) and Pratesi *et al.* (2014) focused on seismic pounding to find the time when seismic pounding occurs, the location and the impact force between two adjacent building. They concluded that time when pounding occurs depends on the distance between buildings, and input earthquakes while the location within buildings where pounding occurs depends on dynamic characteristics of structure and soil underneath. They both also plotted the impact force history. In general, for most of earthquake

excitations, pounding occurs at the floor levels where the mass distribution of structure is higher comparing to column areas. In addition, higher levels tend to experience pounding more often and get higher pounding force comparing to lower levels.

Sołtysik and Jankowski (2015) studied building damage due to structural pounding during earthquakes with numerical modelling and found that earthquake-induced pounding between adjacent buildings causes substantial damage or even total collapse of colliding structures. This non-linear numerical model had two steel building structures with different heights staying near each other and, due to the different dynamic parameters, insufficient separation gap between them and earthquake excitation the seismic pounding occurred. Initially, modal analysis was conducted where the modes of two structures were examined before performing the detailed non-linear dynamic analysis of colliding structures under 1940 El Centro earthquake in both longitudinal and transverse directions.

Mahmoud *et al.* (2013) investigated earthquake-induced pounding between equal height multi-storey buildings considering soil-structure interaction. The comparison was made between colliding three-storey building with and without soil-structure-interaction (SSI) under eight earthquake excitations. In order to model the horizontal and rotational movement of the supporting soil, the spring-dashpot elements were adopted while the nonlinear viscoelastic pounding force was used to model impact force during pounding event. The results of this study in form of structural responses, time-histories of energy dissipated and impact force during pounding indicated that the SSI plays an important role in the system behaviour. The minimum required separation gap for each case of building and earthquake was found and recommended to the engineer to avoid pounding.

The Australian seismic design standard (AS1170.4 2007) requires a separation gap greater than 1% of the height for structures higher than 15 meters to avoid the pounding effect from earthquake loading. Hao (2015) concluded that pounding usually caused local damage around the impacting areas, and in extreme case, collapse of the building structure. In order to examine the adequacy of that specification to preclude seismic pounding between reinforcement concrete frame structures under earthquake loading, the intensive numerical modelling was conducted. The models contained viscous and elastic resistance condition of reinforcement concrete columns while the rigid condition for the floors were adopted. The first frame had unchanged vibration frequency

$f_1 = 1$ Hz while the second frame had varied vibration frequency $f_2 = 0.2$ to 5 Hz with increment of 0.2 Hz. In addition, the damping of the structure was only considered its mass while its stiffness was ignored. The variation of ratio f_2/f_1 caused pounding in several conditions. The result of this study was presented in term of impact forces, displacements and shear forces of two frame structures with and without pounding effect with different separation gaps subjected to earthquake excitations.

Jamal and Vidyadhara (2013) also investigated the seismic pounding of multi-storey buildings and confirmed that during earthquake, the building structures were vulnerable to severe damages. The separation distance between buildings was inadequate to accommodate their relative motion, as a result the buildings vibrated out of phase and collapsed. In order to examine the seismic pounding, numerical modelling was conducted with ETABS software to study two reinforced concrete frames (12 and 19 storeis) using linear static analysis, response spectrum analysis and nonlinear time history analysis. Pounding could occur at the floor level where the gap elements were applied. The results in from of displacement and pounding force history showed that pounding force is non-zero when the difference between displacements of two collision points were equal to the separation gap.

Similarly, Rajaram and Ramancharla (2014) used SAP 2000 sofware to conduct the three dimensional analysis for pounding between adjacent buildings when their floor level were different from each other. In another word, floor level of the first building could hit somewhere in the mid of columns in the second building. However, the obtained result showed that the pounding did not only occur at floor levels but also at mid height of column level. From the results of different floor heights, it was observed that more damage was caused when the collision occurred at mid-height rather that at 3/4 of height.

These aforementioned research studies indicate that most existing studies have only examined the effects of interaction between shallow footings and supporting soil, while only a few considered deep foundations. Although most of these studies investigated the dynamic responses of two conventional buildings of equal or unequal heights using simple lumped mass models, only a few studied the response of retrofitted buildings such as shear wall braced buildings (e.g., Jamal and Vidyadhara 2013; Rajaram and Ramancharla 2014; Kumar and Karuna 2015).

2.9 Summary

A comprehensive literature review has been presented in this chapter in regards to effects of foundation characteristics and separation gap on seismic soil-foundation-structure-interaction. The key findings of the review are summarised below:

(1) The majority of seismic codes for design of building structures have been empirically based on assumptions that structure is fixed at the base, following multiple-step of complexed procedures for design presented in Section 2.3. The effects of seismic soil-foundation-structure interaction (SSFSI) have been frequently ignored in the industry practice. Unfortunately, results obtained from laboratory testing are typically valid for specific problems and are difficult to extend to field problems with different material or geometric parameters. Moreover, obtaining full-scale experiments can be considered as unfeasible for the time being.

(2) Very few rigorous numerical studies have been undertaken to determine seismic induced structural responses of building structures considering seismic soil-foundation-structure interaction. It is generally agreed that existing theories do not adequately describe the dynamic behaviour of soil and its interaction with foundation. Most methods of analysis are based upon the suggestion of Wolf (1985) where the soil-structure-interaction is simplified as a single degree of freedom (SDOF) or Winkler method where the soil is replaced by a range of elastic springs. In addition, the non-linearity of the soil depending on cyclic shear strain (Seed et al. 1986) has been only taken into account in an average sense in order to approximate some effects of non-linearity. A rigorous numerical study of soil dynamic behaviour and its interface with structure using advanced numerical methods is clearly needed.

(3) The characteristics of interaction between soil and foundation have been investigated widely especially for dynamic loading. Existing studies mainly assume that soil and foundation are rough where there is not any sliding allowed between soil-foundation interfaces. However, only a limited number of researchers have proposed well-known Mohr–Coulomb failure criterion for soil-structure-interaction where the soil characteristics depend largely on shear strength τ, cohesion c, internal friction angle φ of the soil and normal stress σ between contacting surfaces. A

rigorous interaction equation is clearly needed which covers both sliding and gap opening.

(4) Very limited attempts have been made to investigate the effects of sizes of shallow foundation and lengths of pile foundation, even though some numerical modelling for shallow and pile foundation have been conducted. In another word, these effects have not been compared and discussed for various sizes of shallow foundation and lengths of pile foundation.

(5) A number of researchers have utilised numerical modelling software to study the pounding effect of adjacent buildings under fixed base condition. However, very few numerical studies have been conducted for the system with combination of seismic soil-foundation-structure interaction (SSFSI) and seismic pounding. In fact, this combination adds another layer of complexity into the study on pounding effects between adjacent buildings.

(6) The literature review gives us a clear view on existing research and highlight areas requiring further research. The four topics related to laterally loaded piles, foundation size effects, influence of size and load-bearing mechanism of pile, and response of mid-rise building sitting on pile foundation to seismic pounding are investigated in this study through rigorous numerical modelling with both geotechnical and structural focuses.

Chapter 3 THREE DIMENSIONAL NUMERICAL SIMULATION TO PREDICT PERFORMANCE OF LATERALLY LOADED PILES ON CLAY-SAND LAYERED SLOPE

3.1 General

Predicting the deformation of the laterally loaded piles constructed on a slope is one of the challenging issues in foundation engineering. Numerical modelling is an efficient method to investigate the effects of the distance from the pile centre-line to the slope crest on the performance of laterally loaded piles considering the shear plastic deformations of the ground. In this chapter, finite element software, ABAQUS, has been employed to simulate the performance of some piles subjected to lateral loads in the sloping ground including sand and clay layers. Appropriate FORTRAN user subroutines have been adopted to simulate the soil-pile interface, capable of incorporating the gapping and sliding in the soil-pile interfaces for both sand and clay layers. The numerical results are used to predict the lateral load-deformation of piles for various cases and validated through comparison with an array of full-scale field measurements.

3.2 Introduction

The escalating demands for complex structures such as highways, retaining walls, ridge bends, abutments or pile foundation under earthquake loading require the piles subjected to lateral forces. These constructions are sometimes placed near or on slopes of variable soil layers, while the piles must satisfy the three following criteria: 1) the pile must have an adequate factor of safety against the most critical (maximum) lateral loading 2) deflections under expected seismic loadings must be small enough to maintain a safe life, and 3) the deflection occurring due to a working load must be in an acceptable range that superstructure can withstand (Poulos and Davis 1980). Currently, one of the most popularly accepted design methods of laterally loaded piles on the horizontal surface is the improved Winkler Spring Method in which the soil resistance is modelled by a number of soil springs along the pile, commonly known as $p-y$ curves method. The spring constants are obtained from analytical calculations or experimental investigations. Application of this method is very challenging particularly when the soil behaviour is nonlinear and the pile is placed on the slope in which the slope behaviour depends on height, the batter angle and other external factors such as rainfall, climate change. To

address this problem, there have been a few investigations in the area of pile engineering, to obtain reliable solutions for the pile deformation under lateral loads on the layered slope (e.g., Rowe and Poulos 1979; Gabr and Borden 1990; Muthukkumaran *et al.* 2008; Georgiadis and Georgiadis 2010).

The system of pile-soil interaction is complex as the contact surface is not a flat plane and the displacements are different in x, y, z directions. Thus, many researchers tend to adopt numerical or experimental approaches to evaluate lateral response piles (e.g., Ng *et al.* 2001; Nimityongskul 2010). Although there have been a number of analytical solutions and design recommendations (e.g. Osman and Randolph (2012), there is no decisive conclusion on how the effects of slopes should be considered in the performance evaluation of piles depending on their distance from the crest of the slope, s, shown in Figure 3.1.

With the availability of high performance computing facilities, the 3D numerical analysis is becoming more popular resulting in the most accurate solutions for problems with 3D nature with complex geometries and nonlinear material behaviour such as piles on layered soil slopes under lateral loading while considering realistic interface behaviour. According to Abdrabbo and Gaaver (2012), the pile-soil interaction plays an important role in the numerical analysis influencing the response of the individual piles and connecting structures significantly.

In this study, the response of a single pile under lateral loading placed in the slope of layered sands and clays is numerically investigated using ABAQUS software version 6.12. The numerical predictions are compared with the exiting field measurements reported by Nimityongskul (2010) for various distances from the pile centre-line to the slope crest.

3.3 Numerical simulation for lateral loaded pile on clay-sand layered slope

3.3.1 Case study description

One of the most recent full-scale investigations took place on the western edge of the Oregon State University, USA presented by Nimityongskul (2010). It consisted of several cases including piles positioned with different distances from the slope crest while the site investigations revealed same geotechnical conditions in all pile locations. The distance

from the slope crest to the pile centre were $-4D, 0D, 2D, 4D$ and $8D$, where D is the outside diameter of the pile. For the sake of presentation, the above mentioned cases are called as -4D_FIELD, 0D_FIELD, 2D_FIELD, 4D_FIELD and 8D_FIELD in order to distinguish with our finite element predictions which are named -4D_ABAQUS, 0D_ABAQUS, 2D_ABAQUS, 4D_ABAQUS and 8D_ABAQUS.

The ground profile and the pile setup tested in the slope in this case study are illustrated in Figure 3.1 and Figure 3.2. A hollow steel pile with a standard nominal diameter of 0.3048 m (1-ft), an outer diameter of D = 0.3239 m (12 ¾ inches) and a length of L = 9.144 m (approximately 30 ft) is placed vertically to the depth of 8.229 m (27-ft). As reported by Nimityongskul (2010), steel piles conform to ASTM specification A252 Grade 3 with pile material density of 8000 kg/m^3, Young Modulus of 1.963E2 GPa, and Poisson's ratio of 0.3. The slope had a length of 20.726 m ($64D$, where D is the outer diameter of pile), height of 14.249 m ($44D$), and width of 13.602 m ($42D$), with the slope angle of 1(V):2(H). Further information about this case study can be found in Nimityongskul (2010).

3.3.2 Finite element model

The finite element software ABAQUS version 6.12 has been used to simulate three dimensional behaviour of the piles adjacent to the slope. The adopted finite element model in ABAQUS consists of two key parts, namely the pile and the layered soil. Each part is partitioned into sub-parts following the ground layers. Material properties and interaction characteristics of each layer is assigned as required.

Table 3.1 summarises the material properties obtained after interpreting the geotechnical profiles reported by Nimityongskul (2010). As can be observed, an over consolidated crust layer (upper clay 1) with a thickness of 0.46 m and the undrained shear strength of 215 kPa followed by a stiff clay (upper clay 2) with an undrained shear strength of 72 kPa has been observed in the top 3 m of the soil profile.

The shear strength of the interfaces between the soil and the pile was defined by Mohr–Coulomb failure criterion (based on two soil properties, namely friction angle, ϕ, and cohesion, c) and the tensile strength of the interfaces is set to zero in order to allow gapping between the piles and the surrounding soil.

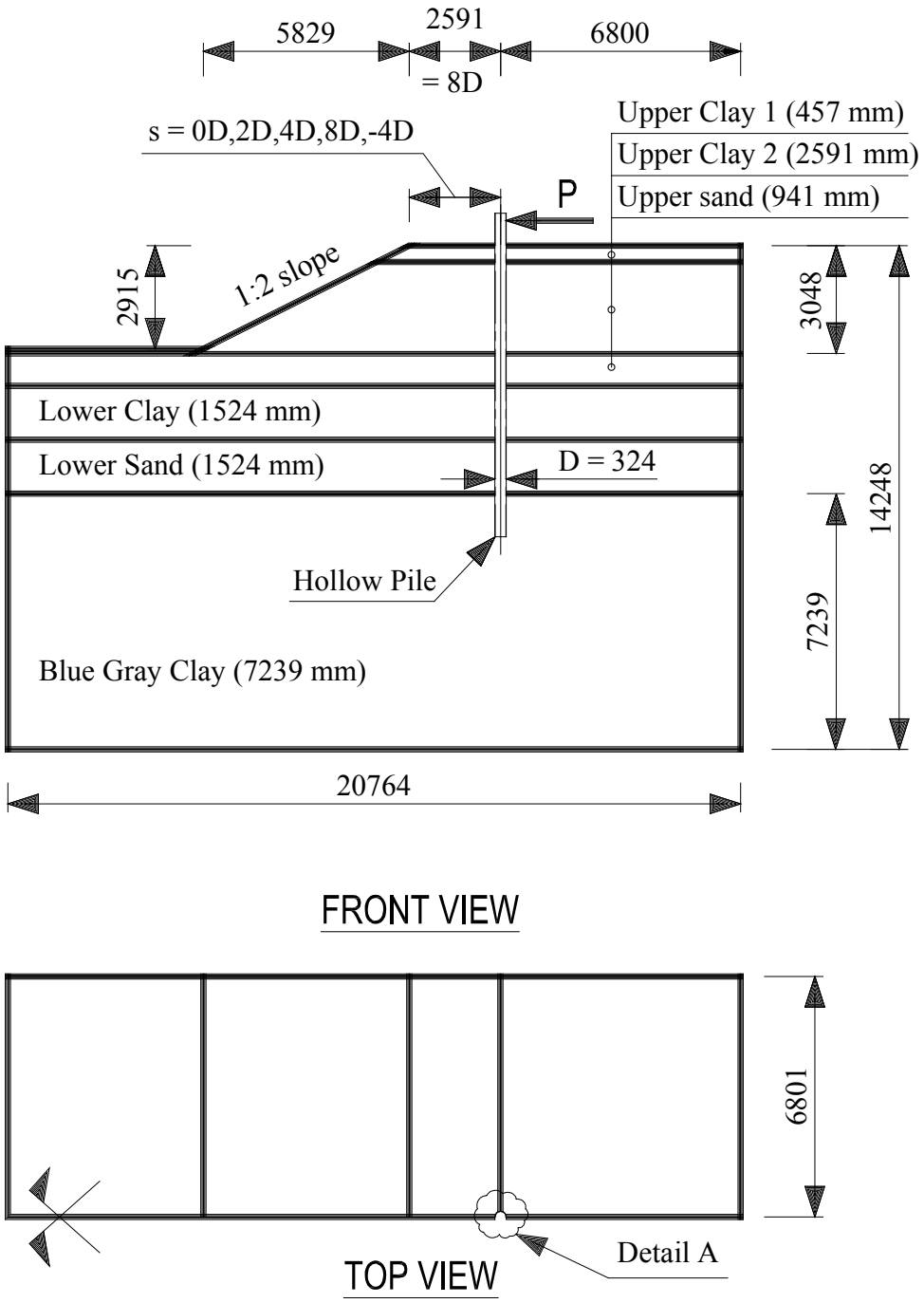

Figure 3.1 Ground profile and the pile location

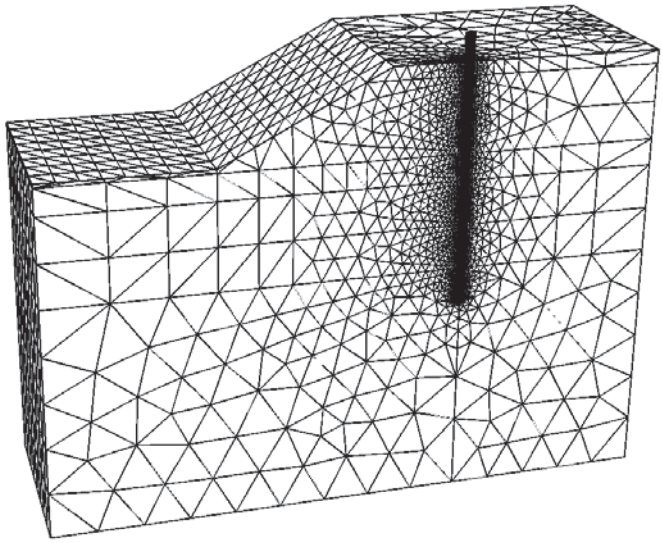

(a) Typical model meshing in 3D

(b) Typical pile meshing for pile

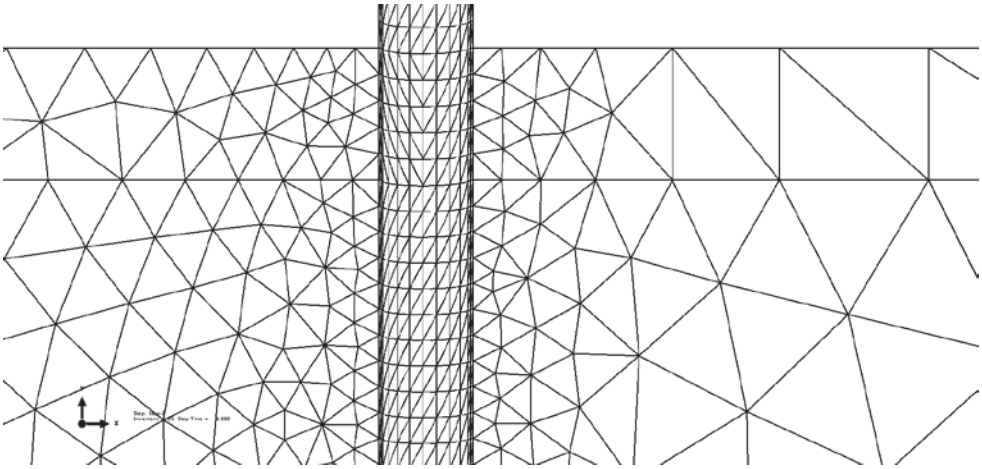

(c) Typical soil-pile meshing in vertical plane

Figure 3.2 A typical adopted meshing scheme

The FORTRAN user subroutine, called $fric\_coef$ (refer to Section 4.4.3 Contact surfaces), has been adopted to include interface elements suitable for both cohesive (clay) and cohessionless soils (sand) required in this study. Surface-to-surface contact pair with finite sliding formulation are adopted in all contact elements between the soil and the pile.

The soil was modelled as an isotropic elastic-perfectly plastic continuum with yielding described by the Mohr-Coulomb yielding criterion. In the numerical model, soil unit weight is taken into account as it affects not only the slope stability but also the load – displacement relationship of the pile under the lateral loading. Furthermore, the steel hollow pile was modelled as an isotropic elastic continuum.

Symmetry has been exploited for the three-dimensional analyses and thus only one-half of the problem domain has been modelled as shown in Figure 3.1 and Figure 3.2. Boundary conditions were introduced along every vertical face and the bottom of the model. The bottom boundary is fixed against movements in all directions, whereas the ground surface is free to move in all directions. The vertical boundaries are fixed against movements in the direction normal to them.

The adopted mesh for the problem of three-dimensional pile simulations under lateral loading in the half symmetrical model is illustrated in Figure 3.2 (a). After several trials, the mesh arrangement and size were finalised resulting in stable and reliable results.

As shown in Figure 3.2 (b) and Figure 3.2 (c), a denser mesh is required close to the pile and the average mesh size can be reduced while moving further away from the pile. The three dimensional element type used to simulate both the soil and the pile is the 10-node quadratic tetrahedron element (C3D10) resulting in the most stable solution without any solution convergence problem.

To simulate the lateral loading applied to the pile head, pile head has moved gradually and the lateral stresses were recorded. The total prescribed displacement was applied over a number of sub-steps and the nodal contact forces along the pile were summed up to compute the equivalent lateral forces. It should be noted that the number of displacement increments is automatically controlled by ABAQUS, within the initial, minimum, and maximum values prescribed by the user.

Table 3.1 Material properties of soil and pile adopted in the numerical simulation

Property	Unit	Upper clay 1	Upper clay 2	Upper sand	Lower clay	Lower sand	Blue gray clay	Pile
Thickness	mm	457	2591	914	1524	1524	7239	9.525
Unit weight (γ)	Kg/m^3	1842.3	1842.3	2082.6	1842.3	2082.6	1762.2	8000
Young Modulus (E)	MPa	43.092	28.728	28.728	22.983	28.728	22.983	1.963E5
Poisson's ratio (ν)	-	0.495	0.495	0.35	0.495	0.35	0.495	0.3
Cohesion (c)	kPa	215.46	71.820	0	114.91	0	167.58	-
Friction Angle (ϕ)	degree	0	0	40	0	45	0	-
Dilation Angle (ψ)	degree	0	0	0	0	0	0	-

To determine the load-displacement curves, the neutral axis of the pile was assumed to be at the centre-line along the pile. A path along the centre of the pile was created and the position of each point in the path was recorded as y to obtain $p - y$ curves. Note that y is the horizontal displacement of each point along the centre-line of the pile and p is the lateral soil resistance per unit pile length. The rotation of the pile is determined by the numerical derivative of y with respect to z as presented in Equation (3.1), where z is the vertical coordinate along the pile.

$$S(z) = \frac{dy(z)}{dz} \tag{3.1}$$

Bending moment of the pile can be determined using Equation (3.2):

$$M(z) = E_p I_p \frac{d^2 y(z)}{dz^2} \tag{3.2}$$

where E_p and I_p are Young Modulus and moment of inertial of the pile, respectively. In this study, $E_p = 1.963E5\ MPa$, and $I_p = \pi(r_{out}^4 - r_{in}^4) = 1.8603E-3\ m^4$, resulting in $E_p I_p = 3.562E8\ Nm^2$. However, in order to carry out the numerical derivation from a number of discrete points at each depth of the pile, polynomial functions in the order of six and five were chosen for curve fitting technique to obtain derivations required in Equations (3.1) and (3.2), respectively.

3.3 Results and discussion

Figure 3.3 summaries the pile head load-displacement curves obtained from both experimental and numerical investigations for different pile arrangements. As shown in Figure 3.3, under the same pile and soil conditions, at the same pile head displacement, the lateral load response/resistance increases while the distance between the pile centre-

line and the slope crest (s) increases. As can be observed, the predicted pile head load - displacement curve at $s = 0D$ is positioned well below the curves for higher values of s (e.g. $4D$ and $8D$).

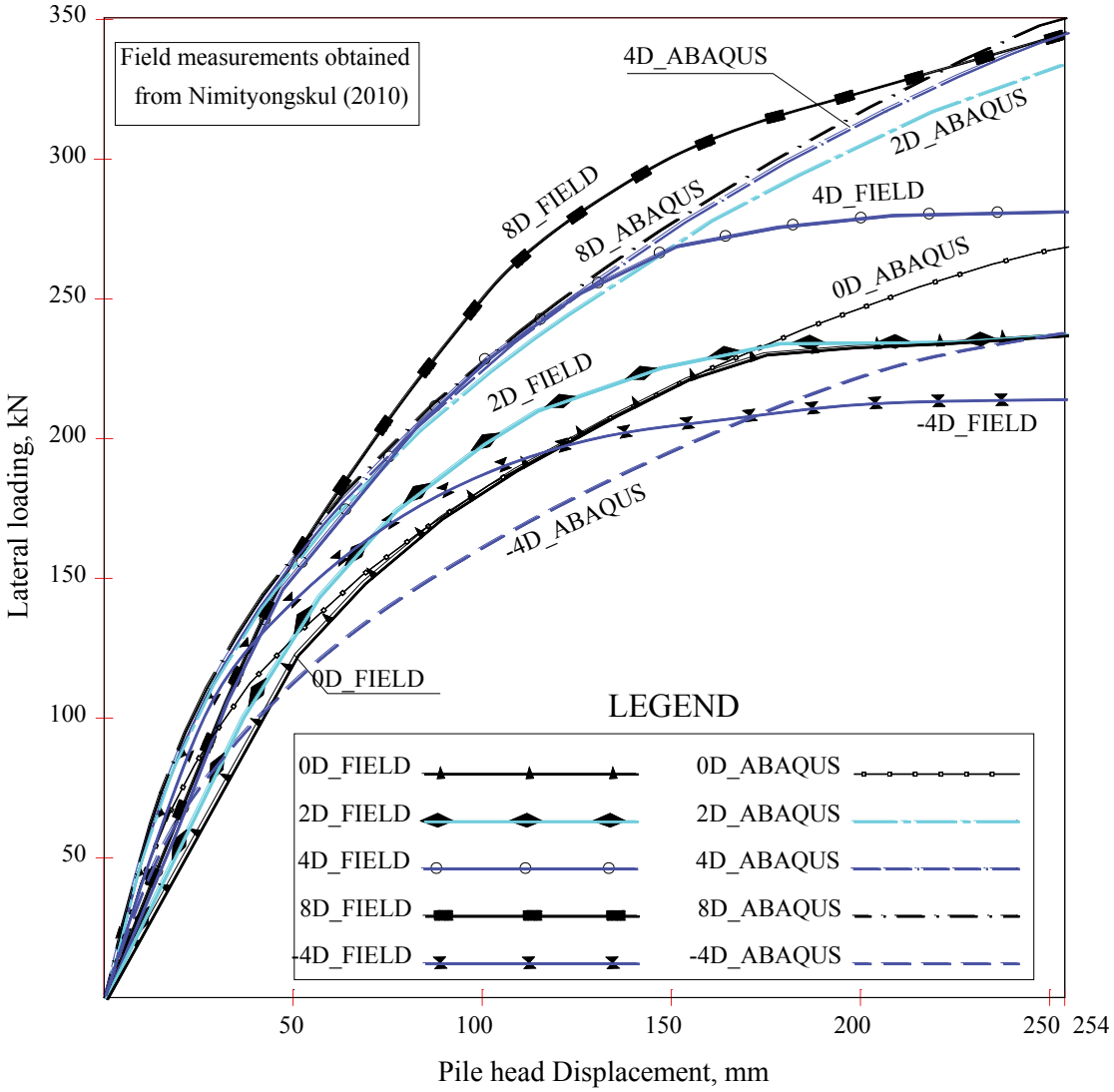

Figure 3.3 Pile head load - displacement curves from both field measurements and numerical predictions

When the pile head displacement is less than 30 mm, the effect of the slope on the lateral resistance of the pile is minor. However, for larger lateral displacements, the effects of the slope on the response of the pile are significant due to the plastic shear strains induced. In other words, for a give lateral pile resistance, the pile head displacement increases when the pile is closer to the slope crest. Based on the numerical predictions, the influence of the slope on the pile head load - displacement relation may

be insignificant when s is greater than $2D$, this is also in a good agreement with Caltrans Bridge Design Specifications(CALTRANS, 2010) for Service Limit State (SLS) design. However based on the field measurements, the slope effects may be significant when the piles are closer than 8D to the slope crest. For the case of $s = 0D$, the predicted and measured load-displacement curves are in a good agreement up to the pile head displacement of 0.15 m. Then the measured lateral resistance stays constant (approximately 220 kN) due to the induced yielding, while the numerical predictions still show a gradual increase (over 250 kN).

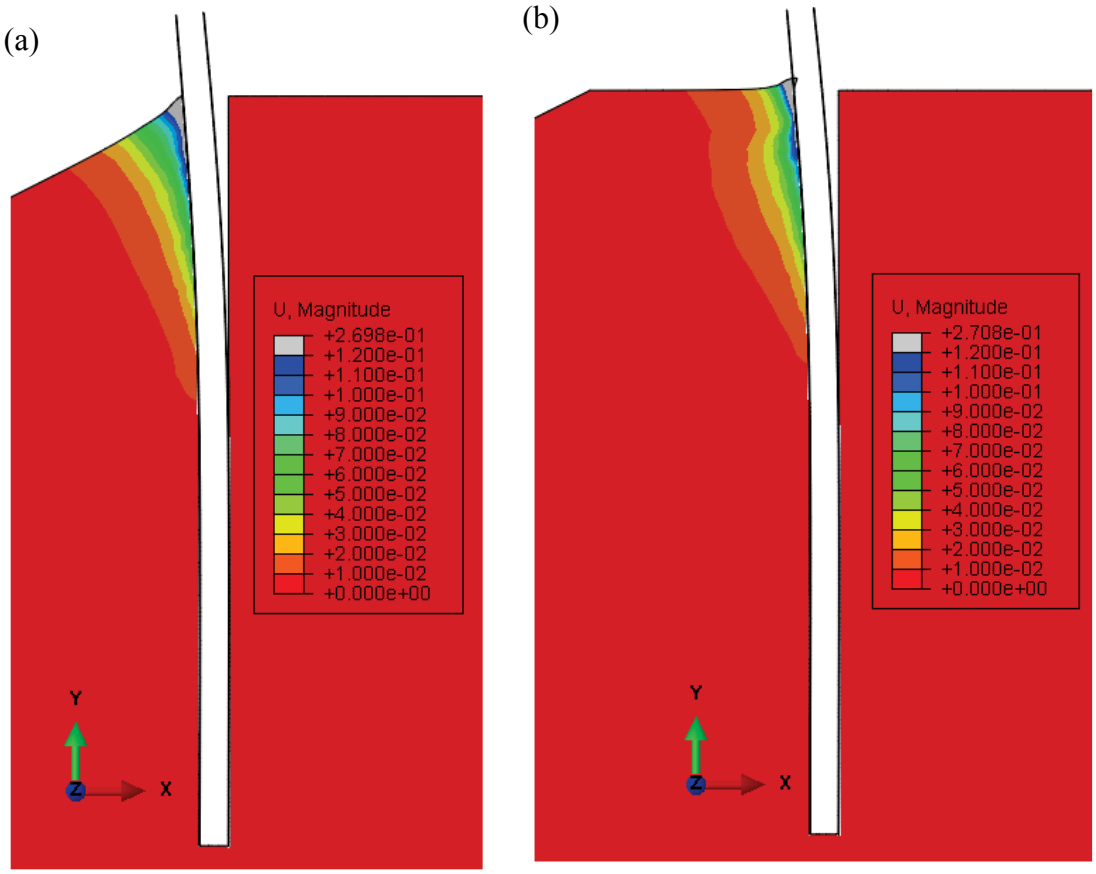

Figure 3.4 Numerical predictions for displacement contours (U) for (a) s = 0D and (b) s = 8D cases in X-Y plane

It can be noted that according to the results reported in Figure 3.3, the measured lateral resistance for all cases kept increasing with the increase of the pile head displacement up to 0.15 m. For larger pile head displacements, the lateral resistance of the pile only increases slightly. Obviously, when the pile is located in the sloping ground

($-4D$ case), it results in the lowest lateral resistance for a particular pile head displacement (e.g., 250 mm) in comparison to the other reported cases.

As can be seen in Figure 3.4, there will be a gap behind the pile when subjected to the lateral loading, which is confirmed by the numerical analysis. A comparison between Figure 3.4 (a) and Figure 3.4 (b) reveals that the gap opens up more and is deeper when the pile is closer to the crest. Obviously, there is a larger mobilised soil body in front of the pile contributing to higher pile lateral resistance when the distance s increases from $0D$ to $8D$. In addition, comparison of Figure 3.4 (a) and Figure 3.4 (b) highlights the effects of the surface crust, as the upper clay layer has influenced the displacement contours due to higher stiffness in comparison to the layers below. This lateral resistance due to the very stiff soil crust is not evident for the other cases (i. e. $0D$, $2D$ and $-4D$ cases).

Figure 3.5 presents the results of the pile deflection, pile rotation and bending moment variations with depth employing Equations (3.1) and (3.2) for $0D$ and $8D$ cases. Comparing the results, it is evident that although the lateral resistance of the pile very much depends on the distance of the pile from the crest, the location of the pile with respect to the slope influences the generated bending moment and pile rotation insignificantly. In addition, when the pile head displacement increases, the location of the maximum bending moment moves to deeper layers and increases as well. For example, for the pile built in the slope crest ($0D$), for the pile head deflections of 50 mm, 100 mm, 150 mm, 200 mm and 254 mm, the maximum bending moment locations (and values) are at the depth of 1.5 m (3 MN.m), 2.2 m (5.2 MN.m), 2.3 m (6.8 MN.m), 2.4 m (8.4 MN.m), and 2.45 m (9.2 MN.m), respectively.

To investigate the influence zone around the pile, the models for $0D$ and $8D$ are selected to demonstrate the view cut section at 1m below the ground surface as shown in Figure 3.6. The mobilised soil zone and the gap between the soil and the pile reveal that there is a larger displaced soil zone in $0D$ case compared to $8D$ case. Hence, it can be concluded that the presence of the slope close to the pile affects the mobilised soil zone, while the pile is under lateral loading.

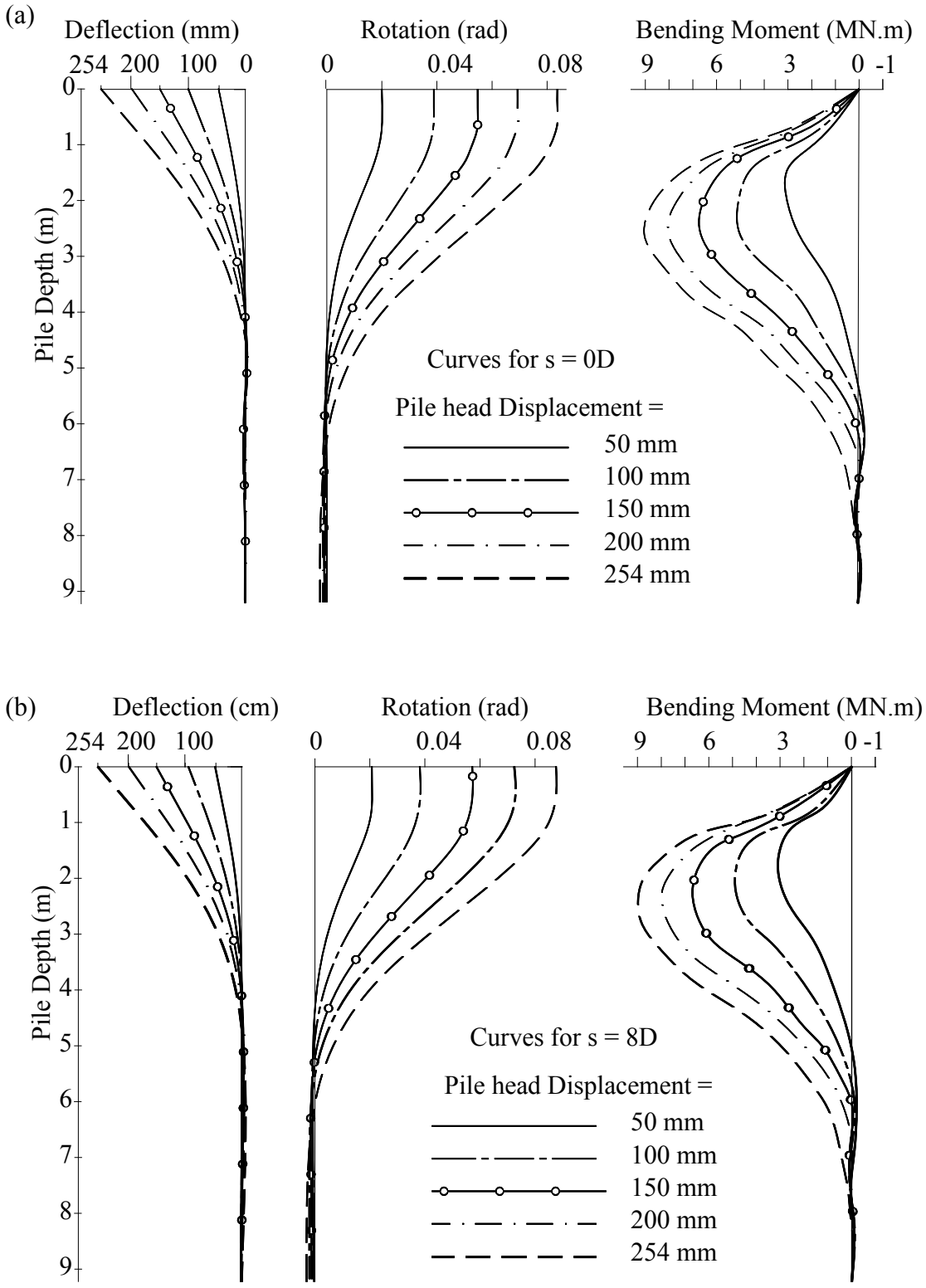

Figure 3.5 Pile Deflection, Rotation, and Bending moment Curves for (a) s = 0*D* and (b) s = 8*D* cases (*D* = the pile outside diameter)

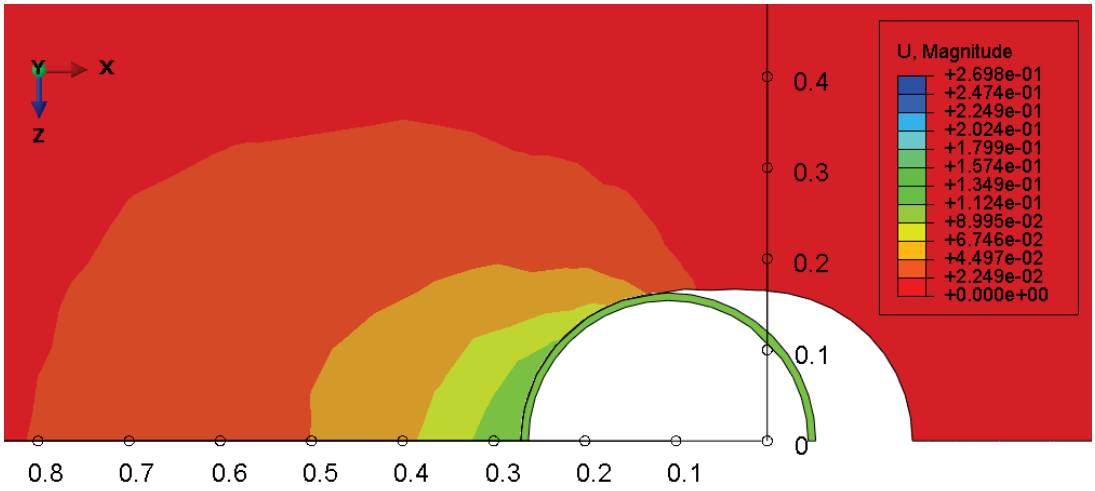

a) Horizontal view cut for $0D$ case

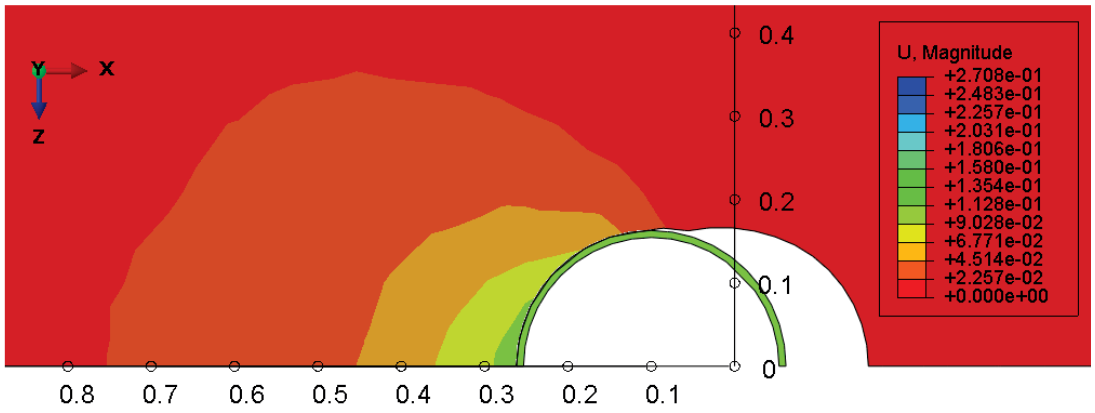

b) Horizontal view cut for $8D$ case

Figure 3.6 Horizontal cross section 1 m below the ground surface indicating total displacements

3.4 Summary

The behaviour of a single pile under lateral loading placed in the slope of layered soil was numerically investigated using ABAQUS software. Finite element predictions are in good agreement with field measurements indicating suitability of ABAQUS and subroutine for simulation of laterally loaded piles. The generated finite element analysis results as well as the field measurements indicate that the lateral resistance of a pile adjacent to a slope is influenced notably by the pile distance from the slope crest, while the effects on the induced pile bending moments and rotations are insignificant. Numerical predictions clearly indicate that for the piles located closer to the slope crest, smaller soil body is mobilised in comparison to the control pile located in the flat ground. The field

measurements and numerical predictions are generally in a good agreement with a similar trend. However, field measurements indicated that the slope affects the lateral resistance of the pile (with an outside diameter of D) was not significant, when the pile was located at least 8D away from the crest, while the numerical predictions shows the same effect when the spacing is greater than 2D away from the slope crest.

Chapter 4 THE EFFECTS OF FOUNDATION SIZE ON THE SEISMIC PERFORMANCE OF BUILDINGS CONSIDERING THE SOIL-FOUNDATION-STRUCTURE INTERACTION

4.1 General

Shallow footings are one of the most common types of foundations used to support mid-rise buildings in high risk seismic zones. Recent findings have revealed that the dynamic interaction between the soil, foundation, and the superstructure can influence the seismic response of the building during earthquakes. Accordingly, the properties of a foundation can alter the dynamic characteristics (natural frequency and damping) of the soil-foundation-structure system. In this chapter the influence that shallow foundations have on the seismic response of a mid-rise moment resisting building is investigated. For this purpose, a fifteen storey moment resisting frame sitting on shallow footings with different sizes was simulated numerically using ABAQUS software. By adopting a direct calculation method, the numerical model can perform a fully nonlinear time history dynamic analysis to realistically simulate the dynamic behaviour of soil, foundation, and structure under seismic excitations. This three-dimensional numerical model accounts for the nonlinear behaviour of the soil medium and structural elements. Infinite boundary conditions were assigned to the numerical model to simulate free field boundaries, and appropriate contact elements capable of modelling sliding and separation between the foundation and soil elements are also considered. The influence of foundation size on the natural frequency of the system and structural response spectrum was also studied. The numerical results for cases of seismic soil-foundation-structure systems with different sized foundations and fixed base conditions (excluding soil-foundation-structure interaction) in terms of lateral deformations, inter-storey drifts, rocking, and shear force distribution of the structure were then compared. Due to natural period lengthening, there was a significant reduction in the base shears when the size of the foundation was reduced. It was concluded that the size of a shallow foundation influences the dynamic characteristics and the seismic response of the building due to interaction between the soil, foundation, and structure, and therefore design engineer should carefully consider these parameters in order to ensure a safe and cost effective seismic design.

4.2 Introduction

The seismic motions experienced by the foundations of a building founded on rocks are similar to the motions that occur in the same point before the structure is built. Therefore, in these cases the seismic response of the building can be calculated by considering a fixed-base assumption subjected to these specified seismic motions. However, where a building is founded on a soft deposit, two main modifications should be applied, as discussed by Wolf (1989); first, free field motion at the site without the superstructure is strongly affected; second, a superstructure built on soft soil alters the dynamic characteristics of the system, unlike the fixed-base assumption.

According to Veletsos and Meek (1974), compared to a fixed-base system, the soil-foundation-structure interaction (SFSI) has two basic effects on the structural response:

(i) the soil-structure system has an increased number of degrees of freedom and thus modified dynamic characteristics, and

(ii) a significant part of the vibration energy of the soil-structure system may be dissipated by radiating waves emanating from the vibrating foundation-structure system back into the soil, or by hysteretic material damping in the soil. Either way this means that a soil-structure system has a longer natural period of vibration than its fixed-base counterpart.

Two key mechanisms are generally involved during a seismic soil-foundation-structure interaction: kinematic interaction and inertial interaction. Kinematic interaction occurs because stiff foundation elements in the soil cause the foundation motion to deviate from the free field ground motion. Kinematic interaction could also be due to ground motion incoherence, foundation embedment effects, and wave scattering or inclination (Stewart *et al.* 1999). Inertial interaction results from the inertia developed in the structure as its own vibration produces base shear, moment, and torsional excitation. These loads in turn cause displacements and the foundation to rotate relative to the free field condition (Kramer and Stewart 2004). Fundamentally, the size of a foundation can influence the kinematic and inertial interactions mainly by altering the mass and stiffness of the soil foundation system, as shown in Figure 4.1, which in turn influences the seismic response of the superstructure.

Referring to Figure 4.1, the inertial forces generated in the superstructure can cause rocking during strong earthquake excitations. This creates compression on one side of the foundation and tension on the other side, which in turn results in settlement on one side and possible uplift on the other side of the foundation.

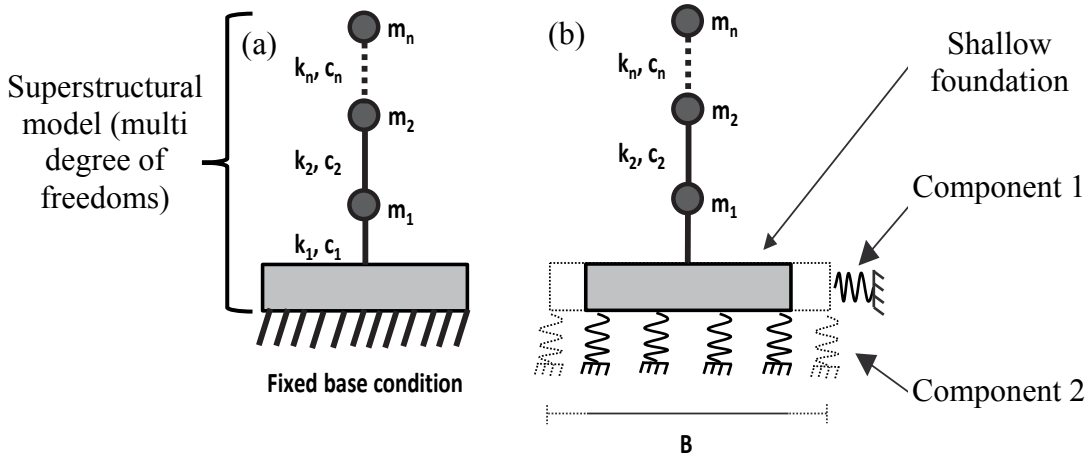

***Component 1**: Horizontal Geotechnical components:*
- Passive properties against site of footing
- Friction properties at bottom of footing

***Component 2**: Distributed Vertical Geotechnical components:*
- Vertical bearing properties of soil
- Component spacing along footing length

Figure 4.1 Schematic modelling of the multi degree freedom structure (a) under fixed based condition excluding soil-structure interaction and (b) supported by shallow foundations considering dynamic soil-foundation-structure interaction

Ma *et al.* (2009) showed that rocking may be the most critical mode of vibration for a foundation because the very low hysteretic (material) damping will lead to high motion amplitude when the excitation frequencies are close to the resonance state. Shallow foundations with varying sizes experience different amounts of rocking under a particular earthquake excitation and it is the rocking component that amplifies the lateral displacement of the superstructure and may influence its total stability. Despite this, a significant amount of earthquake energy may be dissipated due to rocking-dissipation which actually directs less shear forces to the superstructure. Gazetas and Mylonakis (1998) pointed out that in reality, the supporting soil medium allows some movements due to its natural flexibility, and this may reduce the overall stiffness of the structural

system and hence, may increase the natural periods in the system. The influence that this partial fixity of the structures has at the foundation level due to soil flexibility, which is very dependent on the foundation size, in turn alters the response. Therefore, understanding the influence that a shallow foundation size has on the seismic response of buildings during earthquake excitations with respect to the soil-foundation-structure interaction can help design engineers select foundations that are the proper size for the structures and thus deliver a cost effective and safe design.

The procedures regulated in codes such as ATC-40 (1996), BSSC (2009), and ASCE 7-10 (2010) do not account for the influence of foundation size, while a simplified method that represents subsoil by a series of springs and dashpots (impedance functions), and the superstructure as a simple degree of freedom oscillator, has been adopted in the regulated codes.

Moreover, a linear equivalent for the subsoil has also been adopted in these codes without directly capturing any soil non-linearity that depends on the input motion and level of induced shear strain, particularly where the stiffness and damping are assumed to be constant during the solution process.

Several researchers (e.g., Sameti and Ghannad 2014; Chen 2015; Sbartai 2015) studied the seismic soil-foundation-structure interaction phenomena and its influence on the seismic response of buildings by adopting the Winkler (substructure) methods and the numerical methods. Adopting advanced numerical models has a number of advantages over the Winkler methods, especially their ability to conduct time history analyses while considering effects such as the nonlinear stress–strain behaviour of the soil and the superstructure, material and radiation damping, advance boundary conditions, and interface elements (e.g., Hokmabadi *et al.* 2014b; Tabatabaiefar and Fatahi 2014; Tabatabaiefar *et al.* 2014b; Hokmabadi and Fatahi 2015). Another advantage of using numerical methods is their ability to perform the analysis in a fully-coupled manner without resorting to independent calculations of site or superstructure response (Meymand 1998). Consequently, numerical modelling predictions can capture the different parameters involved in soil-foundation-structure interaction (SFSI) that are closer to reality (e.g., Dutta and Roy 2002; Reza Tabatabaiefar *et al.* 2013; Fatahi *et al.* 2014), which is why they were used in this study.

The aim of this study was to investigate the influence of shallow foundation size on the seismic response of a regular mid-rise moment resisting building frame during earthquake excitations. To achieve this goal, a numerical simulation of a soil-foundation-structure system was carried out in ABAQUS software (version 6.14) as a fully coupled nonlinear time history analysis. The effects of foundation size on the natural frequencies of the system as well as the response spectrum and structural performance are investigated. The results of this study can help design engineers assess the influence that foundation size has on the seismic performance of buildings sitting on soft soil, while aiming to achieve an optimised design.

4.3 Characteristics of the soil-foundation-structure system

4.3.1 Characteristics of the adopted moment resisting building frame

In this study, a fifteen storey concrete moment resisting building frame, 45 m high and 12 m wide, consisting of three spans in each direction, was selected. This building frame represents a conventional mid-rise moment resisting buildings. The structural sections were specified after conducting a routine design procedure regulated in the relevant building codes (e.g., AS1170.4 2007; AS3600 2009; CSI 2010) software was utilised for the structural analysis and design of the cross sections of beams and columns. Gravity loads, including the permanent (dead) and imposed (live) actions were determined and applied to the structural model in accordance with AS1170.1 (2002) (Permanent, imposed and other actions). The values of permanent action (dead load) and imposed action (live load) were determined as uniformly distributed loads over the floors according to AS/NZS1170.1-2002, while considering the spacing of the frames as being 4 metres (Permanent Action $G = 6\ kPa$ and Imposed Action $Q = 2\ kPa$). Then, a nonlinear time-history dynamic analysis under the influence of the four earthquake ground motions shown in Figure 4.10 and Table 4.5 was carried out. In this dynamic analysis the geometric non-linearity and $P - \Delta$ effects were considered according to AS3600 (2009). Moreover, cracked sections for the reinforced concrete sections were considered by multiplying the coefficients of the cracked sections by the stiffness values of the structural members (EI) according to ACI318-08 (2008). Based on this standard, the coefficients of the cracked section were 0.25 and 0.7 for slabs and columns, respectively.

After finalising the dynamic analyses, concrete sections of the model were designed according to AS3600 (2009) (Australian Standard for Concrete Structures). Various load combinations were considered while designing the concrete structural members subjected to Permanent (G), Imposed (Q), and Earthquake (E_u) actions according to AS/NZS1170.0-2002 (Australian Standard for structural design actions).

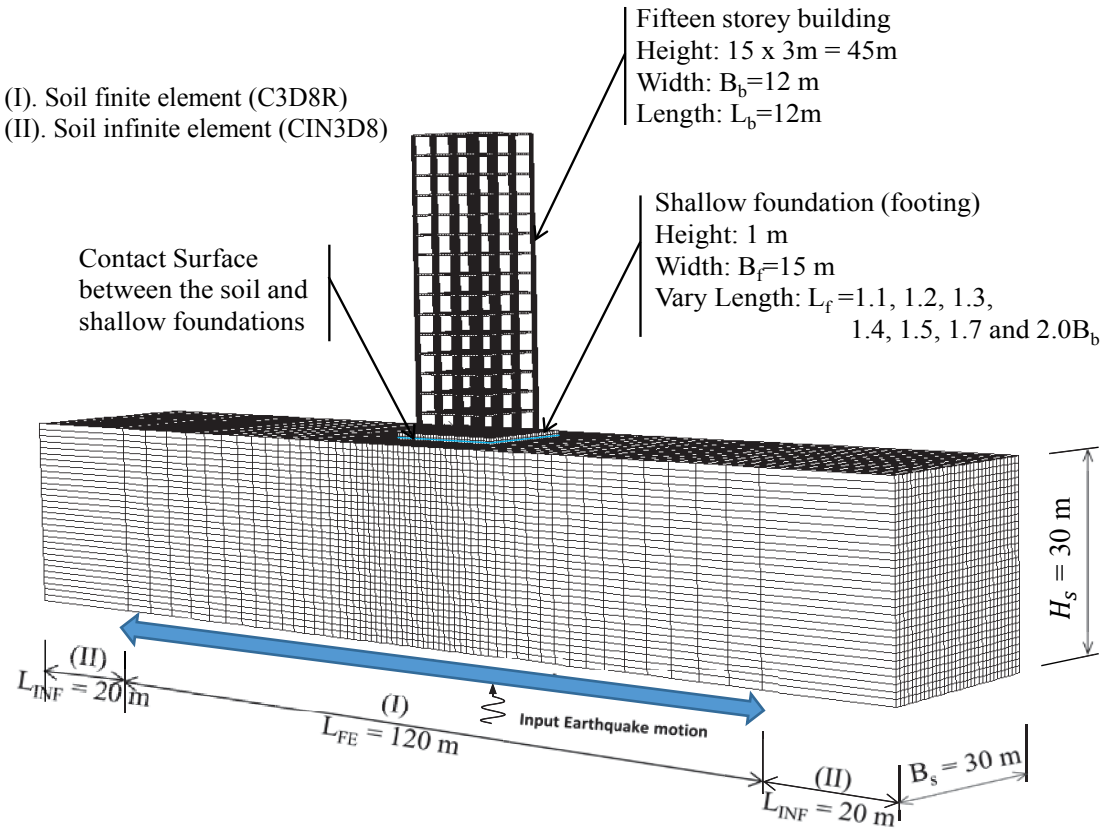

Figure 4.2 Problem definition of shallow foundation on soft soil

Figure 4.2 shows the structural sections which represent the structural norms and construction practises of conventional buildings in mega cities, and which were specifically used to investigate how foundation size influences the seismic response of buildings. The fundamental frequency of the adopted building was 0.830 Hz and its total mass was 1683 tonnes. It should be noted that the research team had previously conducted comprehensive shake table tests on a scaled structure similar to the adopted structure in this study and measurements and trends are in line with the reported numerical predictions (Tabatabaiefar *et al.* 2014b).

4.3.2 Characteristics of the soil and shallow foundations

The fifteen storey superstructure used in this study sits on 30 m deep soft soil that is categorised as Class E_e according to the Australian standard (AS1170.4 2007), and which is defined as a site with more than 10 m depth of soil with a shear wave velocity of 150 m/s or less.

In this study, the sub-soil is a soft clayey soil with a density of $1470\ kg/m^3$, a shear wave velocity of $150\ m/s$, and an-undrained shear strength of 50 kPa. The properties of this subsoil were extracted from actual in-situ and laboratory tests (Rahvar 2006), so these parameters have merit over the assumed parameters which may not be completely conforming to reality. It was assumed that the water table was below the level of the bedrock.

The shallow square foundations (footings) were designed to support the structure against static and dynamic loads, and followed routine engineering design procedures (e.g., Poulos and Davis 1980; Bowles 2001; AS2159 2009; Nguyen *et al.* 2013), to satisfy the requirement for bearing capacity and maximum settlement.

All the shallow foundations were 1 m thick and were made from reinforced concrete. Shallow foundations with various sizes have been adapted to investigation the effect of foundation size on the seismic response of building considering the soil-foundation-structure interaction. These foundations had seven different sizes, including: 1.1B, 1.2B, 1.3B, 1.4B, 1.5B, 1.7B and 2.0B, where B is the width of the building (=12 m). All these foundation sizes were acceptable from an engineer's perspective and satisfied the requirements for bearing capacity and maximum settlement, although the safety factor of the smaller foundations was less than the large ones.

Moreover, although the 1.7B and 2.0B foundations are not common in practice, a wider range of foundation sizes was considered in this study to better understand how foundation size affects the seismic response of a building during strong earthquakes. The seismic response of these foundation sizes are compared and discussed in the following sections via a three-dimensional finite element numerical simulation.

4.4 Numerical model

The governing equations of motion for the structure incorporating foundation interaction and the method of solving these equations are relatively complex because unlike ordinary dynamic time history equations of motions, these dynamic equations of motion of the soil and structure system are a combination of different vectors and matrices of the soil and the structure. This combination makes the equation too mathematically sophisticated to be solved by conventional methods, so a simplified approach to the substructure where the SFSI problem was decomposed into (a) an evaluation of a Foundation Input Motion (FIM), (b) a determination of the impedance function, and (c) a dynamic analysis of the structure supported on a compliant base but represented by the impedance function and subjected to a base excitation consisting of the FIM, has been used extensively by practising engineers and researchers. However, according to (Wolf 1988), since this method is based on the principle of superposition, any predictions would only be accurate for linear soil and structural behaviours, while approximations of soil non-linearity by means of iterative wave propagation analyses, would allow the superposition to be applied to moderately-nonlinear systems.

The direct method of analysis where the entire soil-structure system is modelled in a single step (no need to decompose the system to sub-structure and super-structure), can result in the most realistic modelling and analysis, but more advanced computer programs are required in this method. Since assumptions of superposition are not required, true and accurate nonlinear analyses are possible in this case (Borja *et al.* 1994). Therefore, the direct method, which is better at modelling the complex nature of the soil-foundation-structure interaction in dynamic analysis, was used in this study. ABAQUS v 6.14 finite element analysis software was used in this study for the numerical simulation of the soil-foundation-structure systems. This software package can simulate complex problems that require large computational memories using a direct method of analysis. A number of researchers (e.g., Chu and Truman 2004; Koskinen 2005; Moss *et al.* 2010; Matinmanesh and Asheghabadi 2011) used ABAQUS to study soil-structure interaction problems. The numerical modelling procedure used to simulate structural elements and soil models, as well as the contact surfaces and boundary conditions, is explained below.

4.4.1 Structural model

Beam and shell elements were used to simulate the columns and floor slabs of the superstructure in this numerical model. The characteristics of the columns and floor slabs are presented in Table 4.1 and Table 4.2, respectively, while taking the cracked sections into consideration in accordance with ACI318-08 (2008). The structural elements were modelled using an elastic-viscoelastic constitutive model while considering the Rayleigh damping described below.

According to Ryan and Polanco (2008), the damping matrix in Rayleigh damping is a linear combination of mass-proportional and stiffness-proportional terms:

$$[C] = \alpha[M] + \beta[K] \tag{4.1}$$

where $[C]$, $[M]$, and $[K]$ are the damping, mass, and stiffness matrices, respectively, α and β are the model coefficients used to specify the model damping ratio in two modes.

Table 4.1 Characteristics of designed reinforced concrete column sections adopted in 3D finite element modelling

Section Type	I_x (m^4)	I_y (m^4)	Area (m^2)	E (kPa)	v
Type *I (Levels 1 – 3)*	5.33E-3	10.87E-3	0.302	2.86E7	0.2
Type *II (Levels 4 – 7)*	3.64E-3	7.45E-3	0.250	2.86E7	0.2
Type *III (Levels 8 – 11)*	2.40E-3	4.89E-3	0.203	2.86E7	0.2
Type *IV (Levels 12 – 15)*	1.50E-3	3.05E-3	0.160	2.86E7	0.2

Table 4.2 Characteristics of the designed reinforced concrete floor slabs and foundations adopted in 3D numerical model

Properties	Denote	Unit	Value
Floor slab thickness	h_s	*m*	0.25
Foundation thickness	h_f	*m*	1.0
Density	ρ	kg/m^3	2400
Young's modulus	*E*	*kPa*	2.86E8
Possion's ratio	*v*	-	0.2

According to (Chopra 2007), by assuming the same damping ratio (ξ) for two modes with natural frequencies f_i and f_j, or natural angular frequencies ω_i and ω_j of the model must satisfy by coefficients α and β as following system of equations:

$$\begin{cases} \xi = \dfrac{\alpha}{2\omega_i} + \dfrac{\beta\omega_i}{2} \\ \xi = \dfrac{\alpha}{2\omega_j} + \dfrac{\beta\omega_j}{2} \\ \omega_i = 2\pi f_i \\ \omega_j = 2\pi f_j \end{cases} \tag{4.2}$$

There is a MATLAB code can help to solve this system of equations to determine the model coefficients α and β. However, the hand calculation also help within some expression as follows:

$$\begin{cases} \alpha = \xi \dfrac{2\omega_i\omega_j}{\omega_i+\omega_j} \\ \beta = \xi \dfrac{2}{\omega_i+\omega_j} \end{cases} \tag{4.3}$$

where natural angular frequency, $\omega_i = 2\pi f_i$ and $\omega_j = 2\pi f_j$ (rad/sec).

In this study, a structural damping ratio (ξ) of 5% together with model coefficients of $\alpha = 0.3996$ and $\beta = 0.0049$, calculated based on the first and second mode frequencies of the structure (see Table 4.3 and Figure 4.3), was used to simulate structural damping in the dynamic analysis.

Table 4.3 Natural frequencies of the adopt 15 storey fixed base structure

Motion mode	Mode 1 (f_1)	Mode 2 (f_2)	Mode 3 (f_3)	Mode 4 (f_4)
Frequency (Hz)	0.830	2.341	4.018	5.781

Furthermore, the inelastic behaviour of structural elements was simulated using elastic-perfectly plastic material behaviour by specifying the yield stress. The elastic-perfectly plastic material model used in this study for inelastic analysis and design assumed that structural elements behave elastically until they reach the defined yield stress. The element that reaches the yield stress can continue to deform without inducing additional stresses. According to Shing and Tanabe (2001), the yield stress of concrete

material (σ_y) was assumed to be equal to the compressive strength of concrete (f_c'). Figure 4.4 illustrates the elastic-perfectly plastic behaviour of the structural elements used in this study. For the structural concrete utilised in this design and analysis, the specified compressive strength (f_c') and mass density (ρ) were assumed to be 32 MPa and 2400 kg/m^3, respectively. The modulus of elasticity of concrete (E) was calculated according to clause 3.1.2.a of the Australian Standard for Concrete Structures (AS3600 2009).

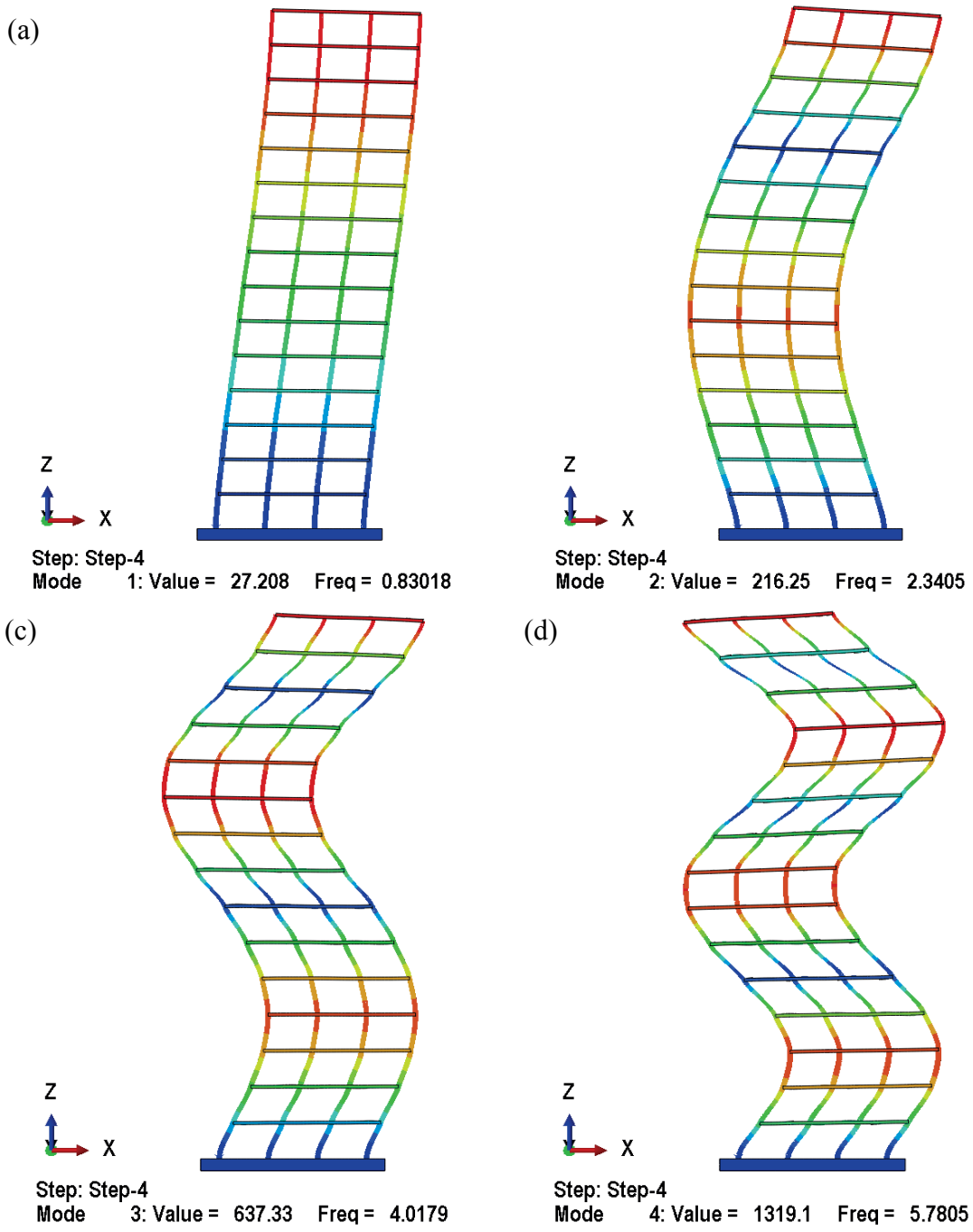

Figure 4.3 Representation of structural deformations for fixed base structure (a) first mode, (b) second mode, (c) third mode, and (d) forth mode

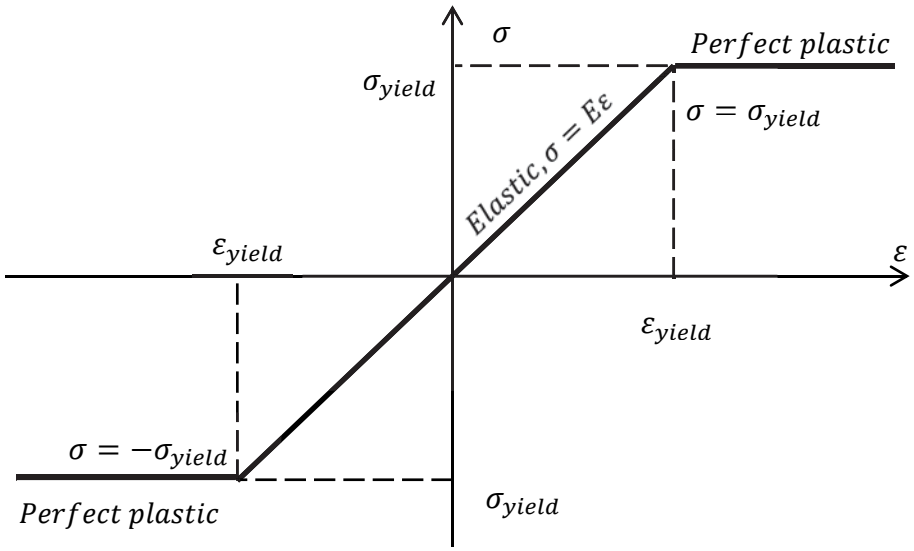

Figure 4.4 Elastic-perfectly plastic behaviour of structural elements

4.4.2 Soil model

The non-linearity of soil during an earthquake plays an important role in the dynamic response of soil-structure systems. The equivalent linear method has been in use for many years to calculate the wave propagation (and response spectra) in soil and rock at sites subjected to seismic excitations. In an equivalent-linear method adopted in this study, a linear analysis is carried out with some assumed initial values for the damping ratio and shear modulus in various regions of the model. Then the maximum cyclic shear strain is recorded for each element and used to determine the new values for damping and modulus by referring to the backbone curves relating the damping ratio and secant modulus to the amplitude of shear strain. Some empirical scaling factors are usually utilised when relating these strains to the model strains, and then these new values for the damping ratio and shear modulus are used in the next stage of the numerical analysis. The whole process is repeated several times, until there is no further change in the properties and the structural response. At this stage, "strain compatible" values of damping and modulus are recorded, and the simulation using these values is deemed to be the best possible prediction of the real behaviour. As described by Seed and Idriss (1969), the equivalent-linear method uses linear properties for each element because they remain constant under the influence of seismic excitations; those values are estimated from the mean level of

dynamic motion, as explained before, but since trial and error utilising nonlinear backbone curves to find the "strain compatible" values of damping and modulus is used, soil non-linearity was captured by this method.

Hysteresis of typical soils subjected to the cyclic loading can be described using two important characteristics of the hysteresis loop shape: inclination and breath. As explained by Kramer (1996), the inclination of the loop represents stiffness of the soil, which can be described at any point during the loading process by the tangent shear modulus. The breath of the hysteresis loop, which is related to the area of one hysteresis loop, represents the energy dissipation and can be described by the damping ratio. The parameters G_{sec} and ξ were used to describe the cyclic behaviour of soil in the equivalent linear analysis and are often referred to as the soil equivalent linear parameters Kramer (1996) in Equation (4.4) and (4.5)

$$G_{sec} = \frac{\tau_c}{\gamma_c} \tag{4.4}$$

$$\xi = \frac{W_D}{4\pi W_s} = \frac{1}{2\pi}\frac{A_{loop}}{G_{sec}\gamma_c^2} \tag{4.5}$$

where τ_c and γ_c are the shear stress and shear strain amplitudes, respectively;

W_D is the dissipated energy;

W_S is the maximum strain energy;

A_{loop} is the area of the hysteresis loop.

In addition, (Vucetic and Dobry 1991) conducted a comprehensive study on the number of cyclic test results available and concluded that the soil Plasticity Index (PI) controls the location of the backbone curves for a wide variety of cohesive soils. The numerical model developed in this study adopts the ready-to-use charts (Figure 4.6) provided by Vucetic and Dobry (1991) to estimate the modulus degradation and damping ratio of cohesive soils in dynamic analysis. These charts provide a design tool for practising engineers because the PI of soil is readily available.

It should be noted that as the plasticity index PI increases, G_{sec}/G_{max} increases while the damping ratio ξ decreases.

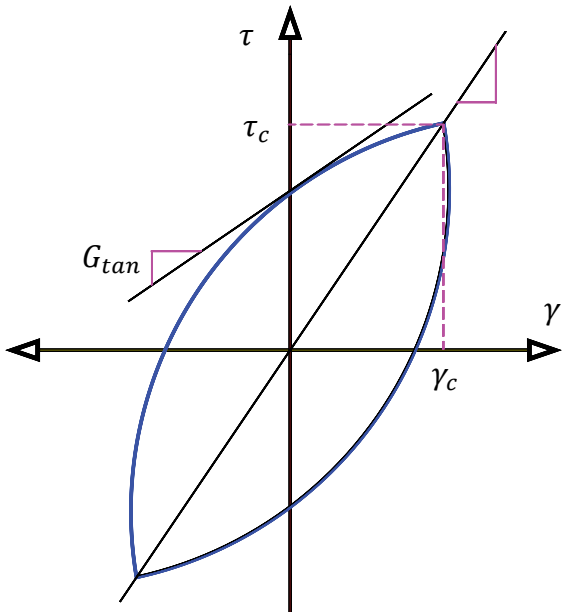

Figure 4.5 Secant shear modulus, G_{sec} and tangent shear modulus G_{tan}

Since each earthquake record induces different levels of shear strain in the soil deposit, the values for soil damping and modulus would be different for each earthquake when the non-linearity of the soil is considered. Table 4.4 summarises the "strain compatible" parameters of soil used in this study when developing the 3D numerical model for four earthquakes. As mentioned earlier, since the properties of the subsoil were extracted from actual in-situ and laboratory tests (Rahvar 2006), they have merit over those assumed parameters which may not completely conform to reality.

Soil damping, which simulates the absorption of energy by particles of soil and their interaction during wave propagation, reduces the wave amplitude and has a significant influence on how the superstructure performs. Das (1983) mentioned that the most commonly used mechanism for representing energy dissipation is viscous damping which assumes that the dissipative forces are a function of particle velocity. In this study the nonlinear variations of energy losses in the soil during an earthquake were simulated using the Rayleigh damping formulation.

Park and Hashash (2004) investigated whether the Rayleigh damping formulation could perform a nonlinear dynamic analysis of soil deposits and concluded that it can provide acceptable results for many applications as long as the parameters for the deposit of soil are selected accurately.

Table 4.4 Adopted soil parameters in three dimensional finite element model for the soil-foundation-structure system

Soil Properties		Denote	Unit	Value	Reference
Mass density		ρ	kg/m^3	1470	Rahvar (2006)
Shear wave velocity		V_s	m/s	150	
Poisson's ratio		v	-	0.4	
Plasticity index		PI	-	15%	
Mass damping factor	Northridge (γ_{max}=0.26%, G/G_{max}=0.25, ξ=15.9%)	α	-	0.937	Vecetic and Dobry (1991); (Park and Hashash, 2004)
	Kobe (γ_{max}=0.20%, G/G_{max}=0.3, ξ=14.6%)		-	0.942	
	Hachinohe (γ_{max}=0.03%, G/G_{max}=0.65, ξ=7.2%)		-	0.141	
	El-Centro (γ_{max}=0.13%, G/G_{max}=0.35, ξ=12.8%)		-	0.893	
Stiffness damping factor	Northridge (γ_{max}=0.26%, G/G_{max}=0.25, ξ=15.9%)	β	-	0.020	
	Kobe (γ_{max}=0.20%, G/G_{max}=0.3, ξ=14.6%)		-	0.017	
	Hachinohe (γ_{max}=0.03%, G/G_{max}=0.65, ξ=7.2%)		-	0.019	
	El-Centro (γ_{max}=0.13%, G/G_{max}=0.35, ξ=12.8%)		-	0.014	

Considering the frequency dependent nature of these Rayleigh damping formulations, the frequencies/modes selected to define the damping function govern the accuracy of the time domain solution, but care should be exercised when selecting frequencies to avoid any negative damping in the resulting frequency dependent damping (Park and Hashash (2004)). The two significant frequencies can be chosen in part to cover the range of frequencies where there is significant content of input motion. Kramer (1996) presented the following equation to calculate the natural frequencies of the soil deposit:

$$f_n = \frac{V_S}{4H}(2n-1) \tag{4.6}$$

where n is the mode number, f_n is the natural frequency of the corresponding mode, V_S is the shear wave velocity of the soil deposit, and H is its thickness. Referring to Figure 4.7, the two significant frequencies are chosen covering the range of dominant frequencies of the ground motion. In this study, following the recommendations by Park and Hashash (2004), a set of frequencies corresponding to the "strain compatible" shear modulus values for different earthquakes are selected.

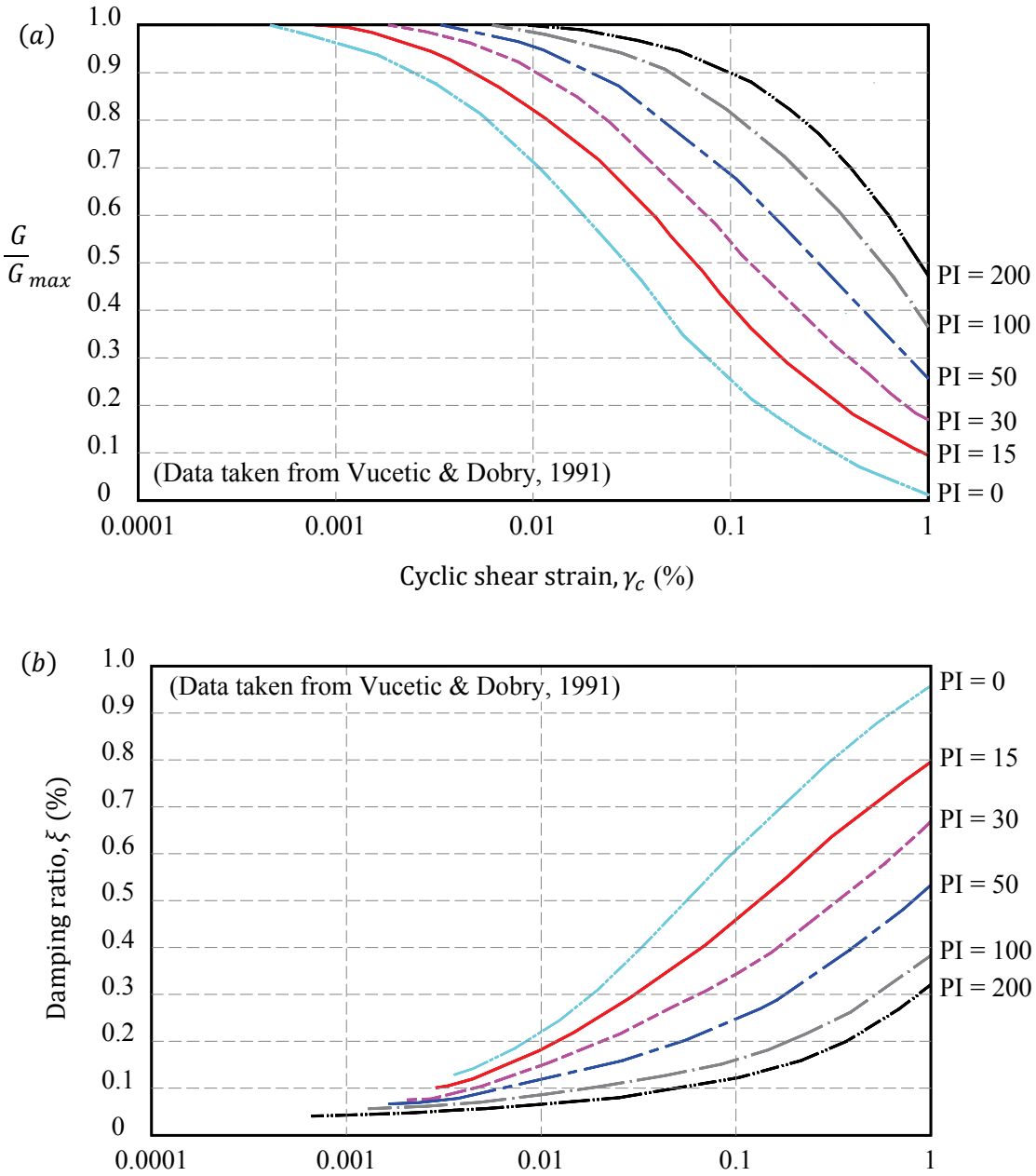

Figure 4.6 Backbone curves relating (a) shear stiffness and (b) damping ratio to cyclic shear strain for cohesive soils

The Rayleigh damping parameters used in the numerical model are summarised in Table 4.4 and Figure 4.7.

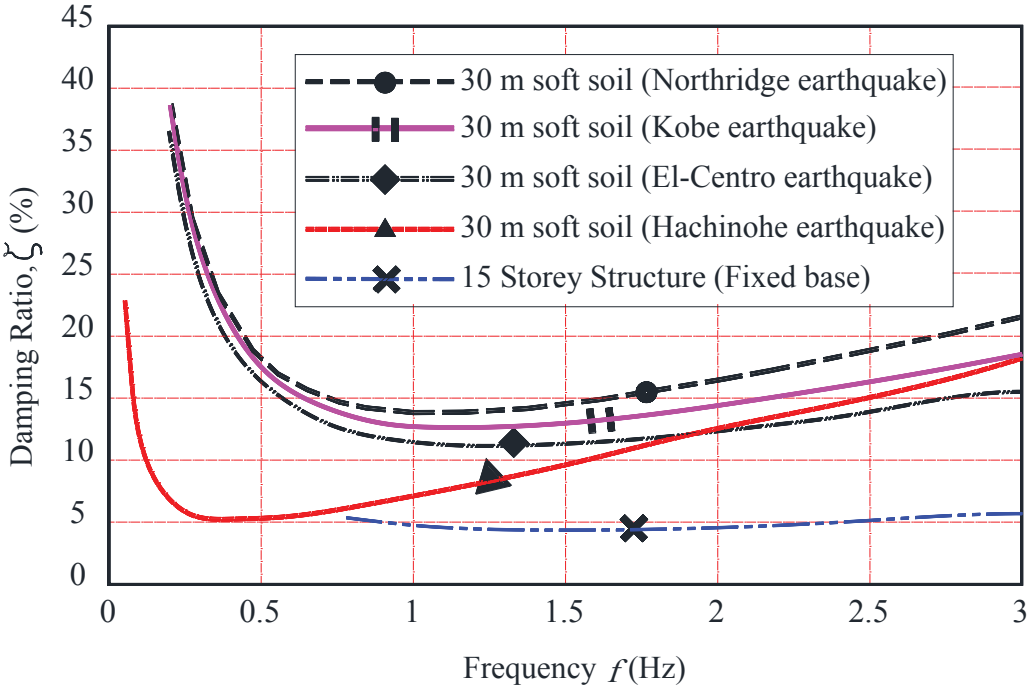

Figure 4.7 Adopted damping variations in this study for soft soil deposit and structure for numerical simulation of dynamic soil-foundation-structure interaction

The soil medium was modelled using C3D8R elements (three-dimensional, 8-node linear brick, reduced integration, hourglass control elements), as shown in Figure 4.8 (a) where, due to reduced integration, the locking phenomena does not occur, but the element tends to be not stiff enough in bending, which is not critical when modelling soil. Moreover, since the integration point is located in the middle of this element, small elements are needed to capture a stress concentration at the boundaries.

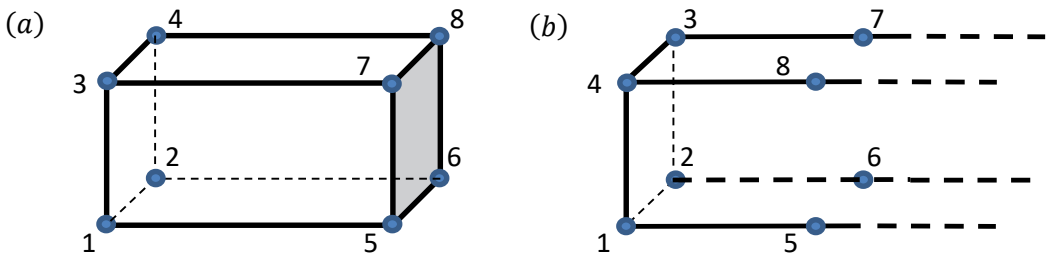

Figure 4.8 Employed element types in the finite element numerical model: (a) soil elements (C3D8R); and (b) infinite elements (CIN3D8)

4.4.3 Contact surfaces

The contact surfaces were used to incorporate the different mechanical characteristics of the soil and the shallow foundation, while capturing any possible uplift and sliding of the foundation over the subsoil during shaking excitations. In ABAQUS, contact elements or surfaces can be used to model the interface between the foundation and the soil surface during shaking excitations. For the soil-foundation-structure interaction analysis in this study, surface-based contacts were defined such that the master surface is the top surface of the soil and the slave surface is the bottom surface of the foundation. Moreover, finite sliding formulation and the surface-to-surface discretisation method were utilised for the contact simulation to consider the shape of the master and slave surfaces when defining the contact constraints. In addition, the "Augmented Lagrange method" was used in conjunction with the penalty stiffness being 1000 times more than the representative underlying element stiffness as recommended by ABAQUS (2012). Lagrange multipliers are only used for the augmented Lagrange method if the penalty stiffness exceeds 1000 times the representative underlying element stiffness; otherwise, no Lagrange multipliers are used. In this numerical modelling, since the penalty stiffness ratio does not exceed 1000, there was no need to incorporate the Lagrange multiplier.

The mechanical properties of the contact surfaces defining the tangential and normal behaviour of the contact surfaces can influence the results of the numerical simulation and should be chosen with great rigor. Normal behaviour adopts hard contact in a pressure-over closure relationship, where a hard contact implies that the surfaces transmit no contact pressure unless the nodes of the slave surface make contact with the master surface, no penetration is allowed at the location of each constraint (depending on the method used to enforce constraint, this condition will either be strictly satisfied or approximated), and there is no limit to the magnitude of contact pressure that can be transmitted when the surfaces are in contact. The hard contact with pressure-over closure relationship in the method used to enforce constraint expressed using Figure 4.7, is illustrated in Figure 4.9. In Figure 4.7, p is the contact pressure and h is the clearance or gap between two contacting surfaces.

$$p \times h = 0, p \geq 0 \text{ and } h \geq 0 \tag{4.7}$$

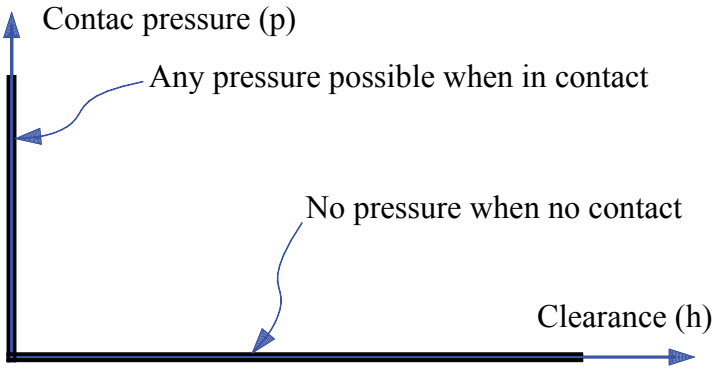

Figure 4.9 Pressure - over closure relationship for 'hard' contact to define the normal behaviour of contact surfaces in the numerical model

A subroutine developed in the FORTRAN programming language and linked to ABAQUS was used to model the tangential behaviour of contact surfaces in the finite element model. This subroutine defines the variable required in the numerical simulation in a way that corresponds to the classical Mohr-Coulomb failure model. Since the Mohr-Coulomb failure model cannot be directly defined in the simulation, a modified version of this model (Equation (4.8)) was coded in the FRIC_COEF subroutine to define the isotropic frictional coefficient between the contacting surfaces.

$$\mu = \frac{\tau}{\sigma} = tan(\varphi) + \frac{c}{\sigma} \tag{4.8}$$

where μ is the coefficient of friction, τ is the shear strength, σ is the normal stress, c is the cohesion intercept of the failure envelope, φ is internal frictional angle and υ is the slope of the failure envelope or the internal friction angle.

4.4.4 Boundary conditions

The boundary conditions in the numerical model were prescribed at the boundaries of the numerical grids. The far-field soil was represented by infinite elements to account for the energy absorbed from the unbounded soil domain while horizontal deformation was also simulated realistically Figure 4.2. The three-dimensional, 8-node linear one-way infinite brick (CIN3D8) elements were used to model the infinite elements, as shown in Figure 4.8 (b), but unlike the other numerical elements, these infinite elements have defined orientations. Referring to Figure 4.8 (b), nodes 1, 2, 3 and 4 were connected to

defined finite elements (subsoil), while the other nodes (nodes 5, 6, 7 and 8) were oriented outwards from the defined finite elements.

During dynamic steps, the infinite elements introduced additional normal and shear tractions on the finite element boundary that were proportional to the normal and shear components of the velocity of the boundary. These boundary damping constants were chosen to minimise the reflection of dilatation and shear wave energy back into the finite element mesh. The infinite elements maintained the static force that was present at the end of the gravity (static) analysis stage, so there was no need to displace the boundaries for the time-history dynamic analysis stage (ABAQUS 2012).

The dynamic response of the infinite elements was based on a consideration of the plane body waves travelling orthogonally to the boundary. The governing equation of motion in the boundaries is presented in Equation (4.9), and the distributed damping on the infinite boundaries of the developed numerical model in the normal and shear directions are as presented in Equation (4.10).

$$\rho\ddot{u}_i = G\frac{\partial^2 u_i}{\partial x_i \partial x_j} + (\lambda + \mathrm{G})\frac{\partial^2 u_j}{\partial x_i \partial x_j} \tag{4.9}$$

$$d_p = G\frac{\lambda + 2\mathrm{G}}{c_p};\ d_s = \rho c_s \tag{4.10}$$

where ρ, G, λ are the soil properties, c_p and c_s are the velocities of the normal wave and shear wave, respectively, d_p and d_s are the distributed damping of the boundary in the normal and shear directions, respectively, u_i, u_j is the material particle displacement, x_i and x_j are the positions of noted i and j.

The values of the boundary damping were built into the infinite elements in ABAQUS. As discussed earlier, these boundaries can transmit all the normally impinging plane body waves, and even for problems that involve non-plane body waves that do not impinge on the boundary from an orthogonal direction, the defined boundaries work well (Cohen and Jennings 1983). Since the boundaries were "quiet" rather than silent (perfect transmitters of all waveforms), and because the boundaries relied on the medium adjacent to them being linear elastic, they should be placed a reasonable distance away from the region of main interest; which was carried out in this study. During the dynamic response

analysis following the static gravity preload (as is common in geotechnical applications), the traction provided by the infinite elements to the boundary of the finite element mesh consisted of the constant stress obtained from the static response with the quiet boundary damping stresses added.

Table 4.5 Characteristics of the adopted earthquake records

Earthquake	Country	Year	PGA (g)	M_w (R)	Duration (s)	Type	Hypocentral Distance* (km)
Northridge	USA	1994	0.843	6.7	30.0	Near field	9.2
Kobe	Japan	1995	0.833	6.8	56.0	Near field	7.4
El Centro	USA	1940	0.349	6.9	56.5	Far field	15.69
Hachinohe	Japan	1968	0.229	7.5	36.0	Far field	14.1

(*) Obtained from (PEER 2012)

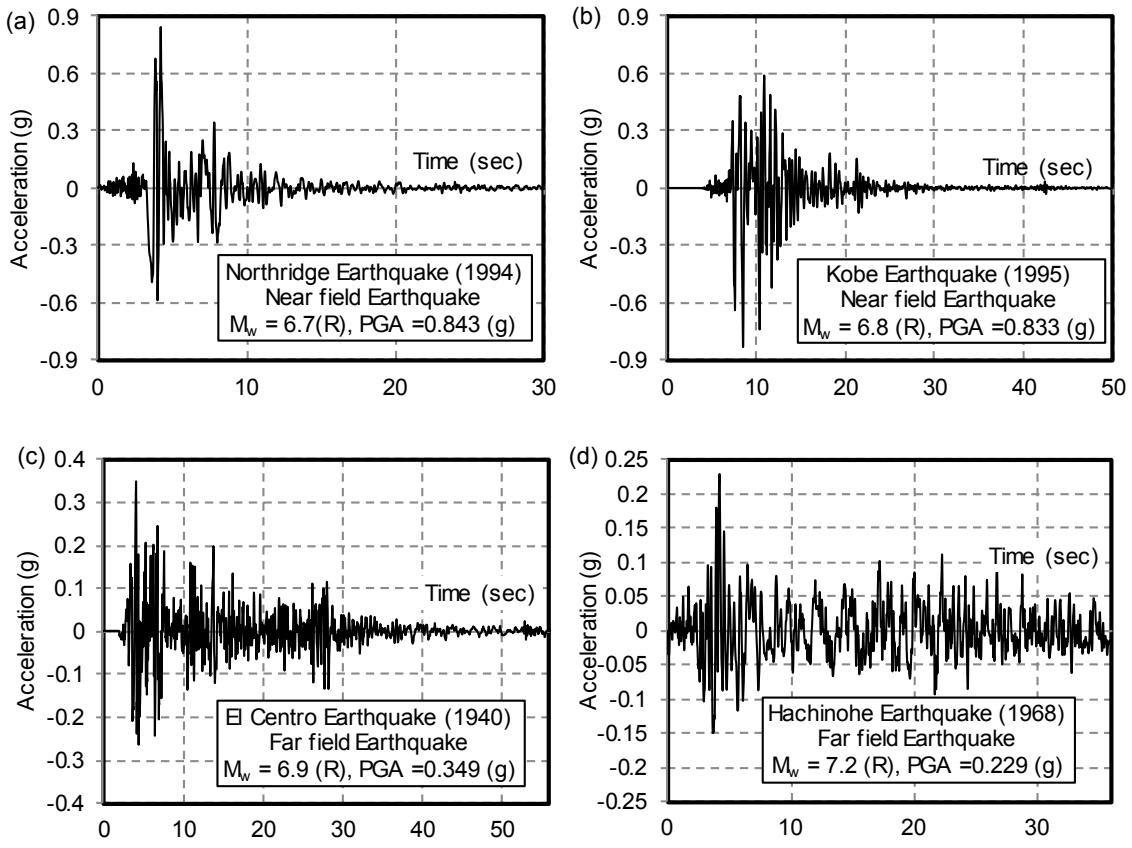

Figure 4.10 Adopted earthquake records: : (a) 1994 Northridge earthquake; (b) 1995 Kobe; (c) 1940 El Centro earthquake; and (d) 1968 Hachinohe earthquake

Note that the material properties assigned to the infinite elements must match the material properties of the adjacent finite elements in the model (Table 4.4). Moreover, only linear behaviour can be associated with infinite elements, but since they are located in the far field, the effect of this simplified assumption on the response of the superstructure under shaking excitations is negligible.

A rigid boundary condition was used to simulate bedrock (the bottom of the soil medium grid) in the seismic soil-foundation-structure interaction analysis, as suggested by other researchers (Fatahi and Tabatabaiefar 2013), while the earthquake input motions were applied at the bedrock propagating upwards through the entire model.

4.4.5 Input earthquake records

Four benchmark earthquake input motions, including the 1994 Northridge, the 1995 Kobe, the 1940 El Centro, and the 1968 Hachinohe earthquakes (referring to Table 4.5 and Figure 4.10), were imposed onto the finite element numerical model while conducting a time-history analysis. Figure 4.2 shows the model components and the numerical mesh for the building supported by the shallow foundations. Note that to make the results comparable for different size foundations without being affected by the meshing variables, the same generated mesh was used for all sizes of the shallow foundations. The generated mesh shown in Figure 4.2 consisted of 42123 elements and 61021 nodes.

Due to the large size of the model (around 70 Giga-bytes for a single case), the fast computation facilities at the University of Technology Sydney were used to conduct this time-history analysis, and even then it took around 50 hours to run a single case under the applied earthquake excitation.

The results of the 3D finite element numerical simulation are presented and discussed in the following section.

4.5 Results and discussion

At first, the fixed-base structure excluding SFSI was simulated. The responses of the fixed-base structure under the influence of four earthquake excitations were used as a comparison benchmark to investigate the influence of SFSI on structures with various shallow foundation sizes. The natural frequencies of the fixed-base structure are presented

in Table 4.3 and Figure 4.3 shows the deformed shape of the structure on its natural modes.

The results of the 3D numerical model developed for the fifteen-storey building supported by shallow foundations of different sizes and the fixed-base building subjected to the 1994 Northridge, 1995 Kobe, 1940 El Centro, and 1968 Hachinohe earthquakes are summarised and compared in Figure 4.11, Figure 4.12, Figure 4.13, and Figure 4.14, respectively. To determine the lateral deflections, the movement of the foundation was subtracted from the movement of the storeys, which means that all the records are relative to the movements of the foundation on the soil surface level.

$$d_i(t) = u_i(t) - u_0(t), \qquad i = 1,2,3,\dots,15 \tag{4.11}$$

where $d_i(t)$ is deflection history at level (i); $u_i(t)$ is horizontal displacement history at level (i); $u_0(t)$ is horizontal displacement history at level (0).

This data was based on the lateral deformation of each storey when maximum deflection at the top level occurred because as Hokmabadi *et al.* (2012) stated, this approach gives a more reasonable pattern of structural deformations than approach where the maximum absolute deformation of the storeys, regardless of the time they occurred and were recorded.

According to Figure 4.11 (a), Figure 4.12 (a), Figure 4.13 (a), and Figure 4.14 (a), SFSI amplified the maximum lateral deflection of the superstructure during shaking excitations, as was expected. For instance, the maximum lateral deformation of the fixed-base building (excluding SFSI) under the 1994 Northridge earthquake was 395 mm, while the same building experienced a lateral deformation of up to 590 mm (49% more) when it was supported by a 1.1B shallow foundation that accounts for SFSI. Moreover, as a general trend, by increasing the size of the shallow foundation from 1.1B to 2.0B the structure experiences less lateral deformation. For instance, an increase in the size of the foundation from 1.1B to 1.5B resulted in up to 25% less lateral deformation under 1940 El Centro earthquake Figure 4.13 (a). This is a considerable reduction in the lateral deformation of a structure subjected to strong earthquakes.

In addition, the upper level has higher maximum lateral deflections for all cases of the four earthquakes. Details of the maximum lateral deflections at the top of the

superstructures (level 15) for different foundation sizes subjected to the four earthquakes were listed on Table 4.7.

Table 4.6 Variations of natural frequencies of soil-structure systems with different foundation size

		Frequency (Hz)							
Soil Properties (Adopted Earthquake)		G/G_{max}=0.25, ξ=15.9% (Northridge)		G/G_{max} =0.3, ξ=14.6% (Kobe)		G/G_{max} =0.65, ξ=7.2% (Hachinohe)		G/G_{max} =0.35, ξ=12.8% (El-Centro)	
Motion mode		Mode 1 (f_1)	Mode 2 (f_2)	Mode 1 (f_1)	Mode 2 (f_2)	Mode 1 (f_1)	Mode 2 (f_2)	Mode 1 (f_1)	Mode 2 (f_2)
Model/ Foundation Size	L=1.1B	0.425	2.266	0.465	2.275	0.604	2.305	0.485	2.279
	L=1.2B	0.431	2.267	0.472	2.276	0.615	2.307	0.492	2.280
	L=1.3B	0.443	2.271	0.486	2.280	0.637	2.311	0.508	2.284
	L=1.4B	0.449	2.274	0.493	2.283	0.648	2.313	0.515	2.287
	L=1.5B	0.453	2.275	0.498	2.284	0.657	2.315	0.521	2.288
	L=1.7B	0.457	2.279	0.505	2.288	0.673	2.320	0.529	2.293
	L=2.0B	0.462	2.282	0.513	2.292	0.692	2.328	0.539	2.297
Fixed base Structure		Mode 1 (f_1)= 0.830 Hz & Mode 2 (f_2) = 2.341 Hz							

Table 4.7 Variations of maximum lateral deflection at top of level 15 with different foundation size

		Maximum lateral deflection (mm)			
Earthquake		1994 Northridge	1995 Kobe	1940 El-Centro	1968 Hachinohe
Shallow foundation with Foundation Size	L=1.1B	589.197	381.643	184.296	138.280
	L=1.2B	577.056	377.971	172.136	136.028
	L=1.3B	549.976	374.207	151.660	133.103
	L=1.4B	535.456	371.341	143.831	131.541
	L=1.5B	521.766	369.609	138.151	128.315
	L=1.7B	502.134	362.451	135.074	125.475
	L=2.0B	477.877	346.839	129.397	124.418
Fixed base Structure		394.826	300.484	104.867	104.726

The corresponding maximum inter-storey drifts of the building for shallow foundations with different sizes were calculated using the following equation, and based on the Australian standard (AS1170.4 2007) as following:

$$Drift = \frac{d_{i+1} - d_i}{h} \tag{4.12}$$

where d_{i+1} is deflection at level $(i + 1)$;

d_i is deflection at level (i);

h is the height of the level, it is the same for all fifteen floors for these models.

The seismic performance (performance level) in the performance-based seismic design is described by considering the maximum allowable damage state (damage performance) for an identified seismic hazard (hazard level). The performance levels describe the state of structures after being subjected to a certain hazard level, and based on (BSSC 1997) are classified as: fully operational, operational, life safe, near collapse, or collapse. Overall lateral deflection, ductility demand, and inter-storey drifts are the most commonly used damage parameters. These above mentioned five qualitative levels are related to the corresponding quantitative maximum inter-storey drifts (as a damage parameter) of: <0.2%, <0.5%, <1.5%, <2.5%, and >2.5%, respectively (BSSC 1997). Moreover, most of the force-based design codes use an additional check in terms of limiting the inter-storey drifts to ensure that particular deformation-based criteria are met. For example, ASCE 7-10 (2010) defines allowable storey drift for structures by considering the type and risk category of the structure. The Australian Earthquake Code (AS1170.4 2007) indicates 1.5% as the maximum allowable storey drift. According to Figure 4.11 (b), Figure 4.12 (b), Figure 4.13 (b), and Figure 4.14 (b) increasing the size of a shallow foundation reduces the maximum inter-storey drifts experienced by the building. For instance, an increase in the size of the foundation from 1.1B to 1.4B reduces up to 23% inter-storey drift under the 1940 El Centro earthquake. As a result, a larger foundation size is an option that design engineers can use to control the performance level of buildings under shaking loads rather than using larger structural sections. Figure 4.15 presents the time-history rocking response of a fifteen-storey structure supported by shallow foundations of various sizes. Rocking occurs when the inertial forces generated in a superstructure cause compression on one side and tension on the other, which in turn results in settlement on one side and a possible uplift on the other side.

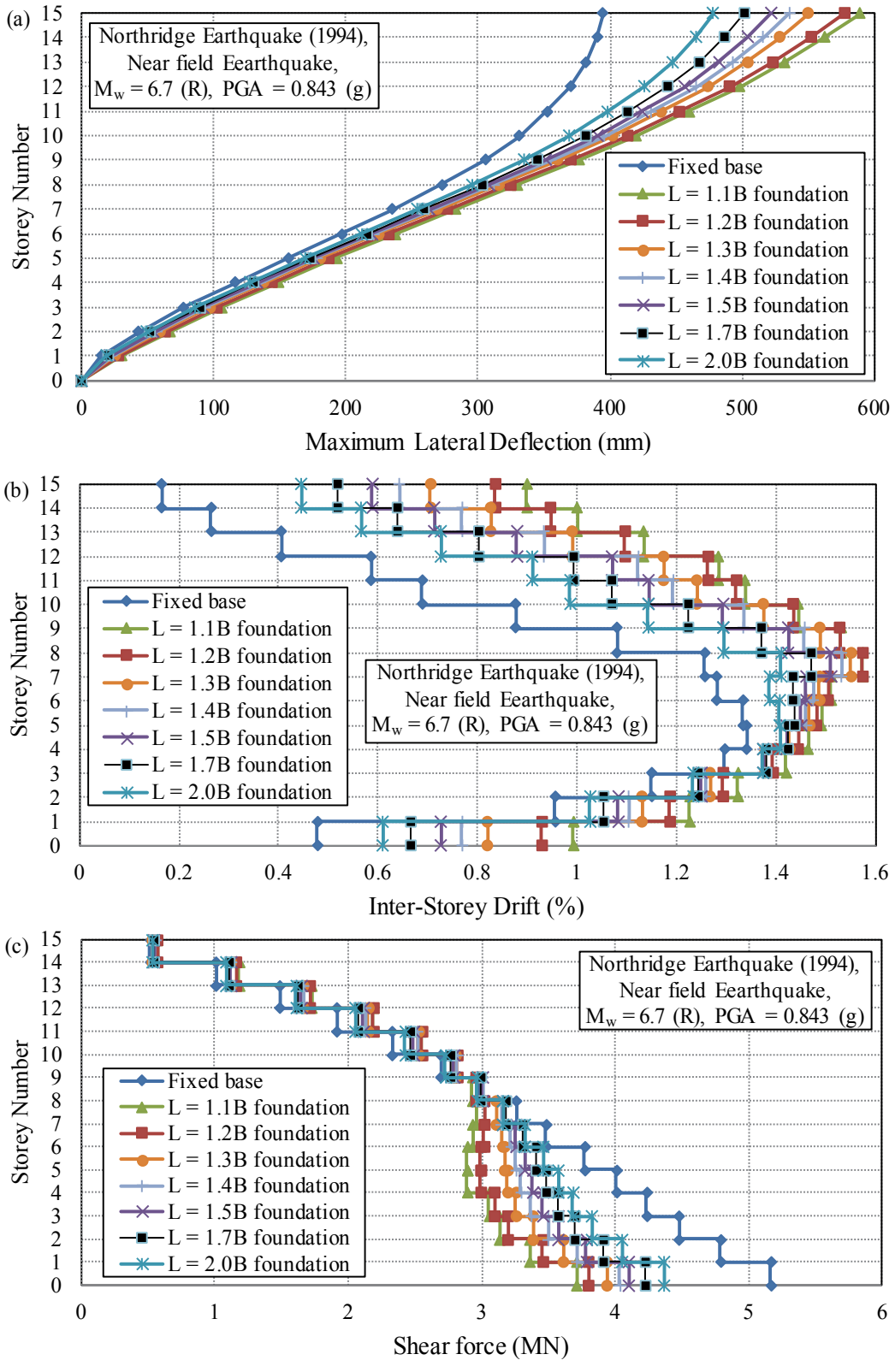

Figure 4.11 Response of the fifteen-storey structure supported by shallow foundations with varies sizes under the influence of 1994 Northridge earthquake: (a) maximum lateral deflection; (b) maximum inter-storey drifts; (c) maximum shear force distribution.

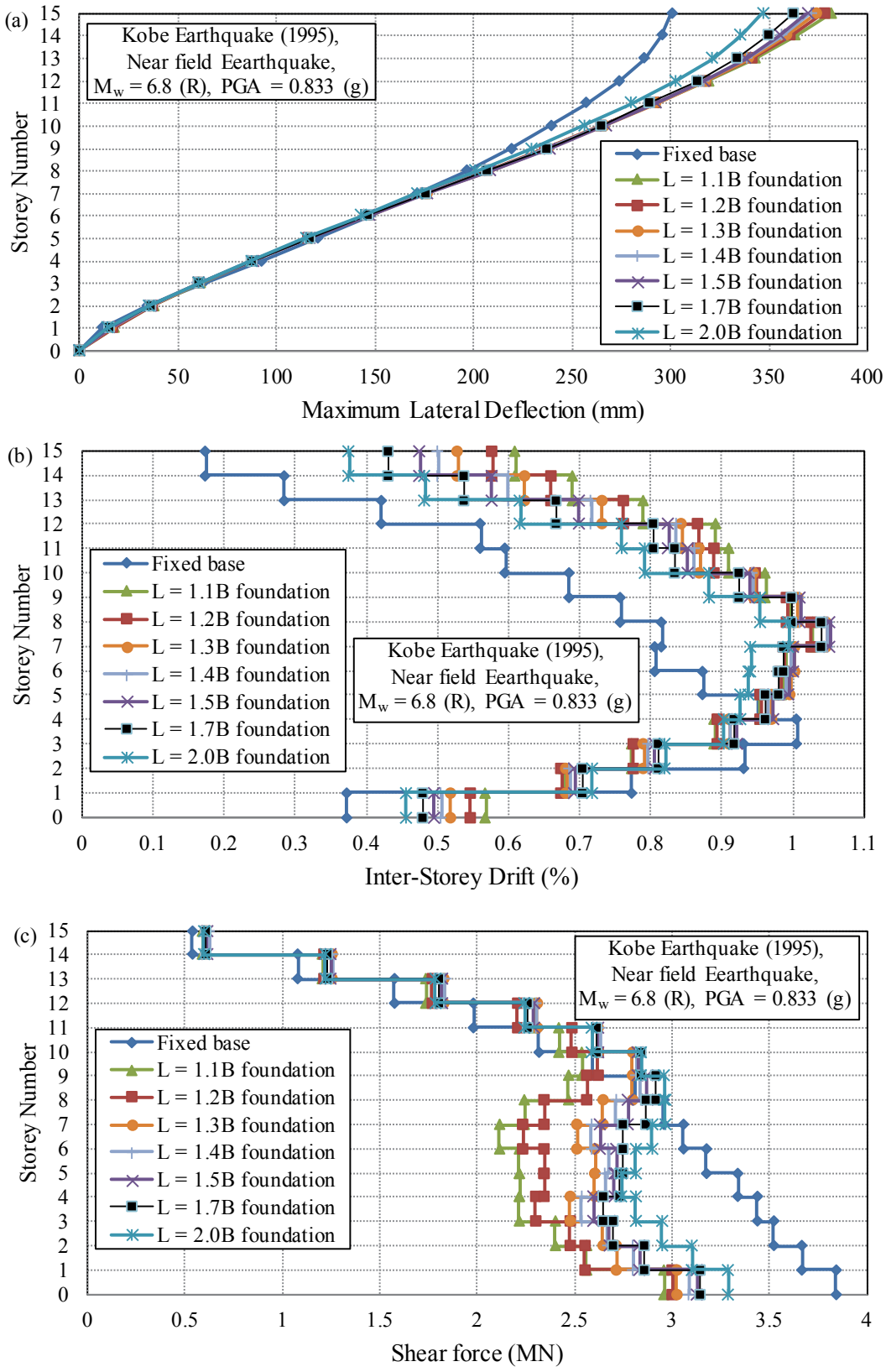

Figure 4.12 Response of the fifteen-storey structure supported by shallow foundations with varies sizes under the influence of 1995 Kobe earthquake: (a) maximum lateral deflection; (b) maximum inter-storey drifts; (c) maximum shear force distribution.

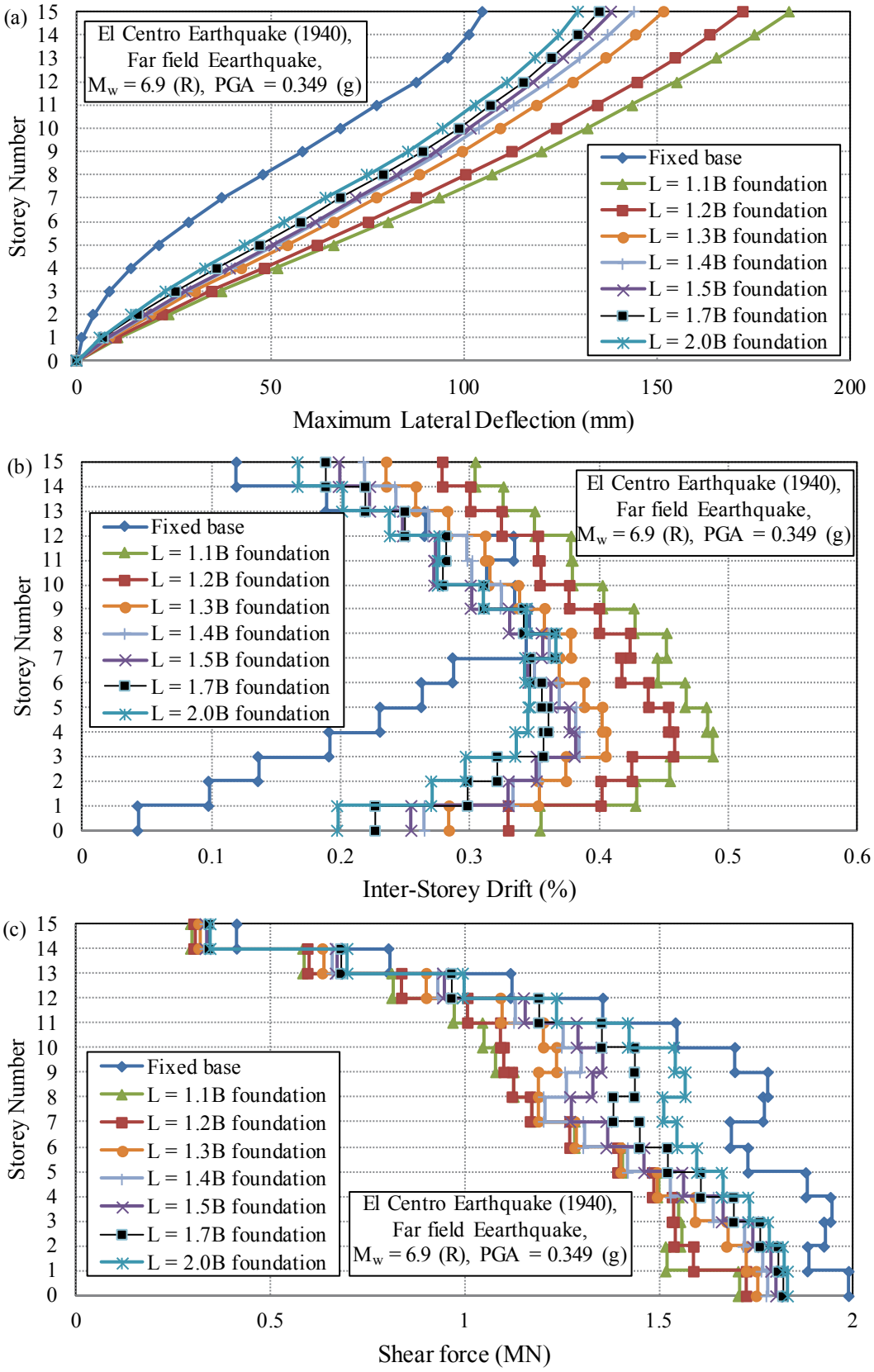

Figure 4.13 Response of the fifteen-storey structure supported by shallow foundations with varies sizes under the influence of 1940 El Centro earthquake: (a) maximum lateral deflection; (b) maximum inter-storey drifts; (c) maximum shear force distribution.

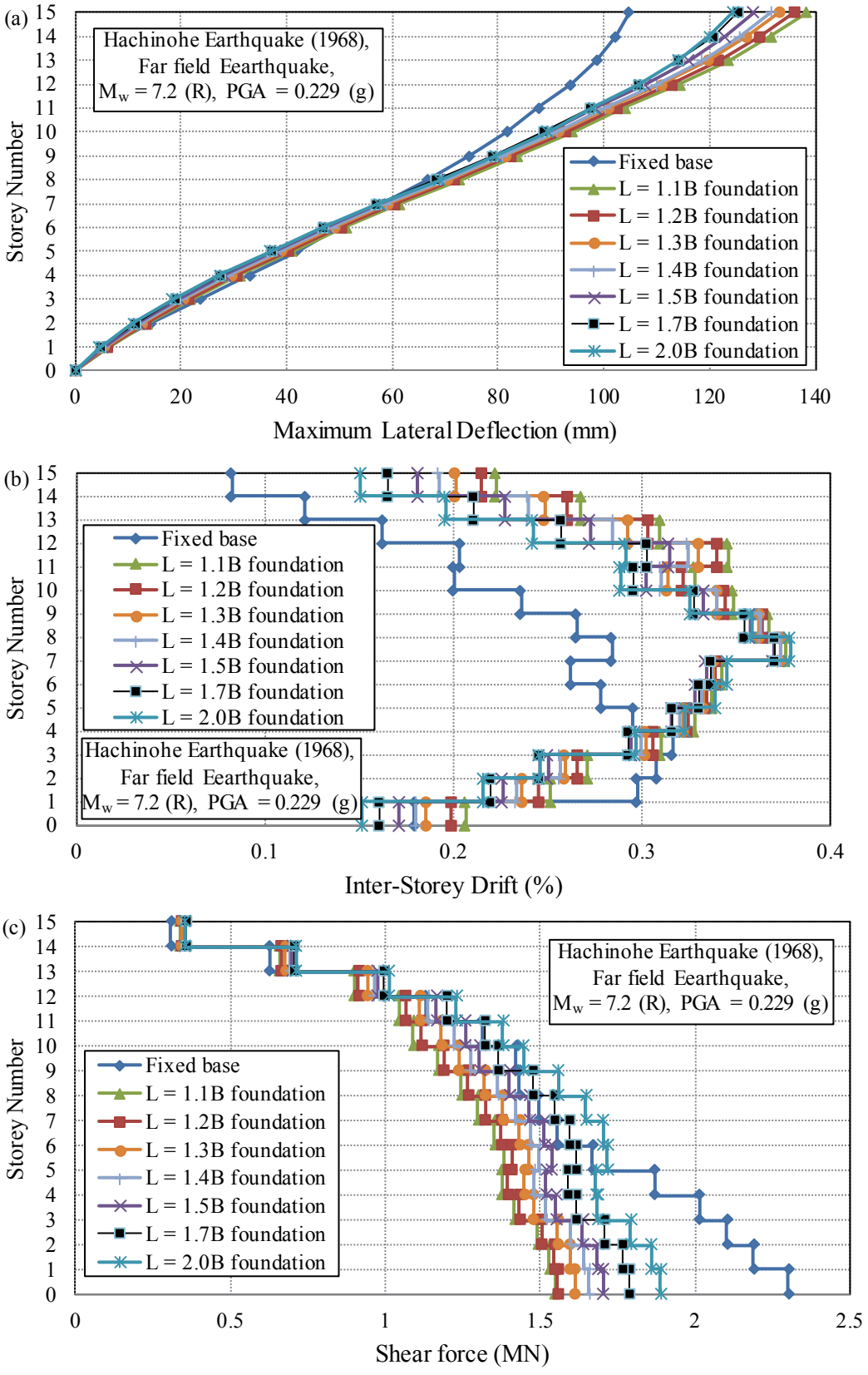

Figure 4.14 Response of the fifteen-storey structure supported by shallow foundations with varies sizes under the influence of 1968 Hachinohe earthquake: (a) maximum lateral deflection; (b) maximum inter-storey drifts; (c) maximum shear force distribution.

other, which in turn results in settlement on one side and a possible uplift on the other side. The maximum rocking of a fifteen-storey structure supported by shallow foundations of various sizes under the influence of four earthquake excitations is shown in Figure 4.16. Accordingly, there was a direct correlation between the size of the shallow foundation and the maximum rocking experienced by a structure, where a superstructure supported by a larger shallow foundation experienced much less rocking than the building supported by a smaller shallow foundation. For instance, the maximum rocking angle of the structure supported by 1.1B foundation under 1940 El Centro earthquake was 0.144 degree, while the corresponding value for the structure supported by 1.5B foundation was 0.084 degree (42% less rocking). How far a structure will rock is the key parameter that directly influences the maximum lateral deflections and inter-storey drifts experienced by the structure during strong earthquakes. Consequently, adopting larger shallow foundations caused less rocking (Figure 4.16) which resulted in less lateral deformation (Figure 4.11 (a) - Figure 4.14 (a)) of the structure under shaking excitations.

Figure 4.17 illustrates the response spectrum of the ground motions at the base of the structure supported by shallow foundations of various sizes. The response spectrum presents the peak acceleration of a single degree of freedom (SDF) system with 5% damping, and with different natural periods for the recorded earthquake motions on the ground surface. The size of a shallow foundation may influence the characteristics of earthquake motion at the base of the structure by altering the inertial and kinematic interactions. The inertial force generated by the mass of the structure and the foundation can create more motion at the base than with free field motion (kinematic interaction). On the other hand, as Kramer (1996) explained, the inability of a shallow foundation to match the free field deformation (kinematic interaction) also contributes to the variations in the base motions. Kinematic interaction reduces the foundation motion relative to the free field motion because the stiffness of the foundation and surrounding soil differs, as Veletsos and Prasad (1989) concluded. Referring to Figure 4.7, although by increasing the size of a foundation the mass and stiffness of the system increases, the influence of the size of a shallow foundation on the shape of the base response spectrum was insignificant in the cases investigated in this study and can be omitted.

(a)

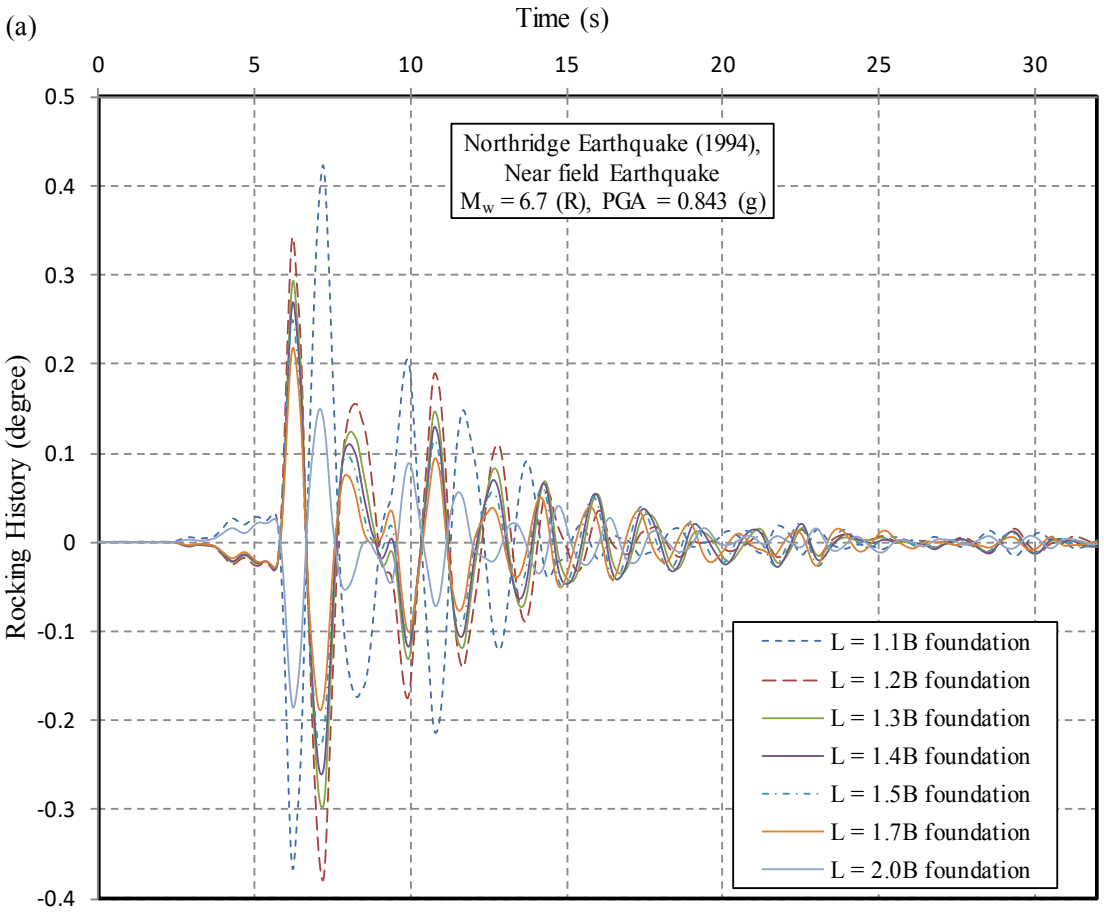
Time (s)
0
5
10
15
20
25
30
0.5
0.4
0.3
0.2
0.1
0
-0.1
-0.2
-0.3
-0.4
Rocking History (degree)
Northridge Earthquake (1994),
Near field Earthquake
Mw = 6.7 (R), PGA = 0.843 (g)
L = 1.1B foundation
L = 1.2B foundation
L = 1.3B foundation
L = 1.4B foundation
L = 1.5B foundation
L = 1.7B foundation
L = 2.0B foundation

(b)

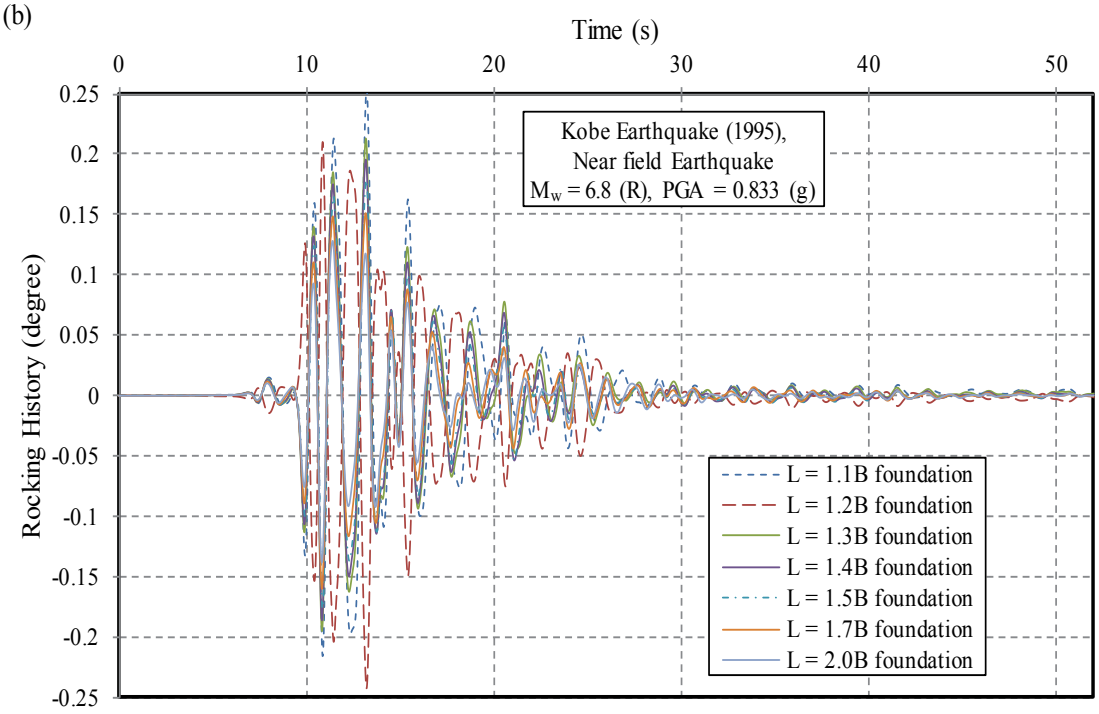
Time (s)
0
10
20
30
40
50
0.25
0.2
0.15
0.1
0.05
0
-0.05
-0.1
-0.15
-0.2
-0.25
Rocking History (degree)
Kobe Earthquake (1995),
Near field Earthquake
Mw = 6.8 (R), PGA = 0.833 (g)
L = 1.1B foundation
L = 1.2B foundation
L = 1.3B foundation
L = 1.4B foundation
L = 1.5B foundation
L = 1.7B foundation
L = 2.0B foundation

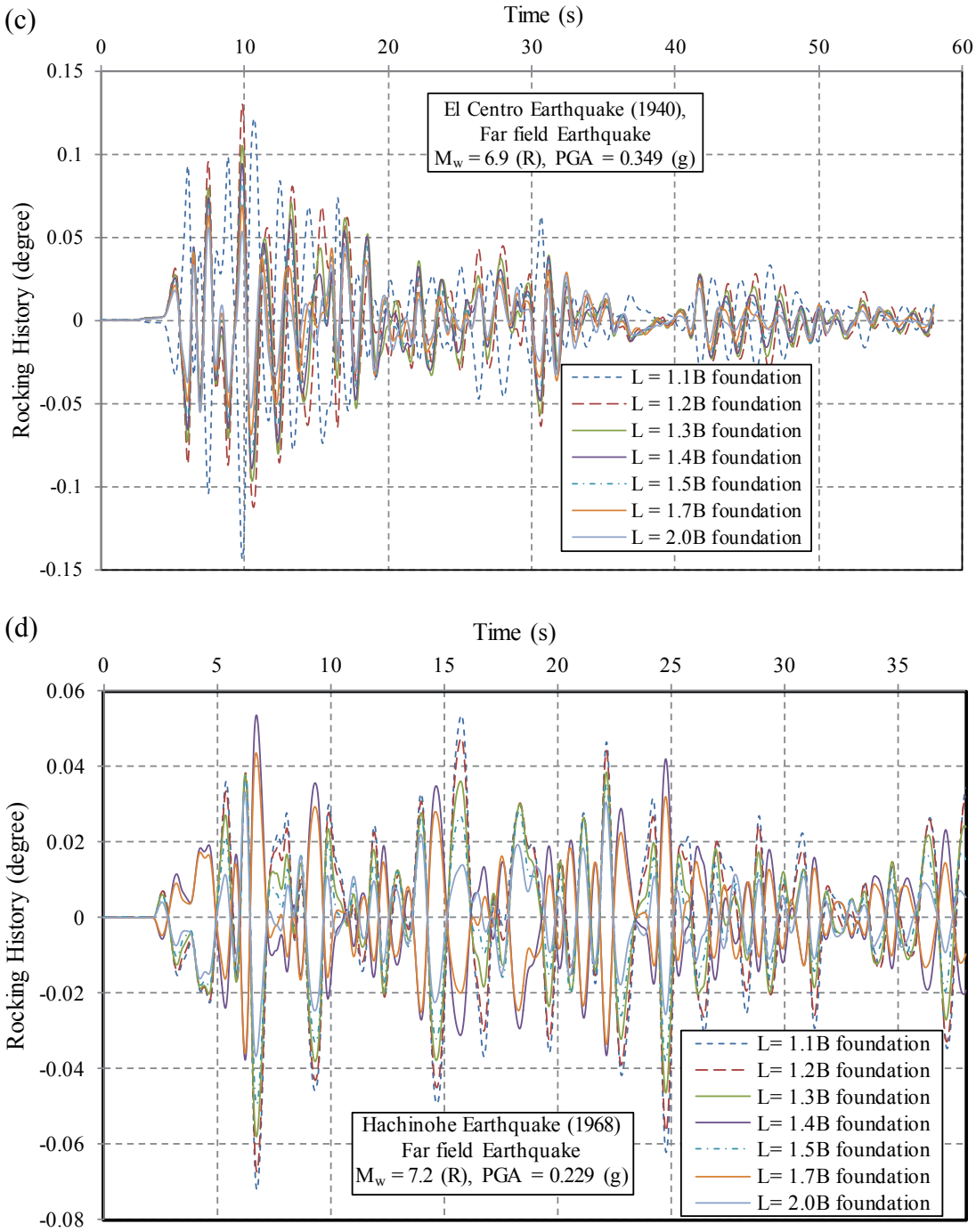

Figure 4.15 Time-history rocking response of the fifteen-storey structure supported by shallow foundations with varies sizes under the influence of: (a) 1994 Northridge earthquake; (b) 1995 Kobe; (c) 1940 El Centro earthquake; (d) 1968 Hachinohe earthquake.

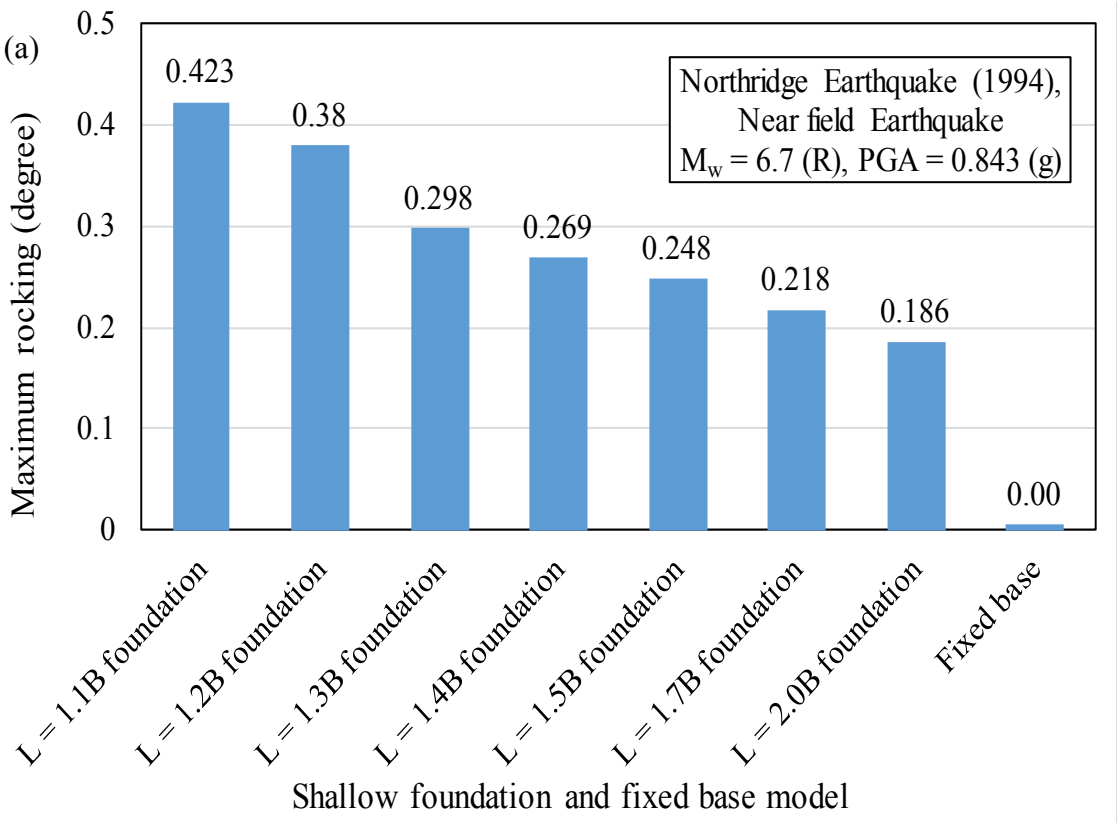
(a)
Maximum rocking (degree)
0.5
0.4
0.3
0.2
0.1
0
0.423
0.38
0.298
0.269
0.248
0.218
0.186
0.00
Northridge Earthquake (1994),
Near field Earthquake
M_w = 6.7 (R), PGA = 0.843 (g)
L = 1.1B foundation
L = 1.2B foundation
L = 1.3B foundation
L = 1.4B foundation
L = 1.5B foundation
L = 1.7B foundation
L = 2.0B foundation
Fixed base
Shallow foundation and fixed base model

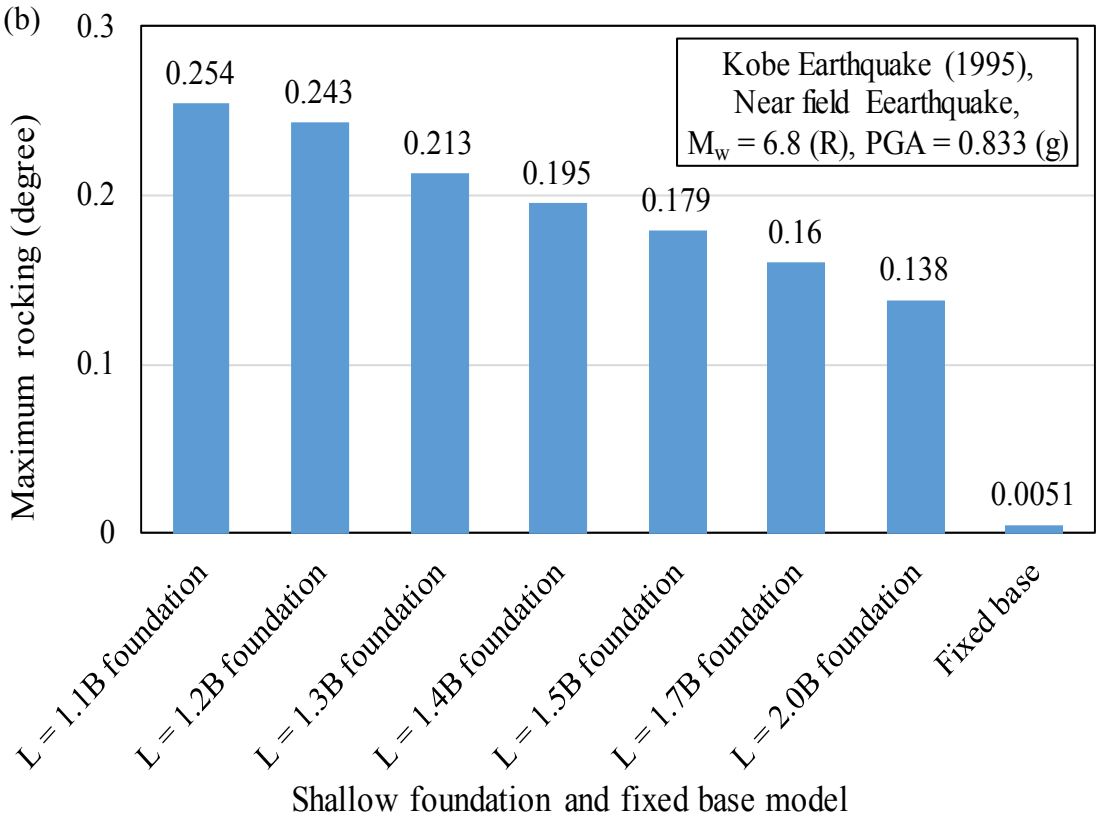
(b)
Maximum rocking (degree)
0.3
0.2
0.1
0
0.254
0.243
0.213
0.195
0.179
0.16
0.138
0.0051
Kobe Earthquake (1995),
Near field Eearthquake,
M_w = 6.8 (R), PGA = 0.833 (g)
L = 1.1B foundation
L = 1.2B foundation
L = 1.3B foundation
L = 1.4B foundation
L = 1.5B foundation
L = 1.7B foundation
L = 2.0B foundation
Fixed base
Shallow foundation and fixed base model

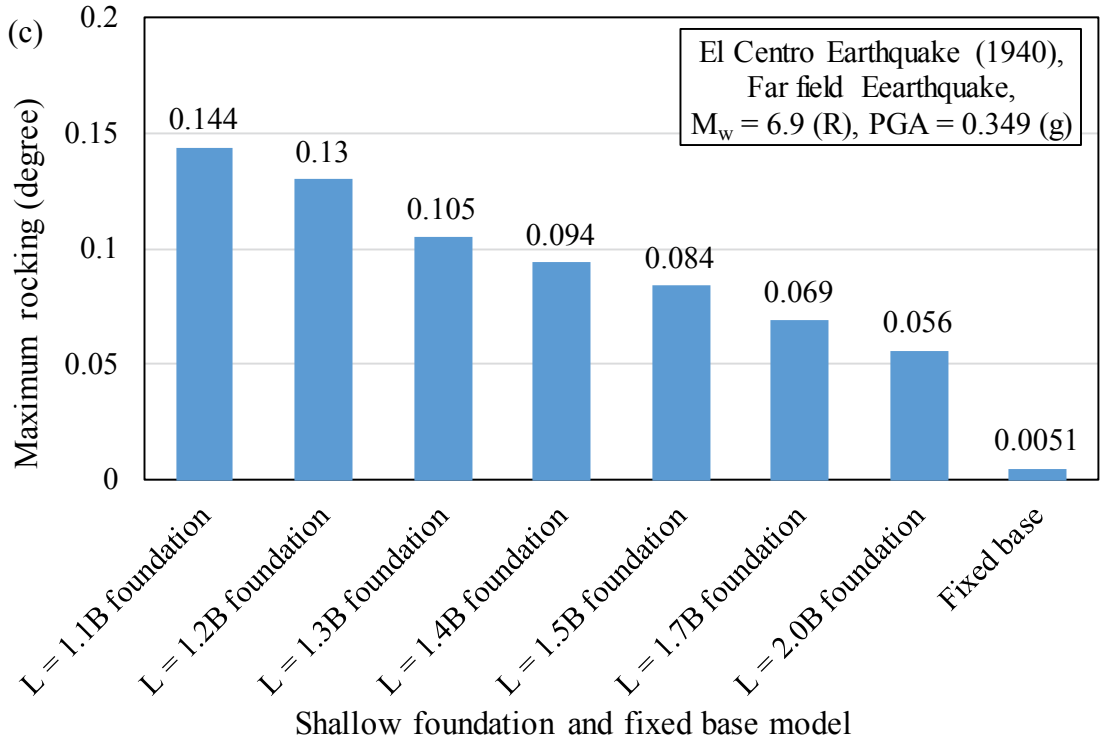

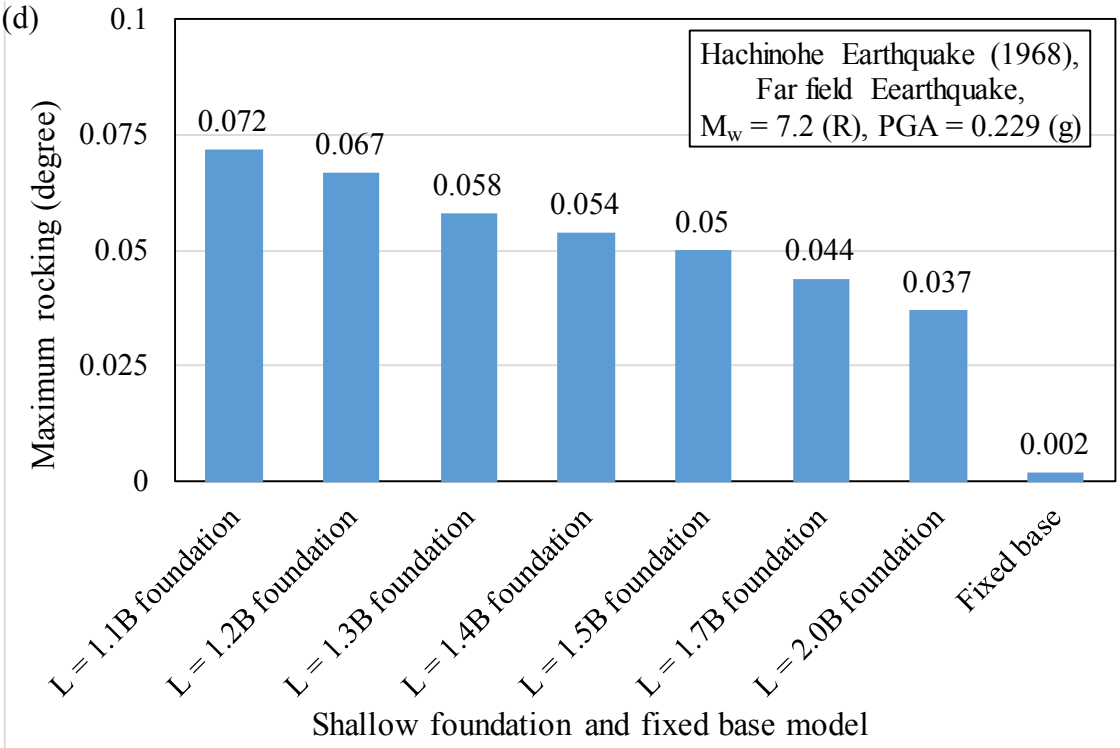

Figure 4.16 Maximum rocking of the fifteen-storey structure supported by shallow foundations with varies under the influence of: (a) 1994 Northridge earthquake; (b) 1995 Kobe; (c) 1940 El Centro earthquake; (d) 1968 Hachinohe earthquake.

(a)

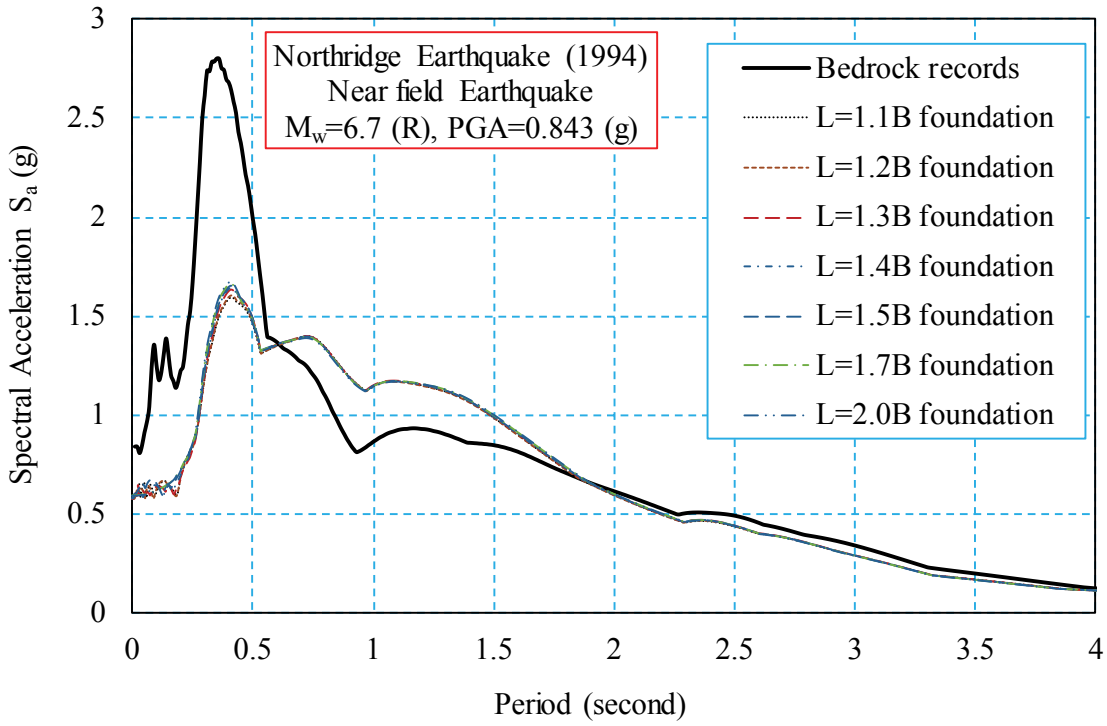
Northridge Earthquake (1994)
Near field Earthquake
Mw=6.7 (R), PGA=0.843 (g)
Bedrock records
L=1.1B foundation
L=1.2B foundation
L=1.3B foundation
L=1.4B foundation
L=1.5B foundation
L=1.7B foundation
L=2.0B foundation
Spectral Acceleration Sa (g)
Period (second)
0
0.5
1
1.5
2
2.5
3
3.5
4

(b)

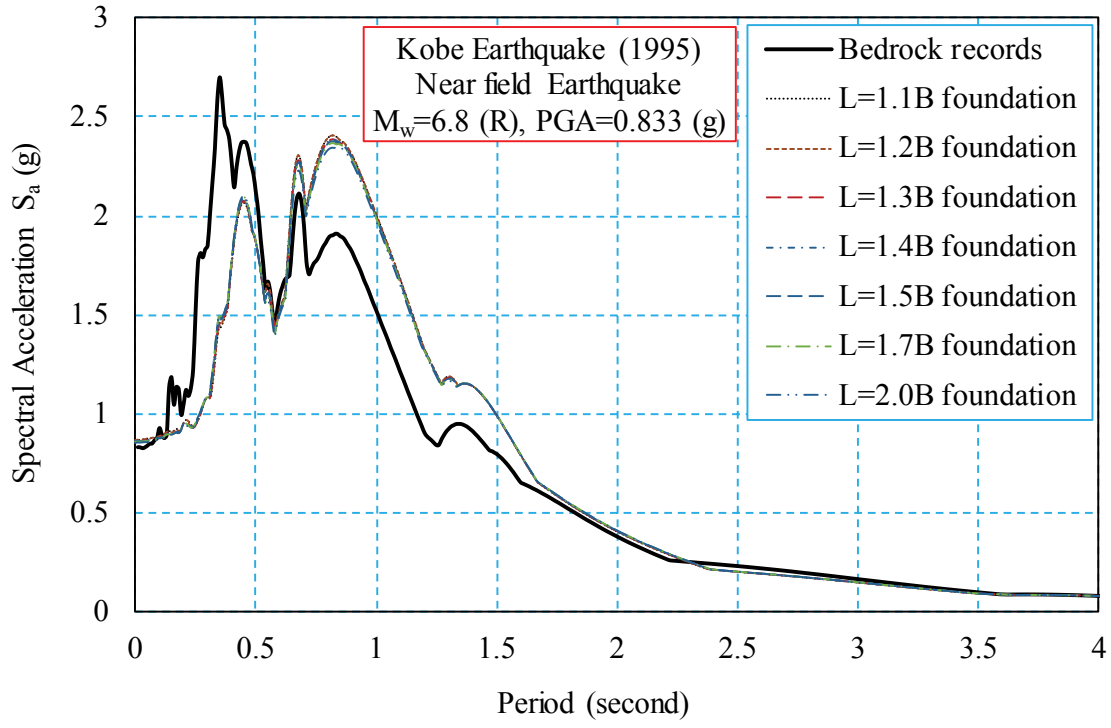
Kobe Earthquake (1995)
Near field Earthquake
Mw=6.8 (R), PGA=0.833 (g)
Bedrock records
L=1.1B foundation
L=1.2B foundation
L=1.3B foundation
L=1.4B foundation
L=1.5B foundation
L=1.7B foundation
L=2.0B foundation
Spectral Acceleration Sa (g)
Period (second)
0
0.5
1
1.5
2
2.5
3
3.5
4

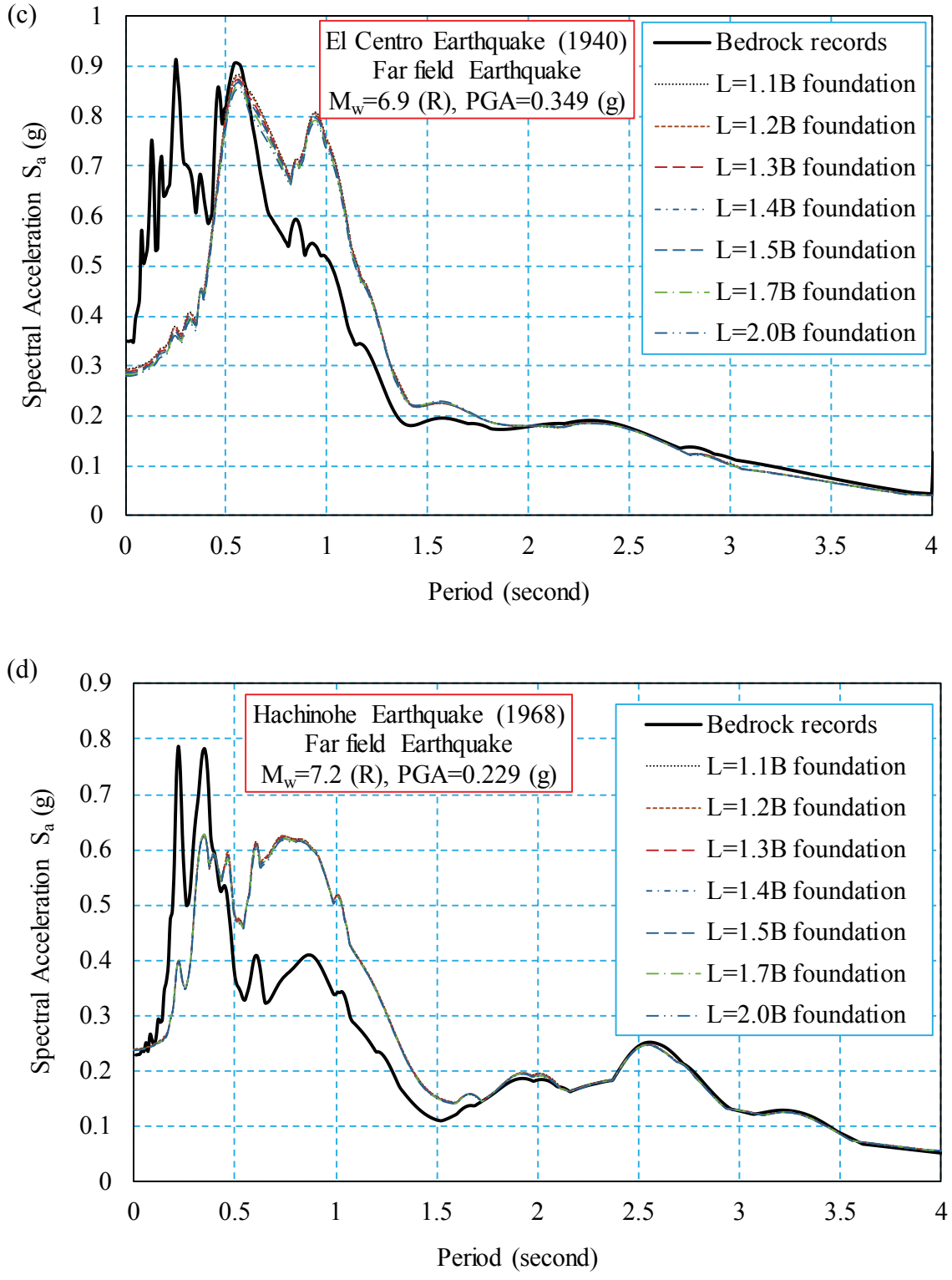

Figure 4.17 Acceleration response spectrum with 5% damping ratio for the structure with different foundation types under the influence of: (a) 1994 Northridge earthquake; (b) 1995 Kobe; (c) 1940 El Centro earthquake; (d) 1968 Hachinohe earthquake

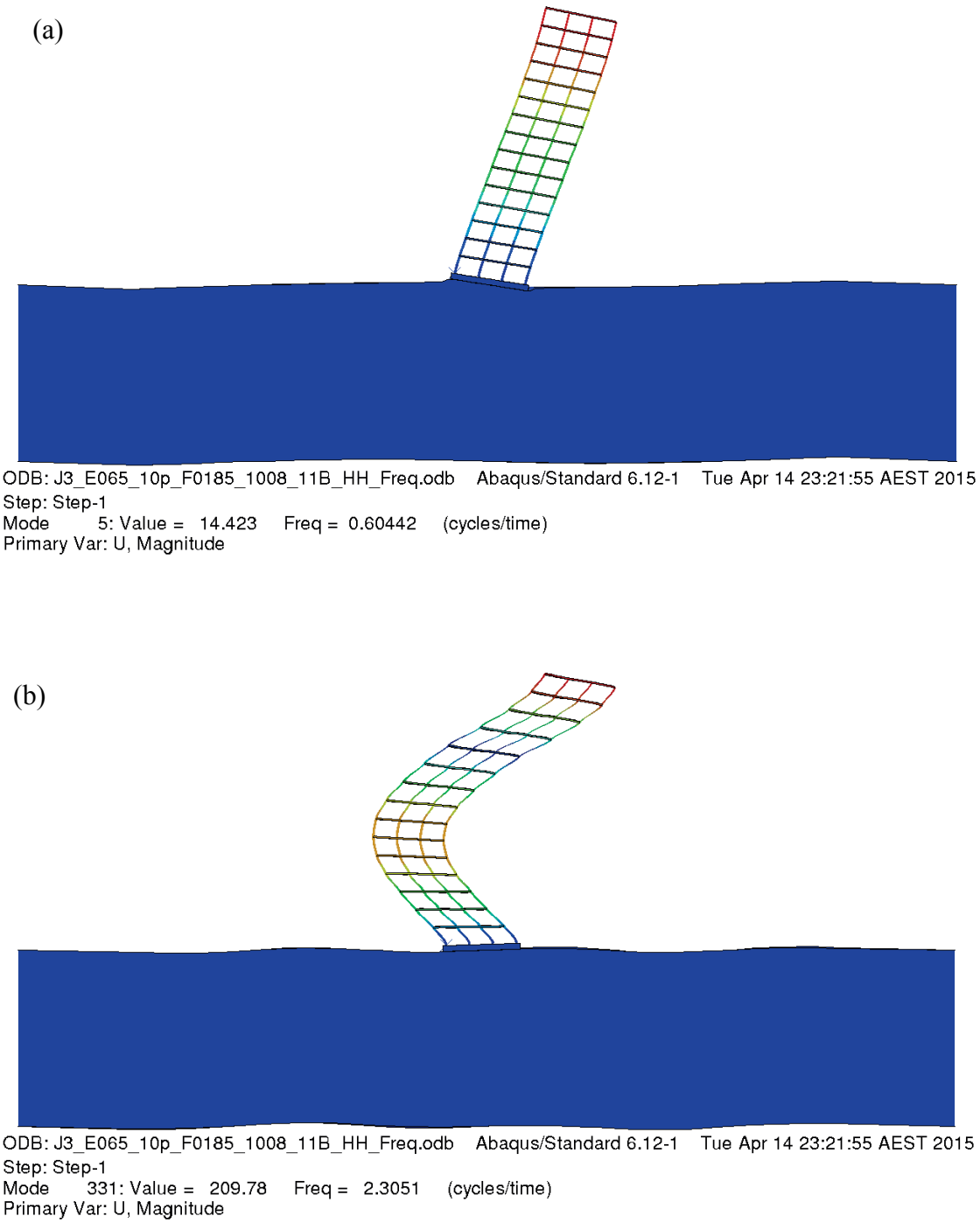

Figure 4.18 Representation of structural deformations considering soil-foundation-structure interaction (a) first mode and (b) second mode

The response spectrums are commonly used to apply the knowledge of structural dynamics to the design of structures and calculate the lateral force requirements (base shears) in building codes as a function of the natural frequency of the system. The size of a shallow foundation alters the natural frequency of the soil-foundation-structure system in comparison to a fixed-base structure, as shown in Table 4.6. The deformed shapes of the soil-foundation-structure system for the two first natural modes are shown in Figure 4.18. For instance, while the first natural frequency of the fixed-base structure in this study was 0.83 Hz, the same structure supported by 1.1B and 1.5B shallow foundations under the influence of 1994 Northridge earthquake possessed a first mode natural frequency of 0.425 Hz and 0.462 Hz, respectively. This change in the dynamic characteristics of the system was one of the main contributors to the amount of energy absorbed by a structure subjected to strong earthquakes. For instance, referring to Figure 4.18 and Table 4.6, the fixed-base structure and the structure supported by 1.1B and 1.5B shallow foundations absorbed different amounts of energy from the imposed earthquake that corresponded to the natural frequencies of each case.

In order to investigate the influence foundation size on the energy absorbed by the structure during earthquakes, the results of the developed 3D numerical model in terms of shear forces were compared for different cases. To determine the maximum shear force at each level, the shear forces generated in every column at that level were summed up in every time increment during the time-history analysis, and the absolute maximum shear force experienced at that level during the earthquake is reported as presented in Figure 4.11 (c), Figure 4.12 (c), Figure 4.13 (c), and Figure 4.14 (c). In general, considering SFSI contributed to the reduction in the shear forces in the structure as expected, whereas larger shallow foundations attracted more inertial forces from the earthquake excitations than the smaller sized foundations. For instance, the maximum base shear of the structure supported by the 1.5B foundation under the 1994 Northridge earthquake was 4.1 MN, while the corresponding value for the structure supported by 1.1B foundation was 3.6 MN (13% less energy absorption). This was due to changes in the dynamic characteristics of the system with various foundations sizes, as discussed earlier.

Decreasing the size of a foundation caused the spectral acceleration to decrease considerably as the natural period lengthened. As a result, such an increase in the natural period substantially changed the response spectral acceleration (S_a).

In the case where the mid-rise moment resisting building frames with a shallow foundation rests on soft soil deposits, the natural period lay in the long period region of the acceleration response spectrum curve. Due to the natural period lengthening induced by a reduction in the size of a foundation, the spectral acceleration (S_a) tended to decrease, which then reduced the base shear of the structure.

Consequently, when a design engineer's primary concern is to improve the total stability of a structure by reducing the rocking component, increasing the size of a shallow foundation might be an appropriate option considering the cases investigated in this study. However, in most cases, where the failure of the structural elements is the main safety concern, structures with smaller shallow foundation size attract less shear forces, and thus the level of damage to a structure with smaller foundations would be less, and it is more likely to survive strong earthquakes. It should be noted that the minimum foundation size is determined based on the bearing capacity requirements.

4.6 Summary

The aim of this study was to evaluate and quantify the influence of shallow foundation size on the seismic response of a regular mid-rise moment resisting building frame during earthquake excitations. In order to achieve this goal, ABAQUS was used to numerically simulate the soil-foundation-structure system by conducting a fully coupled nonlinear time history analysis.

According to the results obtained, the size of a shallow foundation can influence the structural design of the building under seismic loads considering the seismic soil-foundation-structure interaction. Larger shallow foundations can moderate the amplifications of lateral deflection and in turn inter-storey drifts of the structure caused by SFSI. This can be a cost effective alternative to control the performance level of buildings.

The size of a shallow foundation altered the fundamental frequency of the soil-foundation-structure system considerably, whereas its influence on the higher natural modes was insignificant.

As a result, changes in the size of shallow foundations resulted in absorbing an amount of energy from the imposed earthquake that corresponded to the natural frequency of a particular system. It was observed that buildings with larger shallow foundations attracted more inertial forces from earthquake excitations than smaller foundations. In other words, the mid-rise moment resisting building frame with shallow foundations on soft soil had a natural period in the long period region of the acceleration response spectrum curve, and because this natural period lengthened, there was a significant reduction in the base shears when the size of the foundation was reduced.

Chapter 5 INFLUENCE OF SIZE AND LOAD-BEARING MECHANISM OF PILES ON SEISMIC PERFORMANCE OF BUILDINGS CONSIDERING SOIL-PILE-STRUCTURE INTERACTION

5.1 General

Pile foundations are usually used to transmit foundation loads through soil strata of low bearing capacity to deeper soil or rock strata with a higher bearing capacity and stiffness. The type and size of a pile foundation that supports mid-rise buildings in high-risk seismic zones can alter the dynamic characteristics of the soil–pile–foundation system during an earthquake due to soil–structure interaction. To investigate these phenomena, a 15-story moment-resisting frame sitting on differently sized end-bearing and floating pile foundations was simulated numerically. The present study describes a numerical modelling technique for the simulation of complex seismic soil–pile–structure interaction phenomena. By adopting a method of direct calculation, the numerical model can perform a fully nonlinear time history dynamic analysis to realistically simulate the dynamic behaviour of soil, pile foundations, and structure under seismic excitations. This three-dimensional (3D) numerical model accounts for the nonlinear behaviour of the soil medium, the piles, and the structural elements. Results show that the type and size of the pile elements influence the dynamic characteristics and seismic response of the building due to interaction between the soil, pile foundations, and the structure. The findings of this study can help engineers select the correct size and type of pile foundation while considering the seismic performance of buildings sitting on soft soil and aim at optimising their design.

5.2 Introduction

Determining the seismic response of a pile foundation is a complex process that involves inertial interaction between the structure and the pile foundation, the kinematic interaction between piles and soils, and the nonlinear response of the soil to strong earthquake motions. Because simplified approaches are usually implemented in engineering practice, the main reason for considering the seismic soil–pile–structure interaction (SSPSI) in a

design is to ensure that the superstructure will be safe, while making savings on the overall cost of the project by reducing the design-based shear forces.

Although the topic of seismic soil–structure interaction has received considerable attention in the literature recently (e.g., Kim and Roesset 2004; Maheshwari and Sarkar 2011; Iida 2012; Sheil and Finnegan 2016) very limited work has been available on the impact of foundation type and characteristics on the seismic response of buildings. Han and Cathro (1997) analysed the response of a 20-story building supported by a pile foundation and concluded that the seismic behaviour of the tall building supported by the pile foundation is different from the one supported by the rigid base or the shallow foundation. Shiming and Gang (1998) conducted three-dimensional (3D) linear SSPSI analysis using a substructure model and observed that natural frequencies of the structure considering the interaction are greater than that without interaction related to varying soil properties, structural stiffness, and foundation type.

Moreover, the structure with the pile foundation experienced less increase in the natural period compared with the structure on the shallow foundation. Chu and Truman (2004) studied the effects of pile foundation configurations on the soil–structure interaction and noted that although largely spaced pile groups have slightly larger pile head responses than closely spaced pile groups, the general effects of the pile spacing ratio on the seismic responses of the soil–pile systems are insignificant. Although the available studies are valuable contributions, further investigations are essential to fully understand the influence of pile foundation type and characteristics on the seismic performance of buildings due to the complex SSPSI phenomena.

The techniques currently available for modelling SSPSI analysis conceptually follow two scenarios: the substructure method and the direct method. In the substructure method, the soil–pile–structure is partitioned into near-field and far-field cases, such that the near-field case simulates soil–pile–structure interaction, and the far-field case accounts for the semi-infinite nature of the soil medium for a site response analysis. As Kramer (1996) reported, the superposition inherent to this approach requires an assumption of linear soil and structural behaviour. Figure 5.1 shows the following three main steps in the substructure method: (1) evaluate the foundation input motion (FIM), which is the motion that would occur on the base slab if the structure and foundation had no mass; (2) determine the impedance function that describes the stiffness and damping

characteristics of the foundation-soil system; and (3) a dynamic analysis of the structure supported on a compliant base that is represented by impedance functions and is subjected to a base excitation consisting of FIM.

Numerous studies (e.g., Kutanis and Elmas 2001; Allotey and El Naggar 2008; Carbonari *et al.* 2011; Lin *et al.* 2014) have been performed using the substructure method to assess the seismic response of structural systems while considering soil–structure interaction. Gutierrez and Chopra (1978) reported that the principle advantage of the substructure approach is its flexibility. According to Wolf (1989), because this method is based on the superposition principle, which is valid only for linear soil and structural behaviour, approximations of soil non-linearity by means of iterative wave propagation analyses may allow the superposition to be applied to moderately nonlinear systems. Therefore, accounting for the exact non-linearity subsoil in the dynamic analysis may not be easy to achieve using this technique.

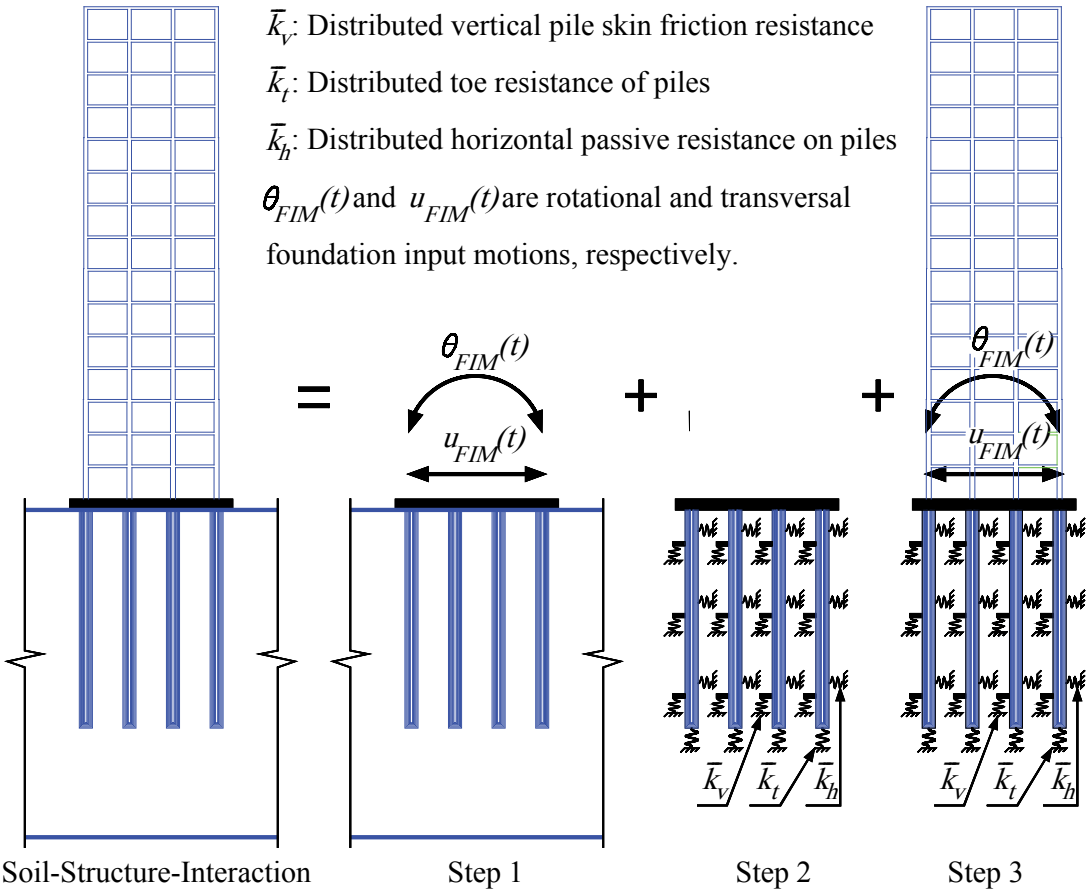

Figure 5.1 Substructure method for modelling soil-pile-structure interaction; Step 1: evaluation of Foundation Input Motion (FIM) using transfer functions; Step 2: evaluation of impedance functions; Step 3: analysis of structure on compliant base subjected to FIM.

In the direct method, the entire soil–pile–structure is modelled at the same time, and the input motions are specified along the base of the model. Typically, the soil is simulated with solid finite elements, whereas the pile and structure are represented with finite beam elements. Several researchers (e.g., Hayashi and Takahashi 2004; Chu and Truman 2004; Carbonari *et al.* 2011; Hokmabadi *et al.* 2014b; Tabatabaiefar and Fatahi 2014; Hokmabadi *et al.* 2014a) have studied the seismic responses of soil–pile–structure systems by adopting the direct method for modelling the soil–structure interaction to achieve accurate and realistic outcomes. Because an assumption of superposition is not required, true and accurate nonlinear analyses are possible in this case, as mentioned by Borja *et al.* (1994). Therefore, because the direct method is better at modelling the complex nature of the soil-pile–structure interaction in dynamic analysis, it is used in this study.

To achieve this goal, a numerical simulation of a soil–pile–structure system was performed in Abaqus 6.12 software as a fully coupled nonlinear time history analysis. The effects that the characteristics of a pile foundation had on the natural frequencies of the system, as well as their response spectrum and structural performance, are investigated. The results of this study can help engineers choose the correct size and type of pile foundation while considering the seismic performance of buildings sitting on soft soil and aim at optimizing their design.

The adopted numerical modelling technique in Abaqus (Dassault Systèmes SIMULIA 2012) is explained with sufficient detail, which can be beneficial for experts from both academia and industry considering the growing interest in the industry in using 3D finite-element modellings in engineering projects for SSPSI problems.

5.3 Overview of the Soil–Pile–Structure System Adopted

A 45-m high 12-m wide 15-story, concrete moment-resisting building with three spans in each direction was selected. The structural sections were specified after conducting a routine design procedure that is regulated in the relevant building codes, such as AS3600 (Standards Australia 2009a) and AS1170.4 (Standards Australia (2007). A nonlinear time history dynamic analysis under the influence of the earthquake ground motions, including the 1994 Northridge, 1995 Kobe, 1940 El Centro and 1968 Hachinohe earthquakes, was

performed. In this dynamic analysis, the geometric non-linearity and $P-\Delta$ effects were considered according to AS3600 (Standards Australia 2009a).

Moreover, the reinforced concrete sections with cracked sections were considered by multiplying the coefficients of the cracked sections by the stiffness of the structural members (EI) according to the American Concrete Institute's (ACI) ACI318-08 (ACI 2008). SAP2000 v 14 software was used for the structural analysis and design of the cross sections of beams and columns. Table 5.1 and Table 5.2 show the material properties and structural sections that represent the structural norms and construction practises of conventional buildings in mega cities. The fundamental frequency of this fixed-base building was 0.830Hz, and its total mass was 1,683 tonnes.

Table 5.1 Characteristics of adopted concrete and steel reinforcement in structural designs

Section type	**Concrete grade**	**Steel reinforcement grade**
Columns	32 (f_c' = 32MPa, E = 30.1GPa)	N500 (f_y= 500 MPa)
Slabs	32 (f_c' = 32MPa, E = 30.1GPa)	N500 (f_y= 500 MPa)

Table 5.2 Designed sections for structural beams, columns and slabs

Section type	Column I	Column II	Column III	Column IV	Slab
Dimensions (m)	0.55×0.55 m	0.5×0.5 m	0.45×0.45 m	0.4×0.4 m	12×12×0.25 m
Distribution	Level 1-3	Level 4-7	Level 8-11	Level 12-15	All level
Cross section area A (m^2)	0.303	0.250	0.203	0.160	0.25 (for 1m width)
Second moment of cross section I (m^4)	0.0076	0.0052	0.0034	0.0021	0.0013 (for 1m width)
Longitudinal reinforcement	8 N24	8 N24	8 N20	8 N24	N16 @250
Tie steel	N10 @80	N10 @125	N10 @200	N10 @225	-
When considering cracked section (according to ACI318-08 (2008))					
Cracked factor	0.7	0.7	0.7	0.7	0.35
Reduced second moment of cross section I_{cr} (m^4)	0.00532	0.00364	0.00238	0.00147	0.000455 (for 1m width)

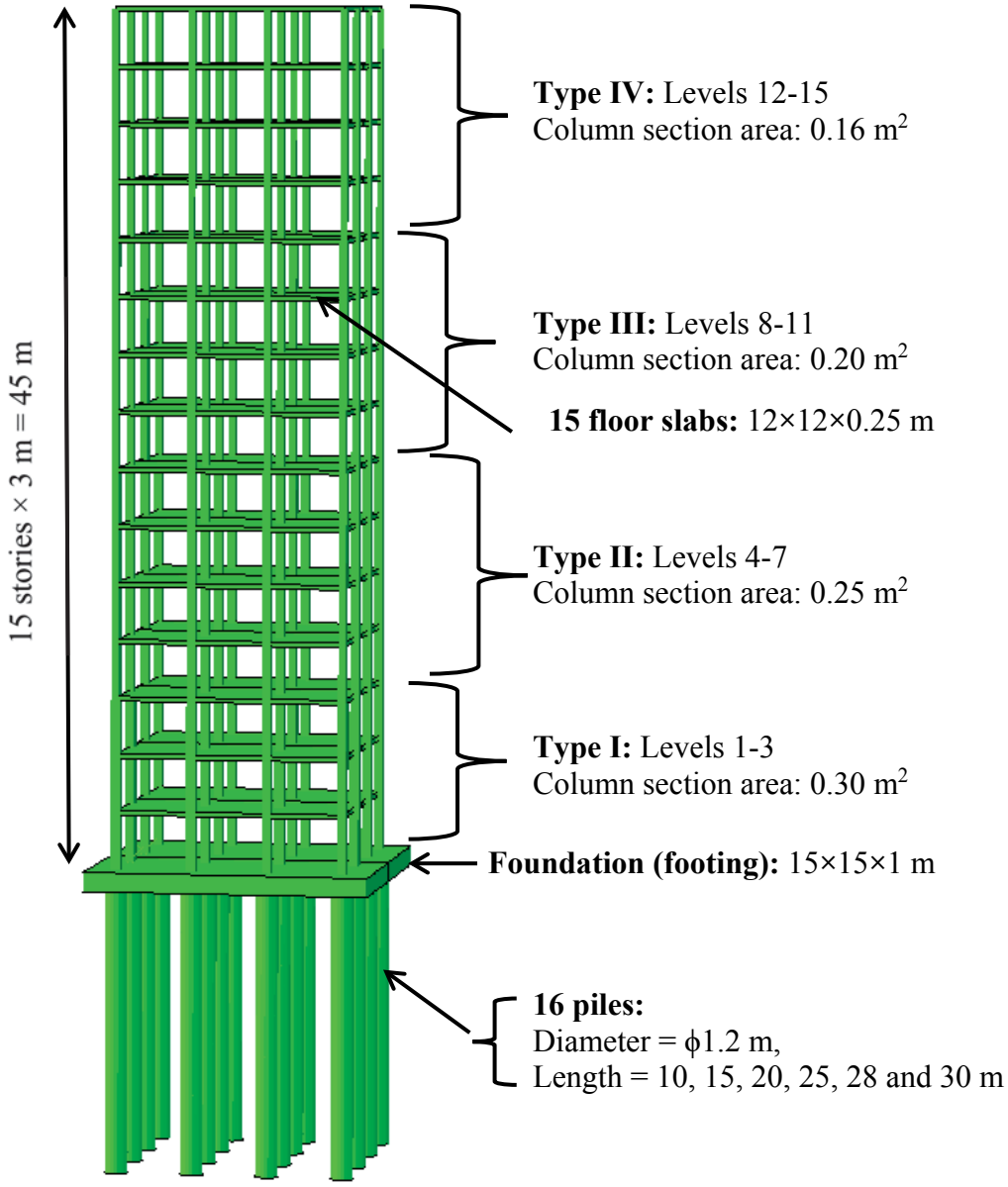

Figure 5.2 Designed sections of 15-story moment-resisting building adopted in the numerical model

The superstructure sits on 30-m deep Class E_e soft soil, and according to the Australian Standard AS1170.4 (Standards Australia 2007), Class E_e soil is a site with more than a 10-m depth of soil with a shear wave velocity of 150 m/s or less. In this study, the subsoil is a soft clayey soil (CL) with a unit weight ρ of 14.42 kN/m3, a shear wave velocity of 150 m/s, and an undrained shear strength of 50 kPa.

The pile foundations were designed to support the structure against static and dynamic loads following routine engineering design procedures (e.g., Poulos and Davis 1980; Bowles 2001; AS2159 2009; Nguyen, Jo*, et al.* 2013; Hokmabadi and Fatahi 2015)

to satisfy the requirements for bearing capacity and maximum settlement. The foundation slab is 15×15 m square and 1 m thick and is made of reinforced concrete. The foundation slab is connected to a group of 4×4 reinforced concrete piles 1.2 m in diameter. The pile spacing is 4 m centre to centre (3.3D), which fundamentally agrees with the dimensions used by other researchers (e.g., Small and Zhang 2002; Shelke and Patra 2008). Because the superstructure consists of three spans with a total width of 12 m, by adopting the previously mentioned pile setup and placing one pile under each column, the pile foundation system has been designed to carry the applied structural loads. Pile foundations with lengths of 10, 15, 20, 25, 28, and 30 m were considered. The 30-m-long pile foundation is connected to the bedrock so it can be considered as having an end-bearing mechanism (socketed pile). Figure 5.2 shows an overview of the system.

From an engineer's perspective, all of the foundations satisfied the requirements for bearing capacity and maximum settlement, although the safety factors of the smaller foundations were less than the large ones. The seismic response of the pile foundations are compared and discussed in the following sections via a 3D finite-element numerical simulation

5.4 Numerical model

Abaqus 6.14 finite-element software was used to numerically simulate the soil–pile–structure systems because it can simulate complex problems that require large computational memories using a direct method of analysis.

Table 5.3 Summary of characteristics of the designed reinforced concrete floor slabs, foundation, and piles

Properties	Denote	Unit	Value
Floor slab thickness	h_s	*m*	0.25
Foundation thickness	h_f	*m*	1.0
Pile diameter	h_p	*m*	1.2
Pile length	l_p	*m*	10, 15, 20, 25, 28 and 30
Density	ρ	kg/m^3	2400
Young's modulus	E	*kPa*	3.01E8
Possion's ratio	ν	-	0.2

A number of researchers (e.g., Chu and Truman 2004; Koskinen 2005; Moss *et al.* 2010; Matinmanesh and Asheghabadi 2011) have used Abaqus to study soil–structure interaction problems. The procedure used to simulate structural elements and soil models, as well as the contact surfaces and boundary conditions, are explained below.

5.4.1 Structural Model and Adopted Earthquake Records

The columns and floor slabs of the superstructure were simulated by beam and shell elements, whereas the foundation and pile elements were modelled with solid elements (continuum elements).

The characteristics of the columns and floor slabs are presented in Table 5.2 and Table 5.3, respectively. The structural elements were modelled using an elastic-viscoelastic constitutive model that considered Rayleigh damping. In this study, a structural damping ratio (ξ) of 5% and model coefficients of $\alpha = 0.3996$ and $\beta = 0.0049$, calculated based on the first and second mode frequencies of the structure, were used to simulate structural damping, whereas the inelastic behaviour of structural elements was simulated using elastic-perfectly plastic material behaviour by specifying the yield stress(Tabatabaiefar *et al.* 2014a; Hokmabadi *et al.* 2014a). The elastic-perfectly plastic material model used here for inelastic analysis and design assumed that structural elements behave elastically until they reach the defined yield stress, after which the element that reaches its yield stress can continue to deform without inducing additional stresses.

Two benchmark earthquakes, including two far-filed earthquakes (1994 Northridge and 1995 Kobe earthquakes) and two near-filed earthquakes (1940 El Centro and 1968 Hachinohe earthquakes), were incorporated into the finite-element numerical model while performing a time history analysis. The adopted earthquake motions are rock outcrop motions; thus, they can be directly applied at the bedrock of the model Table 4.5 and Figure 4.10.

5.4.2 Soil Model

The non-linearity of soil during an earthquake plays an important role in the dynamic response of soil–structure systems. The equivalent linear method has been used for many years to calculate wave propagation (and response spectra) in soil and rock at sites

subjected to seismic excitations. In the equivalent linear method adopted here, a linear analysis with some assumed initial values for the damping ratio and shear modulus in various regions of the model was performed. Then, the maximum cyclic shear strain for each element was recorded and used to determine the new values for damping and modulus by referring to the backbone curves relating the damping ratio and secant modulus to the amplitude of shear strain. Some empirical scaling factors can be used when relating these strains to the model strains, and then these new values for the damping ratio and shear modulus are used in the next stage of the numerical analysis. This process is repeated until there is no further change in the properties and the structural response. At this stage, "strain-compatible" values of damping and modulus are recorded, and the simulation using these values is deemed to be the best possible prediction of real behaviour. As Seed and Idriss (1969) described, the equivalent linear method uses linear properties for each element because they remain constant under seismic excitations. Those values were estimated from the mean level of dynamic motion, but because the nonlinear backbone curves and trial and error were used to find the strain-compatible values of damping and modulus, this method was used to capture the soil non-linearity.

Vucetic and Dobry (1991) comprehensively studied the number of cyclic test results available and concluded that the soil Plasticity Index (PI) controls the location of backbone curves for a wide variety of cohesive soils. The numerical model developed in this study adopts the ready-to-use charts (Figure 5.3) provided by Vucetic and Dobry (1991) to estimate the modulus degradation and damping ratio of cohesive soils in dynamic analysis. These charts are a design tool for practising engineers because the PI of soil is readily available, but note that as the PI increases, $G_{sec} = G_{max}$ increases while the damping ratio decreases.

Because each earthquake record induces different levels of shear strain in soil deposits, the values for soil damping and modulus would differ for each earthquake when the non-linearity of the soil is considered. Table 5.4 summarises the strain-compatible parameters of soil used here to develop the 3D numerical model of the earthquakes. As mentioned earlier, because the properties of the subsoil were extracted from actual in situ and laboratory tests (Rahvar 2006), they have merit over those assumed parameters that may not completely conform to reality.

Soil damping that simulates the absorption of energy by particles of soil and their interaction during wave propagation reduces the wave amplitude and influences how the superstructure will perform. Das (1983) mentioned that the mechanism most commonly used to represent the dissipation of energy is viscous damping, in which the dissipative forces are assumed to be a function of particle velocity. Here, the nonlinear variations of energy losses in the soil during an earthquake were simulated using the Rayleigh damping formulation. Park and Hashash (2004) investigated whether the Rayleigh damping formulation could undertake a nonlinear dynamic analysis of soil deposits, and they concluded that it can provide acceptable results for many applications as long as the parameters for the deposit of soil are selected accurately.

Considering the frequency-dependent nature of these Rayleigh damping formulations, the frequencies/modes selected to define the damping function govern the accuracy of the time domain solution but avoid any negative damping in the resulting frequency-dependent damping (Park and Hashash 2004) when selecting the frequencies. The two significant frequencies can be chosen in part to cover the range of frequencies in which there is significant content of input motion. Kramer (1996) presented the following equation to calculate the natural frequencies of the soil deposit:

$$f_n = \frac{V_S}{4H}(2n - 1) \tag{5.1}$$

where n = mode number, f_n = natural frequency of the corresponding mode, V_S = shear wave velocity of the soil deposit, and H = soil deposit thickness. Here, following recommendations made by Park and Hashash (2004), a set of frequencies corresponding to the strain-compatible shear modulus values for different earthquakes are selected. The Rayleigh damping parameters used in the numerical model are summarised in Table 5.4.

The soil medium was modelled using C3D8R elements (3D, 8-node linear brick, reduced integration, hourglass control elements). This is shown in Figure 5.4, in which, due to reduced integration, locking phenomena do not occur, but the element is not stiff enough in bending, which is not critical when modelling soil. Moreover, because the integration point is located in the middle of this element, small elements are needed to capture the concentration of stress at the boundaries. A summary of all element types used in the finite-element model in this study is presented in Figure 5.4.

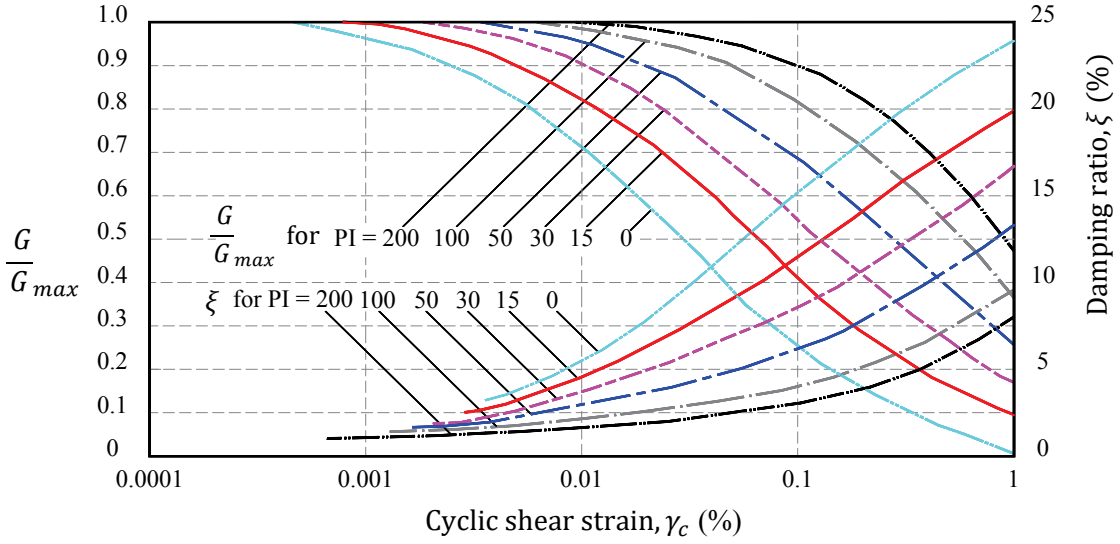

Figure 5.3 Backbone curve relating shear stiffness and damping ratio to cyclic shear strain for cohesive soils

Table 5.4 Adopted soil parameters for the soil-foundation-structure system

Soil Properties		**Denote**	**Unit**	**Value**	**Reference**
Unit weight		γ	N/m^3	14420.7	Rahvar (2006)
Shear strength		S_u	kPa	50	
Poisson's ratio		v	-	0.4	
Shear Wave Velocity		V_s	m/s	150	
Plasticity Index		PI	-	15%	
Northridge earthquake (γ_{max}=0.17%, G/G_{max}=0.31, ξ=13.5%)	Mass damping factor	α	-	0.796	Vecetic and Dobry (1991); (Park and Hashash, 2004)
	Stiffness damping factor	β	-	0.017	
Kobe earthquake (γ_{max}=0.15%, G/G_{max}=0.36, ξ=12.4%)	Mass damping factor	α	-	0.763	
	Stiffness damping factor	β	-	0.015	
El-Centro earthquake (γ_{max}=0.09%, G/G_{max}=0.42, ξ=11.2%)	Mass damping factor	α		0.758	
	Stiffness damping factor	β		0.012	
Hachinohe earthquake (γ_{max}=0.04%, G/G_{max}=0.66, ξ=8.35%)	Mass damping factor	α		0.151	
	Stiffness damping factor	β		0.018	

5.4.3 Pile–Soil Interface and Boundary Conditions

When defining the contacts, contact pressure resists penetration and frictional stress resists sliding; thus, a numerical simulation of contacts can cause severe nonlinearities, particularly due to inequality conditions that lead to discontinuous stiffness in the normal and tangential directions of contact surfaces. To simulate the mechanical contacts in engineering, the interacting surfaces, contact model (e.g., pressure versus overclosure relationship, coefficient of friction), contact formulation aspects (e.g., small sliding or large sliding formulations), and algorithmic contact controls should be defined properly.

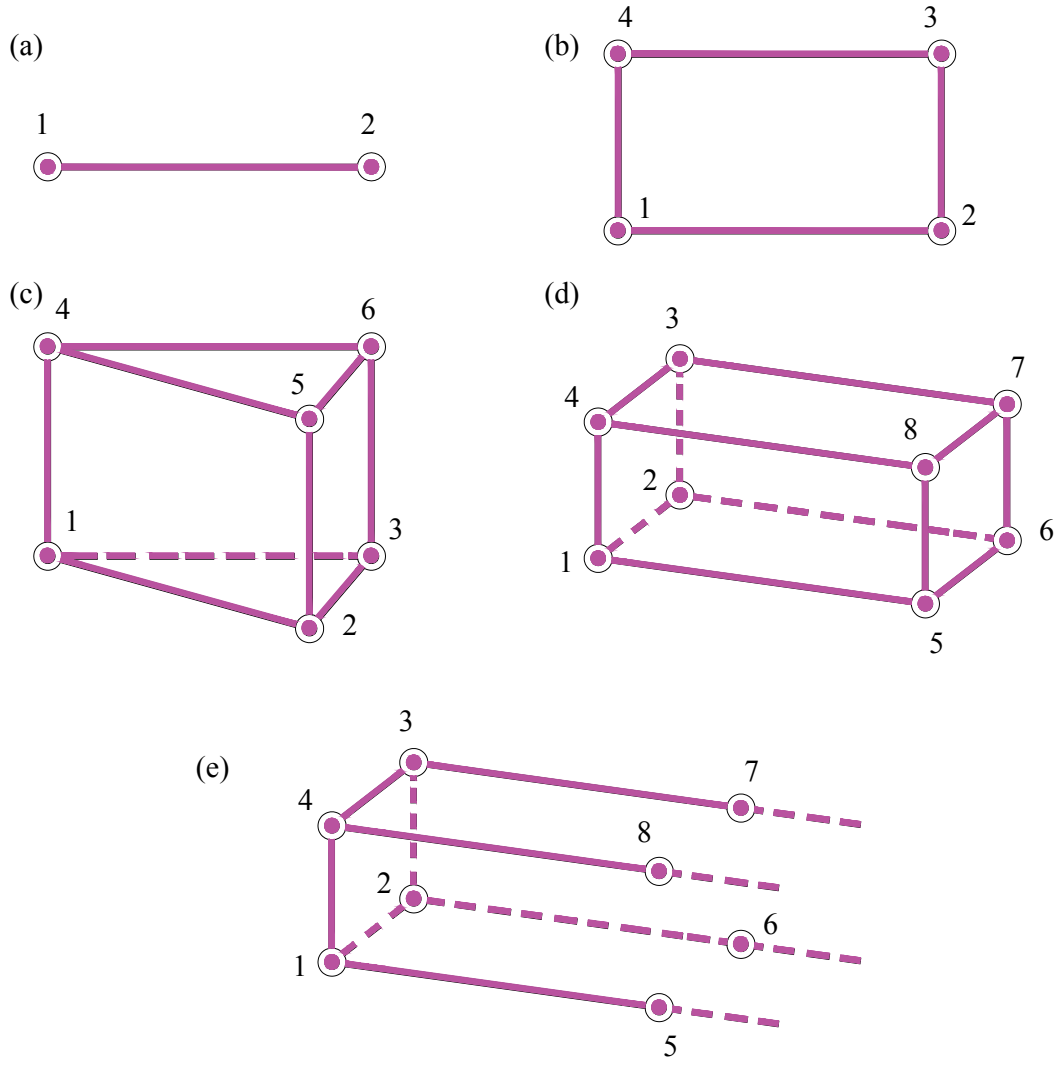

Figure 5.4 Employed element types in the adopted finite element model:

(a) 2-node linear beam element in space (B31) for columns;

(b) 4-node, quadrilateral, stress/displacement shell element with reduced integration (S4R) for slabs;
(c) Three-dimensional, 6-node linear triangular prism elements (C3D6) for pile and foundation footing;
(d) Three-dimensional, 8-node linear brick, reduced integration, hourglass control (C3D8R) for soil;
(e) Three-dimensional, 8-node linear one-way infinite brick (CIN3D8) for soil

Good contact resolution over the entire interface would occur when integrals over the slave surface are considered, but when the slave surface is treated as a collection of discrete points, penetration at the master nodes are not prevented (penetration at slave nodes are only resisted).

In this study, hard surface-to-surface contact that considers the pressure-overclosure relationship is adopted, and surface-to-surface discretization is fundamentally sound when the quadratic or wedge-shaped elements underlie the slave surface. In this hard contact situation, there would be no contact pressure until the nodes make contact and contact pressure would be generated once contact has been established (enforced with a penalty method) and no contact damping is considered. Because the contacting surfaces are curved, representing curved surfaces is crucial for accurate modelling. Representing curved surfaces by a series of facets is sometimes detrimental to accuracy and convergence; thus, the geometric corrections available in Abaqus for the surface-to-surface contact formulation for curved surfaces is used to improve these aspects without degrading the per iteration performance (Figure 5.5). Note that adopting geometric corrections for the curved interfaces avoids the need for matched nodes across the contact interface.

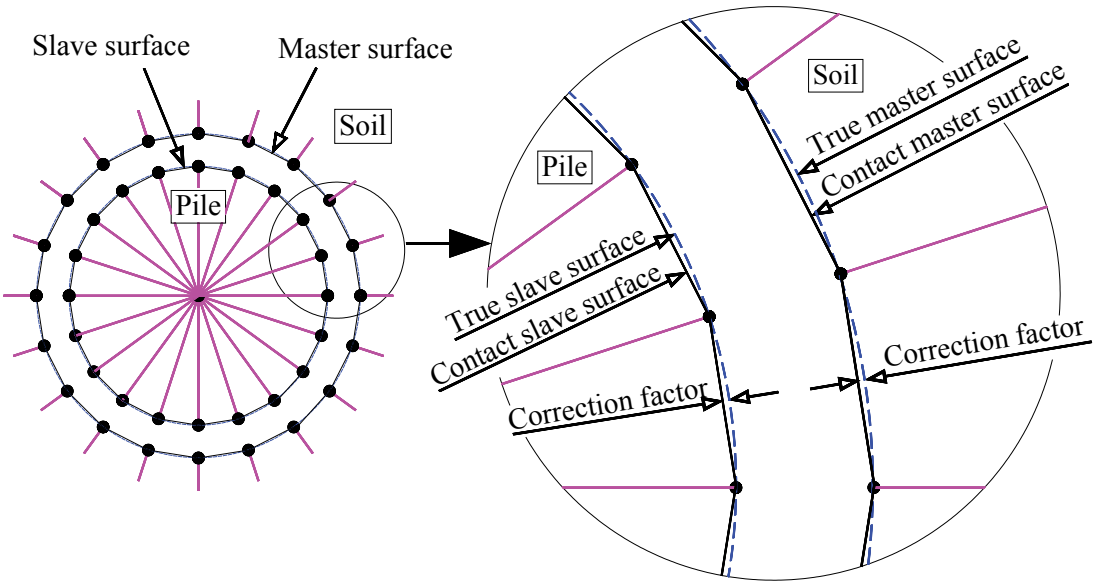

Figure 5.5 Representation of curved surfaces of piles and surrounding soils and adopted geometry correction factors

In the surface-to-surface technique used here to simulate the interaction between soil and piles, contact is enforced in an average sense over a region surrounding each slave node such that each contact constraint is formulated based on an integral over the region surrounding a slave node. Note that computing average penetrations and slips over finite regions has a smoothing effect that avoids snagging, whereas surface-to-surface contact reduces the likelihood of large localised penetrations and sensitivity of results to master and slave roles, and will predict contact stresses more accurately (without matching meshes). Having a slave surface with a finer mesh will yield better results, whereas choosing a more refined master surface tended to increase analysis time. Indeed, the authors' assessment shows that in the pile-soil interface simulated here, the adopted surface-to-surface discretization was not influenced by the choice of master and slave surfaces. Nevertheless, the surface-based contacts between pile and soil were defined such that the master surface is in the soil and the slave surface is the surface surrounding the pile elements.

Modelling stiff interface behaviour with a contact formulation prone to being over-constrained is difficult because simulating hard contacts is susceptible to these issues. However, associating the penalty method with numerical softening can mitigate issues with overconstraint and reduce the number of iterations required in an analysis because the penalty method is a stiff approximation of hard contact. With this method the

contact force is proportional to the distance of penetration, so some degree of penetration will occur (Figure 5.6). Moreover, the penalty method can be implemented such that no Lagrange multipliers are used, which improves solver efficiency. Linear variations of the penalty method are used in this study, in which the so-called stiffness penalty is constant, and the pressure-overclosure relationship is linear. To drive the penetration distance down, the linear penalty method is used within an augmentation iteration scheme when, during the numerical analysis, a converged solution with the penalty method is found. Then, if the slave node penetrates the master surface by more than a specified tolerance, the contact pressure is augmented and another series of iterations is executed until convergence occurs once again. This augmentation of the contact pressure continues until the actual penetration is less than its tolerance. The penetration tolerance here is assumed to be 5% of the characteristic length of the interface.

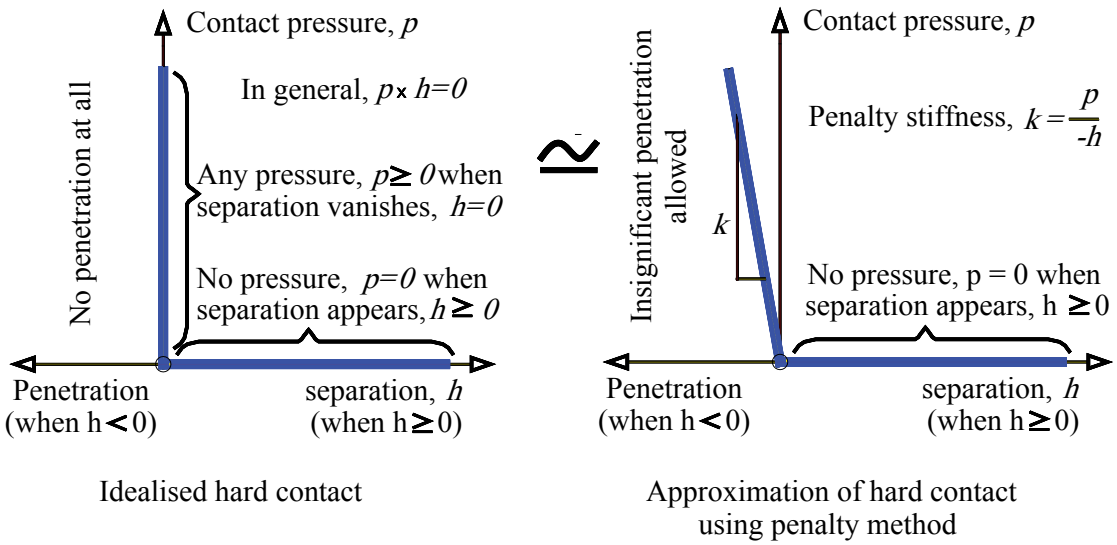

Figure 5.6 Representation of adopted penalty method for stiff approximation of hard soil–pile contact simulation

Lagrange multipliers are only used for the augmented Lagrange method if the stiffness penalty is more than 1,000 times the underlying element stiffness; otherwise, no Lagrange multipliers are used. In this numerical modelling, because the penalty stiffness ratio does not exceed 1,000, there was no need to incorporate the Lagrange multiplier.

To simulate the tangential behaviour of contact surfaces between the pile and the surrounding soil, the classical Mohr-Coulomb failure model is used, and the reduction factor of $R_{int} = 0.75$ to reduce shear strength at the interface $[(S_u)_{int}]$ is used as follows:

$$[(S_u)_{int}] = R_{int} \times (S_u)_{soil} \tag{5.2}$$

The actual interface strength depends on many parameters, such as ground type, roughness of pile outer surface, and the construction method. This value is usually taken between 0.12 and 1.0 (Nor *et al.* 2014; Belinchon *et al.* 2016). In this study, the interface reduction factor of 0.75, which is within the range adopted commonly in geotechnical practice (Kim *et al.* 2010; Fatahi *et al.* 2014), has been used. Although the numerical investigations by Brown and Shie (1991) on laterally loaded piles concluded that it is important to specify a value for a pile-soil friction coefficient, the predictions were not particularly sensitive to the interface friction angle as long as some frictional resistance is included.

Boundary conditions were prescribed at the boundaries of the numerical grids, such that the far-field soil is represented by infinite elements to account for the energy absorbed from the unbounded soil domain, and horizontal deformation is also simulated realistically (Figure 5.7). The 3D, 8-node linear one-way infinite brick (CIN3D8) elements were used to model the infinite elements, as shown in Figure 5.4 (c), but they have defined orientations, unlike the other numerical elements. In Figure 5.4 (b), Nodes 1–4 were connected to defined finite elements (subsoil), whereas the other nodes (5–8) were oriented outward from the defined finite elements.

A rigid boundary condition was used to simulate bedrock (the bottom of the soil medium grid) in the seismic soil–foundation–structure interaction analysis, as suggested by other researchers (Rayhani and El Naggar 2008; Fatahi and Tabatabaiefar 2013), whereas earthquake input motions were applied at the bedrock and propagated upward through the entire model.

Figure 5.7 shows the model components and the numerical mesh for a building supported by pile foundations. Note that to compare the results to piles of different lengths without the meshing variables creating difficulties, the same mesh was used for every size in the pile foundations.

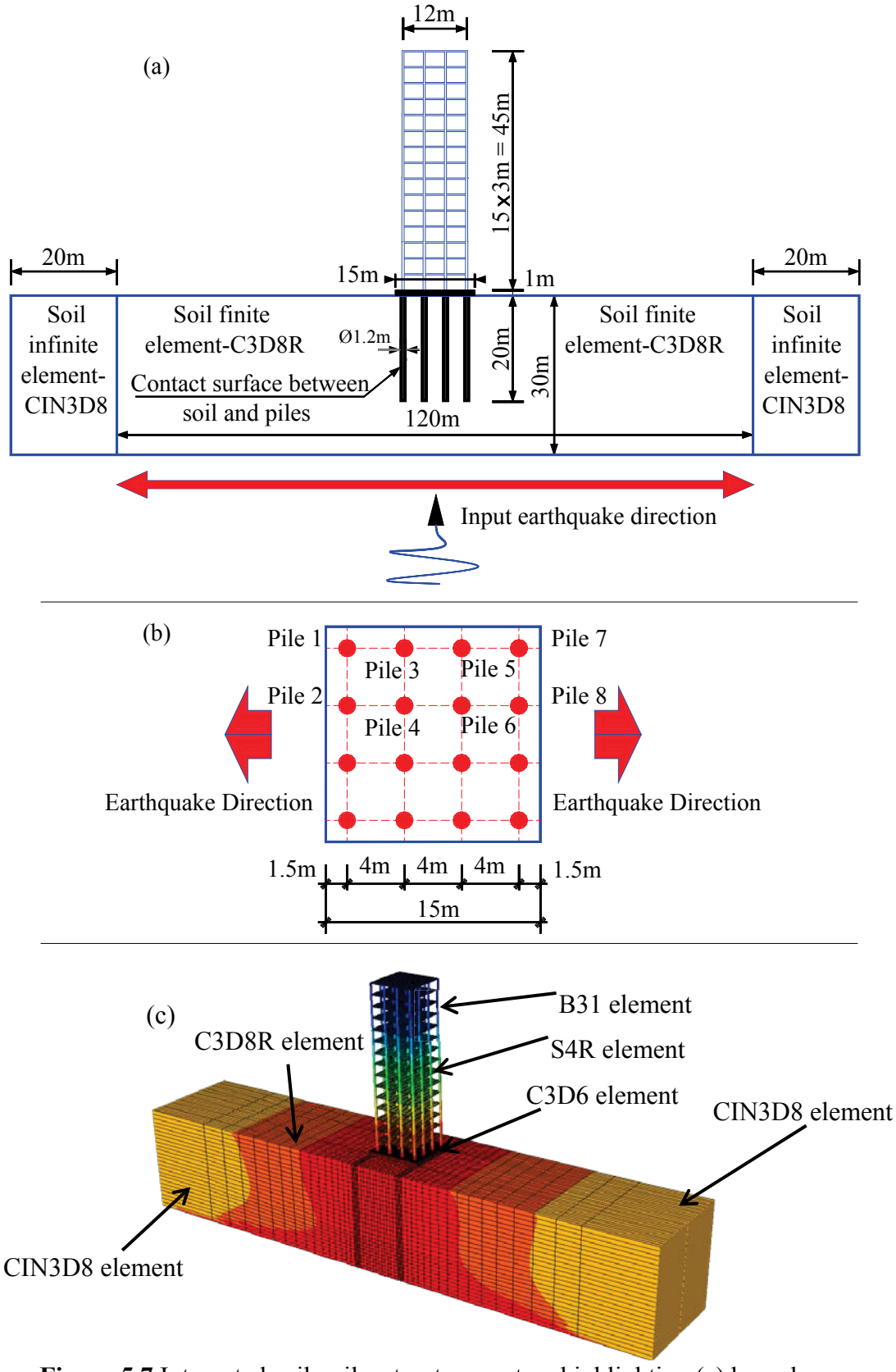

Figure 5.7 Integrated soil– pile–structure system highlighting (a) boundary conditions, main grid, and contact surfaces; (b) numbered pile plan utilised in the numerical simulation; (c) adopted finite element model.

The mesh shown in Figure 5.7 (c) consists of 45,440 elements and 49,816 nodes, and the time histories of the earthquakes applied at the base of the soil–pile–structure models are shown in Figure 4.10. Because this model is large (approximately 80 gigabytes for a single case), the fast computation facilities at the University of Technology Sydney, Sydney, Australia, were used to conduct this time history analysis, and even then it took approximately 60 hours to run a single case under the applied earthquake excitation. The results of the 3D finite-element numerical simulation are discussed in the following sections.

5.5 Results and Discussion

The results are presented and discussed in terms of the lateral deflection of each floor, the maximum inter-story drifts, the total maximum column shear forces, rocking of the foundation, and the bending moments and shear forces in the pile elements.

5.5.1 Flooring Lateral Deflections and Inter-story Drifts

Figure 5.8 (a), Figure 5.9 (a), Figure 5.10 (a) and Figure 5.11 (a) shows the maximum lateral deflection of the building, and to determine the lateral deflection of each floor the movement of the foundation was subtracted from the movement of the stories, which means that all the records are relative to the movements of the foundation on the soil-surface level. These data were based on the lateral deformation of each story when maximum deflection occurred at the top level because, as Hokmabadi *et al.* (2012) stated, it results in a more reasonable pattern of structural deformation than where the maximum absolute deformation of the stories was recorded, regardless of when they occurred.

Referring to Figure 5.8 (a), Figure 5.9 (a), Figure 5.10 (a) and Figure 5.11 (a), SSPSI amplified the maximum lateral deflection of the superstructure during shaking excitations, as was expected. For instance, the maximum lateral deformation of the fixed-base building (excluding SSPSI) under the 1940 El Centro earthquake was 10 4mm, and a lateral deformation of up to 180 mm (73% more) occurred when it was supported by a 28-m-long pile foundation to account for SSPSI. Moreover, increasing the length of the floating piles meant that the structure experienced more maximum lateral deformation; for example, the structure supported by 10-m-long frictional piles experienced a maximum lateral deformation of 148 mm under the 1940 El Centro earthquake, which is

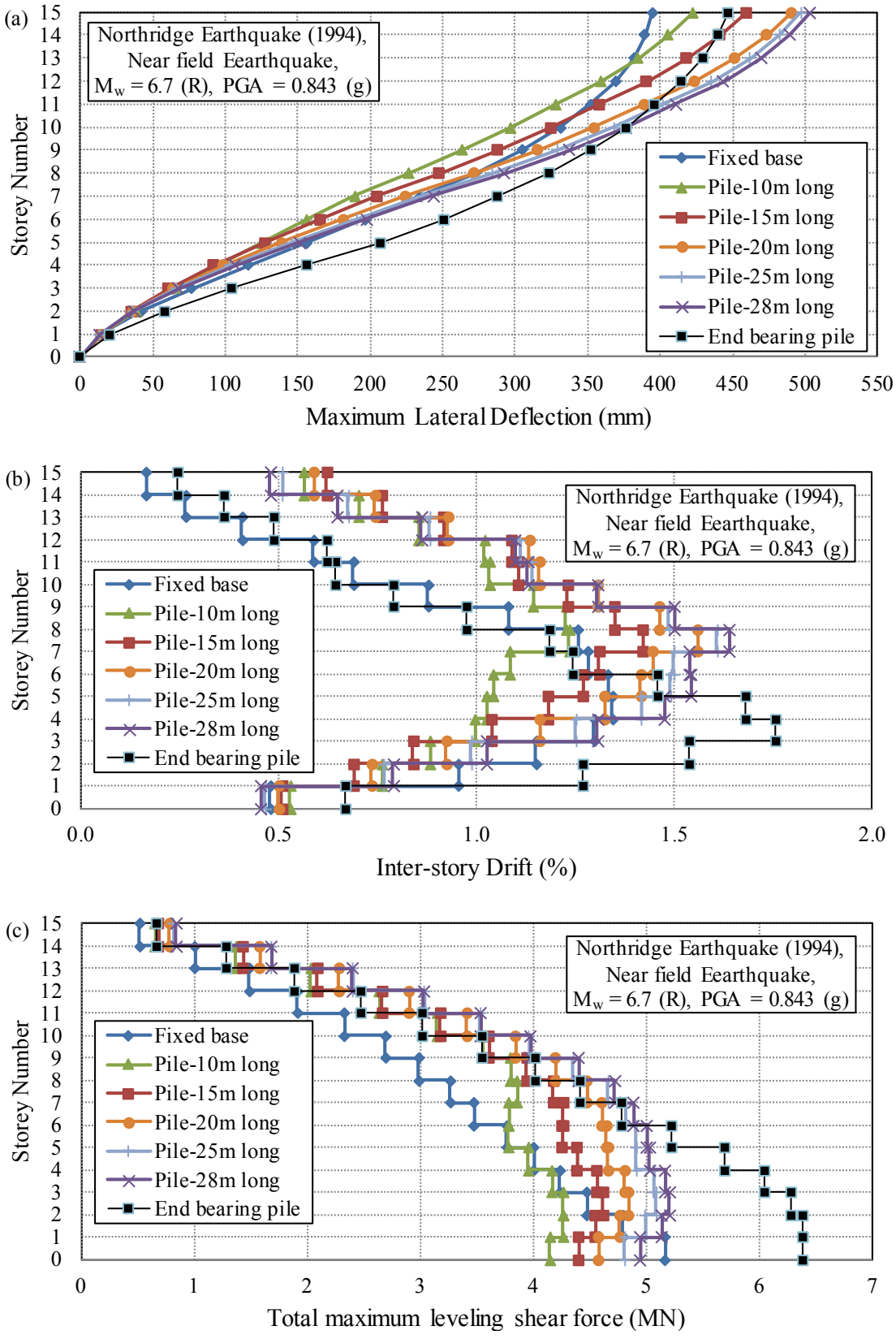

Figure 5.8 Response of the fifteen-storey structure supported by pile foundations with varied lengths under the influence of 1994 Northridge earthquake: (a) maximum lateral deflection; (b) maximum inter-storey drifts; (c) maximum shear force distribution.

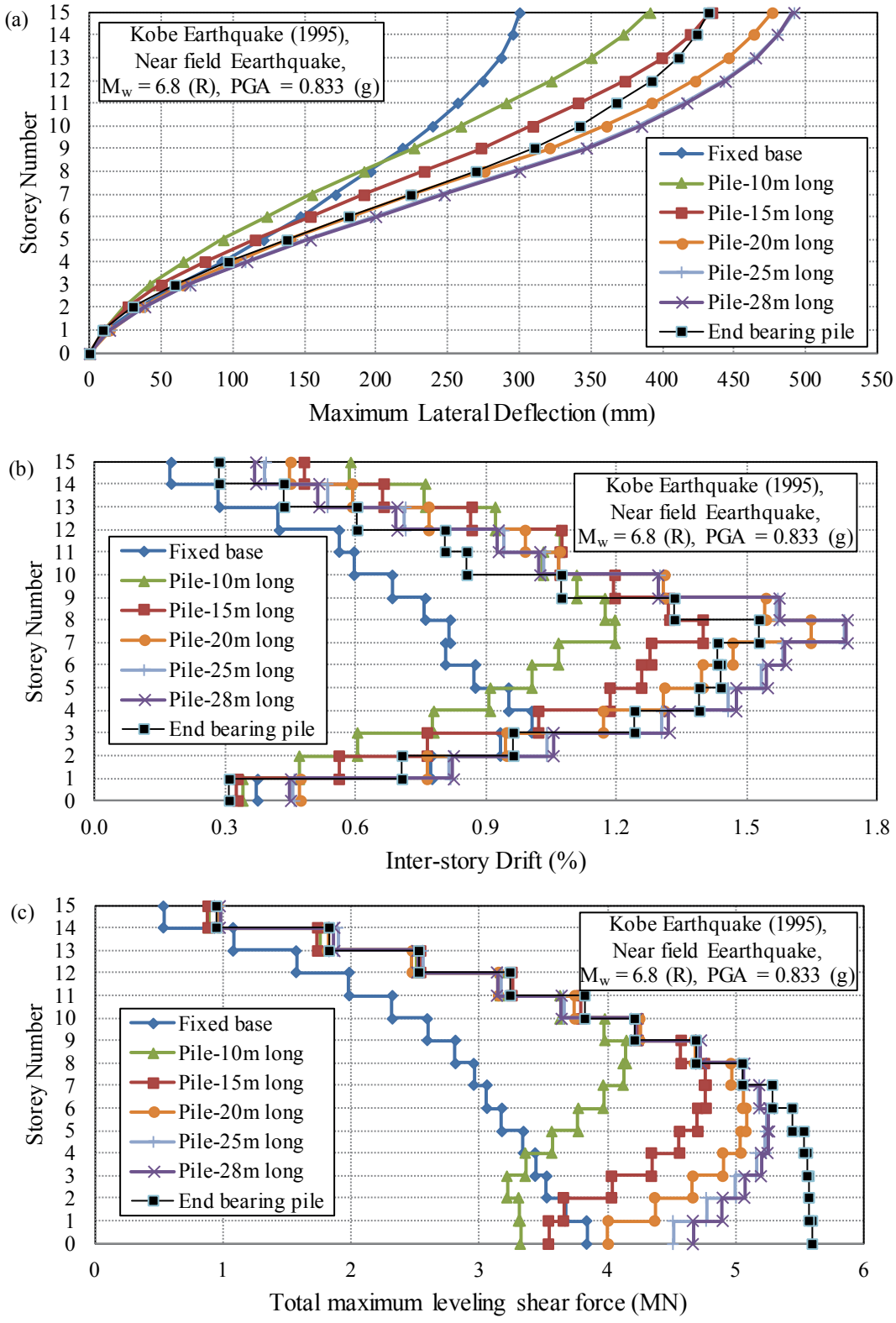

Figure 5.9 Response of the fifteen-storey structure supported by pile foundations with varied lengths under the influence of 1995 Kobe earthquake: (a) maximum lateral deflection; (b) maximum inter-storey drifts; (c) maximum shear force distribution.

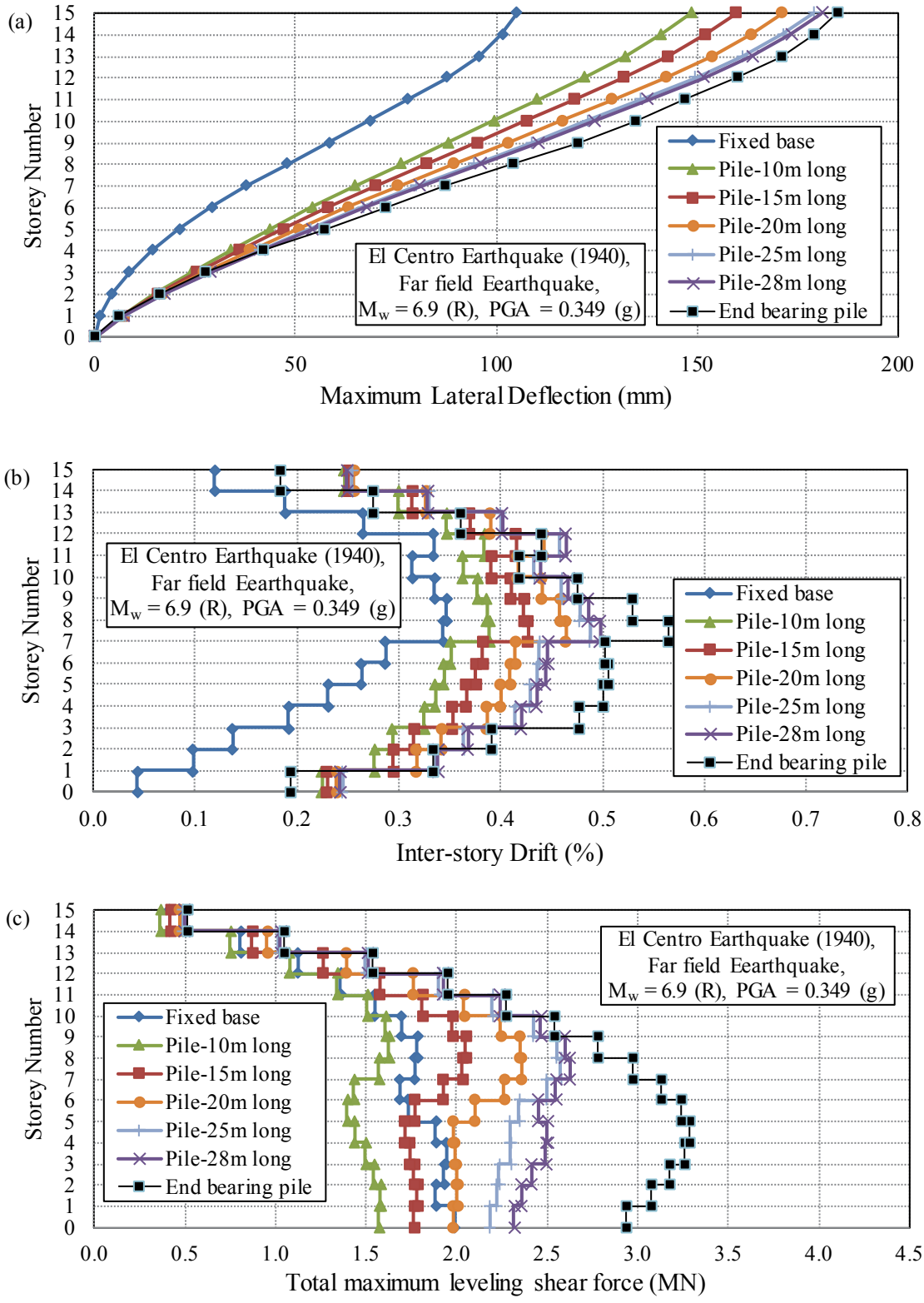

Figure 5.10 Response of the fifteen-storey structure supported by pile foundations with varied lengths under the influence of 1940 El Centro earthquake: (a) maximum lateral deflection; (b) maximum inter-storey drifts; (c) maximum shear force distribution.

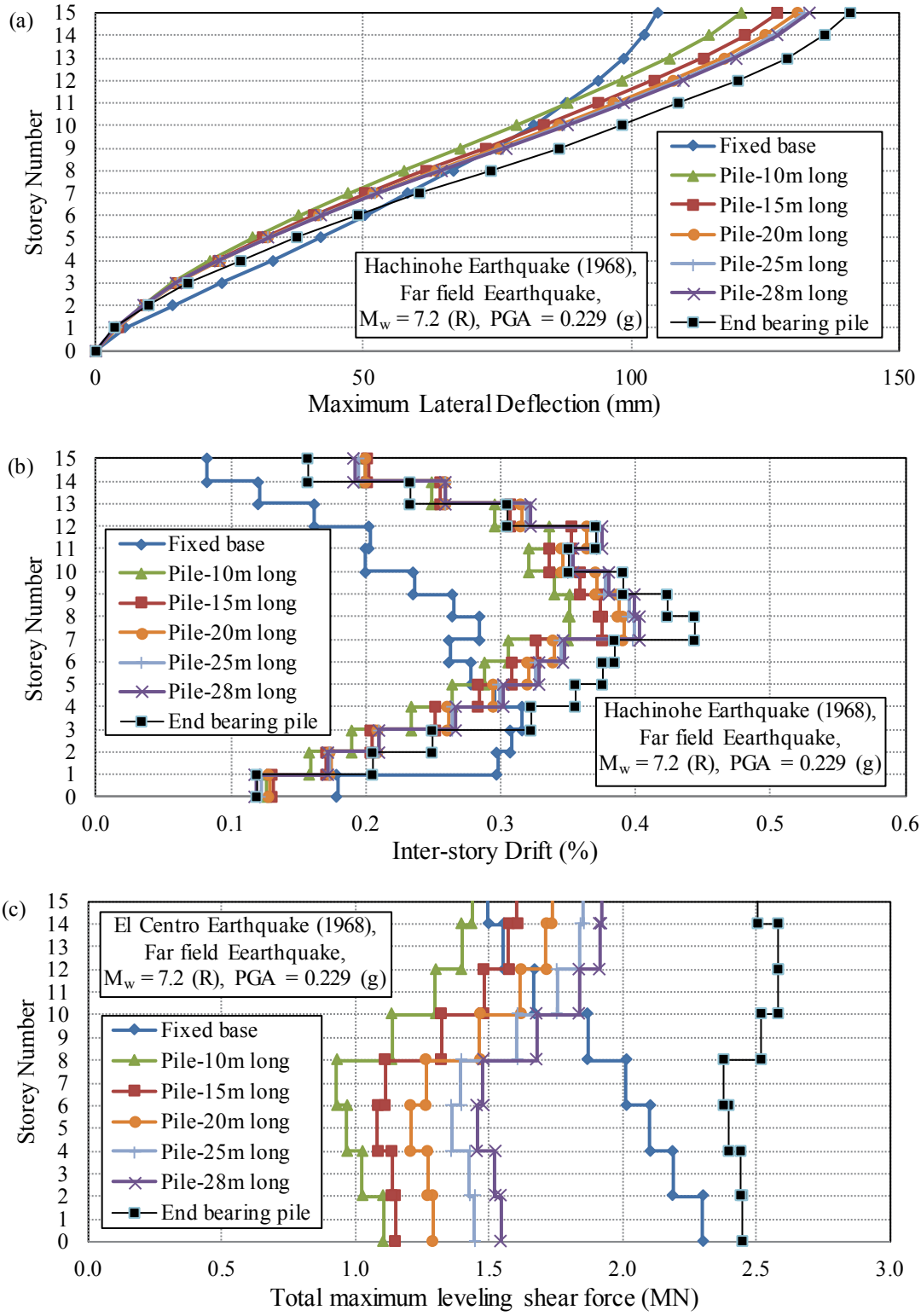

Figure 5.11 Response of the fifteen-storey structure supported by pile foundations with varied lengths under the influence of 1968 Hachinohe earthquake: (a) maximum lateral deflection; (b) maximum inter-storey drifts; (c) maximum shear force distribution.

18% less than the maximum deformation the same structure experienced while supported by 28-m-long frictional piles. This increase in the lateral deflection is related to the amount of inertial energy absorbed by the soil–pile–structure system. The presence of pile elements changes the dynamic characteristics (i.e., natural frequency and damping) of the system, in which longer piles, having higher contact surface with the surrounding soil, absorb extra energy from the earthquake. This extra absorbed energy is then transferred to the superstructure and causes excessive lateral deformations, as observed in the results.

The structure supported by end-bearing pile foundations shows more lateral deformation than the fixed-base case (up to 80%), although the end-bearing pile foundation is not easily compared with the frictional pile foundation due to the totally different load bearing mechanisms. In a floating pile foundation, the transfer of stress between the soil and pile elements occurs mainly through the pile shafts; however, in the end-bearing pile foundation, the rigid connection in which the toe of the pile connects to the bedrock is the main component that governs the load transfer mechanism during shaking excitations.

The maximum interstory drifts of the building were calculated using the following equation (Standards Australia 2007), and the results are plotted in Figure 5.8 (b), Figure 5.9 (b), Figure 5.10 (b) and Figure 5.11 (b):

$$Drift = \frac{d_{i+1} - d_i}{h} \tag{5.3}$$

where d_{i+1} is deflection at level $(i + 1)$;

d_i is deflection at level (i);

h is the height of the story.

Note that the interstory drifts generally follow the same pattern as the lateral deflections, in which longer pile elements cause the structure to undergo extra interstory drifts. These results indicate that a soil–pile–structure interaction can push the interstory drifts to exceed the safe-life zone of performance-based designs, which according to FEMA273/274 (BSSC 1997) limits interstory drifts to 1.5%.

Lateral deflection in the structure consists of structural distortion and rocking, in which structural distortion is directly related to the shear forces generated in the structure. These two components govern the maximum deflection and inter-story drifts experienced by the structure; this ratio depends on the type of pile foundation and load-bearing mechanism. The impact of the pile foundation type and characteristics on the structural distortion and rocking is discussed in detail in the following sections.

5.5.2 Shear forces developed in the columns

To investigate how the length of a pile foundation and the load bearing mechanism influences the amount of seismic energy absorbed by the structure during earthquakes, the structural shear forces resulting from the 3D numerical model were compared for different cases. Shear forces in the structure were generated from relative movement between slabs and columns during earthquake excitations. To determine the maximum shear force at each level, the shear forces generated in every column at that level were summed up (16 columns) in every time increment during the time history analysis. Then, the absolute maximum shear force experienced at that level during the earthquake was reported.

The results are plotted in Figure 5.8 (c) for the 1994 Northridge, Figure 5.9 (c) for the 1995 Kobe earthquake, Figure 5.10 (c) for the 1940 El Centro earthquake and Figure 5.11 (c) for Hachinohe earthquake. Note there is generally a gradual increase in the maximum total shear forces when the pile length increased from 10 m to 28 m. For example, the base shear forces under the 1940 El Centro earthquake for the 28-m pile model was 61% more than for the 10-m-long piles, Similarly, base shears under the 1994 Northridge earthquake is 24% more for foundations with 28-m-long piles than for foundations with 10-m-long piles. These values show that the length of piles influences the total shear forces absorbed by the structure during an earthquake because longer piles have a higher contact surface with the surrounding soil and, thus, absorb extra energy.

Therefore, longer piles do not necessarily result in a safer design under strong ground motions when the interaction between soil and structure is considered. Figure 5.8 (c), Figure 5.9 (c), Figure 5.10 (c) and Figure 5.11 (c) shows that longer piles may result in imposing extra shear forces to columns of the superstructure, which in turn increases the inter-story drifts (Figure 5.8 (b), Figure 5.9 (b), Figure 5.10 (b) and Figure 5.11 (b)).

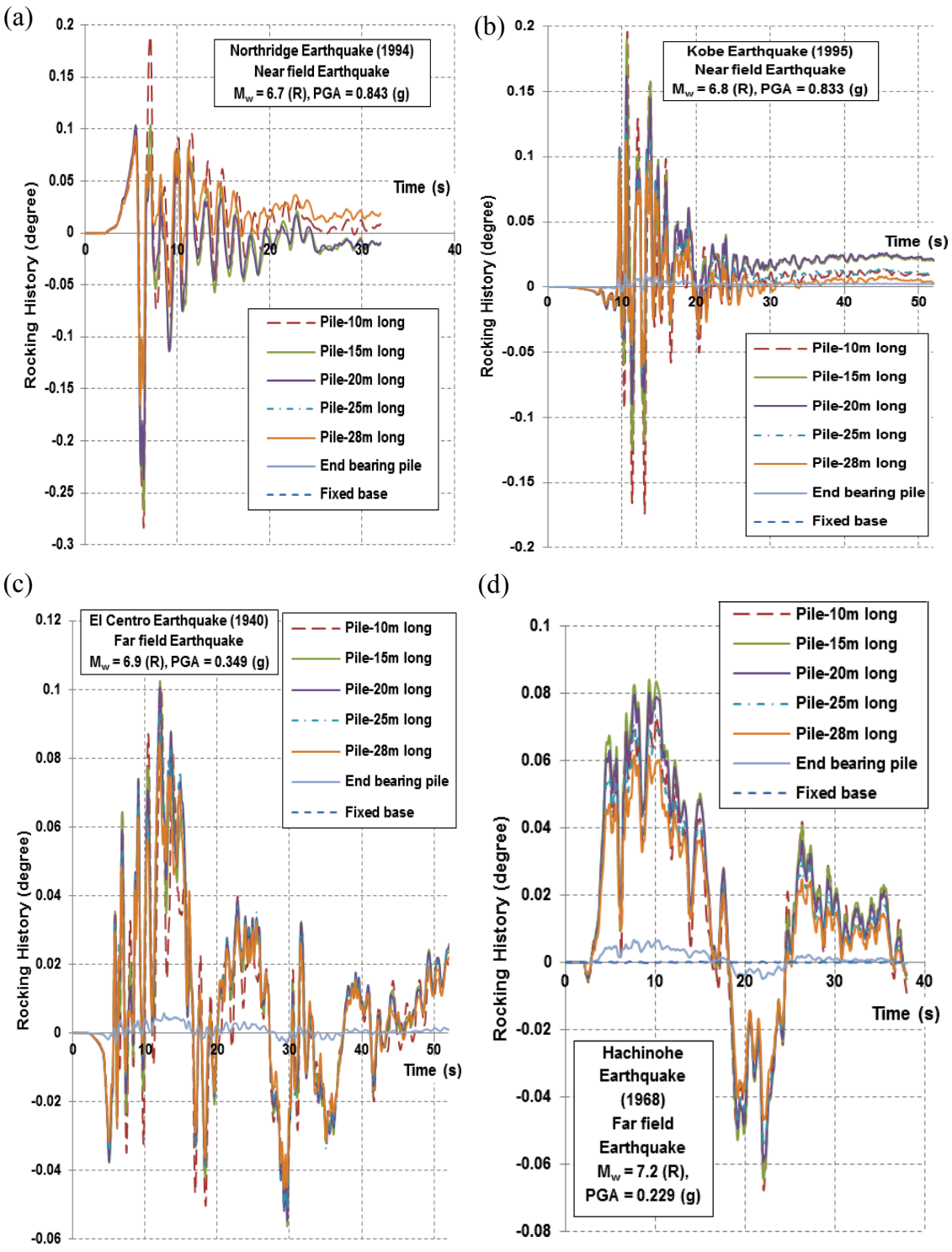

Figure 5.12 Foundation rocking history of the fifteen-storey supported by pile foundation with different pile lengths under: (a) Northridge earthquake, (b) Kobe earthquake, (c) El Centro earthquake and (d) Hachinohe earthquake.

End-bearing pile foundations also produce much higher levelling shear forces than floating piles because end-bearing piles can absorb inertial forces from the toe, which is directly connected to the bedrock, and the shaft of the pile. Moreover, the length of a pile foundation and load-bearing mechanism must influence how the shear forces are distributed along the superstructure because the size and variety of shear forces are not the same at every level. For instance, although the maximum base shear forces under the 1994 Northridge earthquake for a model with 28-m-long piles was 24% more than for 10-m-long piles, level 9 and above experienced almost no changes in the shear force generated between the 10- and 28-m-long pile models.

Depending on the size and load-bearing mechanism of the pile foundation, the soil–pile–structure interaction actually changes the dynamic characteristics (i.e., natural frequency and damping) of the system such that input excitation responses cause different portions of the structure's higher mode to contribute to fluctuations in the shear force distributed along the superstructure. Consequently, practising engineers should be aware that the reduced ratio for the maximum base shear due to the soil–pile–structure interaction cannot be generalised to all levels of the superstructure because the design may prove to be unsafe.

5.5.3 Rocking of Foundations

Figure 5.12 shows how the different lengths of pile foundations supporting a 15-story structure rocked over time. Rocking occurs when the inertial forces generated in the superstructure cause compression on one side of the structure and tension on the other, which then results in settlement on one side and possible uplift on the other side. The models that experienced the same earthquake, albeit the pick values varied, revealed similarly shaped rocking over time, even when the piles changed from 10 m to 30 m long. The maximum rocking of a 15-story structure supported by foundations with different length piles under the earthquake excitations are summarised in Figure 5.13.

Figure 5.13 shows there was less rocking with longer piles than with shorter piles because the longer piles experienced higher shaft friction, which resulted in less rocking. For example, in the 1940 El Centro earthquake, when the piles increased from 10 to 28 m long, maximum rocking gradually decreased from 0.108 to 0.084°. This is a trend that was also observed in the other cases. Note that no rocking occurred in the fixed-base

structure, and the minor rocking observed in the end-bearing piles was caused only by elastic deformation in the pile elements.

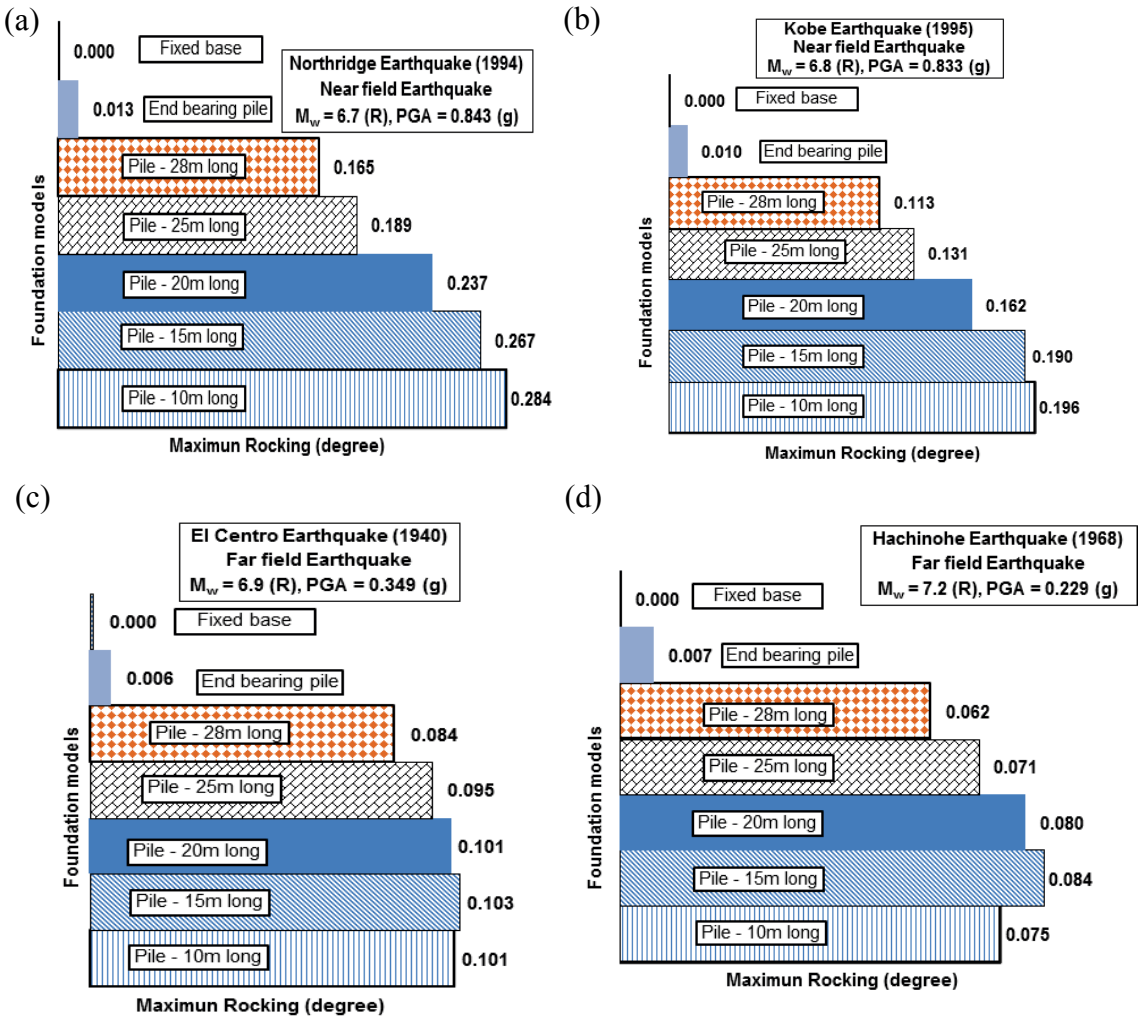

Figure 5.13 Maximum rocking of the fifteen-storey supported by pile foundation with different pile lengths under: (a) Northridge earthquake, (b) Kobe earthquake, (c) El Centro earthquake and (d) Hachinohe earthquake.

5.5.4 Response Spectrum and Natural Frequencies

The soil–structure interaction is defined as a phenomenon in which response of the soil influences the motion of the structure and response of the structure influences the motion of the soil (Kramer 1996). The impact of the soil–structure interaction on soil movement can be illustrated using the response spectrum of the ground motions recorded at the base of the structure supported by pile foundations of various lengths, as shown in (Figure

5.14). Having a better understanding of the ground actual movement during an earthquake, which is different to free-field motion, can help the design engineers evaluate the FIM and analyze the results, particularly when adopting a substructure method for SSPSI analysis. The length of piles in the foundation influenced the characteristic earthquake motions at the base of the structure by altering the inertial and kinematic interactions.

The response spectrum presents the peak acceleration of a single degree of freedom (SDOF) system with 5% damping and different natural periods for the adopted ground motions. Response spectrums are commonly used to apply structural dynamics to the design of structures and calculate the lateral forces required (base shears) in building codes as a function of the natural frequency of the system. Reducing the length of a pile caused the spectral acceleration to decrease as the natural period lengthened (Figure 5.14), such that this increase in the natural period substantially changed the spectral acceleration (S_a) response. Where midrise moment-resisting building frames with pile foundation rest on deposits of soft soil, their natural period lays in the long period region of the acceleration response spectrum curve. Because of natural period lengthening induced by reducing the length of piles in a pile foundation, the spectral acceleration (S_a) decreased, which then reduced the base shear of the structure (Figure 5.8 (c), Figure 5.9 (c), Figure 5.10 (c) and Figure 5.11 (c)).

Abaqus allows the natural frequency of possible motions to be generated; thus, for each pile foundation model there are several possible motions and vibrations that are accompanied by frequency (Table 5.5). Using a linear perturbation procedure and Lanczos method, eigenvalues were extracted to calculate the natural frequencies and the corresponding mode shapes of the soil–pile–structure system. The typically deformed shapes of the soil–foundation– structure system for the first two natural modes are shown in Figure 5.15. For instance, although the first natural frequency of the fixed-base structure was 0.83 Hz, the same structure supported by 10- and 25-m-long pile foundations (for a soil strain level compatible with the 1994 Northridge earthquake) possessed a first mode natural frequency of 0.615 and 0.694 Hz, respectively.

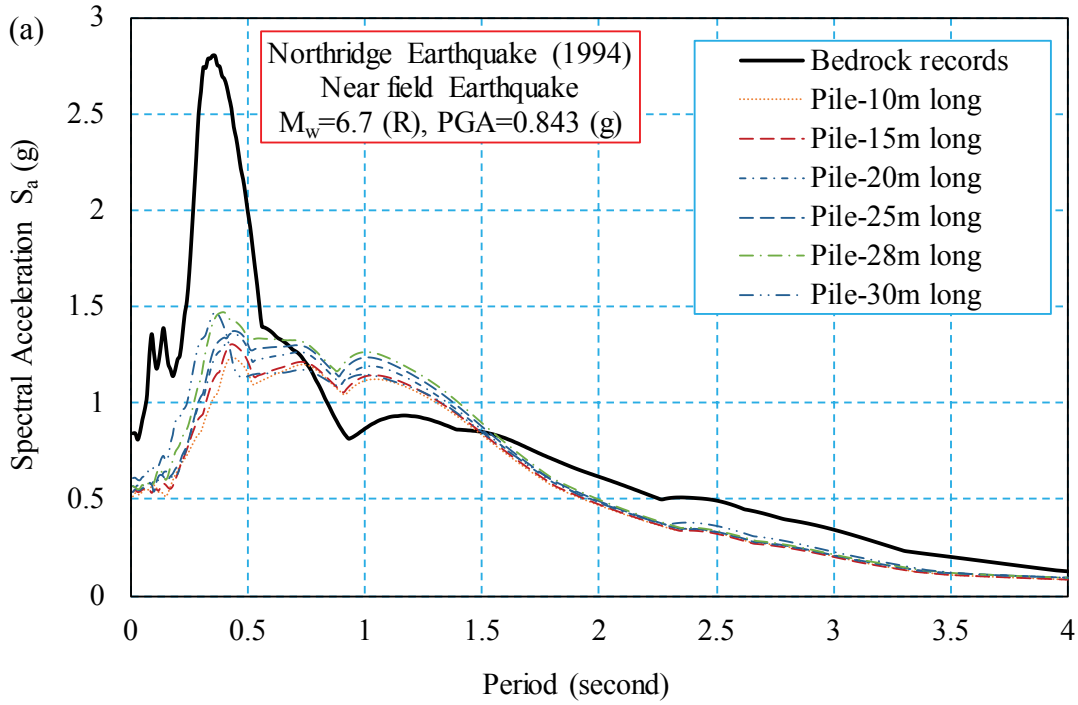
(a)
Northridge Earthquake (1994)
Near field Earthquake
Mw=6.7 (R), PGA=0.843 (g)
Bedrock records
Pile-10m long
Pile-15m long
Pile-20m long
Pile-25m long
Pile-28m long
Pile-30m long
Spectral Acceleration Sa (g)
Period (second)
0
0.5
1
1.5
2
2.5
3
3.5
4

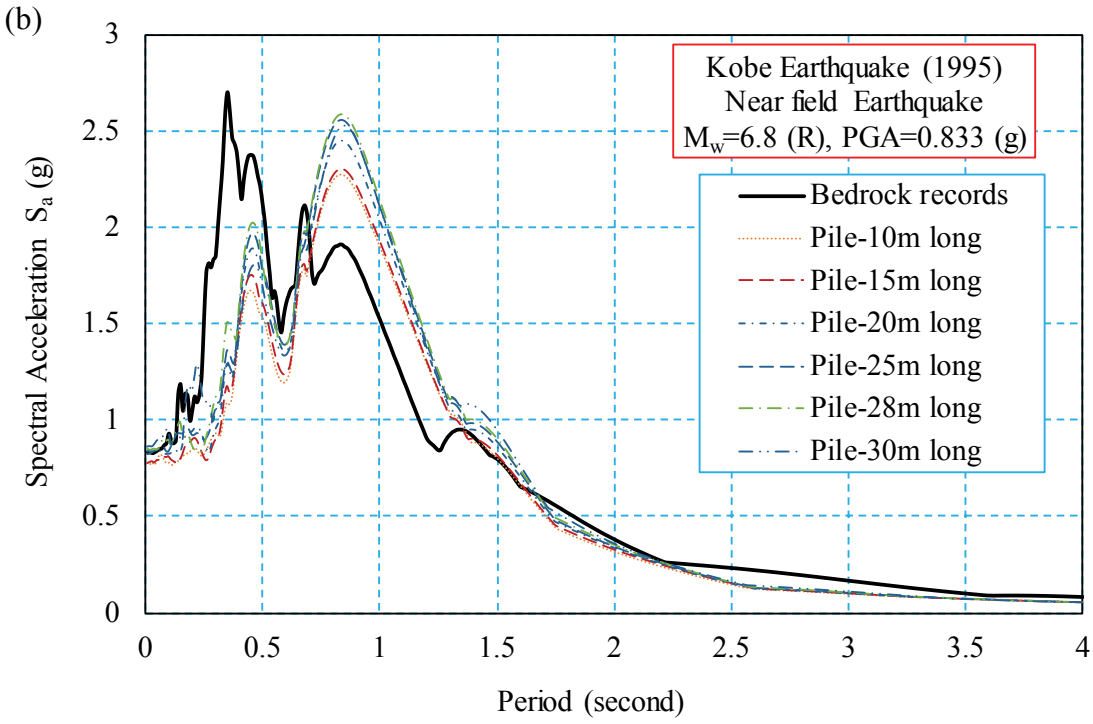
(b)
Kobe Earthquake (1995)
Near field Earthquake
Mw=6.8 (R), PGA=0.833 (g)
Bedrock records
Pile-10m long
Pile-15m long
Pile-20m long
Pile-25m long
Pile-28m long
Pile-30m long
Spectral Acceleration Sa (g)
Period (second)
0
0.5
1
1.5
2
2.5
3
3.5
4

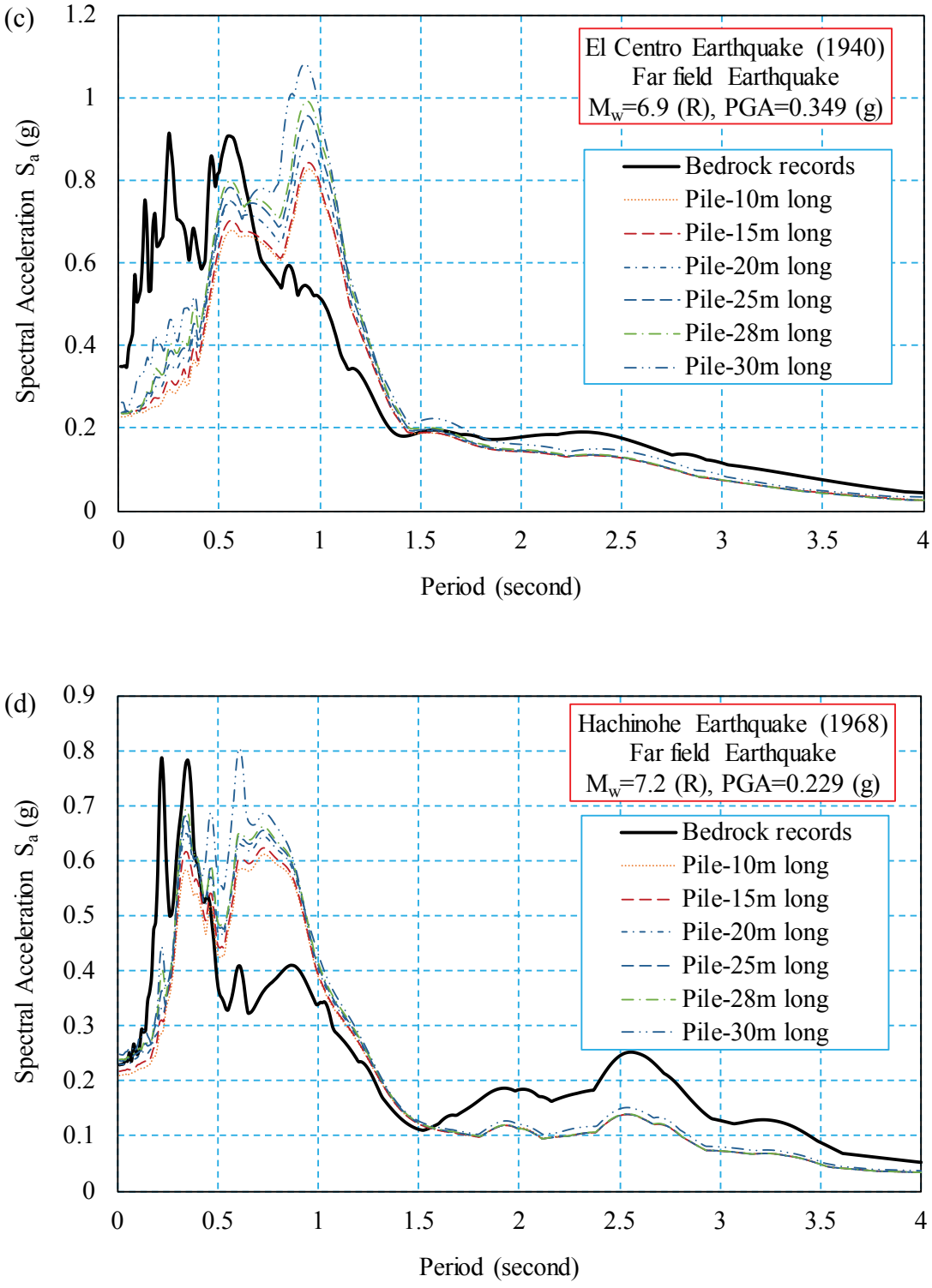

Figure 5.14 Response spectrum of ground motions of the fifteen-storey supported by pile foundation with different pile lengths under: (a) Northridge earthquake, (b) Kobe earthquake, (c) El Centro earthquake and (d) Hachinohe earthquake.

Table 5.5 Variations of natural frequencies of soil-pile-structure systems with different pile lengths

		Frequency (Hz)							
Soil Properties (Adopted Earthquake)		G/G_{max}=0.31, ξ=13.5% (Northridge)		G/G_{max}=0.36, ξ=12.4% (Kobe)		G/G_{max} =0.42, ξ=11.2% (El-Centro)		G/G_{max}=0.66, ξ=8.35% (Hachinohe)	
Motion mode		Mode 1 (f_1)	Mode 2 (f_2)	Mode 1 (f_1)	Mode 2 (f_2)	Mode 1 (f_1)	Mode 2 (f_2)	Mode 1 (f_1)	Mode 2 (f_2)
Pile Length	10 m	0.615	2.217	0.618	2.231	0.620	2.240	0.715	2.302
	15 m	0.648	2.219	0.648	2.235	0.649	2.245	0.719	2.311
	20 m	0.669	2.224	0.675	2.243	0.682	2.251	0.723	2.316
	25 m	0.694	2.230	0.698	2.249	0.705	2.258	0.796	2.322
	28 m	0.695	2.246	0.699	2.268	0.708	2.271	0.802	2.331
	30 m (socketed)	0.788	2.242	0.788	2.261	0.789	2.272	0.821	2.338
Fixed base Building		Mode 1 (f_1)= 0.830 Hz & Mode 2 (f_2) = 2.341 Hz							

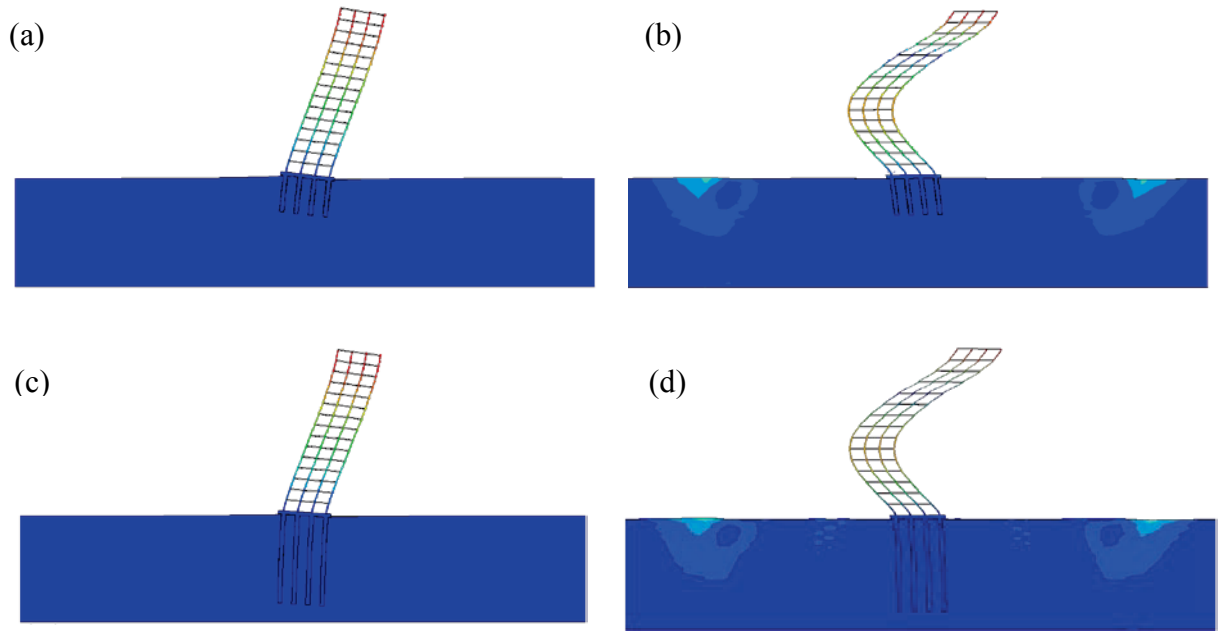

Figure 5.15 Typical possible motions and vibration for natural frequencies

(a) Mode 1 for 10m long pile, natural frequency = 0.615 Hz
(b) Mode 2 for 10m long pile, natural frequency = 2.217 Hz
(c) Mode 1 for 25m long pile, natural frequency = 0.694 Hz
(d) Mode 2 for 25m long pile, natural frequency = 2.230 Hz

This change in the dynamic characteristics of the system was one of the main contributors to the amount of energy absorbed by a structure subjected to strong earthquakes.

The comparison between the natural frequency of the soil–pile–structure system with different length piles and load-bearing mechanisms is shown in Table 5.5. The pile elements increase the equivalent stiffness of the system by an amount related to the volume of the soil medium replaced by the stiff pile elements. As such, longer pile elements result in a stiffer soil–pile–structure system. Note that the natural frequency of the system is a function of damping and mass as well as the stiffness, so although longer pile elements generally increase the natural frequency of the system, as seen in Table 5.5 variations of other influential parameters can alter this pattern.

5.5.5 Bending Moments and Shear Forces in the Pile Elements

The numerical results provide the time history of the relative lateral movement $u_1(z,t)$ of any point along the pile and also rocking (in degrees) of the foundation $\alpha(t)$ (Figure 5.12), where z = depth from the bottom of the foundation to the point being considered; and t = time during excitation. From these two time histories, the lateral pile deflection $d_1(z,t)$ is obtained using the following equation:

$$d_1(z,t) = u_1(z,t) - z\tan[\alpha(t)] \tag{5.4}$$

The time when the toe of the pile deflects laterally and reaches its maximum value was used to plot lateral deflection along the pile $d_1(z)$. The pile elements are numbered, as shown in Figure 5.7 (b), but due to the symmetric characteristics of the model, only eight piles were considered.

Lateral pile deflections are presented in Figure 5.16 (a) for the 1994 Northridge earthquake, Figure 5.19 (a) for the 1995 Kobe earthquake, Figure 5.22 (a) for the 1940 El Centro earthquake and Figure 5.25 (a) for the Hachinohe earthquakes, respectively. The elastic beam theory (Euler-Bernoulli's equation) is used to produce the bending moment and shear force along the length of each pile as follows:

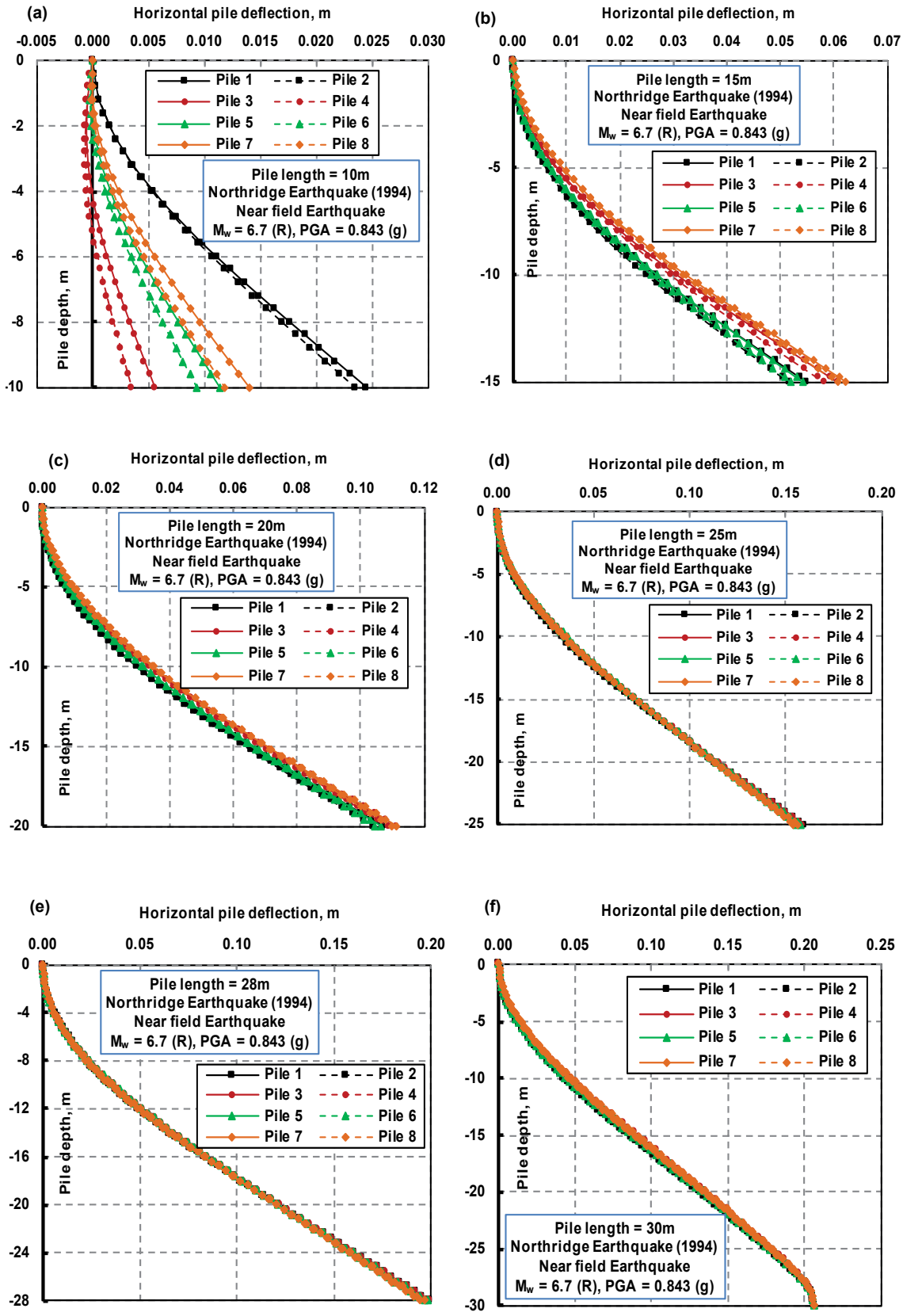

Figure 5.16 Lateral deflection of the piles under the 1994 Northridge earthquake

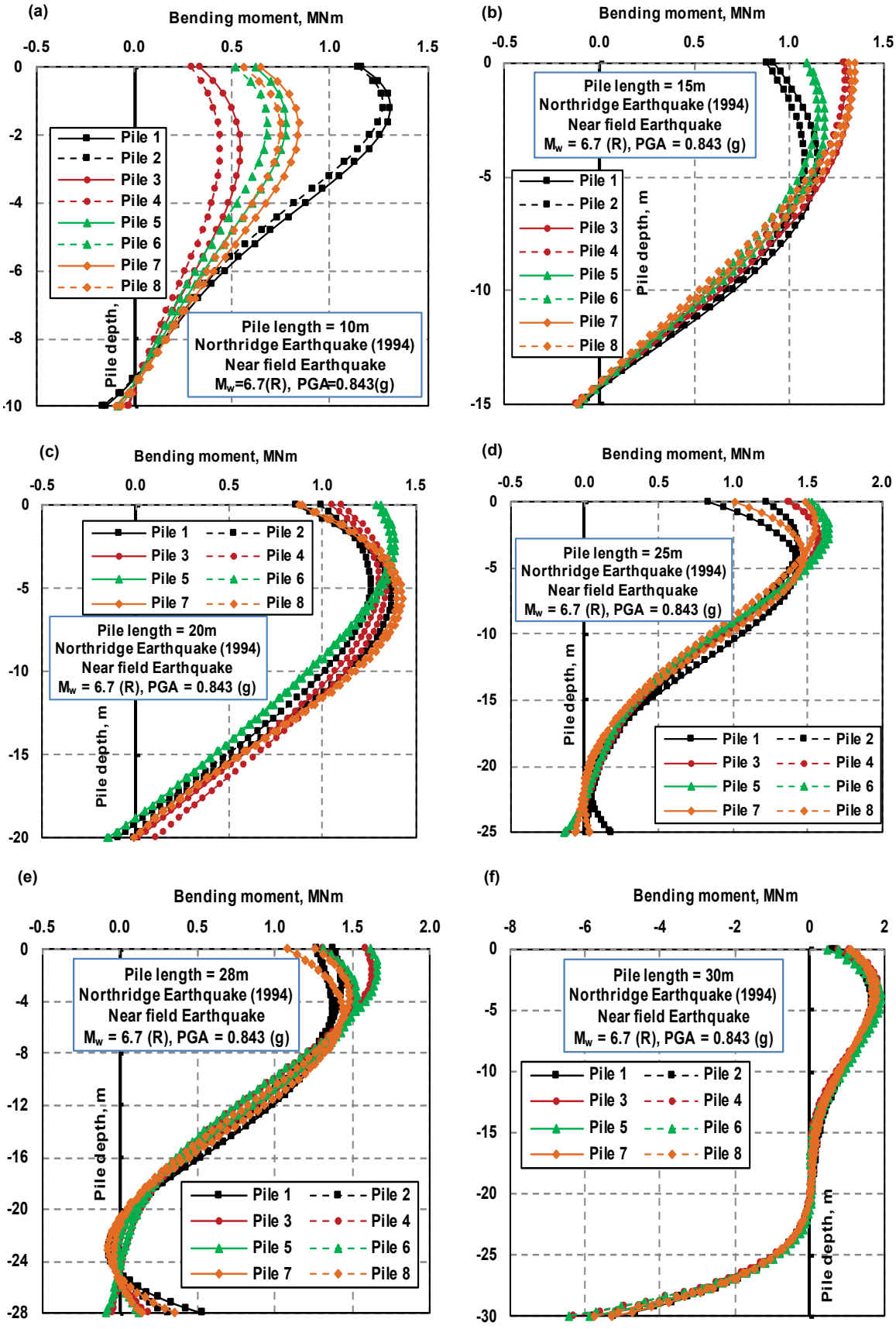

Figure 5.17 Bending moment of the piles under the 1994 Northridge earthquake

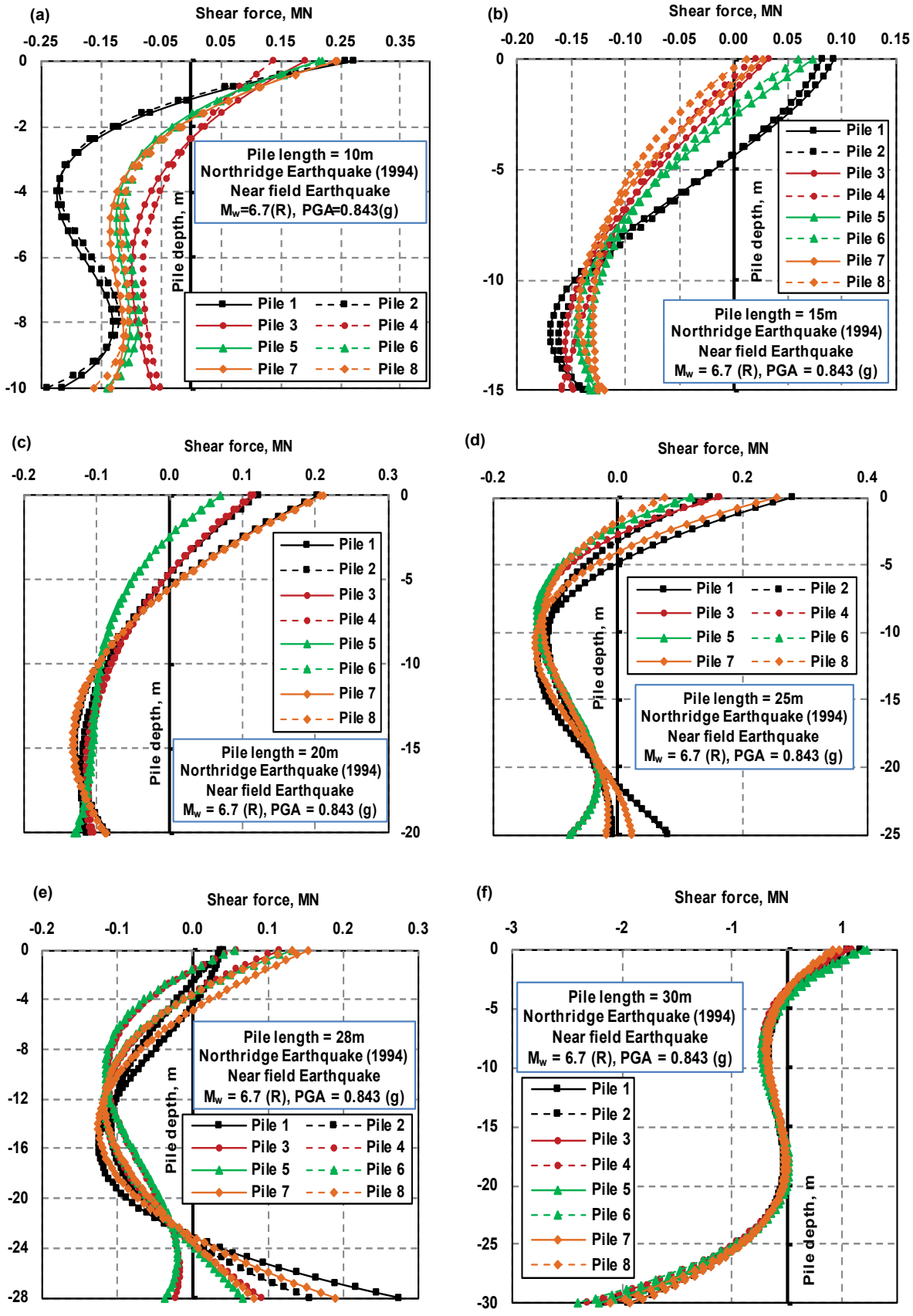

Figure 5.18 Shear force of the piles under the 1994 Northridge earthquake

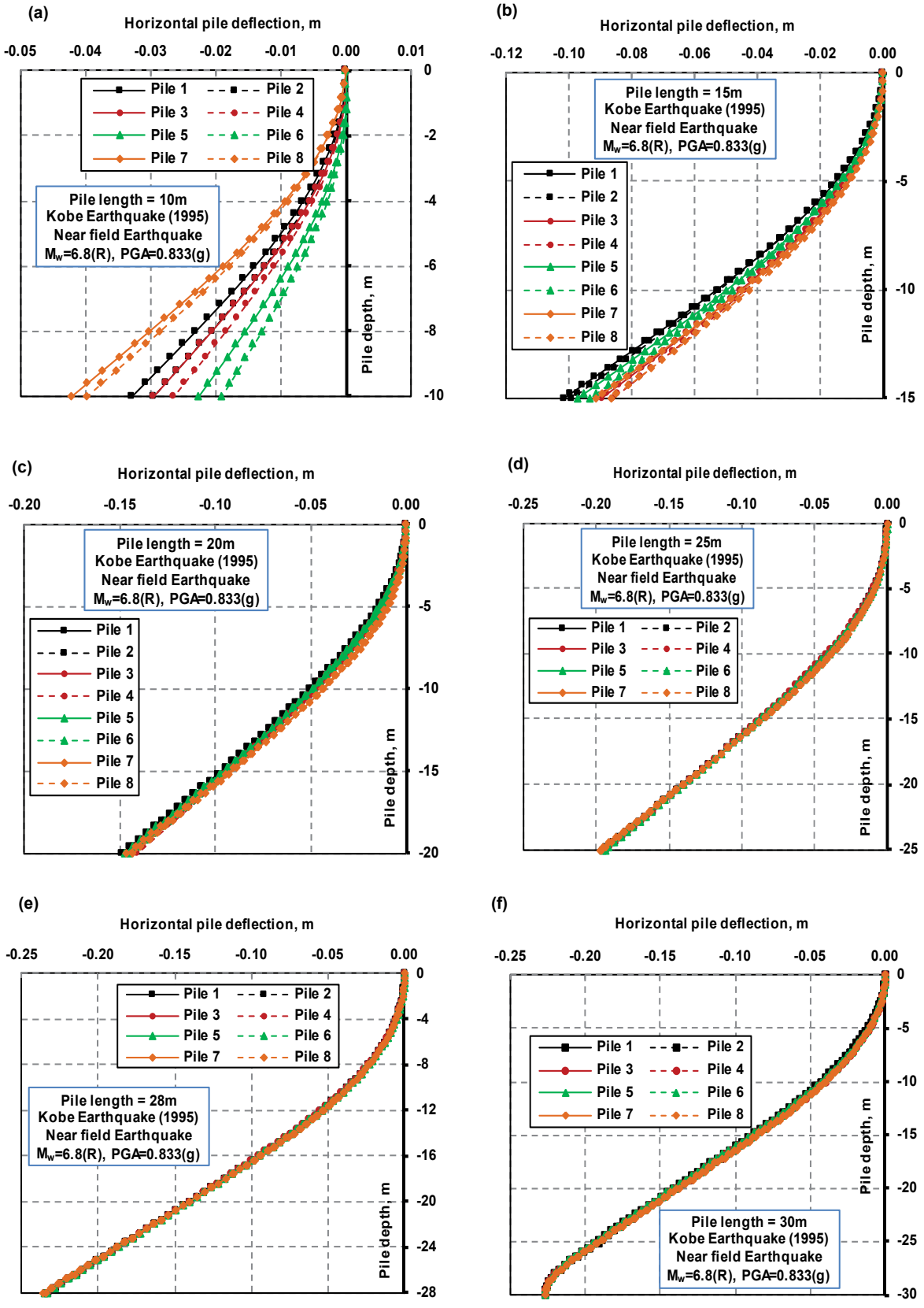

Figure 5.19 Lateral deflection of the piles under the 1995 Kobe earthquake

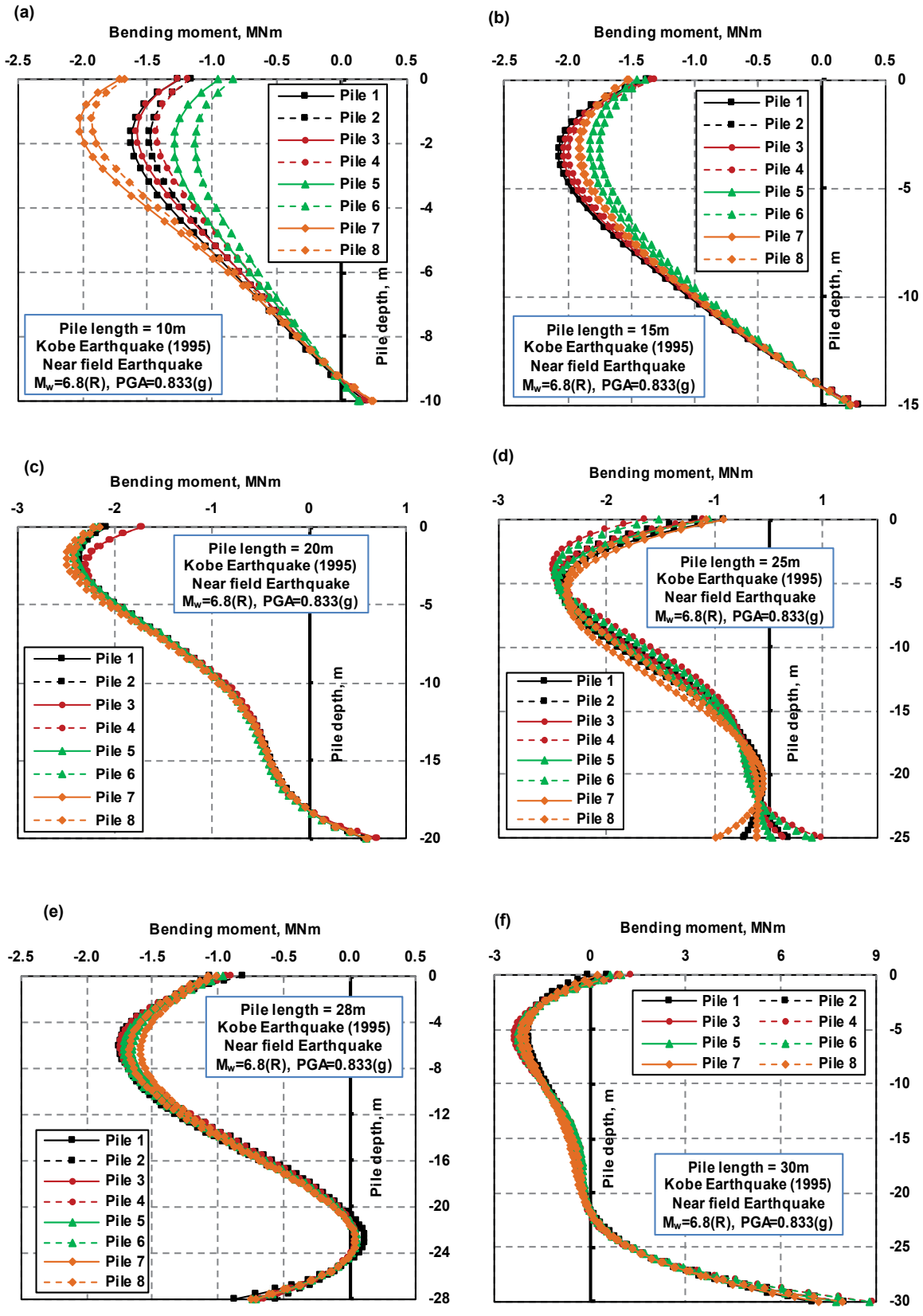

Figure 5.20 Bending moment of the piles under the 1995 Kobe earthquake

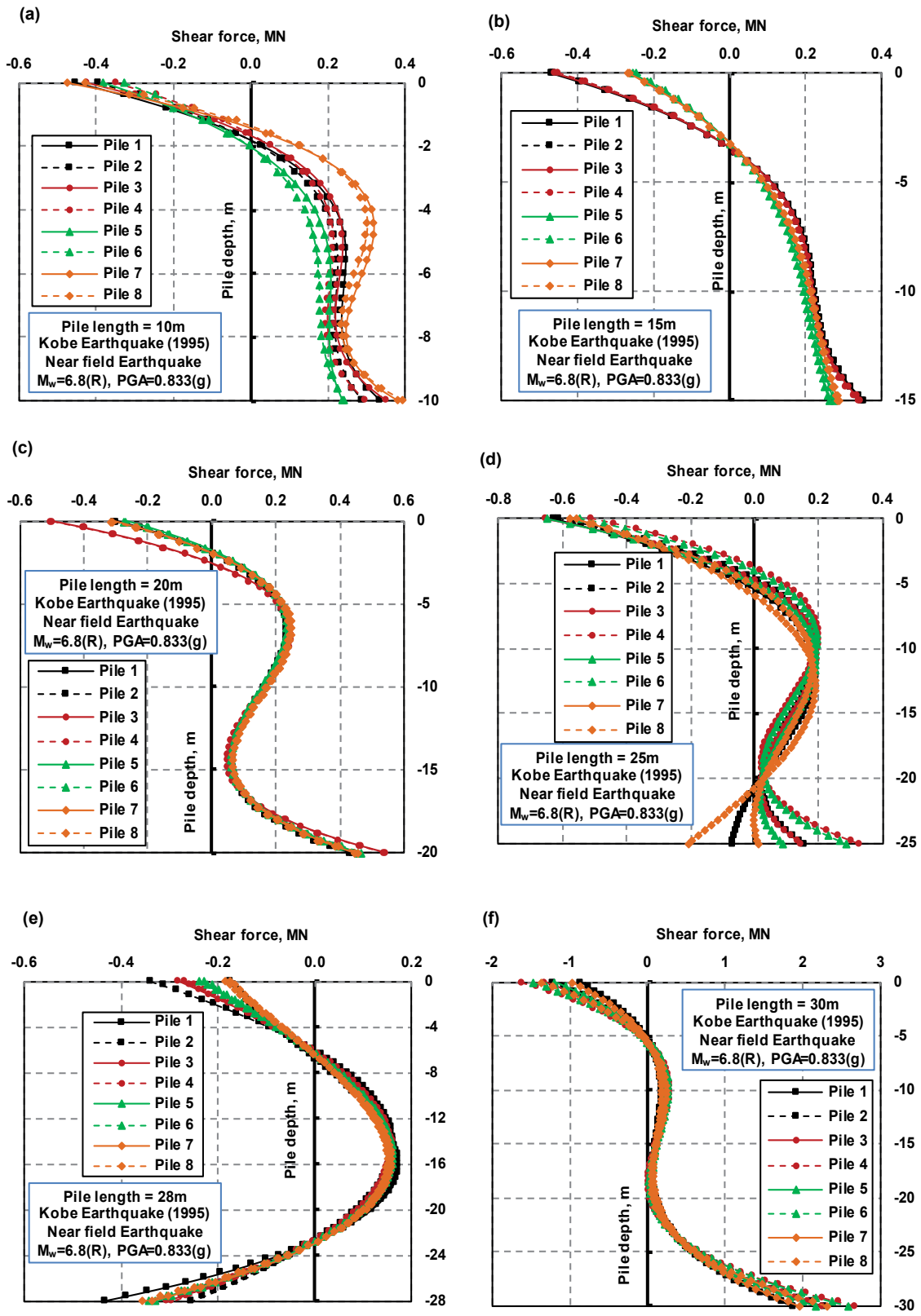

Figure 5.21 Shear force of the piles under the 1995 Kobe earthquake

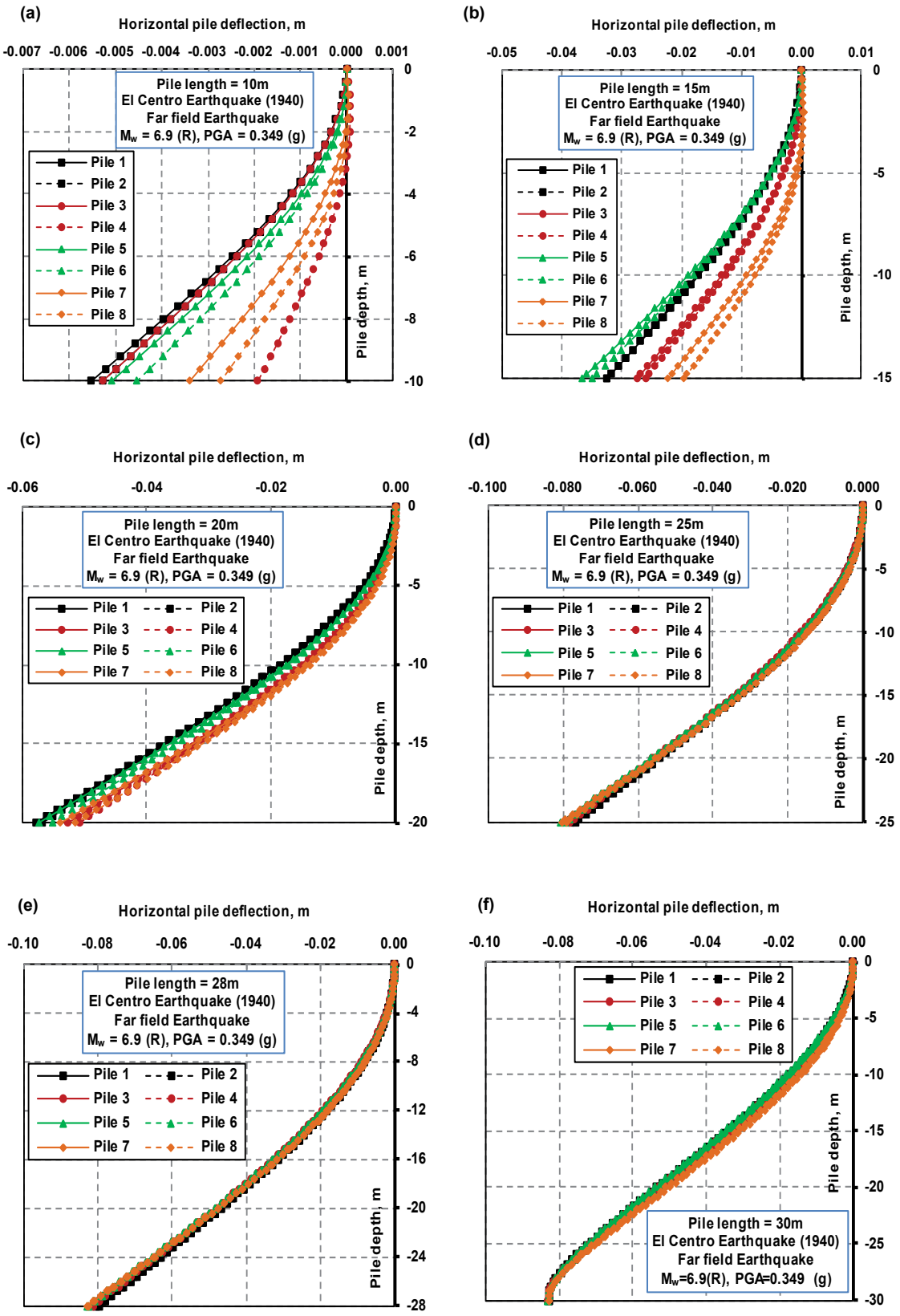

Figure 5.22 Lateral deflection of the piles under the 1940 El Centro earthquake

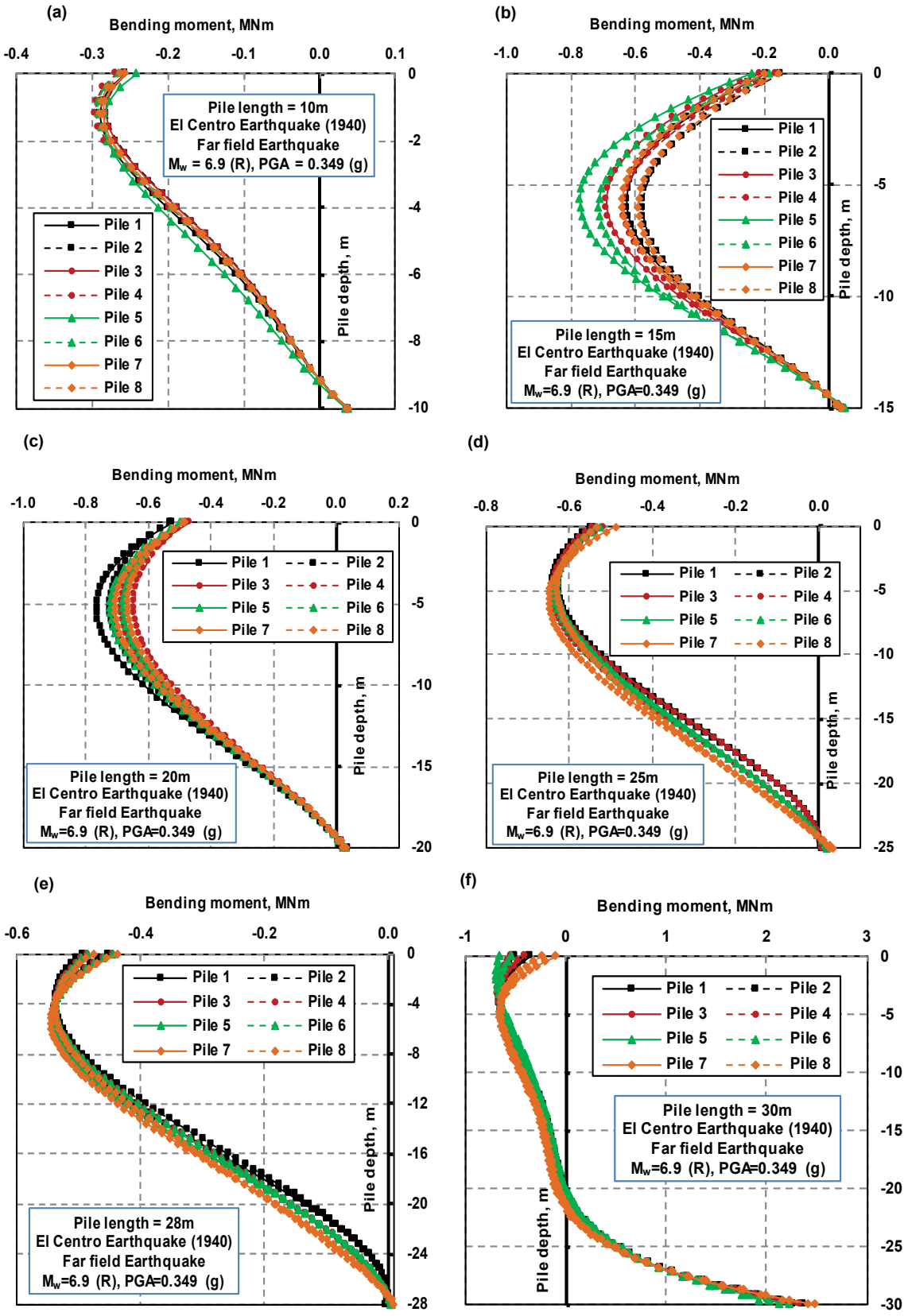

Figure 5.23 Bending moment of the piles under the 1940 El Centro earthquake

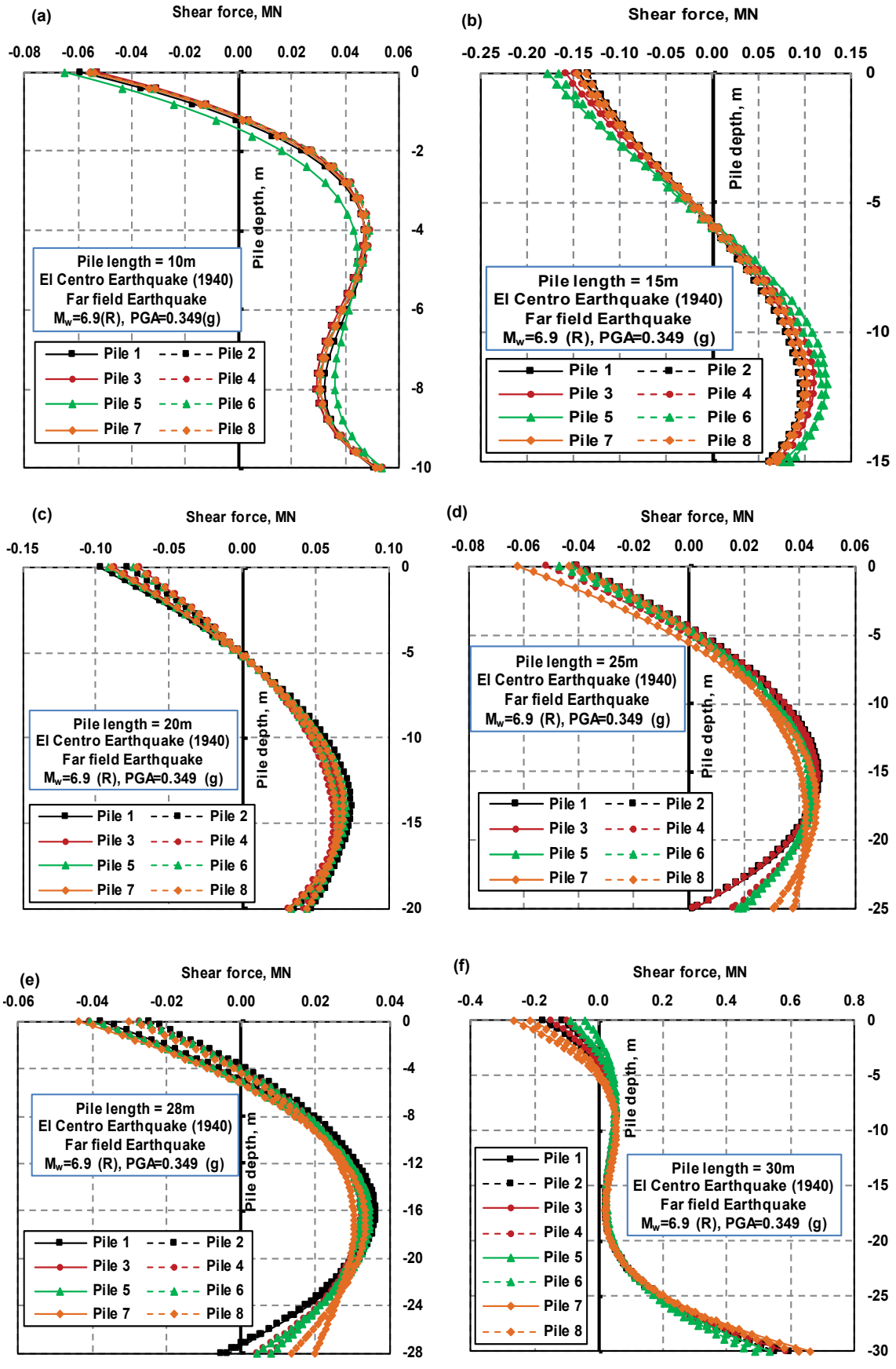

Figure 5.24 Shear force of the piles under the 1940 El Centro earthquake

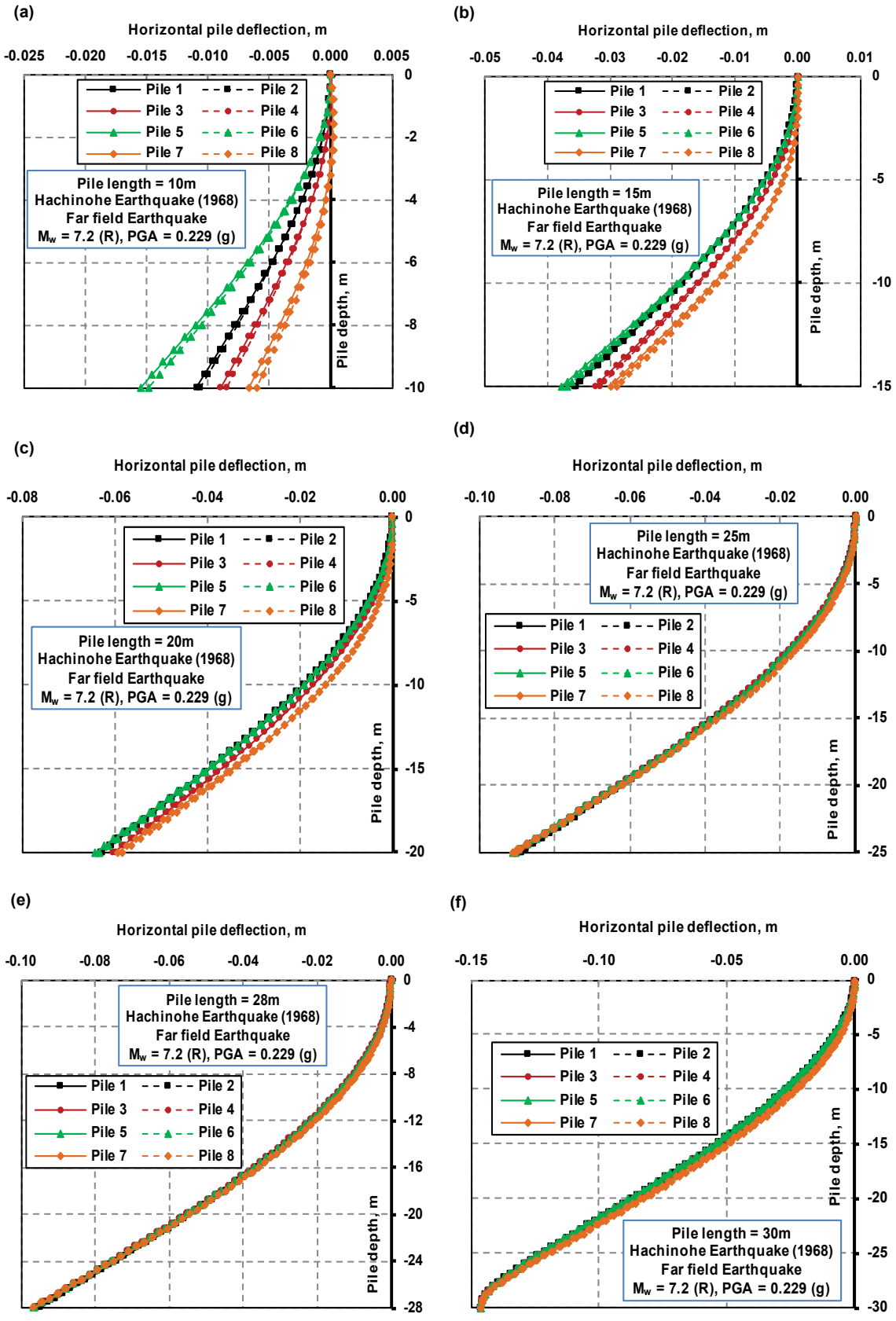

Figure 5.25 Lateral deflection of the piles under the 1968 Hachinohe earthquake

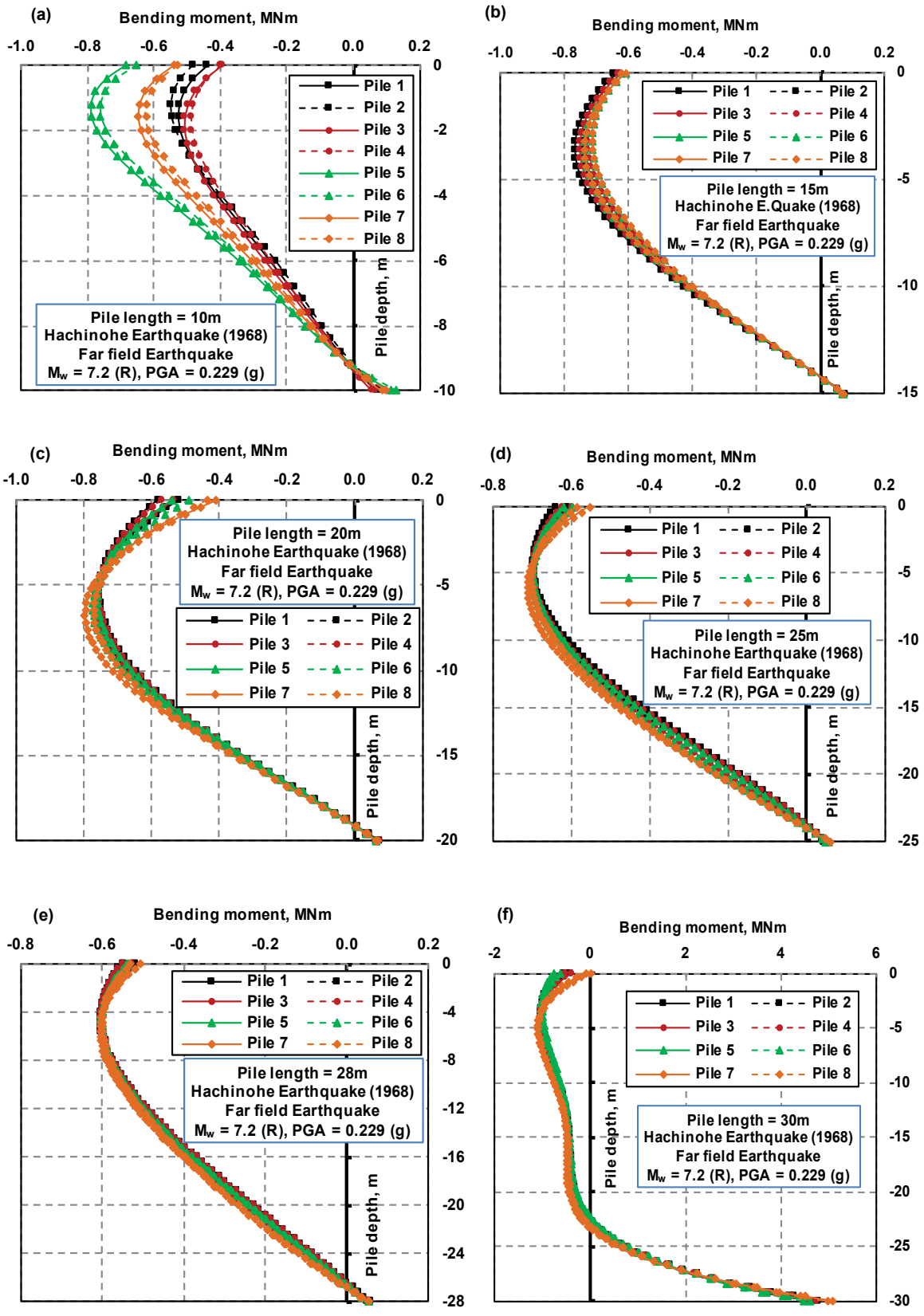

Figure 5.26 Bending moment of the piles under the 1968 Hachinohe earthquake

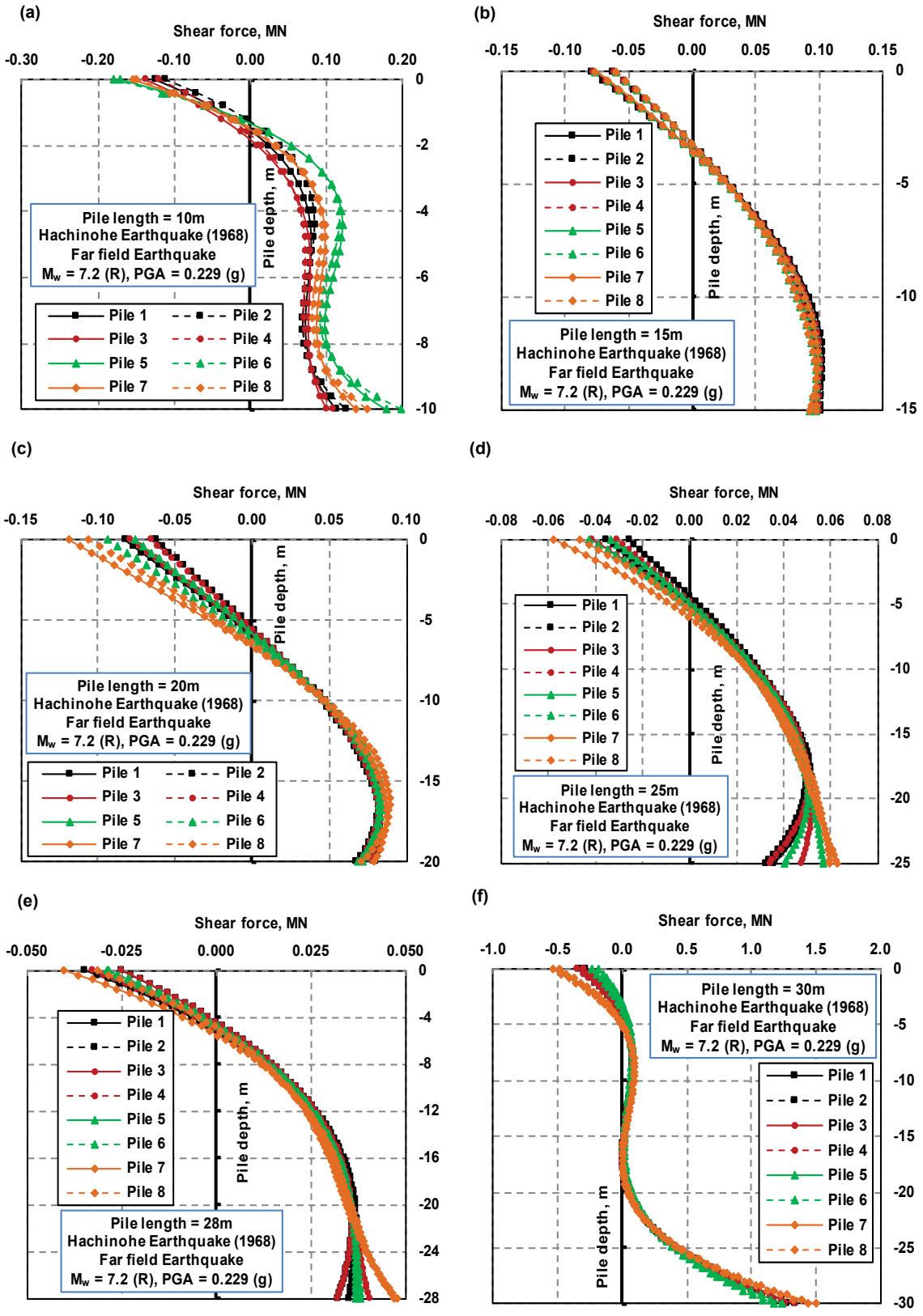

Figure 5.27 Shear force of the piles under the 1968 Hachinohe earthquake

$$M(z) = EI\ \frac{d^2[d_1(z)]}{dz^2} \tag{5.5}$$

$$Q(z) = EI\ \frac{d^3[d_1(z)]}{dz^3} \tag{5.6}$$

where E = Young's modulus of pile material ($E = 3.01 \times 10^5$ MPa); and I = second moment of the pile cross section ($I = \pi r^4 = 0.108\ (m^4)$, r is radius of pile), resulting in $EI = 3.064 \times 10^{10}\ (Nm^2)$. To produce the most accurate curves, the sixth-order polynomial fitting curves were used for deflection, and then the second and third differentials of the polynomial were obtained to calculate the bending moments and shear forces, respectively.

5.5.6 Lateral Pile Deflections

The numerical results reported in Figure 5.16 (a), Figure 5.19 (a), Figure 5.22 (a) and Figure 5.25 (a) show that piles from different positions in the foundation have a similarly shaped lateral deflection. The difference in lateral deflection of the outside rows (numbered 1, 2, 7, and 8) and the middle rows (numbered 3–6) are considerable when the piles are short, but it becomes smaller for longer piles. Furthermore, longer piles experience more lateral deflections compared with the short pile elements. For instance, although the maximum lateral deflection of the 10-m-long pile is around 5.5 mm under the 1940 El Centro earthquake, the 25- and 28-m-long piles experience 79- and 82-mm maximum lateral deflections, respectively. The deformation of the surrounding soft soil under shaking excitations imposes lateral deflection to the embedded pile elements (kinematic forces). As such, longer pile elements were subjected to the larger soil lateral deformations compared with the shorter piles.

Moreover, the inertial shear forces transferred from the superstructure cause further pile lateral deflection. Because the superstructure supported by longer pile elements attracts more inertial energy from an earthquake, extra lateral deflection in longer piles was expected. Also, the maximum kinematic forces and inertial forces are unlikely to occur at the same time due to the phase differences.

5.5.7 Bending Moments along the Piles

The bending moment curves of piles (5.5) were derived by double differentiating their deflection curves (5.4), and the results are compared in Figure 5.17, Figure 5.20, Figure 5.23 and Figure 5.26 for the 1994 Northridge, 1995 Kobe, 1940 El Centro and 1968 Hachinohe earthquakes, respectively. As expected, side piles carry more of the loads applied due to the group effect.

The maximum bending moment in the floating pile elements generally occurs in the top 6 m of the pile, whereas the minimum bending moment always occurs at the toe. A longer pile foundation produced a larger bending moment under the applied earthquakes; for example, in the model with 10-m long piles, the maximum bending moment was less than 0.3 MN·m and occurred in the top 2 m of the outside piles, whereas in the model with 20- and 25-m-long piles, the maximum bending moment was more than 0.5 MN·m and occurred 5–6 m below the ground surface for the 1940 El Centro earthquake.

The load-carrying mechanism in an end-bearing foundation differs entirely from floating piles. End-bearing pile foundations experience an excessive bending moment at the toes of the piles on which they are connected to the bedrock. Comparing the end-bearing pile case with the 28-m-long floating pile case subjected to the 1940 El Centro earthquake, it is evident that the end-bearing piles are highly influenced by the lateral deformations of the surrounding soil. This results in imposing extra kinematic ground forces to the pile elements and the development of high bending moments in deeper areas.

5.5.8 Shear Force along the Piles

The shear force imposed on the pile elements during shaking excitations is another important parameter governing the design of a foundation. The shear forces in pile elements for different cases are presented in Figure 5.18, Figure 5.21, Figure 5.24 and Figure 5.27 for the 1994 Northridge, 1995 Kobe, 1968 Hachinohe and 1940 El Centro earthquakes, respectively. Here, the size of the pile foundation and load-bearing mechanism alters the maximum shear forces and its distribution along the pile elements. This is an important observation showing how the combined kinematic and inertial interactions that influence the loads developing on pile elements can be overlooked in

common design practises in which the superstructure and pile foundation are treated separately.

5.6 Summary

To investigate the type and size of pile foundation needed to support buildings in high-risk seismic zones, a 15-story moment-resisting frame sitting on end-bearing and floating pile foundations with different sizes was simulated numerically using Abaqus software.

The numerical modelling technique used for the simulation of complex seismic soil–pile–structure interaction phenomena in ABAQUS was described. By adopting a method of direct calculation, the numerical model can perform a fully nonlinear time history dynamic analysis to realistically simulate the dynamic behaviour of soil, pile foundation, and structure under seismic excitations.

The results show that by increasing the length of floating piles the structure undergoes more maximum lateral deformation. This can push the inter-story drifts that developed in the superstructure to exceed the life-safe level for the performance-based designs that are usually defined by limiting inter-story drifts to 1.5%.

The lateral deflection of the structure consists of two components: structural distortion, which relates directly to the shear forces generated in the structure, and foundation rocking. This study shows that the length of the pile elements influences the total shear forces absorbed by the structure during an earthquake; longer piles have higher contact surfaces with the surrounding soil, which enables them to absorb extra energy, and they experience less rocking than shorter piles because their resistance is stronger.

The length of the pile foundation and load-bearing mechanism influences the way shear forces are distributed along the superstructure, and the amount and trend of variations in the shear forces were not the same at every level. This means that practising engineers should be aware that the reduction ratio for maximum base shear due to the interaction between the soil–pile–structure cannot be generalised to all levels of the superstructure because it could result in an unsafe design.

The pile foundation and load-bearing mechanism alters the forces and how they are distributed along the pile elements. This observation shows how combined kinematic and inertial interactions influence the developed loads on pile elements, which can be

overlooked in common design practises in which the superstructure and pile foundation are treated separately.

The behaviour of an end-bearing pile foundation is not easy to compare with frictional (floating) pile foundation cases due to the totally different load-bearing mechanism. In a floating pile foundation, the stresses transfer between the soil and pile elements mainly through the pile shafts, but in an end-bearing pile foundation the connection between the toe of a pile and the bedrock governs the load transfer mechanism during shaking excitations and highly impacts the imposed kinematic forces due to the lateral movement of the surrounding soft soil.

The results of this study can help in deciding the size and type of pile foundation best suited to the seismic performance of buildings sitting on soft soil, while aiming to achieve an optimised design, because longer piles do not necessarily result in a safer design under strong ground motions when the interaction between soil and structure is considered.

Chapter 6 THE RESPONSE OF MID-RISE BUILDINGS SITTING ON PILE FOUNDATIONS TO SEISMIC POUNDING

6.1 General

Seismic pounding occurs when the separation gap between buildings and structures is not wide enough, particularly during major earthquake events; this can cause them to collide, causing local damage, or in extreme cases, to collapse. This study investigates the impact that this separation gap has on the seismic response of mid-rise buildings supported on piles considering seismic soil-pile-structure interaction (SSPSI). To achieve this aim, three fifteen-storey reinforced concrete buildings sitting on pile foundations and with five different separation gaps under excitations from the 1994 Northridge and 1995 Kobe earthquakes, were numerically simulated using ABAQUS software. This study uses three-dimensional numerical modelling to simultaneously capture the effects of seismic pounding and SSPSI. The nonlinear behaviour of structural elements was included, and the dynamic soil properties were obtained from field data and backbone curves. A contact pair interface with small-sliding surface-to-surface formulation between buildings was used to capture possible seismic pounding, and contact interfaces with a finite-sliding formulation were used to simulate the interaction between the piles and the soil. The results, including lateral building deflections, inter-storey drifts, structural shear forces, foundation rocking, lateral pile deflections, and the distributions of bending moments and shear forces of the piles are presented and discussed. The findings of this study will give engineers a better understanding of the possible effects of seismic pounding on the seismic performance of buildings, and the response of end-bearing piles in soft soils.

6.2 Introduction

It is not unusual for structures in metropolitan areas to be constructed very close to each other, but during a strong seismic event it is highly likely that they interact due to seismic pounding, leading to severe damage and possible collapse. The lessons learnt from previous earthquake events revealed that seismic pounding is a common phenomenon that can cause failure of non-structural elements, damage to structural elements, and as a

consequence, the partial or total collapse of structures (Rosenblueth and Meli 1986; Park and Hashash 2004; Song *et al.* 2008; Chouw and Hao 2012). Rosenblueth and Meli (1986) reported that in the 1985 Mexico City earthquake, pounding occurred in about 40% of the buildings which partially or entirely collapsed, while 15% of the buildings collapsed primarily due to collisions during this seismic event. In recent earthquake events such as the 2008 Wenchuan earthquake and the 2011 Christchurch earthquake, structural damage due to seismic pounding has also been observed and reported (Song *et al.* 2008; Chouw and Hao 2012).

Many researchers (e.g., (Anagnostopoulos 1988; Hao *et al.* 2000; Karayannis and Favvata 2005; Mahmoud *et al.* 2008; Hao 2015) have pointed out that the effects of pounding should be considered in the structural design stage. According to Hao (2015), the best way to avoid seismic pounding is to provide a sufficient separation gap between buildings. Many modern seismic standards and codes make recommendations on the minimum requirement of the separation gap (also known as the seismic gap) between adjacent buildings. FEMA356 (FEMA 2000) requires a minimum distance (s_i) between adjacent structures at any level i as below:

$$s_i = \sqrt{\Delta_{i1}^2 + \Delta_{i2}^2} \tag{6.1}$$

where Δ_{i1} and Δ_{i2} are the lateral deflections of neighbouring structures. The European seismic design standard (Eurocode8 2005) also has a similar requirement for the size of separation gap. The Chinese seismic design code (GB50011 2010) requires a separation gap of more than 100 mm when the height of a reinforeced concrete building is within 15 meters. When the building height exceeds 15 meters, a 20 mm increment in the separation gap for every 5 m, 4 m, 3 m, and 2 m increments in height is required in regions which correspond to the Chinese seismic intensity level of 6, 7, 8 and 9, respectively. The Australian seismic design standard (AS1170.4 2007) requires a separation gap greater than 1% of the height for structures higher than 15 meters, although existing buildings constructed before the introduction of modern seismic provisions are usually excluded (Anagnostopoulos 1996). However, Anagnostopoulos (1988) stated that these requirements may not be easy to satisfy even for new constructions due to the economic, technical, and legal reasons put forward by property owners, engineers, and developers.

According to Wolf and Skrikerud (1980), the separation gaps between structures may still be insufficient if the plastic displacement of structures and soil beneath the foundations develops during an actual earthquake event. It is common practice to not consider the underlying soil, particularly when structural pounding is analysed, and thus the effect of soil-structure interaction (SSI) is ignored by claiming it will produce a conservative design and the effect of SSI often decreases the fundamental frequency of a structure and increases the effective damping compared to the same structure under a fixed-base condition (Kramer 1996). Based on a comprehensive numerical study, Tavakoli *et al.* (2011) concluded that as the soil under the structure becomes softer, the influence of SSI on amplifying lateral deflections and inter-storey drifts would be more significant, and therefore SSI should be considered for structures supported by relatively soft soil. Furthermore, Carbonari *et al.* (2011) studied the effect of soil-pile-structure interaction (SPSI) on a coupled wall-frame building through a finite element analysis and concluded that the effects of SPSI should be considered in structural design because it would amplify the global seismic response of buildings, particularly the lateral displacement and inter-storey drifts. On this basis the effects of SSI should be considered when studying seismic pounding because it is caused by the relative lateral movement of two adjacent structures. Shakya and Wijeyewickrema (2009) reported that when seismic pounding occurs, the location and the impact force acting on the pounding area are influenced by the dynamic characteristics of the structures and underlying soil, and the distances between neighbouring buildings.

Recently, the issue of coupling the effects of seismic pounding and SSI has received a lot more attention. (Rahman *et al.* 2001) performed a series of time history analyses to study the effect of seismic pounding on two reinforced concrete buildings with different heights, while taking into account the effect of the underlying soil. Chouw (2002) adopted the boundary element method to investigate two colliding buildings modelled by finite element analysis, while considering the flexibility of soil in the Laplace and time domains. Shakya and Wijeyewickrema (2009) conducted an analysis of two buildings with different heights while considering SSI to study the effects of mid-column pounding on the building under the influence of near-field and far-field earthquakes. Uz and Hadi (2011) developed a MATLAB program based on the fourth-order Runge-Kutta method to carry out a response history analysis on two adjacent buildings while

considering the combined effects of seismic pounding and SSI. Moreover, Naserkhaki *et al.* (2012) developed an analytical model of nearby buildings resting on soil where the buildings are connected by the visco-elastic contact elements during pounding. Mahmoud *et al.* (2013) studied the influence of SSI on the seismic pounding of two buildings with the same height but different dynamic characteristics; here the buildings are represented by lumped mass systems and dynamic soil behaviour is considered by using spring-dashpot elements. Furthermore, Zou *et al.* (2013) studied the effect of SPSI on the pounding response of two closely spaced buildings of different heights through analytical modelling. Madani *et al.* (2015) developed a single degree of freedom finite element model which considers SSI and the structure-soil-structure interaction, to investigate the effect of seismic pounding on the dynamic response of structures in which structural and soil non-linearity are considered.

These aforementioned research studies indicate that most of them only examined the effects of interaction between shallow footings and supporting soil, only a few considered deep foundations. Although most of these studies investigated the dynamic responses of two conventional buildings of equal or unequal heights using simple lumped mass models, only a few studied the response of retrofitted buildings such as shear wall braced buildings. As mentioned by Wolf and Skrikerud (1980), the problem of insufficient separation gaps can also be caused by retrofitting structures for increased seismic requirements because this process modifies their dynamic properties and their subsequent seismic response. Moreover, since the effects of seismic pounding on the responses of end-bearing piles has rarely been examined, this study will investigate how seismic pounding between adjacent buildings supported by end-bearing pile foundations influences the seismic response of buildings and piles while considering SPSI. To achieve these goals, ABAQUS software, a three-dimensional finite element numerical simulation package, will be utilised to analyse a fully coupled soil-foundation-structure system by adopting the direct method. Two buildings which represent conventional moment resisting buildings and retrofitted buildings are considered, with the assumption that they are of equal height and with aligned storey levels. The nonlinear behaviour of structural elements is considered, while the dynamic soil properties are obtained from field data and backbone curves. Contact surfaces are assigned to interacting building models to capture possible seismic pounding. To rigorously account for the effect of SPSI, the nonlinear

behaviour of contact surfaces between piles and the surrounding soil medium are captured. The numerical results, including the response spectrum, shear distribution along the buildings, lateral structural displacement, maximum drift envelope, maximum rocking of the foundation slab, lateral pile displacements, and the bending moments and shear forces along the piles are presented and discussed.

6.3 Characteristics of a Soil-Pile-Structure System

6.3.1 Features of adopted buildings

A fifteen-storey three-bay reinforced concrete moment resisting building representing conventional mid-rise buildings, and two fifteen-storey three-bay reinforced concrete buildings with shear wall systems representing retrofitted buildings, have been modelled in this study. The adopted shear wall braced buildings have shear walls at the middle bay in both directions and along their entire height. As Figure 6.1 shows, the conventional moment resisting building is located in the middle with two shear wall braced buildings sitting on each side. Figure 6.2 presents the numerical soil-pile-structure model developed in ABAQUS software.

Table 6.1 Designed sections for columns, slabs and shear walls

Sections Type		**Dimensions (m)**	**Moment of Inertia of Plane Area (m^4)**	**Cracked Factor (According to ACI318-08(2008))**	**Reduced Moment of Inertia of Plan Area I_{cr} (m^4)**
Column	I	0.55×0.55	0.0076	0.7	0.00532
	II	0.50×0.50	0.0052	0.7	0.00364
	III	0.45×0.45	0.0034	0.7	0.00238
	IV	0.40×0.40	0.0021	0.7	0.00147
Floor Slab		0.25×1.0	0.0013	0.25	0.000325
Shear Wall	I	0.55×4.0	2.933	0.7	2.0531
	II	0.50×4.0	2.667	0.7	1.8669
	III	0.45×4.0	2.400	0.7	1.6800
	IV	0.4×4.0	2.133	0.7	1.4931

Both buildings are 45 m high (z direction) and 12 m wide in the x and y directions. Following relevant Australian building codes (AS1170.1 2002; AS1170.4 2007; AS3600 2009) a routine design procedure was carried out for structural analysis and design by utilising SAP2000 V14 (CSI 2010). During the design phase, P-Delta effects were taken into account by following AS3600 (2009). Figure 6.3 shows that the structural sections designed for the moment resisting building Figure 6.3 (a) and the shear wall braced building (Figure 6.3 (b)) satisfy common engineering practice in metropolitan areas. According to AS3600 (2009), grade 32 concrete whose characteristic compressive strength (f'_c) is 32 MPa, the modulus of elasticity (E) is 30.1 GPa, and grade N500 steel reinforcing bars with a characteristic yield strength (f_{sy}) of 500 MPa, were used.

Moreover, the stiffness of all the structural members (EI) was modified according to AS3600 (2009) by using cracked sections for reinforced concrete sections, as presented in Table 6.1. The natural period of the moment resisting building and shear wall braced building in a fixed-base condition was 1.23 seconds and 0.65 seconds, respectively.

Table 6.2 Characteristics of adopted soil

Soil Properties	Value	Reference
Unit weight, γ (kN/m^3)	14.42	Rahvar (2006)
Maximum small strain shear modulus, G_{max} (MPa)	33.1	
Poisson's ratio, ν	0.4	
Effective friction angle, $\emptyset'$ (Degree)	12	
Effective cohesion, c' (kPa)	20	
Plasticity Index, PI (%)	15	
Shear wave velocity, v_s (m/s)	150	

The total mass for the moment resisting building was 1683 tonnes, and 2495 tonnes for the shear wall braced building. As shown in Figure 6.1, the separation gaps between the adjacent buildings considered in this study were 100, 300, 700, 1000 and 1200 mm; these gaps were applied on both sides of the middle building to investigate the effects of seismic pounding.

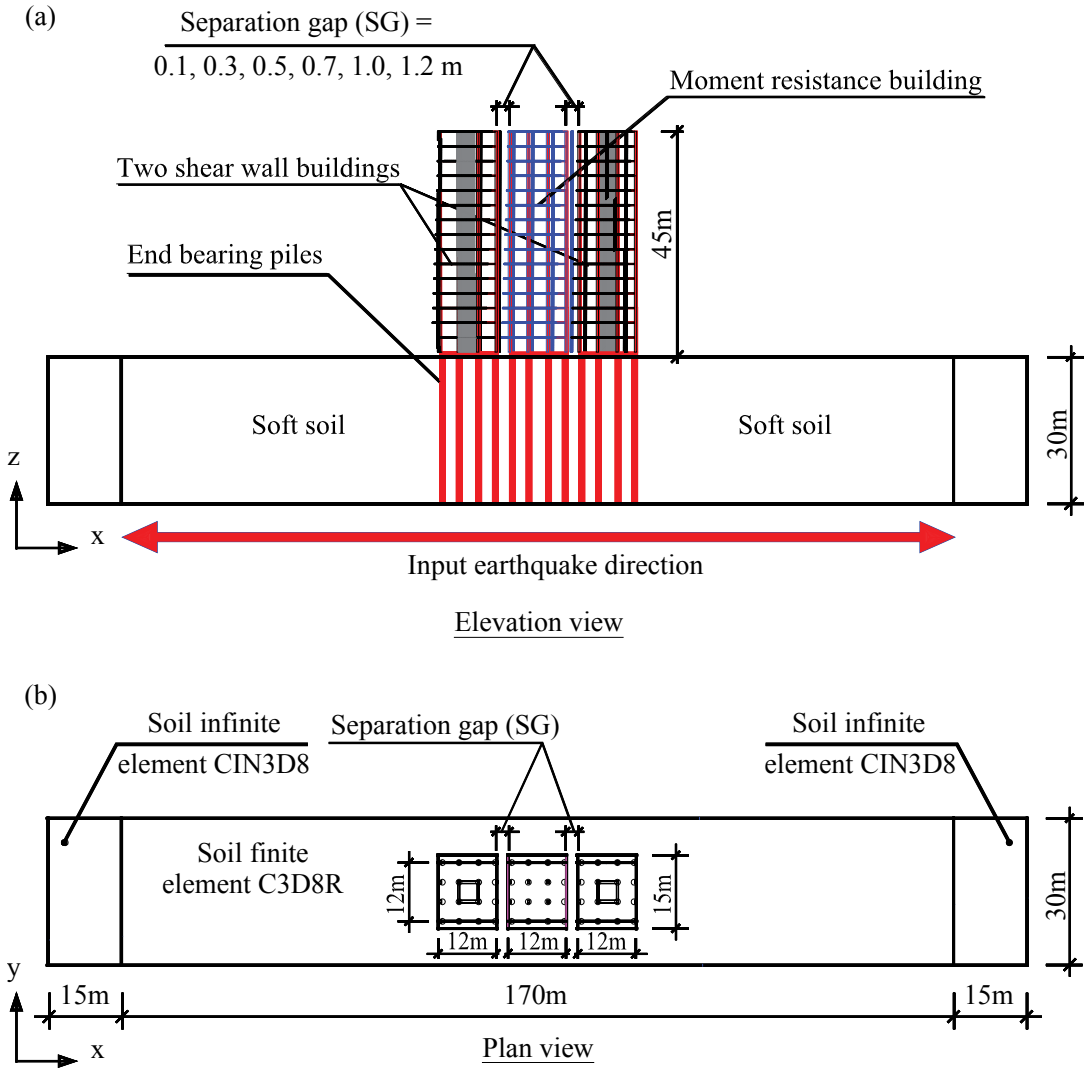

Figure 6.1 General setup of the soil-pile-structure system: (a) elevation view, and (b) plan view

Table 6.3 Mass and stiffness coefficient of Rayleigh damping for adopted buildings

Building Type	1st Mode Frequency (Hz)	2nd Mode Frequency (Hz)	Mass Damping Coefficient (α)	Stiffness Damping Coefficient (β)	Damping Ratio (%)
Moment Resisting Building	0.830	2.341	0.3850	0.0050	5%
Shear wall braced Building	1.522	6.110	0.7656	0.0021	5%

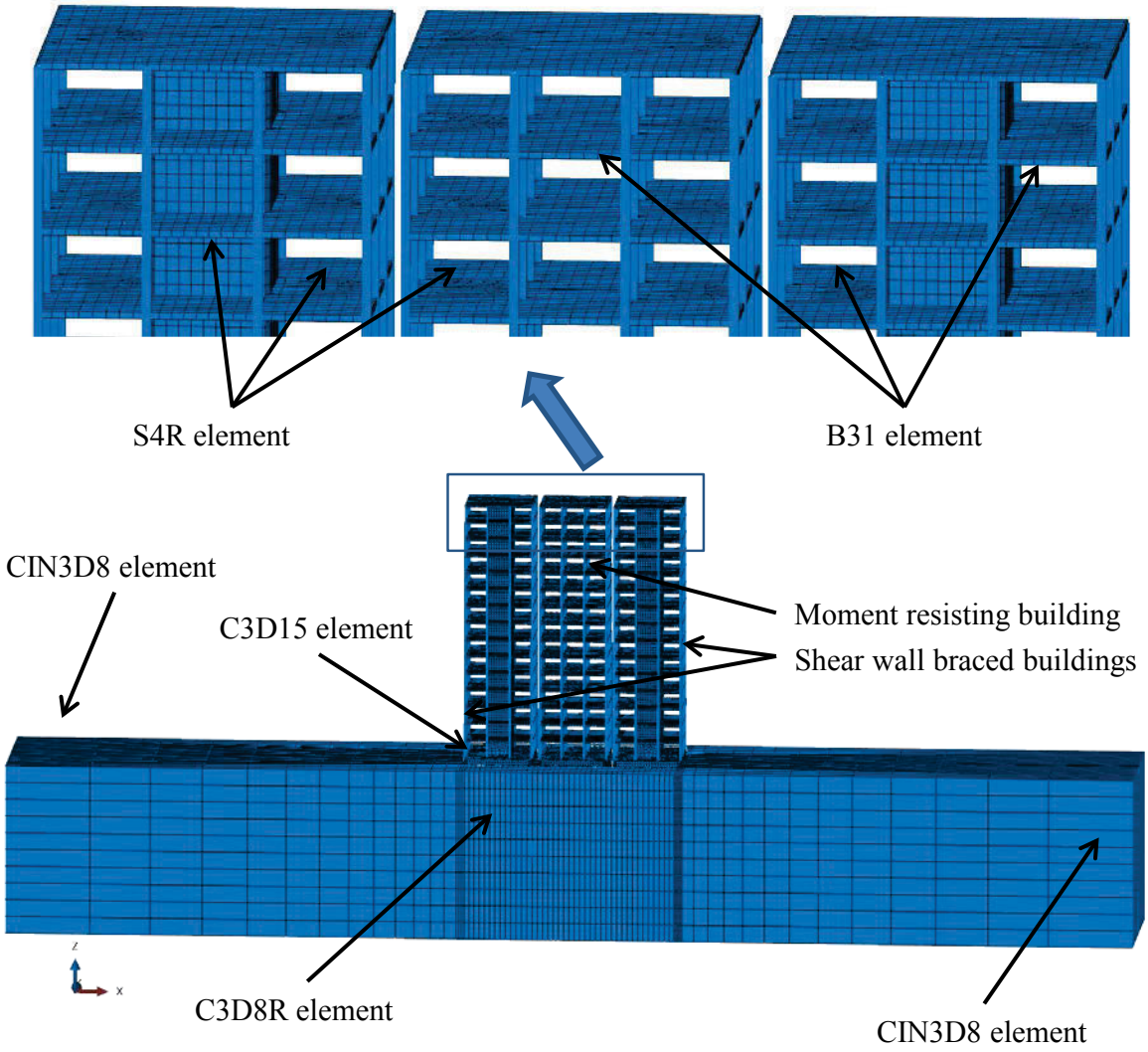

Figure 6.2 ABAQUS 3D numerical model capturing both structural models and adopted soil-structure model

6.3.2 Characteristics of pile foundations

This study considered end-bearing pile foundations to support the adopted buildings. The foundation is designed to fulfil the requirements of bearing capacity and settlement based on a conventional engineering design (Poulos and Davis 1980; Bowles 2001; AS2159 2009) and the foundation material is concrete by assuming a density of 2400 kg/m^3, Young's modulus of 3.01 GPa, and Poisson's ratio of 0.2. As Figure 6.4 shows, the foundation consists of a 12×15×1 m reinforced concrete foundation slab and a group of 4×4 reinforced concrete piles 30 m long by 1.2 m in diameter (D). The pile spacing (centre to centre) is 3.6 m ($3D$) along the x-direction (the same direction as the

applied earthquake) and 4 m ($3.3D$) along the y-direction (the orthogonal direction to the applied earthquake direction); these figures agree with other researchers (Small and Zhang 2002; Shelke and Patra 2008; Kumar *et al.* 2016). It was also assumed that the pile toes were socketed into the strong bedrock, thus creating an end-bearing load mechanism for the piles.

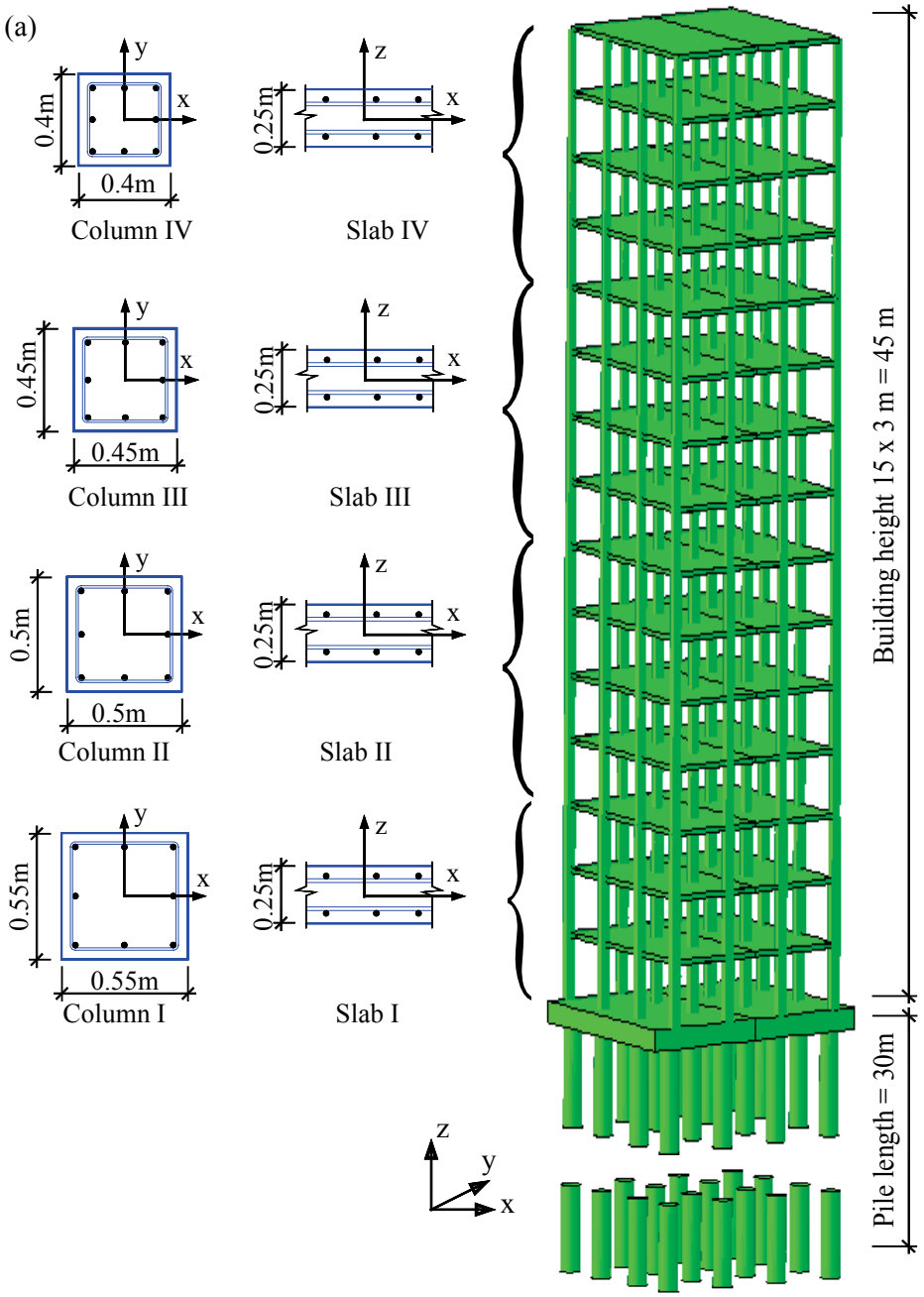

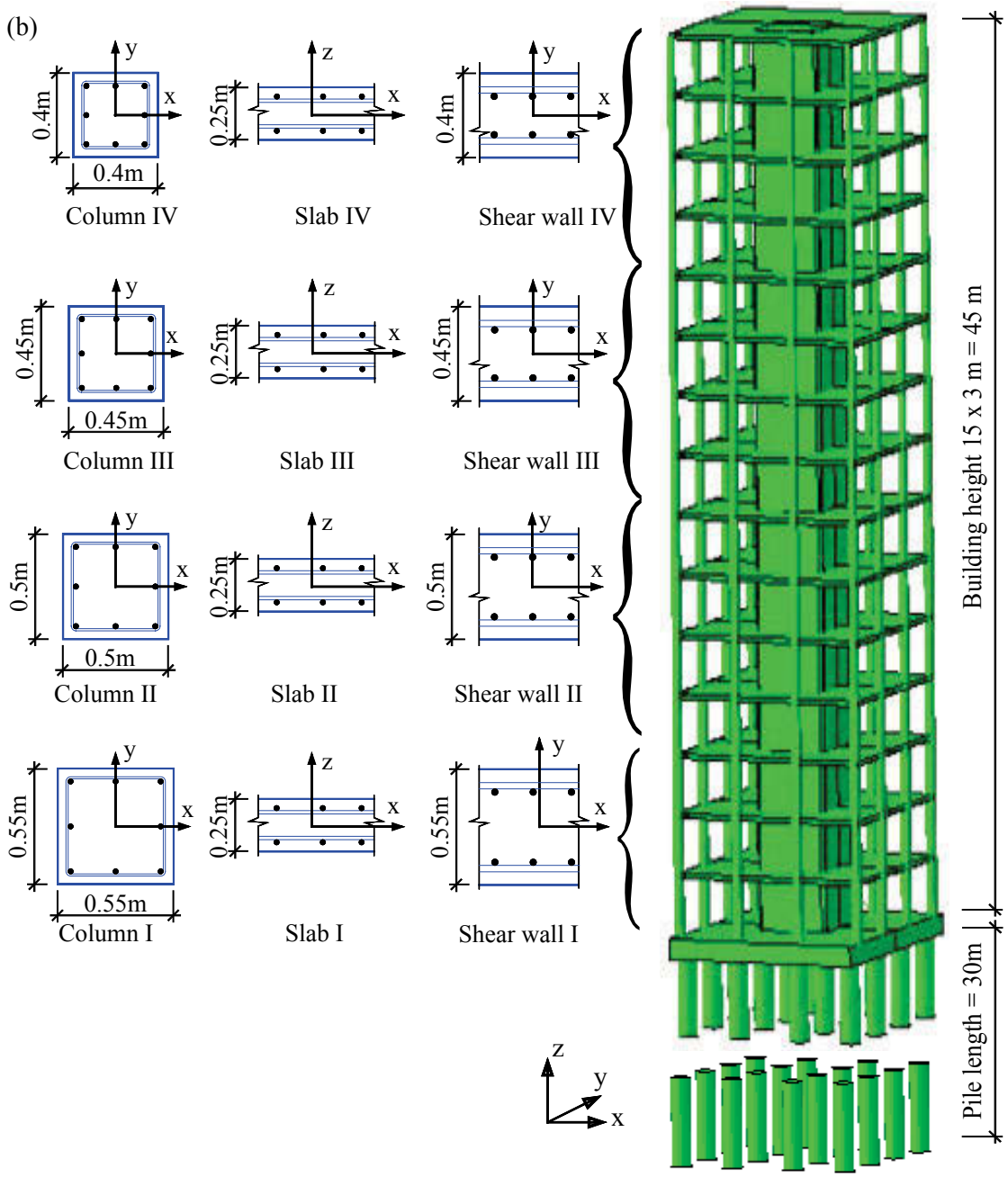

Figure 6.3 Designed structural sections and reinforcement details for (a) the moment resisting building and (b) the shear wall braced building

6.3.3 Characteristics of soil

According to AS1170.4 (2007), a site with more than 10 m depth of soil and a shear wave velocity of 150 m/s or less, should be classified as Class E_e soft soil. Also, the standard evaluates the site effects based on the top 30 m of soil profile because most of the amplification and attenuation occurs within the top 30 m of soil. Therefore, in this study

a 30 m deep soil deposit containing soft clayey soil (CL) is used to represent a Class E_e soft soil site. Table 6.2 summarised the parameters used in this model. Note that the properties of soil were taken from actual in-situ and laboratory tests, which means they have merits over idealised properties which may be unrealistic.

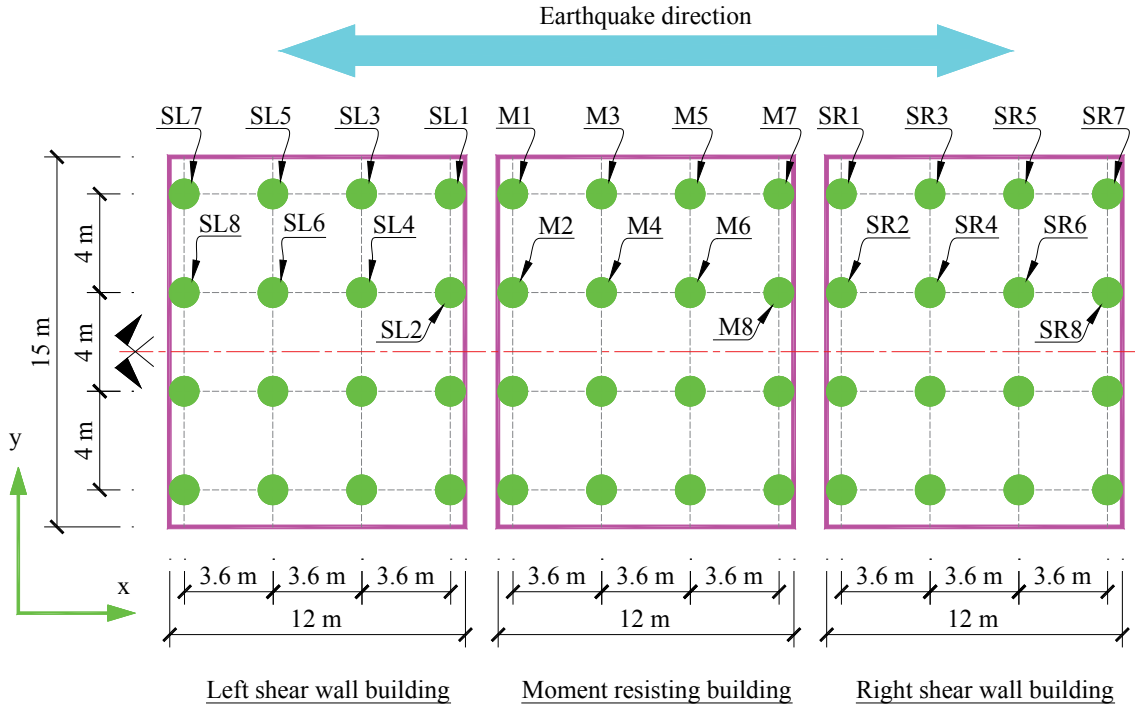

Figure 6.4 Adopted end-bearing foundation setup

Table 6.4 Rayleigh damping for adopted soil deposit considering different earthquake excitations

Earthquake	Maximum Shear Strain (%)	Modulus Reduction Factor	Mass Damping Coefficient	Stiffness Damping Coefficient	Damping Ratio (%)
Northridge 1994	0.14	0.35	1.0694	0.0055	12.8
Kobe 1995	0.10	0.41	1.0405	0.0046	11.5

6.4 Numerical Model

The governing dynamic equations of motion for the soil-foundation-structure system are too complex to be solved by conventional analytical methods due to different vectors and matrices of the soil, the foundation, and the structure, so the substructure method and the direct method are used to tackle this problem. The substructure method

which takes advantage of superposition has been developed and is used widely by practising engineers and researchers. As Wolf (1989) reported, the approximations of soil non-linearity through iterative wave propagation analyses may allow this method to be applied to a moderately-nonlinear system. However, the principle of superposition requires an assumption of linear soil and structural behaviour (Kramer 1996), albeit it is not easy to consider the exact soil and structural nonlinearities in a dynamic analysis.

However, the direct method allows for the soil, foundation, and structure to be simulated simultaneously, and since an assumption of superposition is not required, a correct and accurate model and analysis can be achieved (Borja *et al.* 1994). Moreover, the soil-structure interaction has been studied by many researchers (e.g., Hayashi and Takahashi 2004; Carbonari *et al.* 2011) and accurate and realistic outcomes have been achieved by adopting the direct method, and therefore it was used in this study. The soil-pile-structure system was simulated numerically using the finite element software ABAQUS, version 6.14. This software can simulate complex problems which may require substantial computational memories. In fact some researchers (e.g., Chu and Truman 2004; Koskinen 2005; Matinmanesh and Asheghabadi 2011) have used ABAQUS software to study soil-structure interaction and reported reasonable results. The procedure utilised to perform a numerical simulation while considering the combined effects of seismic pounding and seismic soil-pile-structure interaction is explained below.

6.4.1 Building and foundation models

In this numerical model the beam elements (B31), as shown in Figure 5a, are utilised to model the columns. The B31 beam element is a first-order three-dimensional beam element which considers a three-dimensional continuum in the fashion of one-dimensional approximation. The floor slabs and shear walls are modelled by shell elements (S4R), and as Figure 6.5 (b) shows, this S4R shell element is a 4-node shell element which considers a uniform large-strain formulation.

The elastic-perfectly plastic constitutive model is assigned to structural elements to carry out an inelastic analysis by specifying the yielding stress so that the structural elements will behave elastically until the defined yielding stress is reached. According to Shing and Tanabe (2001), the yielding stress of concrete material is considered to be the same as the characteristic compressive strength (f'_c) of concrete. The energy disspation

of the adopted buildings during earthquakes is accounted for by Rayleigh damping. Table 6.3 shows the adopted mass and stiffness coefficients of Rayleigh damping defined according to the first and second mode frequencies of each structure, and the corresponding damping values.

As suggested by some researchers (e.g., Maheshwari et al. 2004; Ghee and Guo 2011; Comodromos and Papadopoulou 2012; Hokmabadi and Fatahi 2016), solid elements were utilised to model the pile foundations in this study, and as Figure 6.5 (c) and Figure 6.5 (d) show, C3D8R and C3D15 element types were used to model the foundation slabs and piles, respectively.

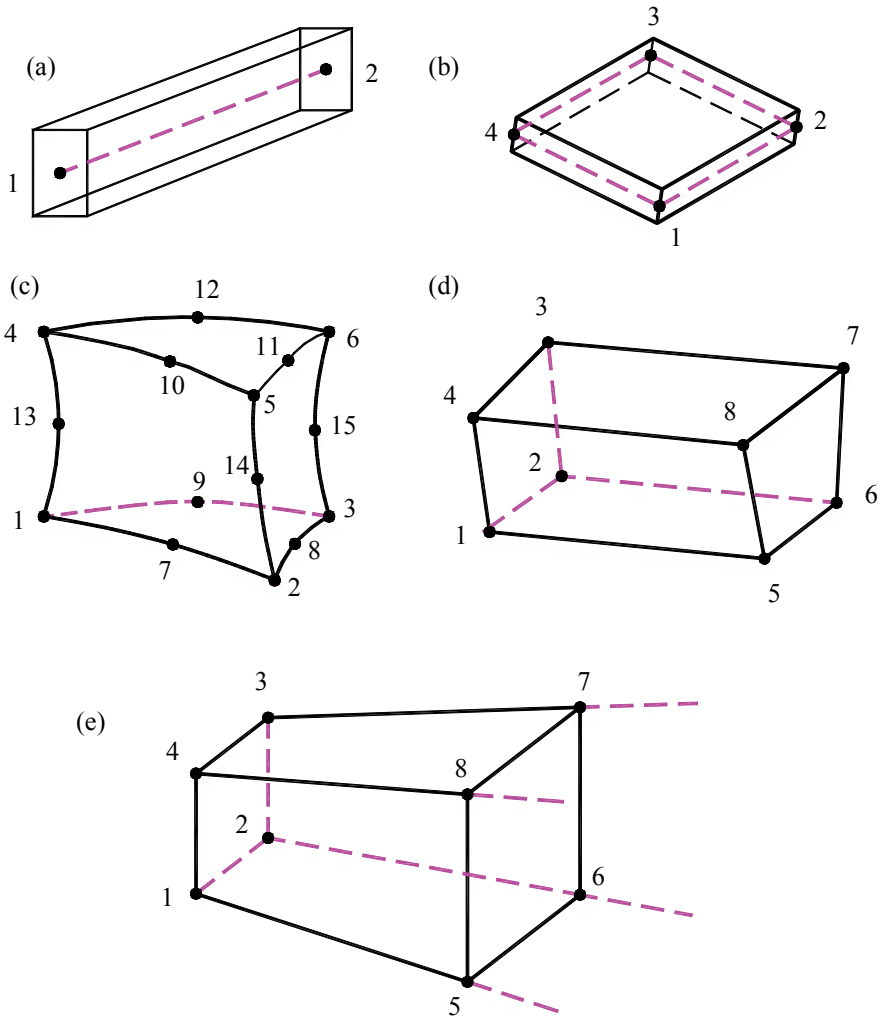

Figure 6.5 Elements employed by adopted finite element model: (a) column element (B31); (b) slab element (S4R); (c) foundation slab element and soil element (C3D8R); (d) pile element (C3D15); and (e) infinite element (CIN3D8)

The C3D8R element is an 8-node, first-order, reduced-integration linear element with an hourglass control that will ensure that the strains calculated at the integration points are more reasonable. The C3D15 element is a three-dimensional 15-node continuum element. All piles have a rigid connection with the foundation slab, and the pile toes are fixed at the bottom of the soil deposit to account for the socket end of piles in strong bedrock.

6.4.2 Soil model

As Figure 6.5 (d) shows, C3D8R elements were also used to model the soil deposit, and although the locking phenomena does not occur due to reduced integration, these elements are not stiff enough in bending, which is not critical when modelling soil, however since the integration points are located in the middle of this element, small elements are needed to capture the concentration of stresses.

The non-linearity of soil during a seismic event is critical in determining the dynamic response of piles (Maheshwari and Watanabe 2006) and so too is the response of the coresponding soil-pile-structure system. The equivalent linear method is the most common method adopted by practising engineers to consider the site effect and non-linearity of soil, and therefore it has been adopted in this study. To carry out the initial analysis, some values of the shear modulus and damping ratio were assumed in various regions of the model, and then the maximum cyclic shear strain of each element is recorded after the analysis. The new values of the shear modulus and corresponding damping ratio for the subsequent analysis were determined by referring the maximum cyclic shear strain to the modulus degradation curves and corresponding damping ratio curves. In this study, ready-to-use backbone curves which included the influence of the Plasticity Index (PI) on the modulus degradation curves and corresponding damping ratio, as provided by Vucetic and Dobry (1991), were adopted. Figure 6.6 shows the particular curves of modulus degradation and damping ratio selected based on the soil properties (see Table 6.2). An iterative procedure was carried out until the difference between the computed values of shear modulus and the damping ratio in two successive analyses was less than a certain value in the model. Finally, the acquired values of the shear modulus and damping ratio were used to obtain the best prediction of the real behaviour of soil and to capture soil non-linearity. Note that due to the characteristics of

each earthquake, the induced shear strain level differs in the soil medium, which is why the adopted shear modulus reduction factor and the corresponding damping ratios were changing with the corresponding earthquake motion inputs to include the appropriate soil non-linearity (see Table 6.4).

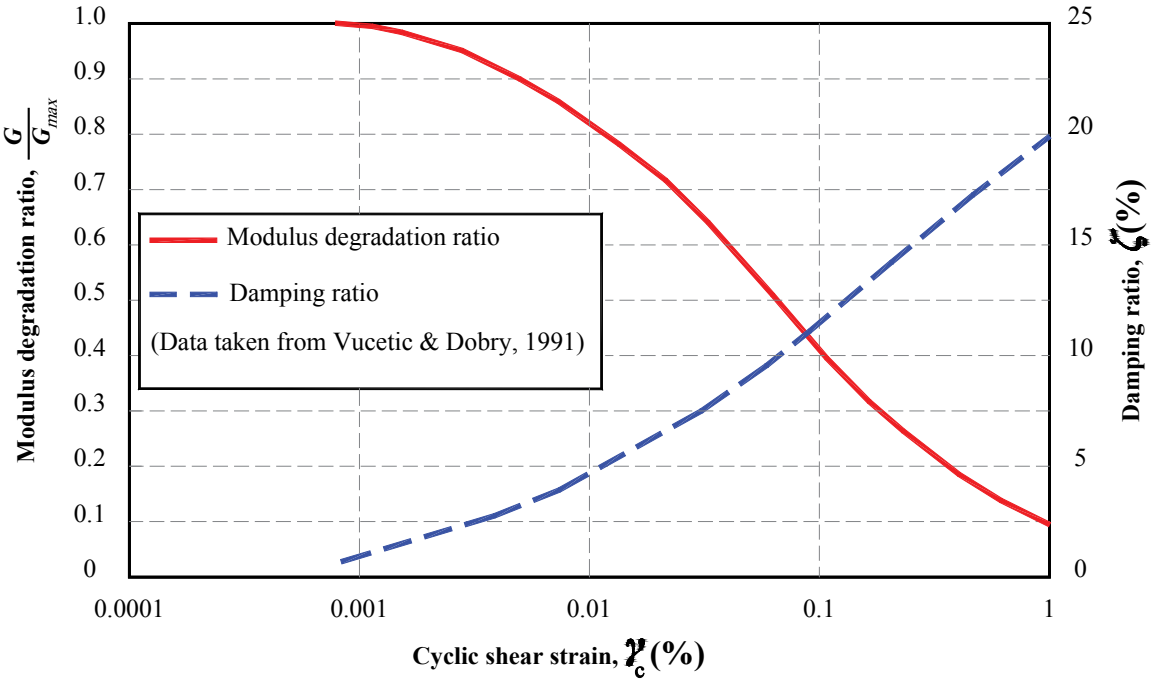

Figure 6.6 Adopted soil modulus degradation curve and corresponding damping ratio curve for cohesive soils with *PI* = 15%

The most common mechanism used to represent the dissipation of energy is viscous damping where the dissipative force is assumed to be a function of particle velocity (Das 1983). Soil damping is one of the essentials needed to simulate the soil-foundation-structure system because it modifies the input motions and influences the dynamic response of structures. Park and Hashash (2004) concluded that Rayleigh damping could provide acceptable results for many applications as long as the parameters for soil media are selected accurately. Thus, in the present study, Rayleigh damping was used to simulate the nonlinear variations of energy losses in the soil during earthquake excitation. The two frequencies which cover the range with a significant amount of input motion were used to define the mass and stiffness coefficient of Rayleigh damping, following recommendation made by Park and Hashash (2004). Table 6.4 contains the corresponding parameters of Rayleigh damping for each earthquake.

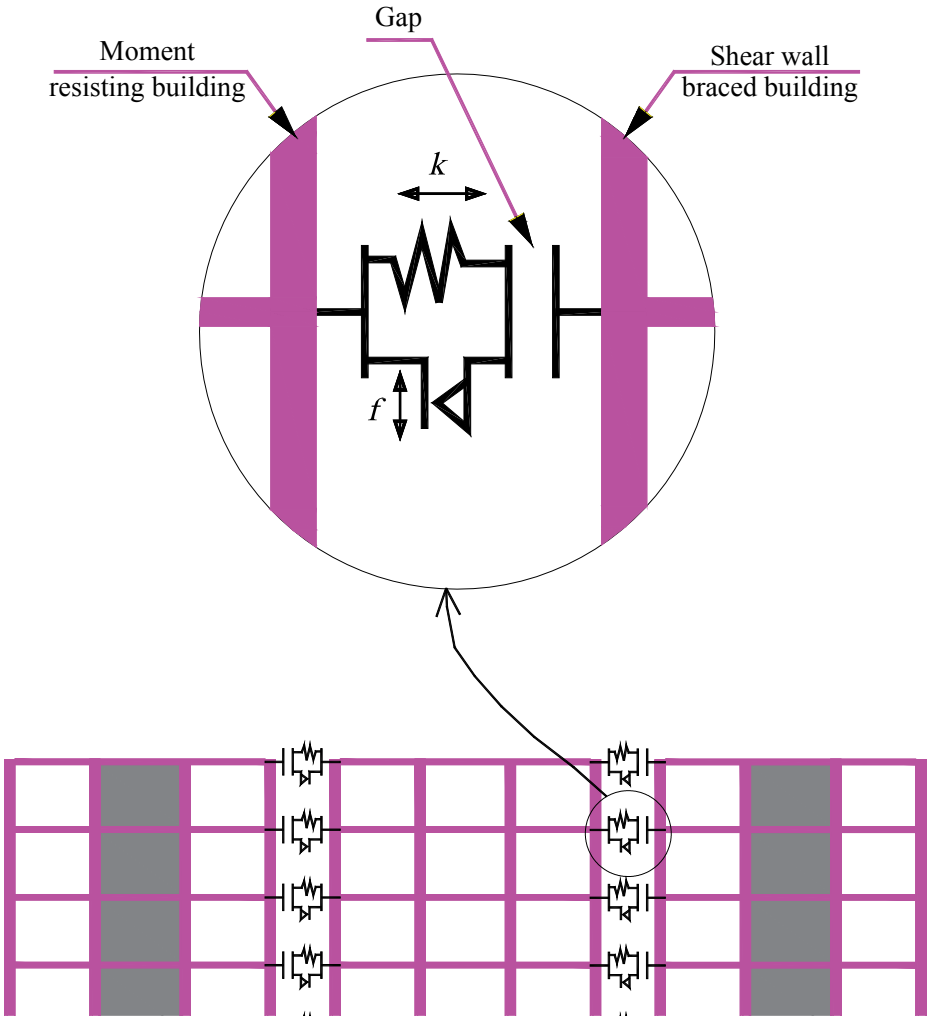

Figure 6.7 Demonstration of adopted mechanical model of contact interaction to capture possible seismic pounding

6.4.3 Contact surfaces for pounding simulation

Contact surfaces were applied to where collisions between the buildings might have been possible. ABAQUS provides more than one approach, including general contact, contact pairs and contact elements, to model the interacting surfaces. In this study a contact pair with small-sliding surface-to-surface contact was used. The contact pair approach needs two surfaces to make contact during analysis, to be defined as a master surface and a slave surface. Here, master surfaces were applied on each side of the floor of the middle building (i.e. the conventional moment resisting building), and the corresponding slave

surfaces were applied on the same level of the other buildings (i.e. the retrofitted buildings). Note that based on the authors' assessment, the location of the master surface would not influence the seismic response of the adopted buildings, which means the analysis would yield the same results irrespective of which master surface in the side or the middle building was selected. A small-sliding tracking formulation was used to capture the behaviour of elements when there was relatively little sliding of one surface over another. Surface-to-surface contact discretisation was used to consider contact interaction as a surface facet rather than a surface node. Specifically, an opening or a penetration distance was considered in the normal direction of the slave surface facet, while the sliding distance was measured perpendicular to the normal direction of the slave surface facet. Based on the distances measured and mechanical properties assigned, the behaviour of these interacting surfaces could be simulated accurately.

Figure 6.7 shows the three essential components needed to account for seismic pounding during dynamic analysis; i.e., a gap to ensure there is no stress transmitted across interface before contact is made. The separation gaps in this study are 100, 300, 700, 1000 and 1200 mm. The normal stresses transferred across the interface include a spring with stiffness k placed in the normal direction, and the frictional forces transmitted through the interface include a slider in the tangential direction.

This means a hard contact pressure-overclosure relationship which defines the properties of gaps and normal springs is used for normal contact interaction between buildings, as shown in Figure 6.7. This particular contact relationship means that no contact stresses will be transmitted until the facet of the slave surface makes contact with the facet of the master surface, i.e., when the gap between the buildings is closed and seismic pounding occurs, contact forces are transmitted across the interface. This implies that no tensile stress can be transmitted across the contact surface and no compressive stress can be transmitted before any contact is made. Technically, this hard contact assumes that no penetration will occur between the slave surface and the master surface when the two corresponding surfaces make contact, but this assumption may lead to over-constraining. To mitigate this possibility, a stiff approximation of hard contact known as the penalty method was used in this study. As Figure 6.8 shows, using the penalty method means allowing for a small degree of penetration for the interacting surfaces, an approach

which resulted in a degree of numerical softening which can alleviate over-constraining and reduce the burden of iterations.

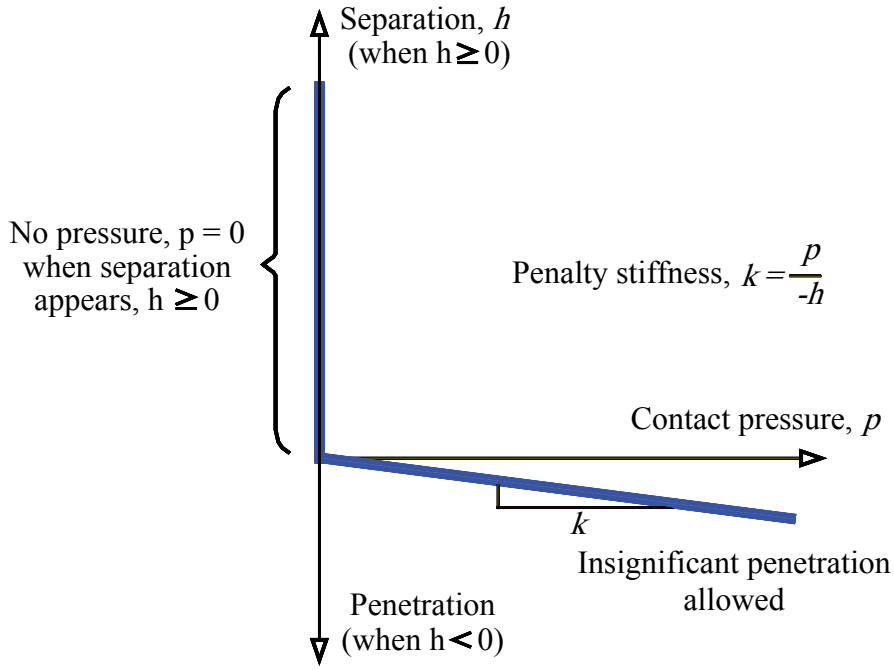

Figure 6.8 Representation of adopted penalty method for numerical softening of hard contact simulation

Tangential behaviour was considered based on the Coulomb friction model and a penalty formulation which specifies the properties of frictional sliders, as shown in Figure 6.7. The Coulomb friction model correlates the critical shear stress (τ_{cr}) and the contact pressure (p) between the contacting surfaces by the coefficient of friction (μ), as presented in Equation (6.2):

$$\tau_{cr} = \mu p \tag{6.2}$$

In this study $\mu = \tan 30°$ is used for the concrete material and it was also assumed to be the same in all frictional directions. The critical stress (τ_{cr}) indicates the states of two contacting surfaces. As shown in Figure 6.9, this state is known as sticking when the equivalent shear stress (τ_{eq}) carried by the two contacting surfaces is below the critical stress (τ_{cr}), and it is called slipping as the applied shear stress (τ_{eq}) reaches the critical stress (τ_{cr}) and the two contacting surfaces start to slide relative to each other. The

equivalent shear stress (τ_{eq}) is a combination of two orthogonal components of shear stress τ_1 and τ_2 by following Equation (6.3):

$$\tau_{eq} = \sqrt{{\tau_1}^2 + {\tau_2}^2} \tag{6.3}$$

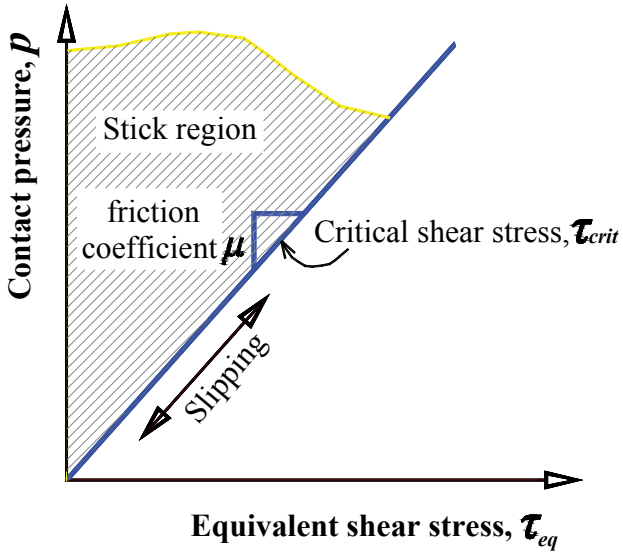

Figure 6.9 Demonstration of adopted Coulomb friction model

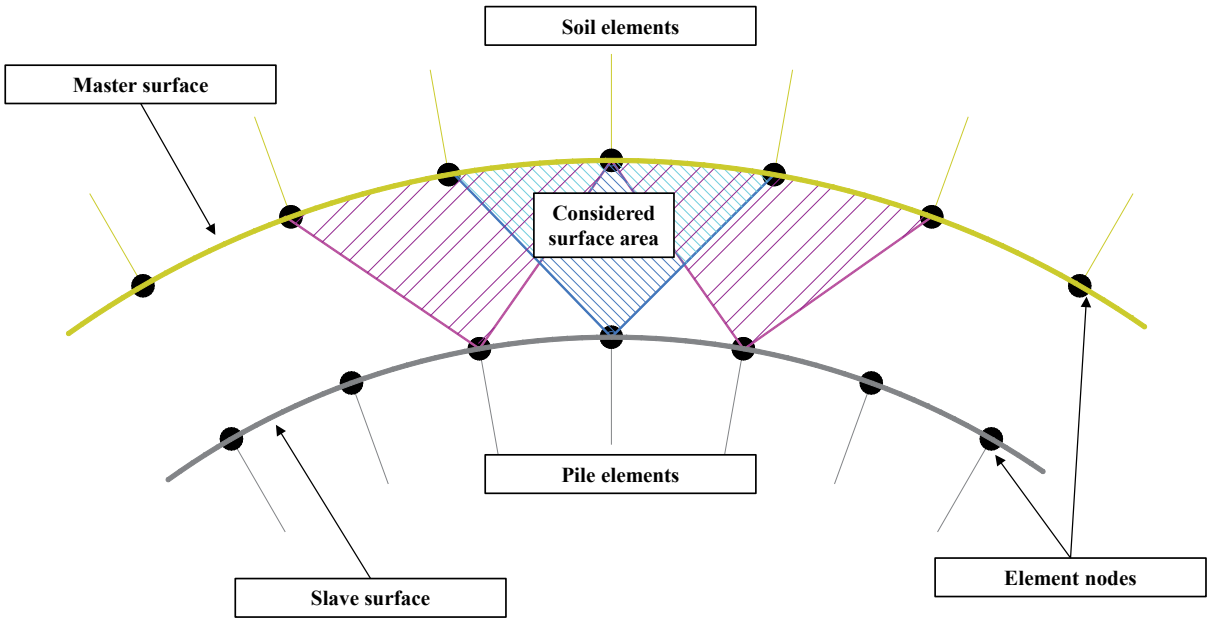

Figure 6.10 Demonstration of the surface-to-surface discretization applied to enforce soil-pile contact conditions

6.4.4 Interfaces between piles and soil

The interfaces between the piles and surrounding soil are essential in the numerical simulation of a soil-pile-structure system in order to incorporate the different properties of these materials and capture any possible separation and sliding which may occur between the piles and surrounding soil during earthquake excitations.

In this study a contact algorithm which includes finite-sliding and surface-to-surface contact formulation between the outer perimeter of each pile and the contacting surface of the surrounding soil has been adopted, whereas general contact requires defining the master surfaces on the soil contacting facets and slave surfaces on the outer perimeter of the piles. This finite-sliding tracking formulation will account for the relative motion of two interacting surfaces and will also capture the arbitrary relative motion of contacting surfaces, thus making it possible to simulate the gapping and sliding between piles and soil during excitation. As Figure 6.10 shows, the surface-to-surface discretisation formulation enforces the contact conditions by including the shapes of the slave and master surfaces, which means each contact constraint will include an individual slave node and the nearby slave nodes, and thus the stress and pressure across the interface are dealt with more accurately. This geometric correction was also applied to alleviate the difficulties with accuracy and convergence which are induced by approximated facets representing an actual curved geometric surface.

The normal interaction between piles and soil was modelled as hard contact due to the penalty method discussed in the preceding section, while the tangential behaviour of the interface follows the classical Mohr-Coulomb model which includes the slip rate dependent coefficient of friction.

Based on Oden and Martins (1985), a model assuming the exponential decay of the coefficient of friction from the peak to the residual coefficient of friction shown in Figure 11 was utilised to simulate the frictional behaviour between the piles and surrounding soil.

The exponential decay function of the coefficient of friction is presented in Equation (6.4):

$$\mu = \mu_r + (\mu_p - \mu_r)e^{-d_c\dot{\gamma}_{eq}} \tag{6.4}$$

where μ_r is the residual coefficient of friction, μ_p is the peak coefficient of friction, d_c is the decay coefficient, and $\dot{\gamma}_{eq}$ is the equivalent slip rate. Thus the peak coefficient of

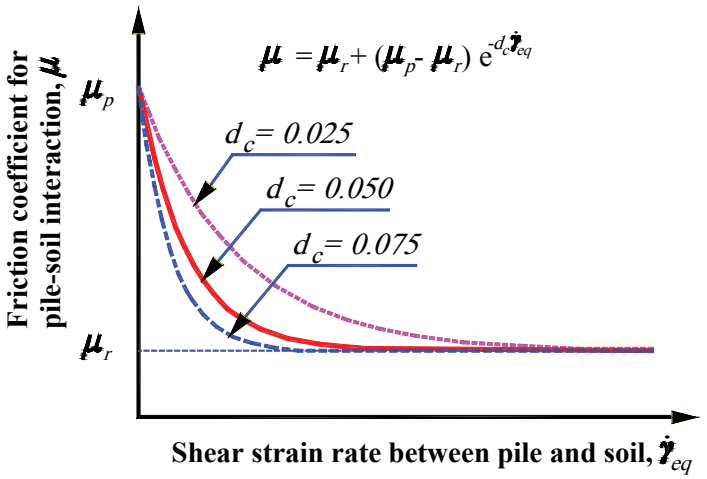

Figure 6.11 Representation of adopted exponential decay behaviour of the friction coefficient

friction (μ_p) is defined based on the classical Mohr-Coulomb model by adopting the following equation:

$$\mu_p = \frac{R_{int}\tau}{\sigma'} = R_{int}(\tan\varphi' + \frac{c'}{\sigma'}) \tag{6.5}$$

where R_{int} (= 0.75) is the reduction factor commonly used by practising engineers, τ is the shear strength, σ' is the effective normal stress, c' is the effective cohesion intercept of the failure envelope, and φ' is the slope of the failure envelope or the effective internal friction angle. As Figure 6.11 shows, the coefficient of friction changes faster against the equivalient slip rate ($\dot{\gamma}_{eq}$) as the decay coefficient (d_c) increases. By referring to Randolph *et al.* (1994), the residual coefficient of friction (μ_r) and the decay coefficient (d_c) are assumed to be $0.2\mu_p$ and 0.05, respectively, to simulate friction between the piles and the soil. Moreover, the equivalient slip rate ($\dot{\gamma}_{eq}$) is calculated by combining the two local slip velocity components $\dot{\gamma}_1$ and $\dot{\gamma}_2$, along the interface between two bodies by using Equation (6.6):

$$\dot{\gamma}_{eq} = \sqrt{\dot{\gamma}_1{}^2 + \dot{\gamma}_2{}^2} \tag{6.6}$$

However, simulating an ideal frictional behaviour can be very difficult because it may cause convergence problems; which is why the use of a penalty formulation allows for a small amount of relative movement when they should ideally 'stick' together, as shown in Figure 6.12, so that the numerical iterations are greatly reduced.

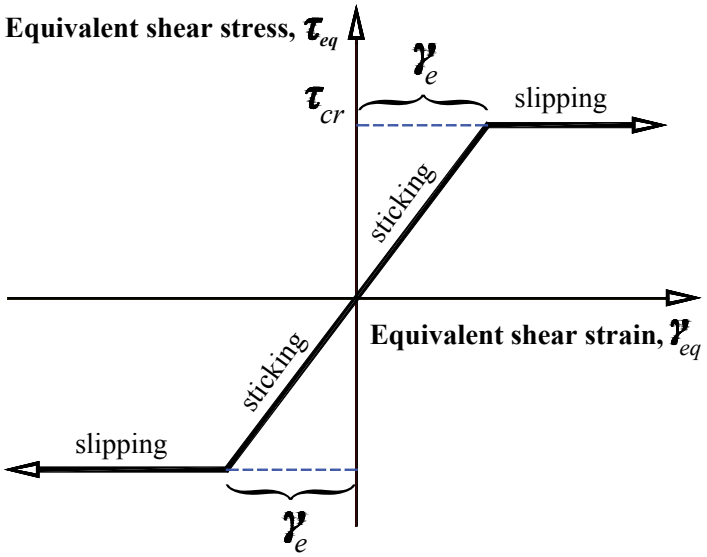

Figure 6.12 Demonstration of adopted friction behaviour with penalty method of soil-pile contact interaction

6.4.5 Boundary conditions

As mentioned by Semblat (2010), the boundaries at the sides of the model must account for free-field motion. In this study, 8-node linear one-way infinite brick (CIN3D8) elements were used to model the infinite elements acting as an unbounded soil domain because plane wave propagation was also modelled. Figure 5 (e) shows that the infinite elements defined the orientations, so nodes 1, 2, 3, and 4 are connected to the solid elements (soil medium), while the other nodes (nodes 5, 6, 7, and 8) are oriented outwards from the soil medium. The soil deposit is five times larger than the adopted buildings in terms of the dimensions in the x direction, as suggested by other researchers (e.g. Rayhani

and El Naggar 2008; Kumar et al. 2015), in order to minimise wave reflection induced by artificial boundaries.

This study simulated a soft soil deposit sitting on a hard bedrock so a rigid boundary is used to represent low-velocity sediment over a high-velocity bedrock.

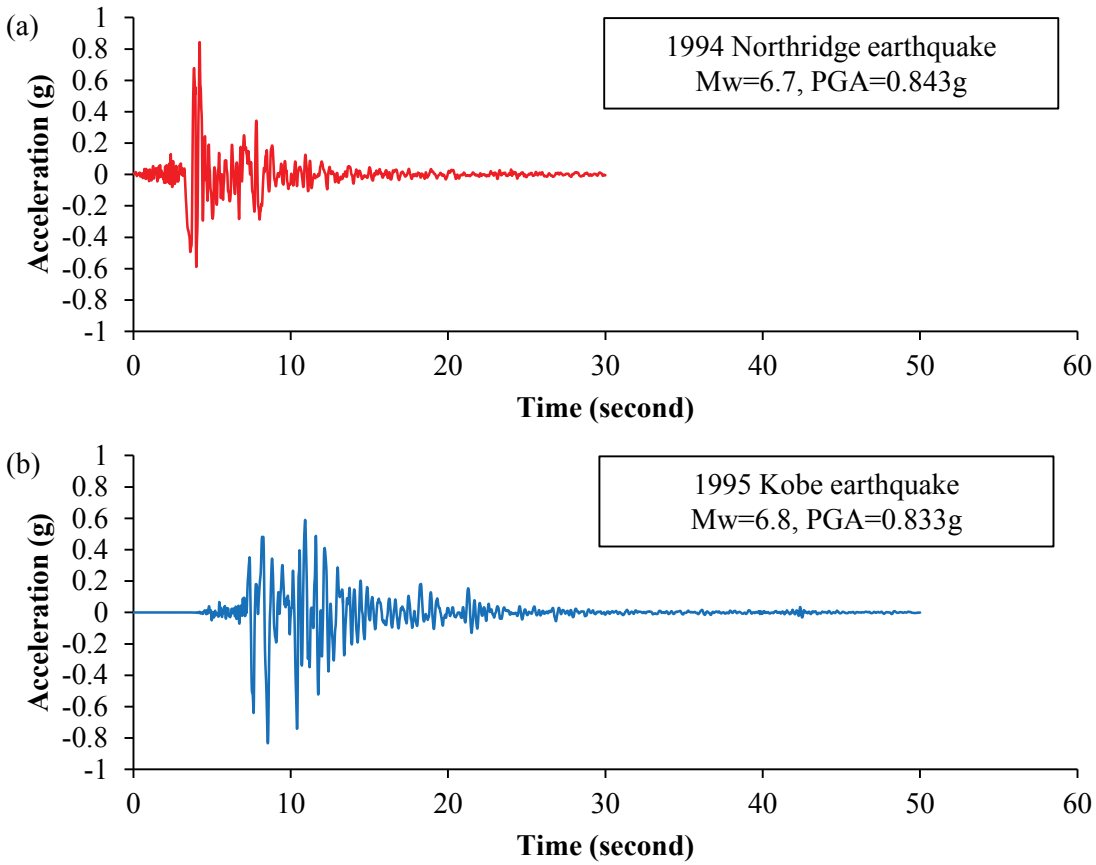

Figure 6.13 Considered earthquake accelerogram: (a) the 1994 Northridge earthquake and (b) the 1995 Kobe earthquake

6.4.6 Input earthquakes

Figure 6.13 also shows two benchmark far-field earthquakes, including the 1994 Northridge earthquake and the 1995 Kobe earthquake, which are used in this study to investigate how seismic pounding affects the response of mid-rise buildings. To conduct a time history analysis, accelerograms of earthquake records have been applied at the bedrock level. A baseline correction has also been applied to modify the accelerograms because when they are used to deduce the velocity and displacement time histories via

integration, particularly for strong ground motions, a significant baseline drift which does not match the field measurements may be observed. This baseline drift can occur due to field conditions, background noise, and the hysteresis behaviour of accelerometers, which is why a baseline correction procedure is often utilised to compensate for baseline drift. This study uses the correction technique proposed by Newmark *et al.* (1973) such that an acceleration correction $a_0(t)$, is added to the raw data record $a(t)$, to produce a corrected acceleration record $a_c(t) = a + a_0$, to minimise the mean square velocity over the time of the event. This corrected acceleration is parabolic over any number of time intervals during the event:

$$\mathrm{a_0(t)} = \mathrm{C_1} + \mathrm{C_2}\left(\frac{\mathrm{t}-\mathrm{T_1}}{\mathrm{T_2}}\right) + \mathrm{C_3}\left(\frac{\mathrm{t}-\mathrm{T_1}}{\mathrm{T_2}}\right)^2, \quad \mathrm{T_1} < t < \mathrm{T_2}\,, \tag{6.7}$$

where T_1, T_2 denote the limits of a time interval and C_k $(k = 1, 2, and\ 3)$ are the constants obtained from the velocity minimisation, as shown in Equation (6.8):

$$\frac{\partial}{\partial \mathrm{C_k}} \int_{\mathrm{T_1}}^{\mathrm{T_2}} [\mathrm{v_c(t)}]^2 \mathrm{dt} \tag{6.8}$$

where $v_c(t)$ is the corrected velocity record obtained by integrating the corrected acceleration record $a_c(t)$. Note that these velocities are obtained by assuming that the uncorrected and corrected accelerations vary linearly over each time increment of the original acceleration history. This is not exact for the corrected acceleration record (because of the parabolic variation of the correction in time), but it is assumed that the acceleration history is discretised at small enough time increments to ensure this is an insignificant error.

6.5 Results and Discussion

The results are presented in terms of the response spectrum at the foundation slab level, the maximum envelope of floor shear, the maximum rocking angle of foundation slabs, the transient maximum lateral building deflection, the maximum inter-storey drifts, the maximum lateral pile deflection and corresponding bending moments, and the shear forces distributed along the piles. The results for both types of buildings are presented and discussed in the following sections.

6.5.1 Response spectra and natural frequencies

In most modern seismic codes and standards, a response spectrum is needed to calculate the lateral force demand (base shears) of a structure in a pseudo-static analysis. The higher spectral acceleration indicates that more seismic energy will be transmitted to the system in a certain natural period and thus the superstructure will attract more base shear. The response spectrum is a function of the natural period of a single-degree of freedom (SDOF) system with a certain damping ratio which is presented by plotting the maximum spectral acceleration which can be experienced by an SDOF system. A higher value of spectral acceleration implies that the structural system will attract more seismic energy of a certain natural period. The response spectra adopted in this study utilised 5% for a system damping ratio under the influence of obtained ground motions.

Figure 6.14 shows the response spectra of the ground motions for a variety of separation gaps (SG); these ground motions were recorded at the foundation slabs under the 1994 Northridge earthquake (Figure 6.13 a) and the 1995 Kobe earthquake (Figure 6.13 b) excitations. This spectrum can help design engineers evaluate the foundation input motion (FIM) and allow them to carry out SSPSI analysis using the substructure method. Referring to Figure 6.14, by considering SSPSI, the response spectra shows an amplification at the longer period range, particularly for the period between 1 and 2 seconds, and attenuation at the shorter period range, such as when the natural period is less than 0.5 seconds. It is also clear that the response spectrum curves are almost identical regardless of the changes in the separation gap, so both shear wall braced buildings, on the left hand and right hand sides, delivered a similar response spectra.

Table 6.5 Variation of natural frequency of adopted moment resisting building and shear wall braced building

Building Type		**Frequency (Hz)**	
		Mode 1	**Mode 2**
Moment Resisting Building	30 m long pile	0.815	2.280
	Fixed base	0.830	2.341
Shear Wall Braced Building	30 m long pile	1.145	4.642
	Fixed base	1.522	6.110

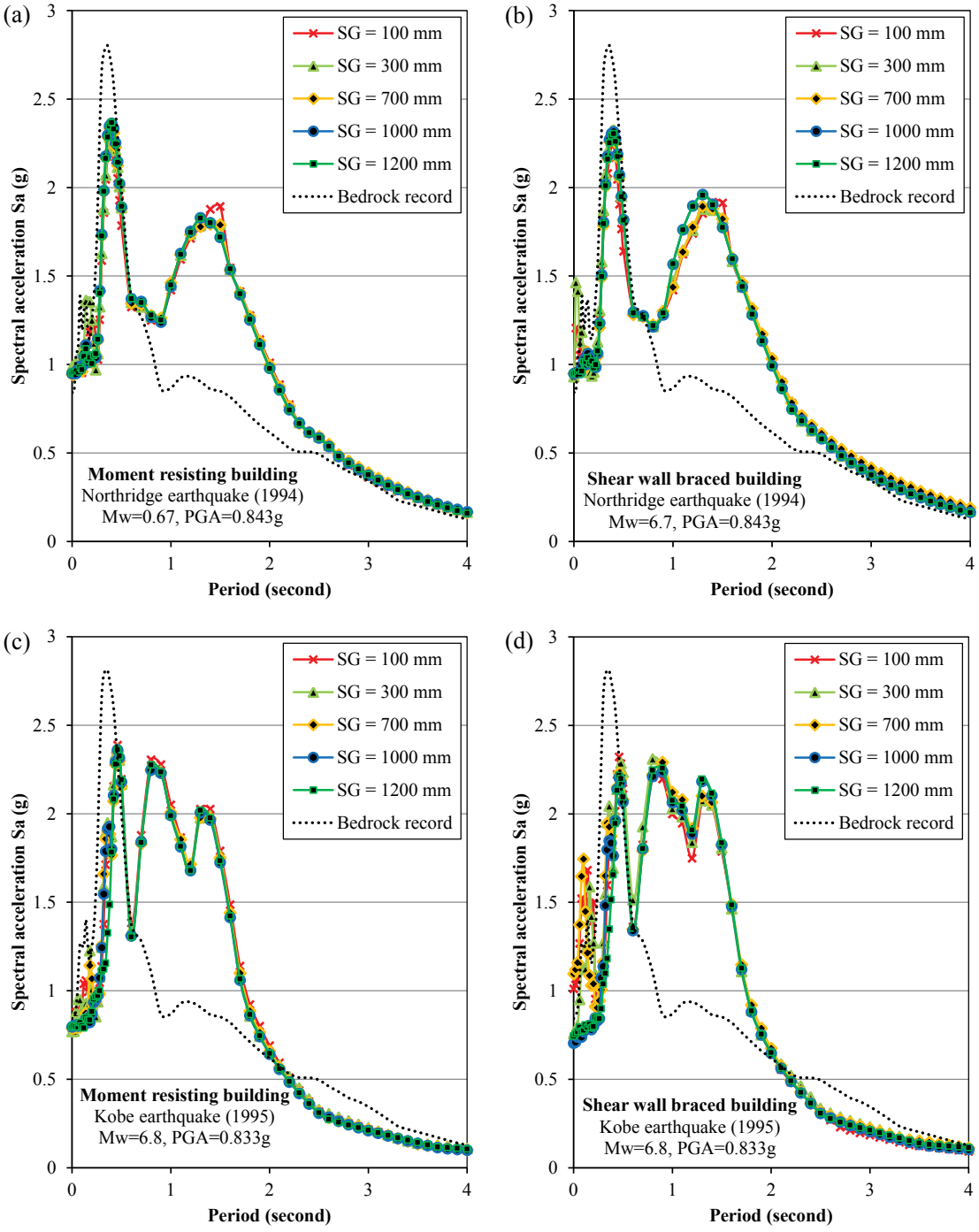

Figure 6.14 Response spectrum of ground motions of (a) the moment resisting building and (b) the shear wall braced building under the 1994 Northridge earthquake; and (c) the moment resisting building and (d) the shear wall braced building under the 1995 Kobe earthquake in conjunction with different separation gaps

(a)

First mode for the moment resisting building

First natural frequency = 0.815 Hz

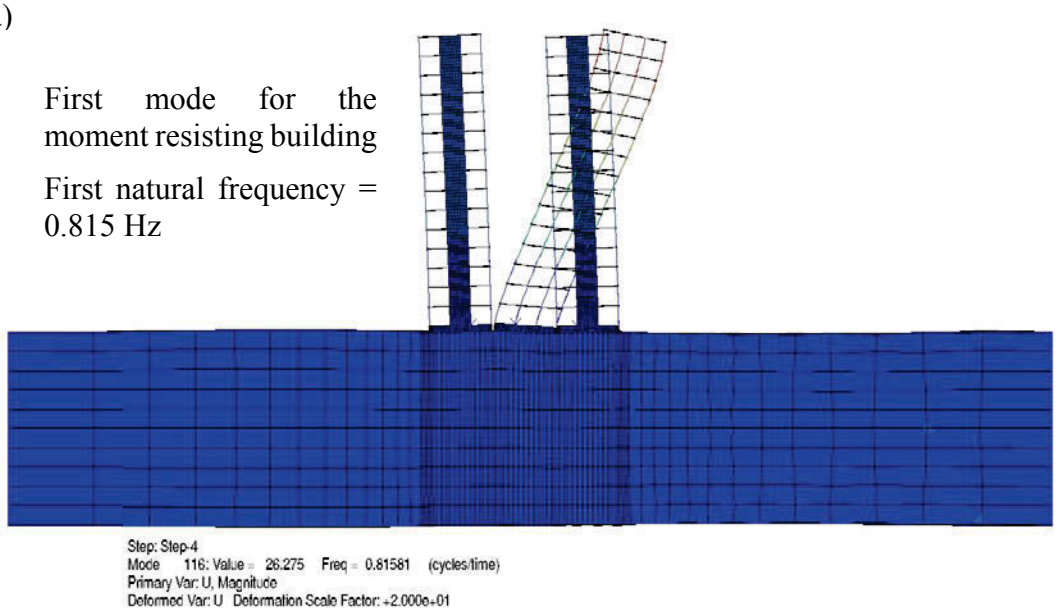

(b)

First mode for the shear wall braced building

First natural frequency = 1.145 Hz

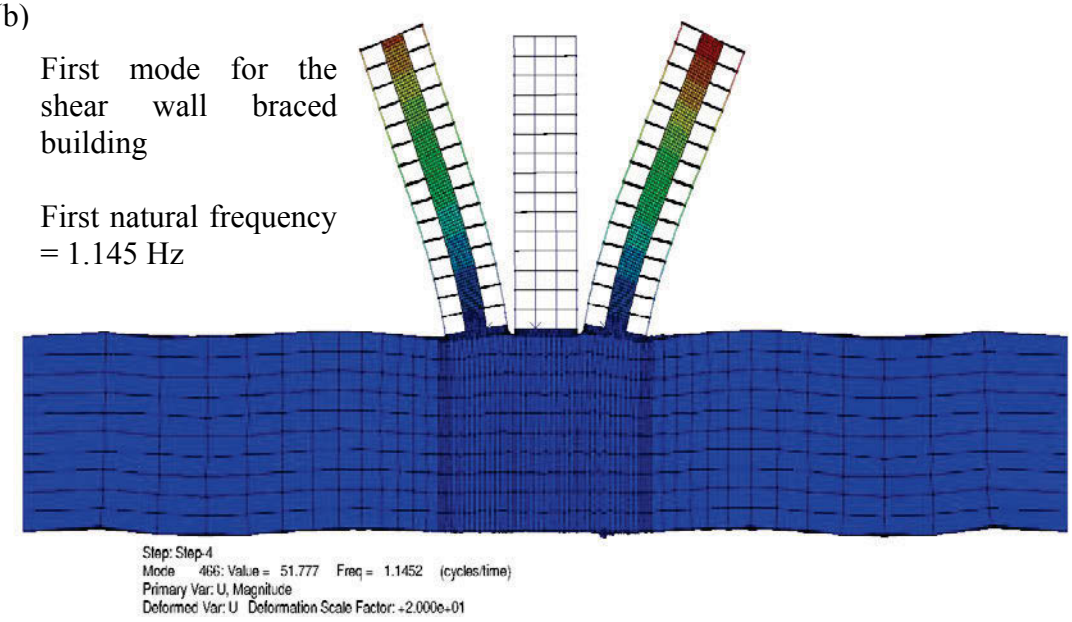

Figure 6.15 Response spectrum of ground motions of (a) the moment resisting building and (b) the shear wall braced building under the 1994 Northridge earthquake; and (c) the moment resisting building and (d) the shear wall braced building under the 1995 Kobe earthquake in conjunction with different separation gaps

A comparison between the first and second mode frequencies of both types of buildings with different foundations is summarised in Table 6.5. A linear perturbation and Lanczos method available in ABAQUS were used to extract eigenvalues to calculate the natural frequencies and corresponding mode shapes of the soil-pile-structure system. Figure 6.15 shows the typical first mode shapes of the soil-foundation-structure system

where the fundamental natural frequency was 0.830 Hz for the moment resisting building in a fixed-base condition, and when sitting on a 30 m long end-bearing pile foundation, provided a first mode frequency of 0.815 Hz. This decrease in natural frequency stemmed from the extra degrees of freedom induced by introducing pile foundations and a soil medium. Moreover, this variation in the dynamic characteristics of the system was the primary governing factor influencing the amount of seismic energy absorbed by structure subjected to strong earthquakes.

6.5.2 Shear forces

Figure 6.16 shows the envelope of shear forces in the building used to study the separation gap (SG), the impact of possible seismic pounding on a moment resisting building, and shear wall braced buildings. This envelope resulted from a 3D numerical analysis of both types of buildings under applied earthquakes. The maximum shear force at each building level, regardless of the direction, is the absolute maximum value of storey shear force, and is the summation of shear forces acting on the columns and shear walls (if existing) at every time interval. The envelope of the shear force was then determined by plotting the maximum absolute shear forces against the corresponding storey levels.

As Figure 6.16 shows, under both earthquake excitations, the envelopes of shear forces are almost identical when the separation gaps are 1000 mm and 1200 mm, thus implying that no seismic pounding occurred during these analyses. However, seismic pounding did occur when the separation gaps were equal to or less than 700 mm because the corresponding envelopes differ markedly from the cases with no pounding.

As plotted in Figure 6.16 (a), the moment resisting building under the 1994 Northridge earthquake experienced 6.3 MN of shear force at level 10 when the separation gap was 100 mm, which is 37% more than the shear force at the same level when the separation gap was 1200 mm. Moreover, where SG = 700 mm, the building experienced an increment of shear force at the roof top of almost three times more than the cases with no seismic pounding. Obviously, seismic pounding occurred at levels 10 and 15 when the separation gaps were 100 mm and 300 mm, and at the rooftop when SG = 700 mm under the 1994 Northridge earthquake.

Figure 6.16 (c) summarises the shear forces developed in the 15 storey moment resisting building under the 1995 Kobe earthquake. Note that the envelopes of shear forces

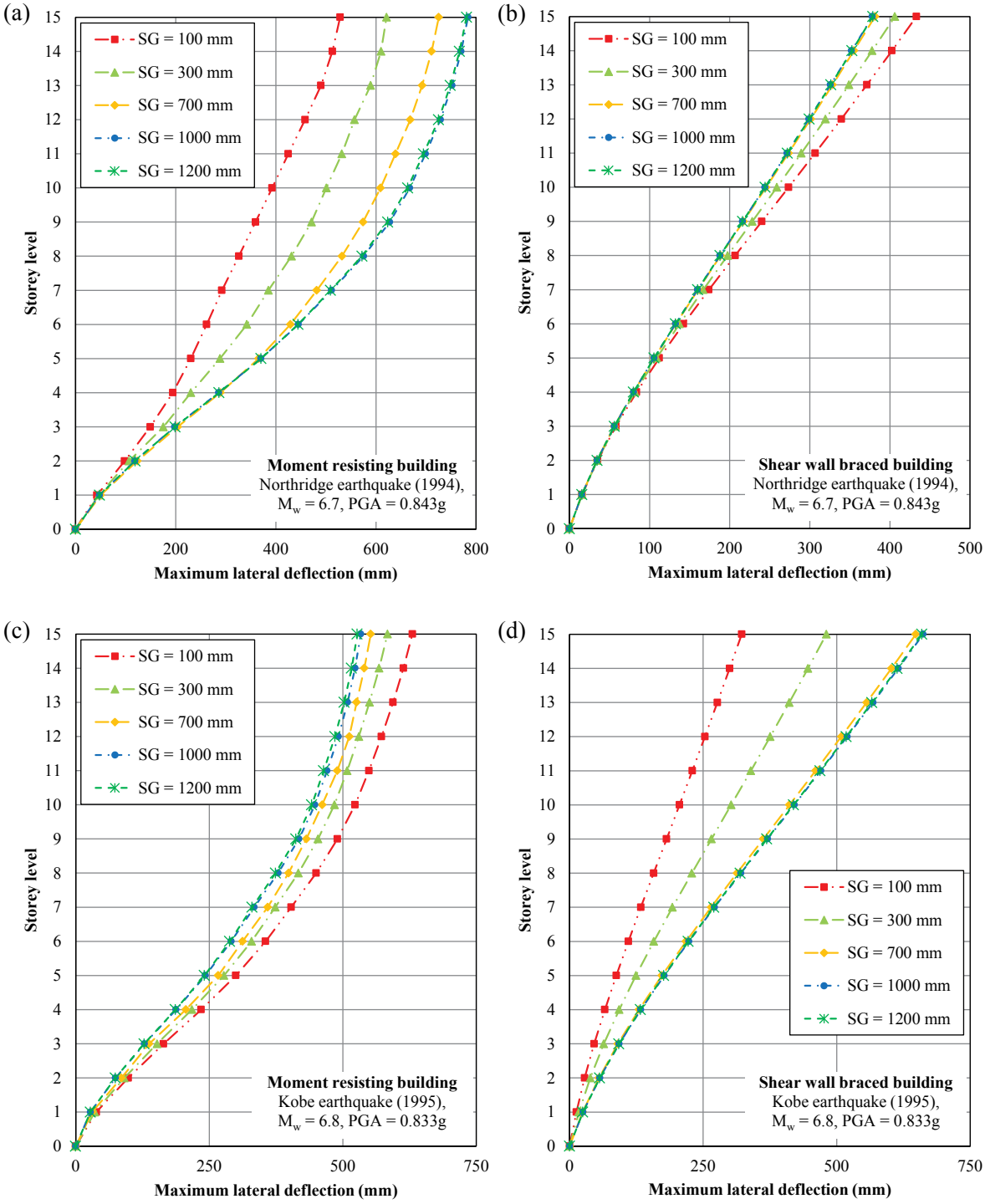

Figure 6.16 Total levelling shear forces of (a) the moment resisting building and (b) the shear wall braced building under the 1994 Northridge earthquake; and (c) the moment resisting building and (d) the shear wall braced building under the 1995 Kobe earthquake in conjunction with different separation gaps

are identical when the separation gaps were 1000 mm and 1200 mm, indicating no pounding, while the increase of shear forces in some particular storey levels with reduced

separation gaps (i.e. SG = 700, 300 and 100 mm) implies that the neighbouring buildings collided. When the SG = 100 mm, the moment resisting building experienced 50% and 400% more shear forces at levels 10 and 15, respectively, compared to the corresponding values for cases with no pounding (i.e. SG = 1200 mm). Furthermore, when the separation gaps were 300 mm and 700 mm, the moment resisting building experienced 5.5 MN and 3.6 MN of shear forces at level 14, respectively. In contrast, taking the case of SG = 1000 mm as an example, the shear force at the same level was only 1.8MN, and therefore the collisions induced by the 1995 Kobe earthquake occurred at levels 10 and 15 when the separation gap was 100 mm, and at level 14 when the separation gaps were 300 mm and 700 mm. These values show that seismic pounding will increase the shear force demand at particular levels, which may threaten column integrity if seismic pounding is not included in the design phase. Referring to Figure 6.16 (b) and Figure 6.16 (d), seismic pounding occurred at the same level of the shear wall braced buildings for the corresponding cases.

In general, the base shear for the moment resisting building (i.e. the middle building) increases when separation decreases, as shown in Figure 6.16 (a) and Figure 6.16 (c). For example, the base shear could have increased by up to 18% and 12% for the 1994 Northridge and the 1995 Kobe earthquakes, respectively. In this present study, the shear forces in the structures stemmed from structural inertia induced by the earthquakes and the collision caused by seismic pounding. In fact, seismic pounding implies that confinement can be induced by the presence of two shear wall braced buildings (i.e. the side buildings), which alters the their natural periods and changes the dynamic characteristics of the system. Moreover, the natural periods of both types of buildings decreases as the separation gap decreases, which means that an increase in the base shear is due to seismic pounding and this decline in the natural period may attract more seismic energy, as shown in Figure 6.14.

On the other hand, Figure 6.16 (d) also shows that under the 1995 Kobe earthquake, the base shear force acting on the shear wall braced structure increases with the separation gap, which implies that the subsequent reduction in base shear induced as the natural period of the building system shifted to a shorter period had more influence on the distribution of shear force along the building, even though seismic pounding occurred when the separation gap was less than 700 mm.

An example of lateral building displacement and pounding force time history where SG = 300 mm due to the 1994 Northridge earthquake is shown in Figure 6.17; it also includes the response of levels 15 and 10 for the moment resisting building and the left shear wall braced building. Indeed, Figure 6.17 shows that at the beginning of dynamic analysis (when the time is equal to 0) the difference in displacement between two buildings is 300 mm, which indicates a 300 mm separation gap. Figure 6.17 (a) indicates that seismic pounding occurred five times at level 15 while Figure 6.17 (b) shows that seismic pounding occurred twice because higher storey levels experience higher accumulated lateral displacement, and thus seismic pounding is more likely to happen at higher storey levels.

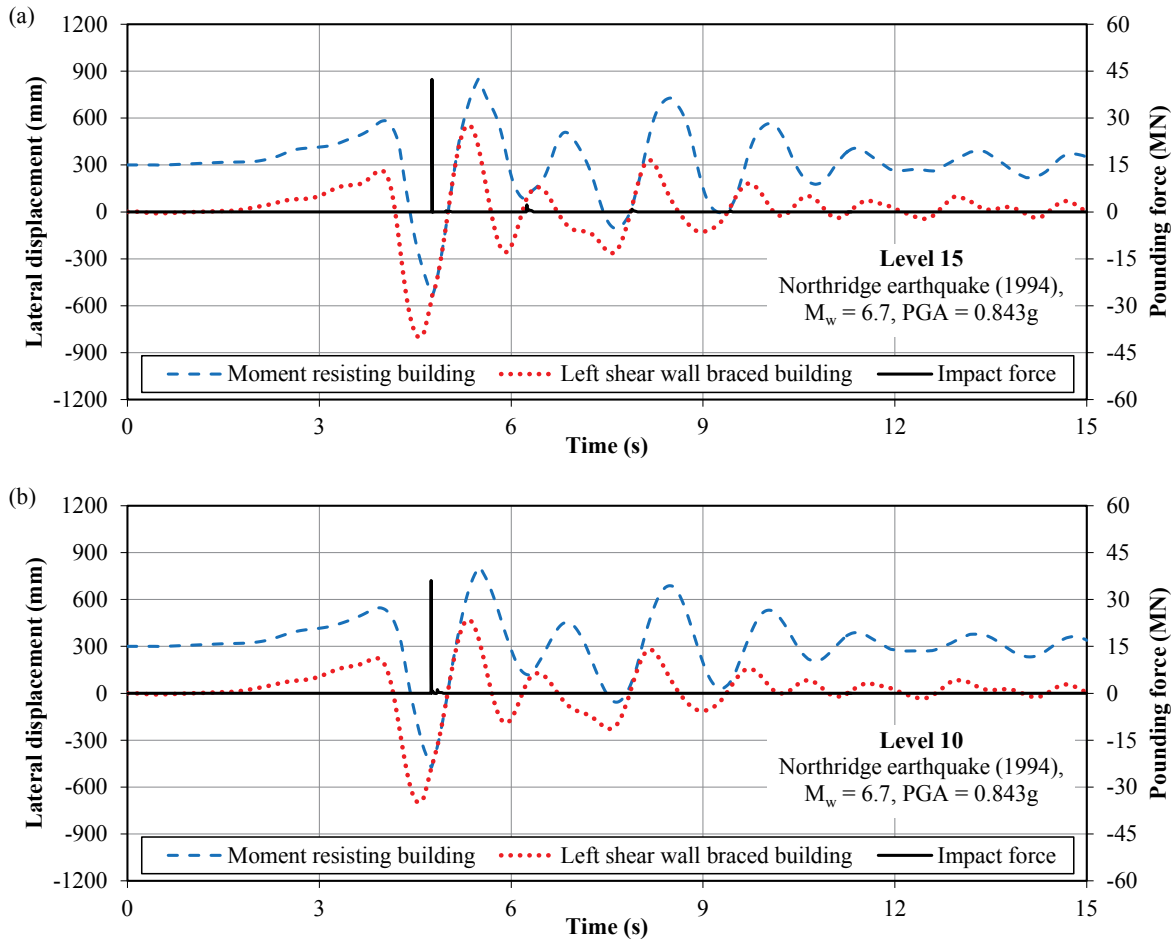

Figure 6.17 Lateral building displacement of the moment resisting building and the left shear wall braced building and pounding force time histories of (a) level 15 and (b) level 10 under the 1994 Northridge earthquake

Moreover, the maximum impact forces induced by seismic pounding are significant but with short durations, and these impact forces are mainly resisted by the mass of the building. Therefore, the impact forces significantly influence the global response of the building and are obviously detrimental to the structural elements around the impact area. Therefore, the coupling effects of seismic pounding and SSPSI should be considered by practising engineers because they can be detrimental to the local and global safety of a building.

It could also be concluded that the minimum separation gap required by some seismic standard (e.g. AS1170.4 and GB50011) is not sufficient because seismic pounding occurred when SG = 700 mm, which is greater than the standard requirement. Basically, neighbouring buildings with similar dynamic characteristics might find the standard separation gap sufficient, but not for neighbouring buildings with different dynamic characteristics such as retrofitted buildings standing next to each other. Retrofitting alters the dynamic characteristics of a building, usually without changing the separation gap, and therefore the pounding issue needs to be re-analysed after retrofitting.

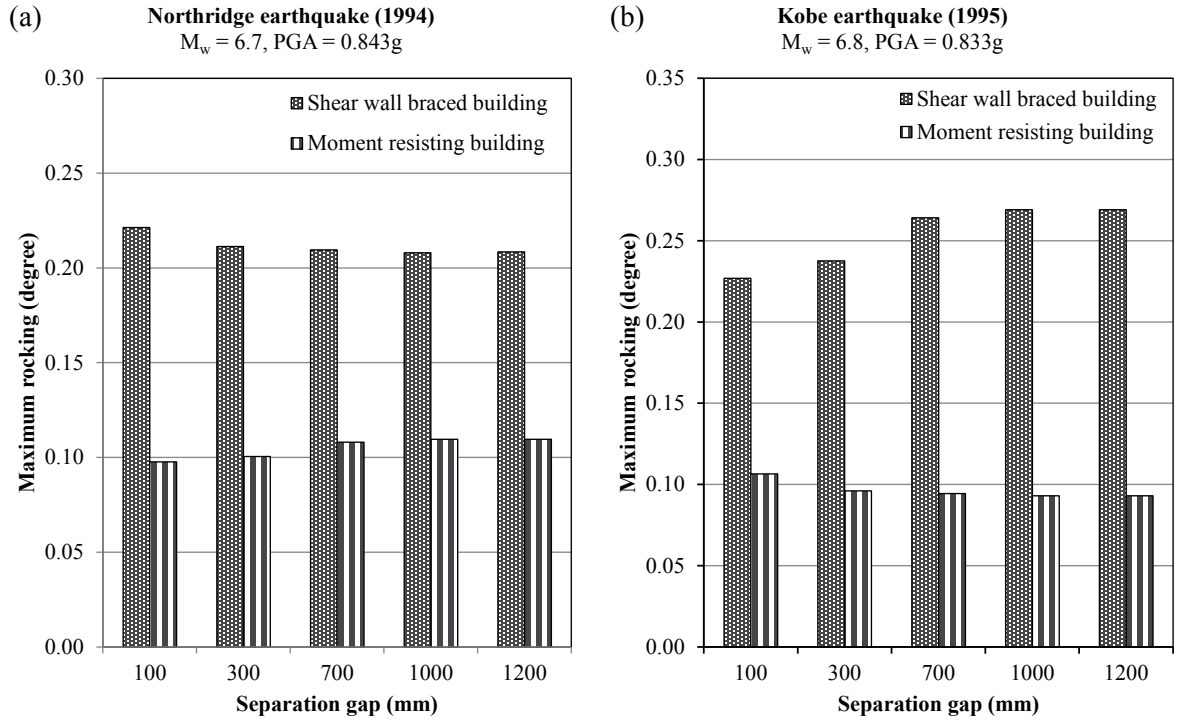

Figure 6.18 Maximum rocking of foundation slab of the moment resisting building and the shear wall braced building in conjunction with different separation gaps under (a) the 1994 Northridge and (b) the 1995 Kobe earthquakes

6.5.3 Rocking of foundation slabs

Figure 6.18 shows the maximum rocking of a foundation slab for both types of buildings in conjunction with five different separation gaps. Maximum rocking is taken as the absolute maximum value of slab rotation during seismic excitation. Foundation slabs rock when the inertial forces generated in the superstructure during earthquakes cause compression on one side and tension on the other side; this causes settlement on the compression side and possible uplift or upward movement on the other side. In this study, confinement induced by two side buildings is another factor which causes a foundation slab to rock, as well as the inertial force generated and the dynamic properties of the underlying soil. Therefore, since the weight of the moment resisting building is less than the weight of the shear wall braced building, and due to the confinement induced by neighbouring buildings on the lateral movement of the moment resisting building, it is expected that the rocking of the foundation slab of the moment resisting building is less than the rocking of the foundation slab of the shear wall braced building.

Under the 1994 Northridge earthquake (Figure 6.18 (a)), as the separation gap decreased, the maximum rocking of the foundation slab of the moment resisting building decreased, but it increased for the shear wall braced building. The increase in base shear with the reduction in the separation gap can be seen in Figure 6.16 (a) for the moment resisting building, and it should result in the foundation slab rocking more. However, due to the confinement caused by neighbouring buildings, foundation movement is restrained, and is even more restrained as the separation gap decreases. Shear wall braced buildings which are free to move on one side means the pattern in which the foundation slab experiences maximum rocking varies with the base shear, thus indicating an increase in the rocking angle as the separation gap decreases; this is shown in in Figure 6.16 (b).

Figure 6.18 (b) shows the trend of maximum rocking of the foundation slab during the 1995 Kobe earthquake, and shows that the maximum rocking of foundation slab increases with the separation gap for the shear wall braced buildings, whereas the trend for the moment resisting building was opposite, mainly due to variations in the base shear for the moment resisting and shear wall braced building, as shown in Figure 6.16 (c) and Figure 6.16 (d), respectively. Thus, the variation of inertial forces had a more pronounced influence on the rocking of the foundation slab.

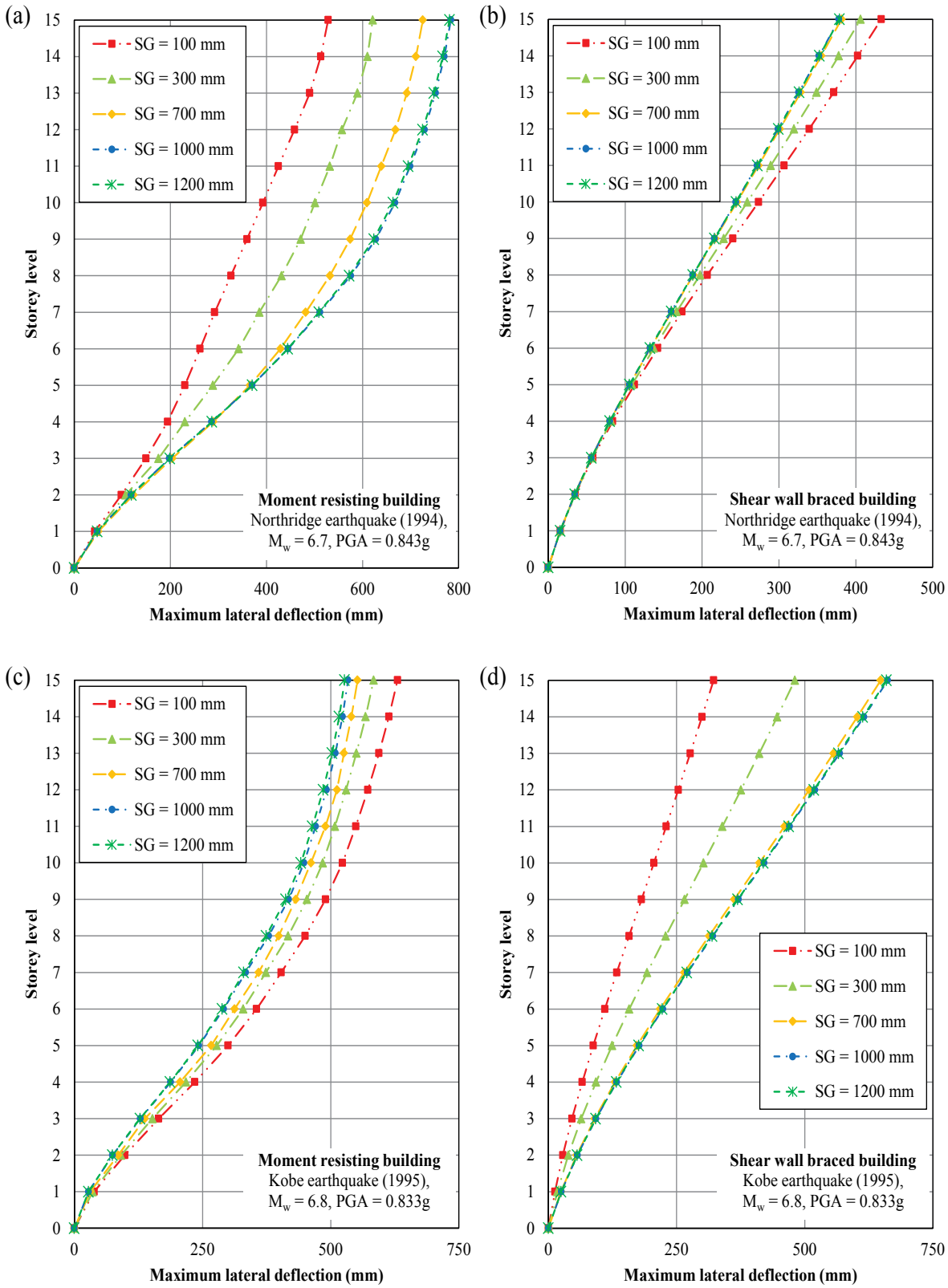

Figure 6.19 Maximum lateral structural deflections of (a) the moment resisting building and (b) the shear wall braced building under the 1994 Northridge earthquake; and (c) the moment resisting building and (d) the shear wall braced building under the 1995 Kobe earthquake in conjunction with different separation gaps

5.4 Lateral deflection and inter-storey drift

Figure 6.19 shows the lateral deflections of both types of buildings when the roof reached its maximum deflection. As Hokmabadi *et al.* (2012) stated, the lateral deflection of a building recorded like this tends to provide a more reasonable structural deformation than recording the absolute maximum values, regardless of when they occurred. In this study the lateral deflections are relative to the movement of the foundation slab at ground level by subtracting the lateral displacement of the foundation slab from the lateral deflection of each storey level.

Figure 6.19 (a) shows that the lateral deflections of the moment resisting building under excitation of the 1994 Northridge earthquake decreased with the decrease in the separation gap (SG). For instance, when SG = 1200 mm, the corresponding maximum lateral deflection was 780 mm, and a maximum lateral deflection of 528 mm was obtained when SG = 100 mm. This decrease in lateral deflection is directly related to the confinement induced by the closely spaced buildings, despite the increases observed in the base shear with the decrease in the separation gap. Moreover, the shear wall braced buildings experienced more lateral displacement as the separation gap decreased due to the extra shear forces induced by seismic pounding and the free side of buildings. Figure 6.19 also shows that the maximum lateral deflection of a moment resisting building is greater than the deflection of a shear wall braced building because a shear wall system induces high structural stiffness in the latter. Thus, the variation in the results of lateral deflections for shear wall braced buildings are not as significant as the corresponding deflections in the moment resisting buildings.

Figure 6.19 (c) shows the lateral deflection of the moment resisting building under excitation during the 1995 Kobe earthquake where maximum lateral deflections increased as the separation gap decreased. However, Figure 6.19 (d) shows that the lateral deflections of shear wall braced buildings decreased with the decrease in the separation gap. This means that lateral building deflection is influenced by three factors, (i) shear force induced building distortion, (ii) the foundation slab rocking, and (iii) the confinement embraced by the neighbouring structures. In those cases which considered the excitation of the 1995 Kobe earthquake, the induced shear forces in the building contributed more significantly to lateral deformation, indeed Figure 6.16 (c) shows that the storey shear forces generally increased as the separation gap decreased, and the shear

forces at some particular levels had increased due to seismic pounding. As a consequence, the moment resisting building experienced more lateral deflection as the separation gap decreased, even though lateral deflection was restricted due to confinement induced by the neighbouring buildings as Figure 6.19 (c) shows, the variation of maximum lateral deflection was only 20%. The shear wall braced building in Figure 6.16 (d) shows that although seismic pounding amplified the shear forces at some levels, the base shear attracted by the building decreased as the separation gap reduced due to changes in the dynamic characteristics. Thus, lateral building deflections decreased with the decrease in the separation gap, as shown in Figure 6.19 (d).

Figure 6.20 presents the maximum inter-storey drifts of both types of buildings. According to the Australian seismic standard (AS1170.4 2007), Equation (6.9) is used to determine the maximum inter-storey drifts:

$$Drift = \frac{d_{i+1} - d_i}{h} \tag{6.9}$$

where d_{i+1} is deflection at level $(i + 1)$;

d_i is deflection at level (i);

h is the height of the story.where d_i is deflection at the i_{th} level, d_{i+1} is deflection at the $(i + 1)_{th}$ level, and h is the storey height. Inter-storey drifts generally follow the same pattern of variation as the lateral deflections for corresponding cases. For instance, during the 1994 Northridge earthquake when the separation gap increased from 100 mm to 1200 mm, inter-storey drift for the moment resisting building increased from 2.08% to 2.94% (see Figure 6.20 (a)), and decreased from 1.11% to 0.94% for the shear wall braced building (see Figure 6.20 (b)). In Figure 6.20 (c) and Figure 6.20 (d), during the 1995 Kobe earthquake the inter-storey drifts decreased by 17% and increased by 107% for the moment resisting building and shear wall braced building, respectively, when the separation gap increased from 100 mm to 1200 mm. Therefore, seismic pounding can increase inter-storey drift and thus seismic pounding interferes with the building's seismic performance level because inter-storey drift is an important parameter for assessing the seismic performance level.

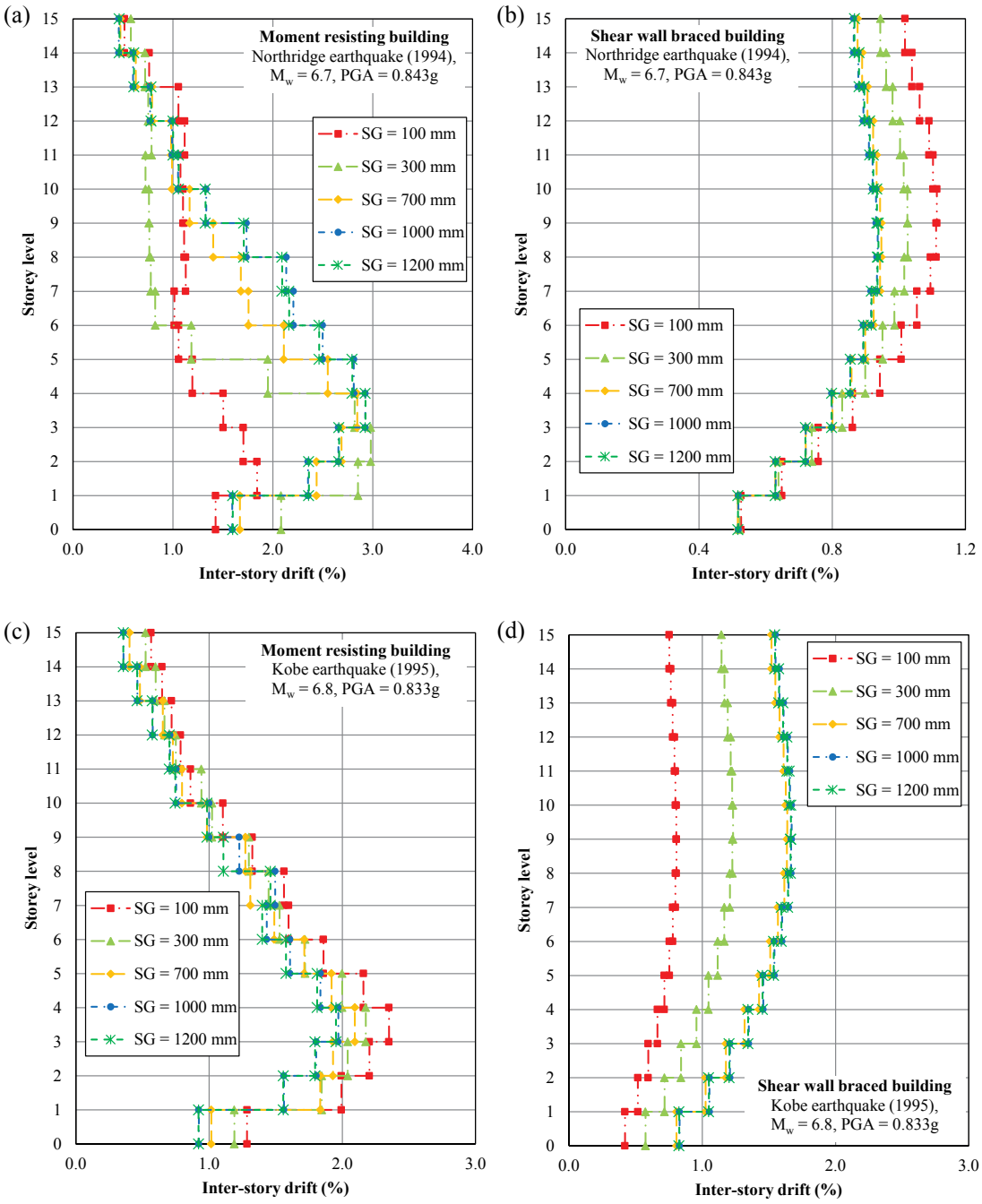

Figure 6.20 Maximum inter-storey drifts of (a) the moment resisting building and (b) the shear wall braced building under the 1994 Northridge earthquake; and (c) the moment resisting building and (d) the shear wall braced building under the 1995 Kobe earthquake in conjunction with different separation gaps

6.5.5 Lateral pile deflections

Figure 6.21 presents the lateral deflection of piles along their depth under an earthquake loading for both types of buildings, in conjunction with different separation

gaps. The numerical model allows the time history of the relative lateral movement $u(z,t)$ of any point along the pile to be accessed, where z is the depth from the bottom of the foundation slab to the considered points, and t is the time during excitation. The time when maximum lateral deflection occurred at the head of a pile is used to plot lateral deflection along the pile $u(z)$. Figure 6.22 shows the deformation of a soil-pile-structure system during a dynamic analysis.

For the moment resisting building, a pile labelled M_1 (see Figure 6.4) is used as an example because all the piles shared a similar amount of lateral deflections in the group of end-bearing piles. The lateral deflections of the pile M_1 during the 1994 Northridge and 1995 Kobe earthquake are plotted in Figure 6.21 (a) and Figure 6.21 (c), respectively, while the results of pile SL_1 (see Figure 6.4) which supported the left shear wall braced building are shown in Figure 6.21 (b) and Figure 6.21 (d).

Figure 6.21 shows that where no seismic pounding occurred during the analysis (i.e. $SG = 1000$ mm and $SG = 1200$ mm) the lateral deflections plotted along the pile are very close to each other, but where the separation gap was equal to or less than 700 mm, the lateral deflections differed compared to the results where no seismic pounding occurred This shows that lateral pile deflection can be influenced significantly by the seismic pounding.

Figure 6.21 (a) and Figure 6.21 (c) show that the lateral deflection of piles increases as the separation gap decreases where piles are supporting the moment resisting building. For instance, under the 1994 Northridge earthquake, when $SG = 1000$ mm, the maximum lateral pile deflection was 112 mm, while the maximum lateral pile deflection increased by 150% when $SG = 100$ mm. Figure 6.21 (b) and Figure 6.21 (d) reveal that the lateral pile deflections of the shear wall braced building increased as the separation gap decreased under excitation by the 1994 Northridge earthquake, whereas this trend was opposite under excitation during the 1995 Kobe earthquake. The foundation slab transmits the inertial forces developed in superstructures from the superstructure to the pile group, and then to the competent bedrock. Thus, the base shear attracted by the superstructure influences the lateral deflection of piles, and as a consequence, it is expected that the lateral deflection of piles and the base shears share the same trend of variation seen in Figure 6.21 and Figure 6.16.

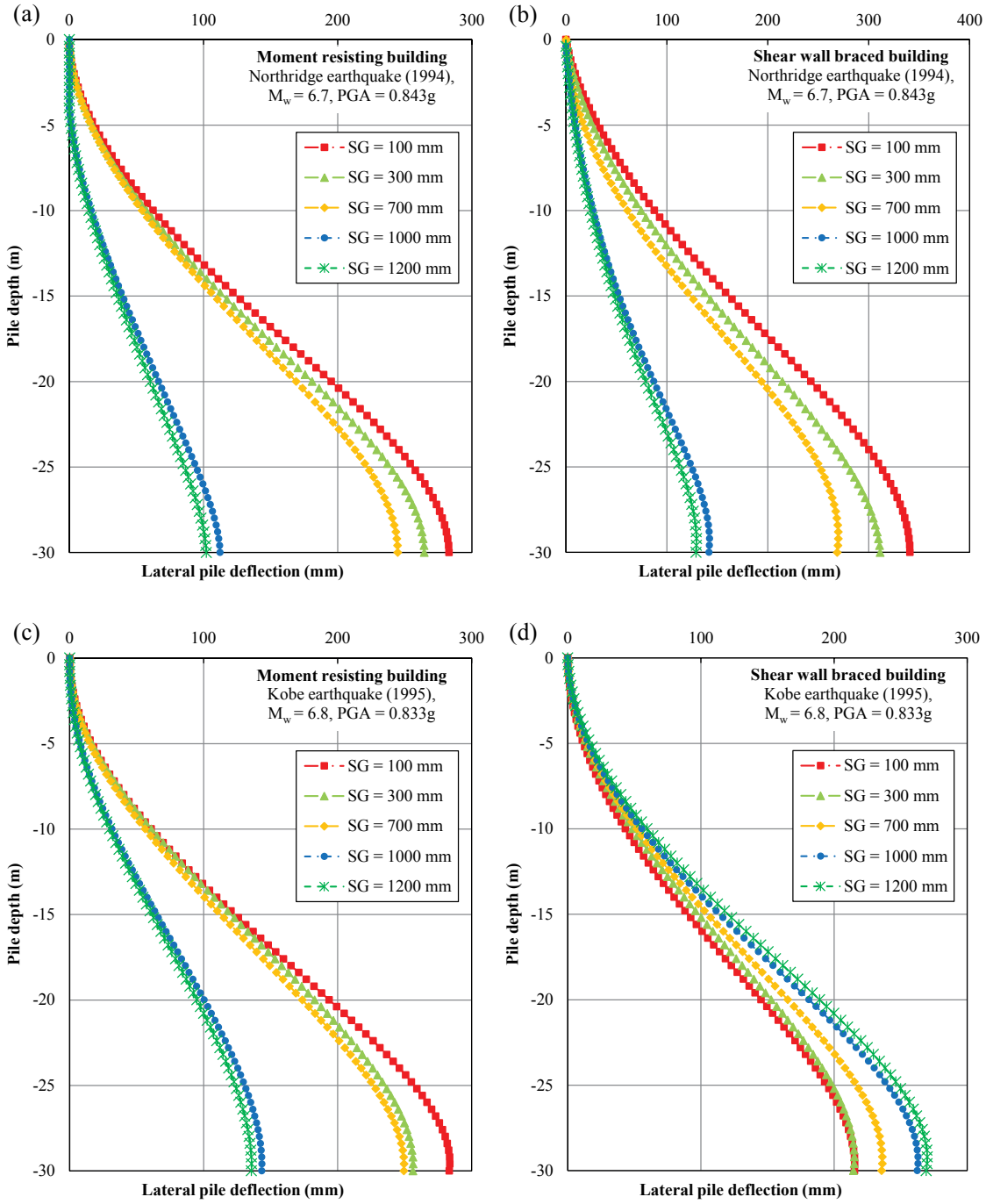

Figure 6.21 Maximum lateral pile deflections of (a) the moment resisting building and (b) the shear wall braced building under the 1994 Northridge earthquake; and (c) the moment resisting building and (d) the shear wall braced building under the 1995 Kobe earthquake in conjunction with different separation gaps

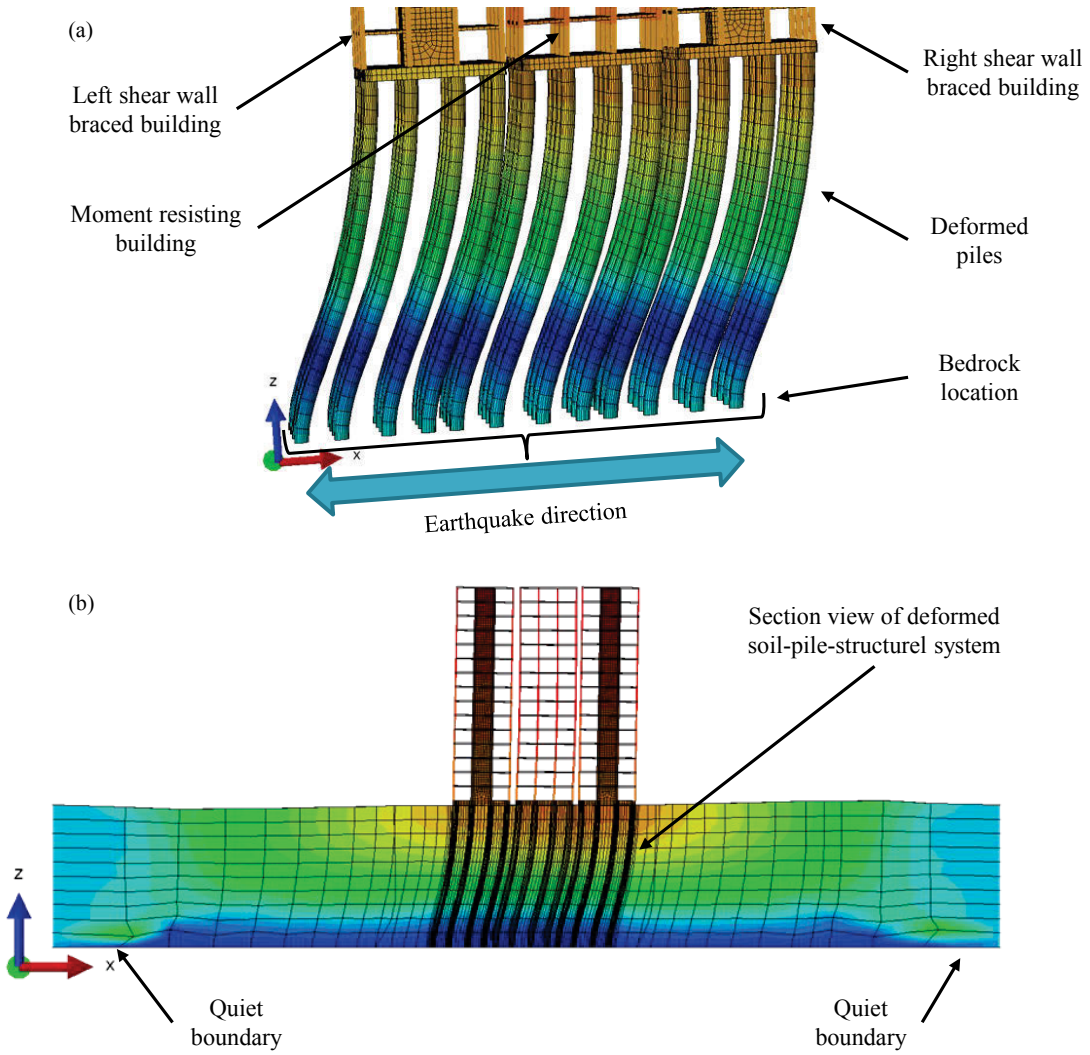

Figure 6.22 Deformation of structure-pile-soil system: (a) deformed piles, and (b) section view of deformed structure-pile-soil system

6.5.6 Bending moments along the piles

Figure 6.23 presents the bending moments along piles under the influence of two seismic excitations and five different size separation gaps. The elastic beam theory (Euler-Bernoulli equation) is used to produce the bending moment along the depth of each pile $M(z)$ as follows:

$$M(z) = EI\frac{d^2(u(z))}{dz^2} \tag{6.10}$$

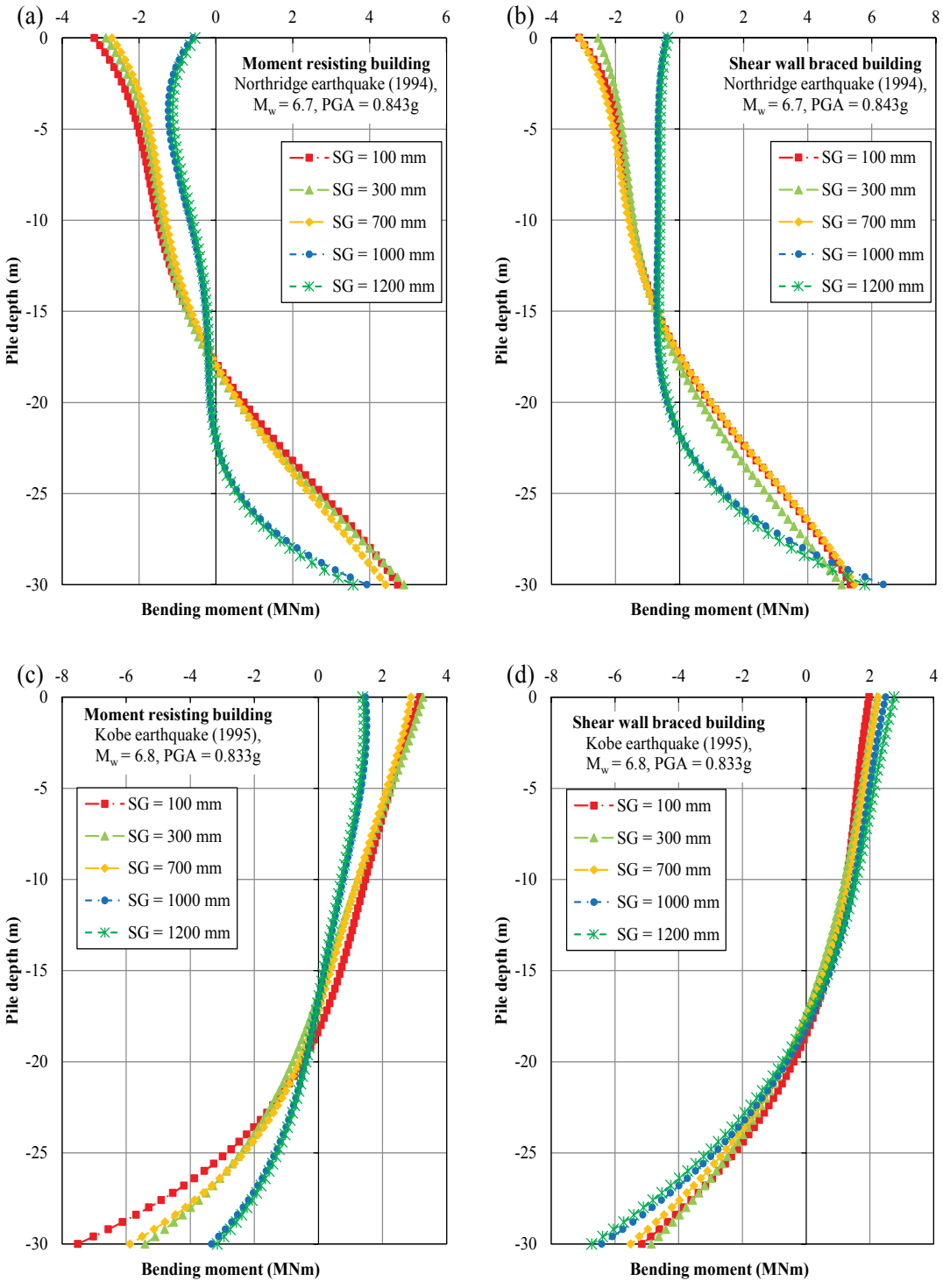

Figure 6.23 Bending moments of the piles of (a) the moment resisting building and (b) the shear wall braced building under the 1994 Northridge earthquake; and (c) the moment resisting building and (d) the shear wall braced building under the 1995 Kobe earthquake in conjunction with different separation gaps

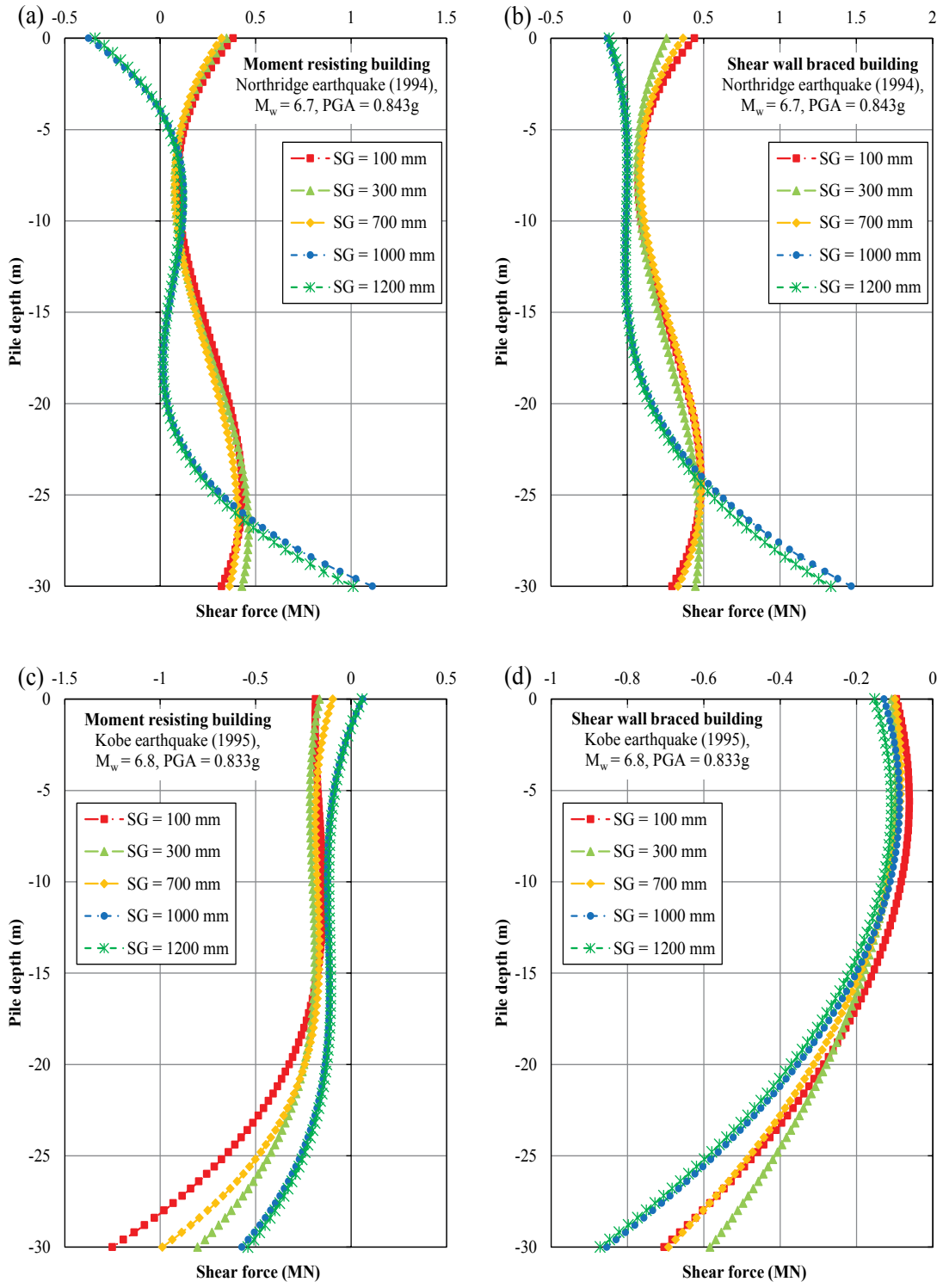

Figure 6.24 Shear forces of the piles of (a) the moment resisting building and (b) the shear wall braced building under the 1994 Northridge earthquake; and (c) the moment resisting building and (d) the shear wall braced building under the 1995 Kobe earthquake in conjunction with different separation gaps

where E is Young's modulus of the pile material, which is assumed to be 30.1 GPa, I is the second moment of the cross section of piles, which is 0.1018 m^4. The 6^{th} order polynomial fitting curves were used to reproduce the most accurate lateral deflections, and then the second differential of the polynomial were obtained to determine the bending moments along the pile.

Due to the load bearing mechanism of an end-bearing foundation, piles experience their maximum bending moment at the toe, where they are connected to the strong bedrock, as shown in Figure 6.23. Overall, the reported pile bending moments for moment resisting building, as shown in Figure 6.23 (a) and Figure 6.23 (c), indicate that the bending moments at the heads of the piles increased as the separation gap decreased. By using the pile M_1 under excitation in the 1994 Northridge earthquake as an example, the bending moment at the head increased by 486% as the separation gap increased from 100 mm to 1200 mm, while Figure 6.23 (b) and Figure 6.23 (d) show that where pile SL_1 supported the shear wall braced building under excitation from the 1994 Northridge earthquake, the bending moment at the pile head increased as the separation gap decreased, but this trend was the exact opposite under excitation from the 1995 Kobe earthquake. As expected, and by comparing Figure 6.23 and Figure 6.21, the maximum mobilised bending moment in a pile increased as deflection in the head increased. Moreover, as the structural shear forces increased, the bending moment generated at head of a pile increased (compare Figure 6.16 and Figure 6.23). Furthermore, bending moments along the pile vary considerably due to seismic pounding which means that seismic pounding can alter the bending moment along a pile. Therefore the effect of seismic pounding must be considered when designing the foundations of closely spaced structures.

6.5.7 Shear forces along the piles

Figure 6.24 shows the shear forces in pile elements for different cases. The shear force imposed on piles during excitation is another important parameter which governs the design of a foundation. The shear force along the pile element $Q(z)$ was obtained also by adopting the elastic beam theory and Equation (6.11).

$$Q(z) = EI\frac{d^3(u(z))}{dz^3} \tag{6.11}$$

Obviously, the third differential of a polynomial was utilised to calculate the shear forces along the pile.

It is evident from Figure 6.24 that a reduction in the separation gap (SG) alters the shear force distribution and maximum shear force along a pile. This is an important observation because seismic pounding has a significant influence on the force developed in the piles. As Figure 6.24 and Figure 6.16 show, seismic pounding changes the shear forces mobilised in the structure and consequently in a pile, and as the base shear in a superstructure increases, the maximum shear forces in piles also increase. It is therefore essential to treat superstructures, foundations, and soil as a whole while considering possible seismic pounding in order to obtain a safe and rational design.

6.6 Summary

To investigate the impact that seismic pounding has on the response of mid-rise buildings sitting on end-bearing piles, a conventional moment resisting building and two shear wall braced buildings resting on end-bearing pile foundations and with different seismic gaps were numerically simulated. Details of how this numerical model accounted for the combined effects of seismic pounding and soil-pile-structure interaction have been presented. The general contact interfaces were simulated to consider the interaction between piles and soil, while the contact pair interfaces between buildings were used to capture possible seismic pounding. The direct calculation method was used to carry out a fully nonlinear time history dynamic analysis to simulate the dynamic behaviour of soil, pile foundations, and structures, and to capture the effects of pounding under seismic excitations accurately.

The results show that seismic pounding influences the distribution of shear force along the buildings and also increases the storey shear forces at the collision level, which poses a significant threat to column safety and the overall stability of buildings. Moreover, neighbouring buildings can have confinement effects which could alter the dynamic characteristics of buildings, and also help to increase the shear forces in structural columns. Therefore, the combined effects of seismic pounding and seismic soil-pile-

structure interaction should be considered by practising engineers because they can be detrimental to the safety of buildings, both locally and globally. In this study, lateral building deflection was influenced by the structural distortion directly induced by the shear force developed in the building, a rocking foundation slab, and confinement caused by neighbouring buildings. The corresponding results reveal that lateral deflection may decrease due to confinement or increase due to variations in the dynamic characteristics.

Due to the load transmission mechanism of an end-bearing foundation, lateral pile deflection can be influenced by the base shear developed in the superstructure, which further indicates that the occurrence of seismic pounding can increase lateral pile deflection. Therefore, the effects of seismic pounding must be considered when designing an end-bearing foundation for buildings. Moreover, the maximum shear forces and their distribution along an end-bearing pile can be impacted by the seismic pounding effect which can be overlooked in common design practice where superstructures and foundations are treated separately. Thus, to obtain a safe and rational design, the superstructure, foundation, and soil must be considered with regards to the possibility of simultaneous seismic pounding. The findings of this paper can provide engineers with a better insight into how seismic pounding affects the seismic performance of buildings, and the response of end-bearing foundations in soft soil. Finally, practising engineers should also consider the presence of the neighbouring structures when designing and analysing a new structure because they may change the dynamic characteristics of the proposed and existing buildings.

Chapter 7 CONCLUSIONS AND RECOMMENDATIONS

7.1 Conclusions

7.1.1 Conclusions based on the research related to laterally load pile on clay-sand layered slope

A numerical model of soil-pile interaction has been verified in this research with strong correlation with full-scale experimental method considering a single pile under lateral loading placed in the slope of layered soil. The results indicated that the lateral resistance of a pile adjacent to a slope is influenced notably by the distance from the pile to the slope crest, while the effects on the bending moments and rotations of the pile are insignificant.

The soil-pile interaction behaviour comprises of both normal and tangential characteristics. The normal behaviour adopts hard contact in a pressure-over closure relationship, where a soft contact implies that the surfaces transmit no contact pressure unless the nodes of the slave surface make contact with the master surface. No penetration was allowed at the location of each constraint (depending on the method used to enforce constraint, this condition will either be strictly satisfied or approximated), and there was no limit to the magnitude of contact pressure that could be transmitted when the surfaces are in contact. The formula for this normal behaviour was expressed in Equation (4.7).

The tangential behaviour was the main focus of this study on soil-pile interaction. A subroutine developed in FORTRAN programming language and linked to ABAQUS was utilised to model the tangential behaviour of contact surfaces in the numerical model. This subroutine defines the variable required in the numerical simulation by adopting the classical Mohr-Coulomb failure model. Since the Mohr-Coulomb failure model cannot be directly defined in the simulation, a modified version of this model (Equation (4.8)) was coded in the FRIC_COEF subroutine to define the isotropic frictional coefficient between the contacting surfaces. The subroutine was verified for further studies by a comprehensive study on several models of soil-pile interaction with different cases of load and pile position in layered soil.

7.1.2 Conclusions based on research on the seismic soil-foundation-structure interaction for shallow foundation

Adopting FRIC_COEF subroutine for dynamics soil-foundation-structure interaction modelling, the shallow foundation size was the main parameter to be investigated and evaluated for the seismic response of a regular mid-rise moment resisting building frame under four selected earthquakes.

The method of direct calculation was adopted, and therefore the numerical model can perform a fully nonlinear time history dynamic analysis to realistically simulate the complicated dynamic behaviour of soil, foundation and structure as well as the interaction between them. In addition, the quiet boundary issue in seismic analysis has been fully resolved in this study via infinite elements in which the orientation is heading outward from the centre of the soil medium. Other dynamic characteristics of the model have been adopted appropriately based on characteristics of the system. Moreover, the main problem for both geotechnical and structural engineering in numerical modelling of these complicated models is the memory and storage spaces. The computer facility from University of Technology Sydney (UTS) clusters and National Computational Infrastructure (NCI) supercomputers provided the abilities to handle those difficulties where, in some cases, the model was not able to be solved in a reasonable time frame.

Details of the building response in terms of lateral deflections, inter-storey drifts, and maximum total levelling shear forces at each level and rocking of foundation for several case of foundation have been quantified. The numerical results confirm that the size of shallow foundation can influence the structural design of the building under seismic loads considering the seismic soil-foundation-structure interaction. The size of a shallow foundation altered the fundamental frequency of the soil-foundation-structure system considerably, whereas its influence on the higher modes of vibration was insignificant.

It was observed that buildings with larger shallow foundations attracted more inertial forces from earthquake excitations than smaller foundations. The outcomes of this study show that when the size of shallow foundation reduced, the natural period would increase, the base shear would reduce significantly while the lateral deformation, inter-storey drift and foundation rocking are also increase considerably.

7.1.3 Conclusions based on research considering the seismic soil-foundation-structure interaction for pile foundation

Numerical modelling of a superstructure founded on a pile group subjected to seismic loading has been conducted. After satisfying the bearing capacity and stress analysis conditions under dead loads and live loads, a parametric study on the effects of pile length on the building response was conducted by increasing the pile length from 10 m to 30 m (30 m being end-bearing pile). In general, the results show that increasing the pile length causes increase in both lateral deflections and inter-storey drifts for all of the four modelled earthquakes. As a result, maximum inter-story drift of this building exceed the life-safety threshold defined in the performance based design, which is usually limited to 1.5%. In addition, the increasing trend of lateral deflection and reducing trend of total levelling shear forces from level 0 to level 15 was observed while the maximum inter-storey drift occurred at the mid-height (level 3 to level 10). Moreover, the pile load-bearing mechanism alters the forces and how they are distributed along the pile elements. This observation shows how combined kinematic and inertial interactions influence the developed loads on pile elements, which can be overlooked in industry practice in which the superstructure and pile foundation are treated separately.

The key difference between floating and end-bearing pile in earthquake loading is that the floating pile absorbs seismic energy from the surrounding soil mainly around the shafts while end-bearing pile absorbs energy of earthquake not only from soil via pile shaft, but also from the toe socketed in the rock. In addition, all pile will have almost zero vertical displacement while the corresponding values for floating piles are significant. As a result, rocking of structure on end-bearing piles is much smaller than rocking of structure on floating piles. Although there is a significant difference in mechanism between floating and end-bearing piles in all four selected earthquakes, the spectral response acceleration of these pile foundations are almost the same. Obviously, the patterns of spectral response acceleration are different from earthquake to earthquake.

Finally, lateral movements of each pile were obtained from numerical results and were results of the lateral displacements due to foundation rocking as well as the lateral deflection of pile elements. The lateral deformations of individual piles in the pile group were considerably different for the case of short pile foundations (i.e. 10 m or 15 m long) while these differences become less significant for longer pile foundations. Bending

moments and shear forces along the piles were graphed in order to assist structural engineers gaining a better understanding about pile response under earthquake loading.

7.1.4 Conclusions based on research on the seismic soil-foundation-structure interaction considering pounding between buildings

The seismic pounding analysis between adjacent buildings on end-bearing pile foundations under two selected large earthquake motions was conducted rigorously in this thesis. In order to obtain the building response under pounding effect, it is ideal to consider buildings with different natural frequencies. A moment resisting building and two shear wall braced buildings having the same height and overall dimensions were used to conduct numerical analysis in this study. The results show that seismic pounding influences the distribution of shear force along the buildings and also increases the storey shear forces at the collision level, which poses a significant threat to column safety and the overall stability of buildings. Moreover, neighbouring buildings can have confinement effects which could alter the dynamic characteristics of buildings, and also help to increase the shear forces in structural columns. Therefore, the combined effects of seismic pounding and seismic soil-pile-structure interaction should be considered by practising engineers because they can be detrimental to the safety of buildings, both locally and globally.

The combination of seismic soil-foundation-structure interaction (SSFSI) and seismic pounding induce a significant difficulty for the structural and geotechnical engineers in terms of analysis and design. Although occasionally there is some decrease in terms of building response such as lateral deflections, inter-storey drift, total levelling shear force of one building due to confinement effect from neighbour buildings, in general, structural designers prefer not to allow any pounding. This research can provide the structural designers and urban planners a clear understanding about how bad the effect of pounding impact could be when considering the seismic soil-foundation-structure interaction.

7.2 Recommendations for future works

Future research work may be carried out in the following areas:

- Current study for effect of foundation characteristics and separation gap on seismic soil-foundation-structure interaction (SSFSI) is for the regular mid-rise building. One of the recommendation for future work should be modelling of irregular superstructures.
- Shallow foundations under buildings are often placed in some depth below the ground surface. Research on the effects of embedded shallow foundations can be another interesting idea while considering seismic soil-foundation-structure interaction.
- Pile foundation for the moment resisting building considered in current study is vertical. The piles also had the same centre-lines with columns of the building which is believed to be the best pile arrangement. It would be possible that the inclined piles are installed. In another words, the inclined piles may be more suitable for buildings under seismic loading, and therefore can be investigated.
- Seismic pounding studied in this research only considered buildings with the same storey height and the pounding occurred between concrete slabs. Further investigation should consider buildings with different storey heights where the pounding may occur between concrete slabs and concrete columns. Those cases may cause more damages to buildings.
- Another interesting direction for future research is studying the effects of soil plasticity under dynamic loading considering number of cycles. In addition, the current research just investigates the seismic soil-foundation-structure interaction (SSFSI) for homogeneous clay deposit. Thus, multiple layers combining clay, sand or rock found in real sites should be investigated further.
- In addition, regarding earthquake excitation, these investigations just addressed horizontal components of earthquakes in the form of accelerations. The recommendation for future work should be consideration of vertical components of earthquakes in the analysis of seismic soil-foundation-structure interaction.
- Finally, the result of these studies and other related works can be used to develop a new revised procedure that can fulfil the current uncertainties in available design codes considering seismic-soil-foundation-structure interaction and pounding.

REFERENCES

Abdrabbo, F. M. and Gaaver, K. E. 2012. 'Simplified analysis of laterally loaded pile groups', *Alexandria Engineering Journal*, 51: 121-27.

ACI318-08. 2008. 'Building Code Requirements for Structural Concrete and Commentary'. American Concrete Institute.

Anagnostopoulos, S. A. 1996. 'Building pounding re-examined: how serious a problem is it'. *Eleventh world conference on earthquake engineering*, 2108. Pergamon, Elsevier Science Oxford, UK.

Anagnostopoulos, S. A. 1988. 'Pounding of buildings in series during earthquakes', *Earthquake Engineering & Structural Dynamics*, 16: 443-56.

AS1170.1, Australia Standard. 2002. 'Structural design actions - permanent, imposed and other actions', *Standards Australia, Sydney, Australia*, 1.

AS1170.4, Australia Standard. 2007. 'Structural design actions, part 4: earthquake actions in Australia', *Standards Australia, Sydney, Australia*, 4.

AS2159. 2009. 'Pilling-Design and installation, Standards Australian', *NSW, Australia.*

AS3600. 2009. 'Concrete Structures, Standards Australia', NSW, *Australia*.

ASCE7-10. 2010. 'Minimum Design Loads for Buildings and Other Structures'. *American Society of Civil Engineers.*

ATC-40. 1996. 'Seismic evaluation and retrofit of concrete buildings'. *Seismic Safety Commission, State of California*.

Badoni, D. and Nicos M. 1996. 'Nonlinear response of single piles under lateral inertial and seismic loads'. *Soil Dynamics and Earthquake Engineering*, 15: 29-43.

Belinchon, P., Sørensen, K. K. and Christensen, R. 2016. 'A Case Study of the Interaction between a Pile and Soft Soil focusing on Negative Skin Friction using Finite Element Analysis'. *Proceedings of 17th Nordic Geotechnical Meeting*. The Icelandic Geotechnical Society.

Borja, R. I., Wu, WH., Amies, A. P. and Smith, H. A. 1994. 'Nonlinear lateral, rocking, and torsional vibration of rigid foundations', *Journal of Geotechnical Engineering*, 120: 491-513.

Boulanger, W.R., Curras, J. C., Kutter, L. B., Wilson, W. W. and Abghari., A. 1999. 'Seismic Soil-Pile-Structure Interaction Experiments and Analyses', *Journal of geotechnical and geoenvironmental engineering*, 125: 750-59.

Bowles, J. E. 2001. *Foundation analysis and design* (McGraw-Hill International,).

Brown, D. A., and Shie, CF. 1991. 'Some numerical experiments with a three dimensional finite element model of a laterally loaded pile', *Computers and Geotechnics*, 12: 149-62.

BSSC, Council Building Seismic Safety. 1997. 'NEHRP guidelines for the seismic rehabilitation of buildings', *FEMA-273, Federal Emergency Management Agency, Washington, DC*.

BSSC. Council Building Seismic Safety, 2009. 'NEHRP recommended seismic provisions for new buildings and other structures (FEMA P-750)'. *Federal Emergency Management Agency, Washington, DC*.

Carbonari, S., Dezi, F. and Leoni, G. 2011. 'Linear soil–structure interaction of coupled wall–frame structures on pile foundations'. *Soil Dynamics and Earthquake Engineering*, 31: 1296-309.

Chang, D.W., Cheng, S.H. and Wang, Y.L. 2014. 'One-dimensional wave equation analyses for pile responses subjected to seismic horizontal ground motions'. *Soils and foundations*, 54: 313-28.

Chang, D.W., Lu, C.W., Lin, S.S., Lai, J.R. 2016. 'Dynamic analyses for performance-based seismic design of geotechnical structures with examples in deep foundations'. *Geotechnical Engineering*, Volume 47, Issue 2, June 2016.

Chau, K.T, Shen, C.Y. and Guo, X. 2009. 'Nonlinear seismic soil-pile-structure interactions: Shaking table tests and FEM analysis'. S*oil Dynamics and Earthquake Engineering* 29, 300-310.

Chen, L. 2016. 'Dynamic interaction between rigid surface foundations on multi-layered half space'. *International Journal of Structural Stability and Dynamics*, 16: 1550004.

Chopra, A. K. 2007. 'Dynamics of structures: theory and applications to earthquake engineering. 2007'. Prentice-Hall.

Chouw, N. and Hong, H. 2012. 'Pounding damage to buildings and bridges in the 22 February 2011 Christchurch earthquake'. *International Journal of Protective Structures*, 3: 123-39.

Chu, D., and Truman, KZ. 2004. 'Effects of pile foundation configurations in seismic soil-pile-structure interaction'. *13th World Conference on Earthquake Engineering*.

Chu, D., 2006. 'Three-dimensional nonlinear dynamic analysis of soil-pile-structure interaction'. PhD thesis, Washington University.

Clough, R. W., and Chopra, A. K. 1966. 'Earthquake stress analysis in earth dams'. *Journal of the Engineering Mechanics Division*, 92: 197-212.

Cohen, M., and Jennings, P. C. 1983. 'Silent boundary methods for transient analysis', *Computational methods for transient analysis*, 1: 301-60.

CSI. 2010. 'SAP2000 v14 Analysis Reference Manual, CSI'. *Computers and Structures Inc., Berkley, California*.

Das, B. M. 1983. *Fundamentals of soil dynamics* (Elsevier New York et al).

Durante, M. G., Sarno, L. D., Mylonakis, G., Taylor, C. A. and Simonelli, A. L. 2016. 'Soil–pile–structure interaction: experimental outcomes from shaking table tests', *Earthquake Engineering & Structural Dynamics*, 45: 1041-61.

Emani, P. K., Kumar, R. and Vedula, P. 2016. 'Inelastic Response Spectrum for Seismic Soil Pile Structure Interaction'. *International Journal of Geotechnical Earthquake Engineering (IJGEE)*, 7: 24-34.

Eurocode8. 2005. 'Eurocode 8: Design of structures for earthquake resistance'. *Standard, British*.

Fan, K., Gazetas, G., Kaynia, A., Kausel, E. and Ahmad, S. 1991. 'Kinematic seismic response of single piles and pile groups'. *Journal of Geotechnical Engineering*, 117: 1860-79.

Fatahi, B. and Tabatabaiefar, S. 2013. 'Fully Nonlinear Versus Equivalent Linear Computation Method for Seismic Analysis of Mid-Rise Buildings on Soft Soils', *International Journal of Geomechanics*, 14 (4).

Fatahi, B., Tabatabaiefar, S. and Samali., B. 2014. 'Soil-structure interaction vs Site effect for seismic design of tall buildings on soft soil'. *Geomech. Eng.*, 16: 293-320.

FEMA. 2000. *Prestandard and commentary for the seismic rehabilitation of buildings* (Prestandard and commentary for the seismic rehabilitation of buildings (FEMA)).

Gabr, M. A. and Borden R. H. 1990. 'Lateral analysis of piers constructed on slopes'. *Journal of Geotechnical Engineering* 116: 1831-1850.

Gazetas, G., Anastasopoulos, I., Adamidis, O. and Kontoroupi, Th. 2013. 'Nonlinear rocking stiffness of foundations'. *Soil Dynamics and Earthquake Engineering*, 47: 83-91.

Gazetas, G. , and Mylonakis, G. 1998. 'Seismic soil-structure interaction: new evidence and emerging issues'. *Proc. 3rd Conf. Geotechnical Earthquake Engineering and Soil Dynamics*. Seattle, USA.

Gazetas, G., Fan, K., Kaynia, A. and Kausel, E. 1991. 'Dynamic interaction factors for floating pile groups'. *Journal of Geotechnical Engineering*, 117: 1531-48.

GB50011. 2010. 'Code for seismic design of buildings (in Chinese)'. Beijing, China: China Building Industry Press.

Georgiadis, K. and Georgiadis M. 2010. 'Undrained Lateral Pile Response in Sloping Ground'. *Journal of Geotechnical & Geoenvironmental Engineering*,136: 1489-1500.

Google map, 2016. 'https://www.google.com/maps/'.

Guin, J, and Banerjee, P. K. 1998. 'Coupled soil-pile-structure interaction analysis under seismic excitation'. *Journal of Structural Engineering*, 124: 434-44.

Gutierrez, J. A., and Chopra, A. K. 1978. 'A substructure method for earthquake analysis of structures including structure-soil interaction'. *Earthquake Engineering & Structural Dynamics*, 6: 51-69.

Hall, J. F., Holmes, W.T. and Somers, P. 1994. 'Northridge earthquake, January 17, 1994'. *Preliminary reconnaissance report*.

Han, Y. 2002. 'Seismic response of tall building considering soil-pile-structure interaction'. *Earthquake Engineering and Engineering Vibration*, 1: 57-64.

Han, Y., and Cathro, D. 1997. "Seismic behaviour of tall buildings supported on pile foundations." *Seismic Analysis and Design for Soil-Pile-Structure Interactions*, 36-51. ASCE.

Hao, H. 2015. 'Analysis of seismic pounding between adjacent buildings'. *Australian Journal of Structural Engineering*, 16: 208-25.

Hao, H., Liu, X. Y., and Shen, J. 2000. 'Pounding response of adjacent buildings subjected to spatial earthquake ground excitations'. *Advances in Structural Engineering*, 3: 145-62.

Hardin, B. O., and Drnevich, V. P. 1972. 'Shear modulus and damping in soils: measurement and parameter effects'. *Journal of Soil Mechanics & Foundations Div*, 98.

Hashimoto, M., Sagiya, T., Tsuji, H., Hatanaka, Y. and Tada, T. 1996. 'Co-seismic displacements of the 1995 Hyogo-ken Nanbu earthquake'. *Journal of Physics of the Earth*, 44: 255-79.

Hayashi, Y., and Takahashi, I. 2004. 'Soil-Structure Interaction Effects on Building Response in Recent Earthquakes'. *Third UJNR Workshop on Soil-Structure InteractionVallombrosa Center, Menlo Park, California*.

Hemple, H. W. 1941. 'Recent progress in geodetic surveys of the United States Coast and Geodetic Survey'. *Eos, Transactions American Geophysical Union*, 22: 340-44.

Hetényi, M. 1971. 'Beams on elastic foundation: theory with applications in the fields of civil and mechanical engineering'. *University of Michigan.*

Hokmabadi, A. S., and Fatahi, B. 2015. 'Influence of foundation type on seismic performance of buildings considering soil–structure interaction'. *International Journal of Structural Stability and Dynamics*, 16: 1550043.

Hokmabadi, A. S., Fatahi, B. and Samali, B. 2012. 'Recording inter-storey drifts of structures in time-history approach for seismic design of building frames'. *Australian Journal of Structural Engineering*, 13: 175-79.

Hokmabadi, A. S., Fatahi, B. and Samali, B. 2014a. 'Physical modelling of seismic soil-pile-structure interaction for buildings on soft soils'. *International Journal of Geomechanics*, 15: 04014046.

Hokmabadi, A. S., Fatahi, B. and Samali, B. 2014b. 'Assessment of soil–pile–structure interaction influencing seismic response of mid-rise buildings sitting on floating pile foundations'. *Computers and Geotechnics*, 55: 172-86.

Hokmabadi, A. S. 2014. 'Effect of Dynamic Soil-Pile-Structure Interaction on Seismic Response of Mid-Rise Moment Resisting Frames'. *PhD thesis*, University of Technology Sydney.

Hong, H.P., Wang, S.S. and Hong, P. 2003. 'Critical building separation distance in reducing pounding risk under earthquake excitation'. *Structural Safety*, 25: 287-303.

Hough, S., and Jones, L. 2002. 'Earthquakes Don't Kill People, Buildings Do'. *San Francisco Chronicle*, 4: 17.

Jamal, K. A., and Vidyadhara, H. S. 2013. 'Seismic pounding of multistoreyed buildings'. *Moment*, 15: 2.

Kanamori, H. 1971. 'Focal mechanism of the Tokachi-Oki earthquake of May 16, 1968: Contortion of the lithosphere at a junction of two trenches'. *Tectonophysics*, 12: 1-13.

Karayannis, C. G., and Favvata, M. J. 2005. 'Earthquake-induced interaction between adjacent reinforced concrete structures with non-equal heights'. *Earthquake Engineering & Structural Dynamics*, 34: 1-20.

Kim, Y., Jeong, S. and Lee, S. 2010. 'Wedge failure analysis of soil resistance on laterally loaded piles in clay'. *Journal of geotechnical and geoenvironmental engineering*, 137: 678-94.

Kramer, S. L. 1996. 'Geotechnical earthquake engineering'. *Pearson Education India*.

Kramer, S. L., and Stewart, J. P. 2004. 'Geotechnical aspects of seismic hazards'. *Earthquake Engineering: from Engineering Seismology to Performance-Based Engineering, Y. Bozorgnia, V. Bertero (Eds.), CRC Press*, 4: 85.

Kumar, A., Choudhury, D. and Katzenbach, R. 2016. 'Effect of earthquake on combined pile–raft foundation'. *International Journal of Geomechanics*, 16: 04016013.

Kumar, K. 2008. 'Basic Geotechnical Earthquake Engineering'. *New age international: India.*

Li, Q., and Yang, Z. 2017. 'P–Y Approach for Laterally Loaded Piles in Frozen Silt'. *Journal of geotechnical and geoenvironmental engineering*, 143: 04017001.

Lin, H., Ni, L., Suleiman, M. T. and Raich, A. 2014. 'Interaction between laterally loaded pile and surrounding soil'. *Journal of geotechnical and geoenvironmental engineering*, 141: 04014119.

Liu, L., and Dobry, R. 1997. 'Seismic response of shallow foundation on liquefiable sand'. *Journal of geotechnical and geoenvironmental engineering*, 123: 557-67.

Lu, Y., Marshall, A. M. and Hajirasouliha, I. 2016. 'A simplified Nonlinear Sway-Rocking model for evaluation of seismic response of structures on shallow foundations'. *Soil Dynamics and Earthquake Engineering*, 81: 14-26.

Ma, X.H., Cheng, Y.M., Au, S.K., Cai, Y.Q. and Xu, C.J. 2009. 'Rocking vibration of a rigid strip footing on saturated soil'. *Comput. Geotech.*, 36: 928-33.

Madani, B., Behnamfar, F. and Riahi, H. T. 2015. 'Dynamic response of structures subjected to pounding and structure–soil–structure interaction'. *Soil Dynamics and Earthquake Engineering*, 78: 46-60.

Maheshwari, B. K., Truman, K. Z., El Naggar, M.H. and Gould, P. L. 2004. 'Three-dimensional nonlinear analysis for seismic soil–pile-structure interaction'. *Soil Dynamics and Earthquake Engineering*, 24: 343-56.

Maheshwari, B. K., and Watanabe, H. 2006. 'Nonlinear dynamic behaviour of pile foundations: Effects of separation at the soil-pile interface'. *Soils and foundations*, 46: 437-48.

Mahmoud, S., Abd-Elhamed, A. and Jankowski, R. 2013. 'Earthquake-induced pounding between equal height multi-storey buildings considering soil-structure interaction'. *Bulletin of Earthquake Engineering*, 11: 1021-48.

Mahmoud, S., Chen, X. and Jankowski, R. 2008. 'Structural pounding models with Hertz spring and nonlinear damper'. *Journal of Applied Sciences*, 8: 1850-58.

Malhotra, S. 2010. 'Seismic Soil-Pile-Structure Interaction: Analytical Models'. *GeoFlorida 2010: Advances in Analysis, Modelling & Design*.

Masaeli, H., Khoshnoudian, F. and Ziaei, R. 2015. 'Rocking soil-structure systems subjected to near-fault pulses'. *Journal of Earthquake Engineering*, 19: 461-79.

Meymand, P. J. 1998. 'Shaking table scale model tests of nonlinear soil-pile-superstructure in soft clay'. *University of California, Berkley.*

Muthukkumaran, K., Sundaravadivelu, R. and Gandhi, S. R. 2008. 'Effect of Slope on PY Curves Due to Surcharge Load'. *Soils and foundations* 48: 353-361.

Mylonakis, G., Nikolaou, A. and Gazetas, G. 1997. 'Soil-pile-bridge seismic interaction: kinematic and inertial effects. Part I: soft soil'. *Earthquake Engineering & Structural Dynamics*, 26: 337-59.

Naserkhaki, S., Aziz, F. N. A. A. and Pourmohammad, H. 2012. 'Earthquake induced pounding between adjacent buildings considering soil-structure interaction'. *Earthquake Engineering and Engineering Vibration*, 11: 343-58.

Newmark, N. M., Blume, J. A. and Kapur, A. A. 1973. 'Seismic design spectra for nuclear power plants'. *Consulting Engineering Services*, Urbana, IL.

Ng, C.W.W. Zhang, L.M. and Ho, K. K. S. 2001. 'Influence of laterally loaded sleeved piles and pile groups on slope stability'. *Can. Geotech. J.* 38: 553–566.

Nguyen, D. D. C., Jo, S.B. and Kim, D. S. 2013. 'Design method of piled-raft foundations under vertical load considering interaction effects'. *Computers and Geotechnics*, 47: 16-27.

Nimityongskul, N. 2010. 'Effects of soil slope on lateral capacity of piles in cohesive soils'. *PhD thesis,* Oregon State University.

Nor, M., Hakimi, M., Yahuda, A. H. and Pakir, F. 2014. 'Analysis of lightweight concrete "cakar ayam" foundation for road construction using plaxis 3D foundation software'. *Applied Mechanics and Materials*, 695.

NZS1170.5. 2004. 'Structural Design Actions, Part 5: Earthquake actions–New Zealand'. *Standards New Zealand Wellington*, New Zealand.

Oden, J. T., and Martins, J. A. C. 1985. 'Models and computational methods for dynamic friction phenomena'. *Computer methods in applied mechanics and engineering*, 52: 527-634.

Osman, A. S., and Randolph, M. F. 2012. 'Analytical Solution for the Consolidation around a Laterally Loaded Pile'. *International Journal of Geomechanics*, 12: 199-208.

Park, D., and Hashash, Y. M. A. 2004. 'Soil damping formulation in nonlinear time domain site response analysis'. *Journal of Earthquake Engineering*, 8: 249-74.

PEER. 2012. 'Ground Motion Database'. *Pacific Earthquake Engineering Research Centre*.

Poulos, H. G., and Davis, E. H. 1980. 'Pile foundation analysis and design'. *No. Monograph.*

Pratesi, F., Sorace, S. and Terenzi, G. 2014. 'Analysis and mitigation of seismic pounding of a slender R/C bell tower'. *Engineering Structures*, 71: 23-34.

Rahman, A. M., Carr, A. J. and Moss, P. J. 2001. 'Seismic pounding of a case of adjacent multiple-storey buildings of differing total heights considering soil flexibility effects'. *Bulletin of the New Zealand National Society for Earthquake Engineering*, 34: 40-59.

Rahvar. 2006. 'Geotechnical investigation and foundation design report of Mahshahr train station, P.O. ', *Rahvar Pty Ltd, Iran Railway Authority, Mahshar, Iran.* .

Randolph, M. F., Dolwin, J. and Beck, R. 1994. 'Design of driven piles in sand'. *Geotechnique*, 44: 427-48.

Reese, L. C., Isenhower, W. M. and Wang, ST. 2006. 'Analysis and design of shallow and deep foundations'. *Wiley Hoboken*, NJ.

Rosenblueth, E., and Meli, R. 1986. 'The 1985 earthquake: causes and effects in Mexico City'. *Concrete international*, 8: 23-34.

Rowe, R. K. and Poulos H. G. 1979. 'A method for predicting the effect of piles on slope behaviour'. *Research report in School of Civil Engineering*, Sydney, Australia.

Ryan, K. L., and Polanco, J. 2008. 'Problems with Rayleigh damping in base-isolated buildings'. *J. Struct. Eng.*, 34: 1780-84.

Sameti, A. R., and Ghannad, M. A. 2016. 'Equivalent linear model for existing soil-structure systems'. *International Journal of Structural Stability and Dynamics*, 16: 1450099.

Sbartai, B. 2016. 'Dynamic interaction of two adjacent foundations embedded in a viscoelastic soil'. *International Journal of Structural Stability and Dynamics*, 16: 1450110.

Seed, H. B., and Idriss, I. M. 1969. 'Influence of soil conditions on ground motions during earthquakes'. *Journal of the Soil Mechanics and Foundations Division*, 95: 99-138.

Seed, H. B., Wong I. M., Idriss, I. M. and Tokimatsu, K. 1986. 'Moduli and damping factors for dynamic analyses of cohesionless soils'. *Journal of Geotechnical Engineering*, 112: 1016-32.

Semblat, JF. 2010. 'Modelling seismic wave propagation and amplification in 1D/2D/3D linear and nonlinear unbounded media'. *International Journal of Geomechanics*, 11: 440-48.

Shakya, K, and Wijeyewickrema, A. C. 2009. 'Mid-column pounding of multi-story reinforced concrete buildings considering soil effects'. *Advances in Structural Engineering*, 12: 71-85.

Shelke, A., and Patra, N. R. 2008. 'Effect of arching on uplift capacity of pile groups in sand'. *International Journal of Geomechanics*, 8: 347-54.

Shiming, W., and Gang, G. 1998. 'Dynamic soil-structure interaction for high-rise buildings'. *Developments in geotechnical engineering*, 83: 203-16.

Shing, P. B., and Tanabe, T. 2001. 'Modelling of inelastic behaviour of RC structures under seismic loads'. *ASCE Publications.*

Small, J. C., and Zhang, H. H. 2002. 'Behaviour of Piled Raft Foundations Under Lateral and Vertical Loading'. *International Journal of Geomechanics*, 2: 29-45.

Sołtysik, B., and Jankowski, R. 2015. 'Building damage due to structural pounding during earthquakes'. In *Journal of Physics: Conference Series*, 012040. IOP Publishing.

Song, E., Ye, L., Zhao, S. & Yang, Q. 2008. 'Analysis on seismic damage of buildings in the Wenchuan Earthquake (in Chinese)'. *Journal of Building structure*, 29: 1-9.

Sorensen, S. P. H., Ibsen, L. B. and Foglia, A. 2015. 'Testing of Laterally Loaded Rigid Piles with Applied Overburden Pressure'. *International Journal of Offshore and Polar Engineering*, 25: 120-26.

Star, L. M., Givens, M. J., Nigbor, R. L. and Stewart, J. P. 2015. 'Field-Testing of Structure on Shallow Foundation to Evaluate Soil-Structure Interaction Effects'. *Earthquake spectra*, 31: 2511-34.

Stewart, J. P, Fenves, G. L. and Seed, R. B. 1999. 'Seismic soil-structure interaction in buildings. I: Analytical methods'. *Journal of geotechnical and geoenvironmental engineering*, 125: 26-37.

Stewart, J. P, Seed, R. B. and , Fenves G. L. 1999b. 'Seismic soil-structure interaction in buildings. II: Empirical findings'. *Journal of geotechnical and geoenvironmental engineering*, 125: 38-48.

Stewart, J. P, Seed, R. B. and , Fenves G. L. 1998. *Empirical evaluation of inertial soil-structure interaction effects* (Pacific Earthquake Engineering Research Center).

Sun, J. I., Golesorkhi, R. and Seed, H. B. 1988. 'Dynamic moduli and damping ratios for cohesive soils'. *Earthquake Engineering Research Center*, University of California Berkeley.

Suzuki, Z. 1971. 'General Report on the Tokachi-oki Earthquake of 1968'. *Keigaku Pub. Co*.

Tabatabaiefar, S., Fatahi B., and Samali, B. 2014a. 'An empirical relationship to determine lateral seismic response of mid-rise building frames under influence of soil–structure interaction'. *The Structural Design of Tall and Special Buildings*, 23: 526-48.

Tabatabaiefar, S., Fatahi, B. and Samali, B. 2014b. 'Numerical and experimental investigations on seismic response of building frames under influence of soil-structure interaction'. *Adv. Struct. Eng.*, 17: 109-30.

Tavakoli, H. R., Naeej, M. and Salari, A. 2011. 'Response of RC structures subjected to near-fault and far-fault earthquake motions considering soil-structure interaction'. *International Journal of Civil and Structural Engineering*, 1: 881.

Thio, H. K., and Kanamori, H. 1996. 'Source complexity of the 1994 Northridge earthquake and its relation to aftershock mechanisms'. *Bulletin of the Seismological Society of America*, 86: S84-S92.

Torabi, H., and Rayhani, M. T. 2014. 'Three dimensional Finite Element modelling of seismic soil–structure interaction in soft soil'. *Computers and Geotechnics*, 60: 9-19.

Uz, M. E., and Hadi, M. N. S. 2011. 'Seismic history analysis of asymmetrical adjacent buildings with soil-structure interaction consideration'. *WIT Transactions on The Built Environment*, 120: 225-36.

Veletsos, A. S., and Meek, J. W. 1974. 'Dynamic behaviour of building-foundation systems'. *Earthquake Engineering & Structural Dynamics*, 3: 121-38.

Veletsos, A. S., and Prasad, A. M. 1989. 'Seismic interaction of structures and soils: stochastic approach'. *Journal of Structural Engineering*, 115: 935-56.

Veletsos, A. S. 1993. 'Design concepts for dynamics of soil-structure interaction'. *Developments in dynamic soil-structure interaction* (Springer).

Vucetic, M., and Dobry, R. 1991. 'Effect of soil plasticity on cyclic response'. *Journal of Geotechnical Engineering*, 117: 89-107.

Wald, D. J. 1996. 'Slip history of the 1995 Kobe, Japan, earthquake determined from strong motion, teleseismic, and geodetic data'. *Journal of Physics of the Earth*, 44: 489-503.

Wald, D. J., Heaton, T. H. and Hudnut, K. W. 1996. 'The slip history of the 1994 Northridge, California, earthquake determined from strong-motion, teleseismic, GPS, and levelling data'. *Bulletin of the Seismological Society of America*, 86: S49-S70.

Wang, S., Kutter, B. L., Chacko, M. J., Wilson, D. W., Boulanger, R. W. and Abghari, A. 1998. 'Nonlinear seismic soil-pile structure interaction'. *Earthquake spectra*, 14: 377-96.

Wolf, J. P. 1985. 'Dynamic soil-structure interaction'. *Prentice Hall, Inc.*

Wolf, J. P. 1988. 'Soil-structure-interaction analysis in time domain*'. Prentice Hall, Inc.*

Wolf, J. P. 1989. 'Soil-structure-interaction analysis in time domain'. *Nuclear Engineering and Design*, 111: 381-93.

Wolf, J. P., and Skrikerud, P. E. 1980. 'Mutual pounding of adjacent structures during earthquakes'. *Nuclear Engineering and Design*, 57: 253-75.

Yegian, M. K., Ghahraman, G. V., Gazetas, G., Dakoulas, P. and Makris, N. 1995. 'The Northridge Earthquake of 1994: Ground Motions and Geotechnical Aspects'. *International Conferences on Recent Advances in Geotechnical Earthquake Engineering and Soil Dynamics.* Feb 1995. St. Louis, Missouri.

Yuen, P. C., Weaver, P. F., Suzuki, R. K. and Furumoto, A. S. 1969. 'Continuous, traveling coupling between seismic waves and the ionosphere evident in May 1968 Japan earthquake data'. *Journal of Geophysical Research*, 74: 2256-64.

Zou, L., Huang, K., Wang, L. and Fang, L. 2013. 'Pounding of adjacent buildings considering pile-soil-structure interaction'. *Journal of Vibroengineering*, 15.